EXPERIMENTAL AND NUMERICAL INVESTIGATION OF A HEAT RECOVERY VENTILATION UNIT WITH PHASE CHANGE MATERIAL FOR BUILDING FACADES

A Thesis Submitted to
the Graduate School of Engineering and Sciences of
İzmir Institute of Technology
in Partial Fulfillment of the Requirements for the Degree of

DOCTOR OF PHILOSOPHY

in Architecture

by
Tuğçe PEKDOĞAN

December 2021
İZMİR

ACKNOWLEDGMENTS

ABSTRACT

EXPERIMENTAL AND NUMERICAL INVESTIGATION OF A HEAT RECOVERY VENTILATION UNIT WITH PHASE CHANGE MATERIAL FOR BUILDING FACADES

This thesis presents a wall-integrated HRV unit design that stores latent heat thermal energy (LHTES). The system's performance is tracked through experimental and numerical studies. The experimental tests of the unit took place in a controlled environment, where two HRV units are inside two wall-integrated ducts. The wall divides two conditioned spaces that represent indoors and outdoors. In one set of experiments, the commercially available system that stores sensible heat thermal energy (SHTES) with ceramic block. On another set of experiments, the newly designed LHTES system with the staggered tube bundle that contains phase change material (PCM). SHTES system shows the best performance in 2-minute, supply efficiency is 82% and exhaust efficiency is 67%. LHTES system shows the best performance in 20-minute and supply efficiency is 55% and exhaust efficiency is 30%.

Numerical parametric studies on the HRV systems use the commercial CFD software ANSYS-FLUENT. These studies include the detailed flow and heat transfer analyses and the optimum operating times for two systems. As a result of these studies, the CFD results show good agreement with the experimental results. At the end of the thesis, the ability to increase the capacity of the HRV unit with PCM was investigated. In addition, the simulations for different climatic data were studied. According to the results, 12mm longitudinal, 12mm transverse pitch size for the ∅4.76mm tube is the most efficient system with total heat capacity of 45.77kJ. In addition, for different climates simulations, LHTES unit can be used throughout the year in Singapore.

ÖZET

BİNA CEPHELERİ İÇİN FAZ DEĞİŞİM MALZEMELİ BİR ISI GERİ KAZANIM ÜNİTESİNİN DENEYSEL VE SAYISAL İNCELENMESİ

Bu tez, duyulur ısıl enerji depolama (DIED) yerine gizli ısıl enerji depolama (GIED) özelliğini kullanan duvara entegre bir ısı geri kazanım (IGK) ünitesinin ısı ve akış performansının incelenmesi üzerinedir. Sistemlerin performansı deneysel ve sayısal parametrik çalışmalarla incelenmiştir. Deneysel kısımda, laboratuvar ortamında şartlandırılan iki mekân arasına örülen duvarda bulunan iki adet kanal içerisine IGK havalandırma sistemleri yerleştirilerek kontrollü parametrik incelemeler yürütülmüştür. Bu iki kanala yerleştirilen, birbirleriyle eş zamanlı çalışan ünitelerin ısı ve akış performansları elde edilmiştir. Birinci deney setinde, piyasada bulunan DIED seramik bloklu sistem için parametrik çalışmalar gerçekleştirilmiştir. İkinci deney setinde ise, GIED sağlayan IGK ünitesi şaşırtmalı tüp demeti şeklinde tasarlanmış ve tüplerin içine faz değişim malzemesi (FDM) yerleştirilerek, ünite içerisindeki sıcaklık değişimleri ve erime/katılaşma süreçleri belirlenmiştir. DIED sisteminde 2 dakika, GIED sisteminde ise 20 dakika boyunca çalıştığında, birim zaman başına en yüksek enerji depolama görülmektedir. Deneysel sonuçlara göre en yüksek verim; DIED için besleme verimi %82, egzoz verimi %67'dir. GIED sisteminde ise besleme verimi %55, egzoz verimi %30'dur.

İki IGK sistemi üzerindeki sayısal parametrik çalışmalar, ANSYS-FLUENT aracılığıyla yapılmıştır. Yapılan çalışmalar neticesinde HAD sonuçları deneysel sonuçlarla uyumludur. HAD çalışmaları kapsamında; sistemler üzerinde detaylı akış ve ısı transferi analizleri ile optimum çalışma süreleri değerlendirilmiştir. Ayrıca daha yüksek performansa sahip GIED ünitesi için kapasite geliştirme çalışmaları araştırılmış ve farklı iklim verileri için simülasyonlar yapılmıştır. Elde edilen sonuçlara göre, 4.76mm çapındaki tüp için 12mm enine 12mm boyuna hatve ölçüsüne sahip olan tasarım 45.77kJ toplam ısı kapasitesi ile en verimli sistemdir. Farklı iklimlerde yapılan simülasyon sonuçlarına göre Singapur'da bu sistemin yıl boyunca kullanılabileceği görülmüştür.

TABLE OF CONTENTS

LIST OF FIGURES

LIST OF TABLES

LIST OF ABBREVATIONS

AHU — Air Handling Unit

ASHRAE — American Society of Heating, Refrigerating and Air-Conditioning Engineers

EPBD — Energy Performance of Buildings Directive

AECB — Association for Environment Conscious Building

BEP — Basic Energy Plan

BEP-TR — Building Energy Performance Turkey

BREEAM — Building Research Establishment Environmental Assessment Method

CFD — Computational Fluid Dynamics

CVS — Centralized Ventilation System

DIN — Deutsches Institut für Normung

DVS — Decentralized Ventilation System

EN — European Standards

EPA — Environmental Protection Agency

GEMS — Greenhouse and Energy Minimum Standards

HRV — Heat Recovery Ventilation

HTF — Heat Transfer Fluid

HVAC — Heating, Ventilation, and Air Conditioning

IAQ — Indoor Air Quality

LHTES — Latent Heat Thermal Energy Storage

LEED — Leadership in Energy and Environmental Design

MOHURD — The Ministry of Housing and Urban-Rural Development

PCM — Phase Change Material

PMV — Predicted Mean Vote

PPD — Predicted Percentage of Dissatisfied

SHTES — Sensible Heat Thermal Energy Storage

WHO — World Health Organization

LIST OF NOMENCLATURE

A	area (m^2)
β	thermal expansion
c_p	specific heat capacity (J/kg°C)
h_{sf}	latent heat of fusion (J/kg)
h	height (m)
H	total volumetric enthalpy
f	friction factor
F_s	safety factor
g	gravity
m	mass (kg)
$\dot{m}$	mass flow rate (kg/s)
η	efficiency
N	total number of the cell
Nu	Nusselt number (hD/k)
Q	thermal energy (J)
$\dot{Q}$	heat transfer rate (W)
p	pressure (Pa)
ρ	density (kg/m^3)
R	total uncertainty of the value
Re	Reynolds number
T	temperature (°C)
t	time (s, min)
ΔT	temperature difference (°C)
ΔP	pressure drop (Pa)
Δt	time difference (s)
x_1	independent variables
V	volume (m^3)
v	velocity
W_R	uncertainty in the independent variables

CHAPTER 1

INTRODUCTION

1.1. Research Area and Context

Today, people spend more than 90% of their time indoors, either in the office or home (EPA 2018). Therefore, buildings should provide adequate accommodation and create a healthier environment. Such studies have increased recently considering the COVID-19 pandemic, which has raised concerns about indoor air quality (IAQ) (Afshari 2020). In an attempt to slow or stop the transmission of the virus, scientists and government officials have focused on implementing infectious disease prevention measures such as asking people to stay at home. Such recommendations have increased interest in ensuring IAQ and related mechanical ventilation systems.

On the other hand, since the building sector consumes more energy than the industry and transportation sectors (Köktürk and Tokuç 2017), many studies focus on the effect of building energy use on the environment and methods to reduce this energy use. Many countries have implemented compulsory measures to decrease energy consumption while maintaining thermal comfort in response to environmental concerns. The most common criteria include properly insulating the building envelope and reducing infiltration loads (Chandel and Agarwal 2017). However, this creates airtight buildings that are not well-ventilated and lead to decreased IAQ. This can lead to health problems, and disturbances called Sick Building Syndrome, Building-Related Diseases, and Building-Related illness, directly caused by the indoor environment and air.

Air pollution can result from both natural causes as well as human activities. In addition, building materials can also be critical interior pollutants and affect indoor air quality. Carbon dioxide is a significant indoor air pollutant, and its concentration is usually considered an indicator for IAQ and adequate ventilation. Although indoor CO_2 concentrations vary from country to country, 1000 ppm CO_2 concentrations are considered the threshold for the IAQ (ASHRAE Standard 62.1 2016). If the amount of CO_2 is lower than this level, the indoor air is of acceptable indoor air quality. CO_2 is not a toxic gas, but when the concentration value exceeds 35000 ppm, the central breathing

receptors are triggered and lead to inadequate breathing, and the central nervous system cannot function due to the lack of oxygen (Işık and Çibuk 2015). Clean air is essential for human health, and acceptable CO_2 levels can be ensured by using CO_2 sensors with ventilation systems.

Figure 1.1 shows the relationship between the levels of CO_2 in one area and ventilation rates. As can be seen at the point of demand control based on CO_2, it is thought that energy costs can be reduced by meeting the ventilation needs of the area more accurately. CO_2 concentration is appropriate to take place in the open air at around 400 ppm. However, a ventilation rate of about 10 L/s per person is required when the outdoor level is 500 ppm, while a good fresh airflow can be achieved with a ventilation rate of 7 L/s, even if the outdoor level is 700 ppm. The American Society of Heating, Refrigerating and Air-Conditioning Engineers recommends a ventilation rate of 7-10 L/s per person in ASHRAE Standard 62.1 (2016).
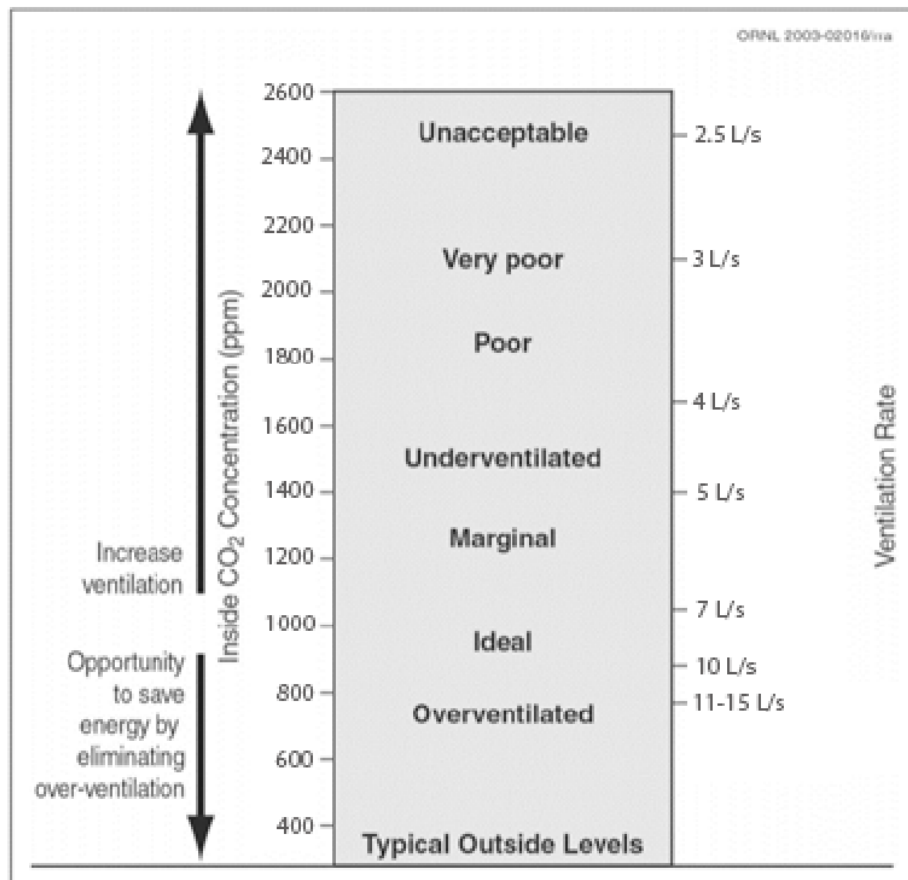
Figure 1.1. The relationship between CO_2 and ventilation rates (converted to SI unit). (Source: Bas 2003)

In addition, previous studies have reported that the impact of ventilation rate on sick building syndrome symptoms has been concluded to be often substandard, and it is not unusual to find CO_2 levels above less than 1000 ppm in classrooms and offices (Persily 2017; Özdamar and Umaroğulları 2017; Çotuker and Menteşe 2017; Bulut 2011; Ekren et al. 2017). Good ventilation systems not only provide thermal comfort, but they should also distribute adequate fresh air to occupants and remove pollutants.

Understanding and controlling building ventilation can improve the air quality and reduce the risk of indoor health concerns, including preventing the virus that causes COVID-19 from spreading indoors (WHO 2020). Depending on the climate and conditions, unique solutions and building components are used to ensure fresh air inflow from the outside. Ventilation is a concept related to the exchange of air in an enclosed space and has brought with it the quality and comfort criteria frequently mentioned in architecture in recent years. Yeang (2006) summarizes the purposes of ventilation as:

- To keep the oxygen concentration of the air in a particular range and prevent it from decreasing,
- To prevent the excessive increase of CO_2, moisture, cigarette smoke content in the closed air,
- To remove or control the air pollutants from the area,
- To remove the heat and humidity increases caused by the users, lighting, and machines,
- To keep the temperature and humidity at the comfort level,
- To remove toxic gases and dust from the environment,
- To reduce the number of harmful microorganisms and bacteria

Good ventilation is essential for a healthy and efficient building and indoor environment. So, a top priority is to understand the building's HVAC system that needs the building occupants throughout the day. Natural and mechanical ventilation methods can help provide fresh air inside the buildings. The pressure difference between the indoor and outdoor environment is the driving force for natural ventilation. However, mechanical ventilation systems are preferred if the wind-driven ventilation and stack effect are insufficient or cannot be controlled. When the differences between mechanical and natural ventilation in terms of indoor air pollutants were compared, occupants living in mechanically ventilated houses had a better health status, and their health was significantly improved (Cuce and Riffat 2015). Healthcare units' IAQ results indicate that

adequate control of CO_2 concentration and relative humidity balance effectively reduces the risk of infection through the air using mechanical ventilation systems (Shao, Riffat and Gan 1998). When ventilation rates investigated the air quality in schools, the concentrations of pollutants in low-energy school buildings were lower than naturally ventilated (Mardiana-Idayu and Riffat 2011). Comparing mechanically ventilated buildings with naturally ventilated buildings can better understand the IAQ of buildings because different ventilation systems can have other effects on indoor particle concentrations. Considering IAQ conditions, mechanical ventilation can reduce indoor particle concentrations in residential buildings (Zeng, Liu and Shukla 2017). Also, some publications have discussed and examined mechanical ventilation systems' energy use potential in different climates (Wallner et al. 2017; Fonseca et al. 2019).

Advanced designs of new buildings are beginning to have mechanical systems that bring outdoor air into the indoor environment. Some of these designs include energy-efficient heat recovery ventilators to improve IAQ (EPA 2018). Heat recovery ventilation (HRV) systems ensure the efficient use of energy by transferring heat from the exhaust air to the fresh air supply (Verriele et al. 2016). There are various methods to recover heat from exhaust air for mechanical system applications (Park, Jee and Jeong 2014), and these systems typically recover 60-95% of the energy in the exhaust air, thereby significantly improving buildings' energy performance (Kim and Baldini 2016; Pekdogan et al. 2021a; Pekdogan et al. 2021b). Although several studies on HRVs, shortcomings remain in the research and development of using recovery systems in building applications and wall-integrated systems (Merzkirch et al. 2016).

Considering heat recovery effectiveness, fan and pump energy consumptions are limited (Wallner et al. 2017) and decentralized ventilation systems (DVSs) have lower pressure losses (Fonseca et al. 2019) when DVSs and centralized ventilation systems (CVSs) are compared. Also, the large volume requirements of a CVS (Etheridge and Sandberg 1996) can be avoided by using a DVS and embedding HRV systems into the building wall. HRV systems that store sensible heat (SHTES) are commercially available in this scope. However, wall integrated HRV systems can only meet the fresh air requirement of relatively small spaces by using multiple units because of the low capacity of their SHTES units and small fans. These wall integrated HRV systems usually involve electronically driven two-way fans. The indoor air expelled to the outdoors flows through a ceramic material and transfers its thermal energy to the ceramic block and occurring sensible heat storage corresponds to the temperature variations within the ceramic block.

After completing the expelling process, the fan transfers fresh outdoor air indoors in the opposite direction. Removable filters in the system control the outdoor contaminants and two units running simultaneously prevent indoor pressure imbalances.

The commercially available wall-integrated DVSs generally consist of an air supply grill, an air filter, an axial fan, and a ceramic HRV unit. These products can provide different fresh air flow rates depending on their fan capacities and the selected control levels. The fans usually work in one direction for 70 seconds. The number and placement of units inside a space depend on the size of the space to be ventilated, the desired air change rate, and the homogeneous fresh air distribution. In addition to considering aesthetic value in architectural designs, DVSs are easier to control and generate less noise than CVSs.

However, the proper design, selection, and implementation of energy-efficient ventilation systems require a holistic approach to the buildings and users. According to ASHRAE Standard 62.1 2016, the sensible effectiveness of air-to-air energy recovery equipment for the room-based DVS installed in the exterior walls is typically 80% to 90%. Also, HRV systems that store latent heat (LHTES) with phase change materials (PCM) are possible in condensing conditions (i.e., heating mode). LHTES is frequently used today in the heating and cooling sector due to its energy-saving and high efficiency (Khudhair, Razack and Al-Hallaj 2004; Promoppatum et al. 2017). Therefore, heat recovery DVSs can achieve higher thermal energy storage capacities by using latent heat in addition to sensible heat.

1.2. Purpose of the Study

In the previous research, many energy-efficient systems have been developed and evaluated to recover waste heat energy from buildings. Several studies mentioned wall integrated HRV systems, a new concept DVS, and evaluated their potential applications for residential ventilation. However, these studies only mention and evaluate units that store sensible energy.

Based on the literature review, there are no numerical and experimental studies into the energy and flow analysis of a decentralized wall integrated HRV system with PCM. Thus, this dissertation's purpose is to design a wall integrated HRV unit with PCM to achieve more thermal energy storage capacity than the sensible energy storage solution.

Therefore, in this study, two different types of decentralized HRV units are investigated experimentally and numerically. These two systems are named ceramic HRV unit and tube bundle HRV unit. Both systems' thermal performance and airflow behaviors are evaluated experimentally and numerically.

Several items can be provided to characterize the current dissertation's objectives:

- To thermally characterize decentralized HRV units (with ceramic HRV unit (SHTES) and tube bundle HRV unit (LHTES) working under controlled conditions in a real-scale experimental setup).

- To investigate experimentally how the different cycle periods affect the energy consumption of HRV units.

- To suggest appropriate solutions to evaluate the parameters affecting airflow and energy performance on different tube bundle unit designs via conducting numerical studies on LHTES.

- To guide the designer in selecting the wall integrated ventilation system in different climates by analyzing the energy performance of the tube bundle prototype under three different climatic conditions.

1.3. Research Methodology

This study will approach the problems described above in a systematic way. First, a thorough analysis and a literature review on related subjects are undertaken. The major area of published research reviewed focuses on current and in-development decentralized and centralized heat recovery devices. Following this, all measurements are tested under laboratory conditions. All measuring instruments are calibrated by an accredited calibration laboratory for accurate and traceable measurements. Despite this, all measurements have uncertainty caused by sources such as repeatability, calibration, and the environment. Thus, the uncertainty of the measurements is calculated as well. Computational Fluid Dynamics (CFD) is used for the 2D flow analysis. The CFD model can produce data about the airflow through the heat recovery device and the temperature change used. The data generated from the CFD model is validated against real-scale experiments. Then results of the decentralized ventilation units are analyzed and the conclusions on the performance of these units are given. Finally, the answer to the question of how to improve the produced prototype is searched with the different

refinement of the LHTES unit. Figure 1.2. shows the flowchart of the main steps of this study.

```
┌─────────────────────────────────────────┐
│  Wall integrated heat recovery ventilation │
│            units' analysis                │
└─────────────────────────────────────────┘
                    │
                    ▼
┌─────────────────────────────────────────┐
│       Overview of the past research      │
└─────────────────────────────────────────┘
                    │
                    ▼
┌─────────────────────────────────────────┐
│    Measurements in laboratory conditions │
│    Indoor temperature, Outdoor temperature, │
│  HRV unit temperature distribution, Air temperature at │
│   ducts, Air velocity, Pressure drop, Calibration of the │
│     measurements and Uncertainty analysis │
└─────────────────────────────────────────┘
```
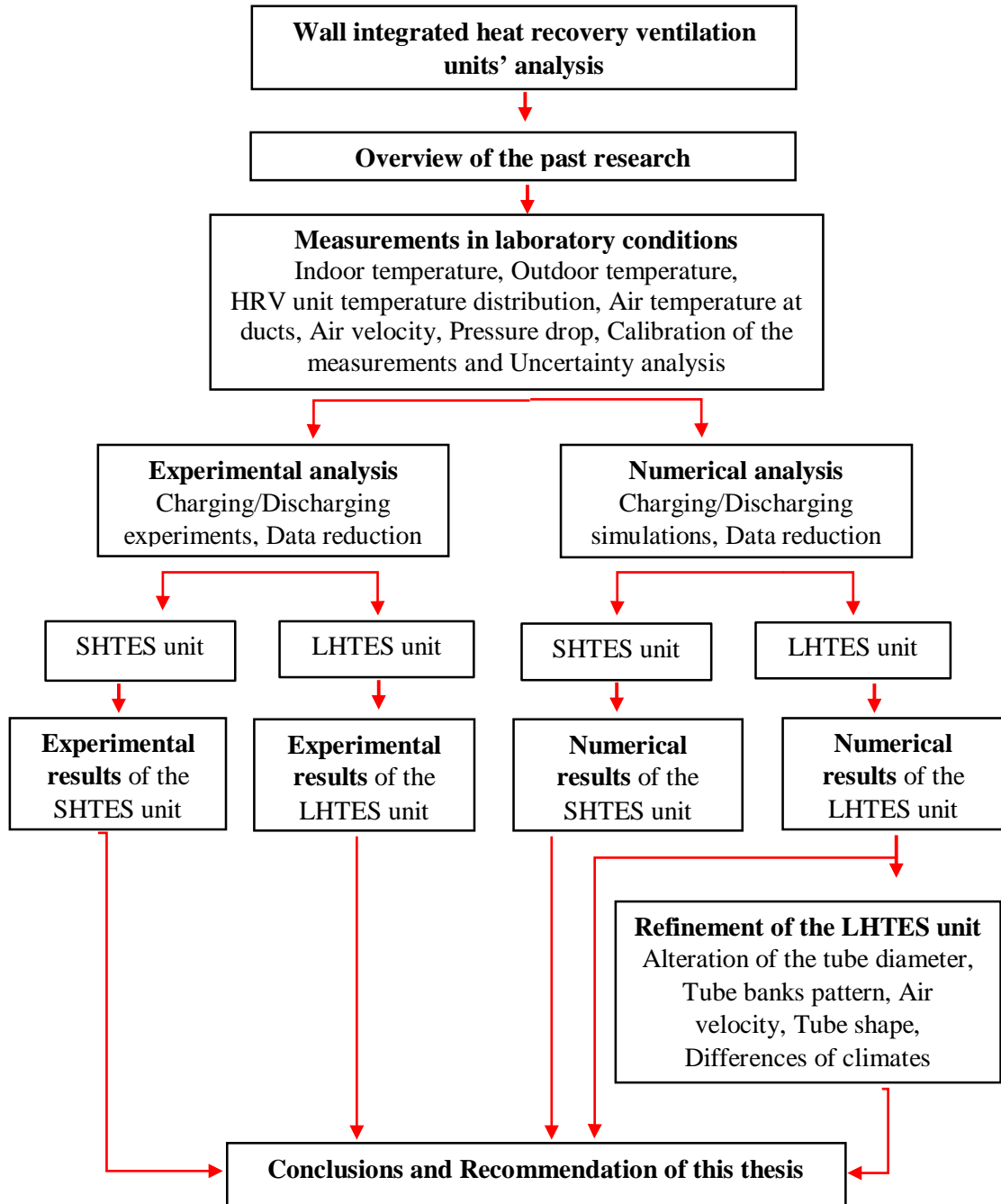
Figure 1.2. The flowchart of the studies to calculate heat recovery unit performance.

7

1.4. Contents of the Study

This thesis contains six main chapters. These sections are organized according to the underlying objectives based on the classification of the research problem and the method of the study.

Chapter 1 is an introduction to the study. This chapter covers the background of the research, the purpose of the study, the research methodology, and the organization of the thesis.

Chapter 2 covers the literature of the study that discusses thermal comfort and indoor air quality and reviews the thermal energy storage used in buildings and the classification and application of different PCMs. This chapter also deals with HVAC systems using several methods.

Chapter 3 demonstrates the methodology and research framework, experimental setup, and measurement devices. The calibration process and uncertainty analysis of the measurements is included as well.

Chapter 4 shows the computational fluid dynamics modeling solution for two types of decentralized HRV systems.

Chapter 5 presents the results of each type of HRV system, including experimental results and simulation results. And also, this chapter provides the perspectives of refinement of the tube bundle prototype facade unit with different scenarios and the simulation studies on the prototype with different climate data.

Chapter 6 concludes based on the results of the investigations. This chapter also details the results and discussions from the CFD analysis and the prototype experiments.

Appendix 1 provides the air velocity calibration results and Appendix 2 provides the fan characteristics manufacturer document. Appendix 3 shows the thermocouple calibration results in the different temperature ranges.

CHAPTER 2

DEFINITIONS AND LITERATURE REVIEW

2.1. Indoor Environment

A good indoor environment, essential for successful building design, has not only a significant impact on energy consumption but also provides occupant comfort. Built environments consist of various functions, sizes, and forms. The diversity and availability of building materials also reflect basic factors such as climate and culture. Different thermal conditioning is applied according to each climate to provide indoor and thermal comfort according to the outdoor weather conditions. While cooler conditions are provided in hot climates, a warmer environment is desired in cold climates. Controlling thermal comfort and other aspects of the indoor environment is associated with using and applying climate control technologies (Maroni, Seifert, and Lindvall 1995). Indoor environments often contain various toxic or hazardous substances and biologically sourced pollutants. Due to some biological pollutants, diseases have been seen frequently in human history. In developed countries, concerns have increased over the last few decades about indoor pollutants and potential exposure risks, including ambient air pollution, water pollution, hazardous waste (Godish 2016).

Indoor environmental quality (IEQ) and occupant comfort are closely related. Current indoor environmental assessment includes four aspects, namely thermal comfort (TC), indoor air quality (IAQ), visual comfort (VC), and aural comfort (AC) (Clausen and Wyon 2008; Wong, Mui and Hui 2008). Frontczak et al. (2012) identified the effect of indoor environmental quality studies on building occupants' satisfaction. And the result of this review found that these aspects, visual, thermal, acoustics, and IAQ, contributed to occupant satisfaction. Astolfi and Pellerey (2008) found that the indoor environment was associated with thermal, acoustic, visual, and air quality satisfaction. However, indoor environmental quality is affected by chemical, biological, and psychological factors. The characteristics of the built environment are defined IEQ, such as building materials, furnishing, building design, mechanical systems, etc. Ultimately, this can lead to health effects (Fig. 2.1.) (Wu et al. 2007).

Sources	Chemical	Users	Diseases
-Building design -Building materials -Mechanical systems -Furnishing -Cleaning Products -External sources -Smoking -Wastes	**Chemical** -Asbestos -Inorganic fibers -Tobacco smoke -Volatile compounds -Pesticides **Biological** -Viruses, bacteria -Fungi, mold **Physical** -Heat/cold -Humidity Noise -Lights -Radon	-Occupant characteristics -Medical history -External exposures -Lifestyle -Environmental factors -Building maintenance	-Injuries -Asthma -Allergic disorders -Infection -Mucosal irritation -Nervous effects -Psychiatric disorders (depression etc.) -Cardiovascular diseases -Cancer

Figure 2.1. The pathway from the built environment to health effects.
(Source: Wu et al. 2007)

However, achieving improved indoor environmental quality involves multiple stakeholders. But according to occupants' satisfaction, thermal comfort is important than air quality and much higher than visual comfort (Frontczak et al. 2012).

So, the following section focuses on the thermal comfort and IAQ definitions and the applicability of the indoor environment. The literature background is divided into two sections. The first is definitions of comfort and parameters, and the second is international standards and local regulations for thermal comfort, IAQ, and energy recovery requirements.

2.1.1. Indoor Air Quality

IAQ refers to the quality of air in and around buildings and structures, especially in terms of the health and comfort of occupants of buildings (EPA 2018). Health can be influenced by the quality of indoor air, which is a result of outdoor and indoor air contaminants, thermal comfort, and sensory loads (odors, "freshness" (McDowall 2007). Monitoring common contaminants contained indoors will help us reduce the risk of concerns about indoor health (EPA 2018). To ensure sufficient IAQ, continuous ventilation of occupied spaces is essential. The decrease in IAQ is directly related to Sick Building Syndrome. The levels of the pollutants such as CO_2, CO within the indoor air

affect the IAQ. Various government agencies, organizations, and researchers have prepared guidelines for assessing the IAQ.

The appropriate application of three techniques is required to maintain satisfactory IAQ. The essential way to keep indoor air quality at a safe level is to control contaminants and pollutant sources. The other method is to remove contaminants from the air. Choosing a filter is important for balancing initial purchase, operating, and effectiveness requirements. And also, the third essential method is dilution. The standard method of controlling general pollutants in buildings and the methods and quantities necessary is dilution ventilation (Megahed and Ghoneim 2020).

Megahed and Ghoneim (2020) reviewed the design strategies in post-pandemic architecture, which is the management of IAQ related to the COVID-19. This research aims to show architects the increased risk of disease transmission by providing solutions to understand the health and environmental issues of COVID-19. This study provides a conceptual model based on this issue that discusses the integration of engineering controls, design methods, and techniques for air disinfection to achieve a better IAQ. Buildings include a holistic IAQ management strategy for human-centered designs that requires adequate ventilation system, air filtration, regulation of humidity, and control of temperature.

Mentese et al. (2020) studied 121 homes in Çanakkale, Turkey, collected data throughout a year. Especially, some air pollutants like; CO_2, VOCs, temperature, and humidity were monitored. Finally, the SBS symptoms varied seasonally and some diseases occurred frequently. The frequency of SBS symptoms, the calculated IAQ parameters, and personal factors is correlated ($p < 0.05$).

Ma et al. (2021) proposed an analytical model and its variables of IAQ related to thermal comfort and health. The first part of this paper has the thermal comfort model and its variables. The second part of this paper focuses on indoor air pollutants and their relationship to ventilation requirements. And the final part of this paper explains the factors required for thermal comfort and IAQ to be expected. To sum up, factors such as outdoor/indoor temperature, wind velocity, outdoor/indoor relative humidity, physical features of the room, natural/mechanical ventilation, the number of occupants, and air exchange rate were determined to define health, IAQ, and thermal comfort.

Zender (2020) analyzed the office building using a DVS to improve IAQ. The object of the research carried out was to determine the efficiency of the wall-integrated ventilation unit for pollution reduction. The DVS works 2 min, 4 min, and 10 min cycles

with supply and exhaust mode in this study. The experimental research was conducted using the tracer gas method to determine the air change rate. As a result, the DVS embedded in the wall sufficiently reduces the concentration of air pollutants. The cyclic air supply and exhaust provide an adequate rate of hourly air change to dilute emissions.

Kozielska et al. (2020) measured indoor air pollutants in a residential building in Poland. The samples were collected outside and inside of the buildings includes kitchens, living rooms, and bedrooms. According to results, CO_2 concentrations increased with many people living in the home and a lower volume of rooms. NO_2 (Nitrogen dioxide) concentrations increased during cooking activities in the kitchen. Results indicated that occupants are particularly exposed to PM_4 (with an aerodynamic diameter $\leq$ of 4 μm) which can be dangerous for their health. Because of poor ventilation, some pollutants concentration levels were high.

Seppänen and Fisk (2001) reviewed ventilation systems and the effect systems had on occupant health and instances of SBS symptoms. Compared to natural ventilation systems, mechanical systems face a higher risk of pollution but have a significantly higher level of temperature, humidity, and ventilation control. In contrast to more simple mechanical ventilation, air-conditioned buildings were found to have the highest rates of SBS symptom levels.

As seen in the literature, controlling the IAQ is important to reduce SBS symptoms. Continuous ventilation of the indoor environment is sufficient to maintain the IAQ below the recommended pollutant limits. However, the air quality perception and ventilation rates are correlated with each other. So, adequate ventilation should be a major focus of design or remediation efforts.

2.1.2. Thermal Comfort

Comfort conditions vary concerning an occupied residence's function, but physiological characteristics such as ventilation, humidity, cooling, and heating are primary qualities in offering comfort standards. Thermal comfort is when a building occupant is content with the ambient conditions within a building. It is subjective and personal, and there is no single condition that can be defined at any time as comfortable for all occupants. In practice, there is a temperature range where most occupants will feel comfortable. Generally, there are many conditions, such as a range of temperature groups,

where the great majority of people will feel acceptably comfortable (CIBSE-TM52 2013). According to Fanger Model (Fanger 1970), thermal comfort, the same comfort conditions, can be applied worldwide. However, personal variables are also important in determining and interpreting perceived thermal comfort conditions. Also, parameters identified as climatic comfort conditions designate the comfort value of any indoor space. These parameters are categorized under two main groups as personal and environmental variables (Fanger 1970).

- Environmental Variables: Air Temperature, Mean Radiant Temperature, Relative Air Velocity, Air Humidity,
- Personal Variables: Activity level, Clothing type, Expectation.

A list of values suggested for indoor spaces is as given below (Özbalta and Çakmanus 2008);

Table 2.1. Environmental Variables according to summer and winter.
(Source: ASHRAE Standard 62.1 2016)

Environmental Variables	Summer	Winter
Air Temperature	23-26°C	20-22°C
Relative Humidity	30%<RH<60%	30%<RH<50%
Air Velocity	0.1-0.2 m/s	0.05-0.1 m/s
Mean Radiant Temperature	20-22°C	16-18°C

Over time, people may adapt to the changes in the conditions, although it depends on the rate of change of adaptation conditions. For example, a sudden hot air may feel uncomfortably warm in April, while similar temperatures can be tolerated on average in July. Similarly, a room may feel extremely hot when entering from the outside first, but it may feel quite comfortable after a while. The consideration of overheating can be defined as aiming to minimize the discomfort rather than aiming for the idealized comfort level (CIBSE-TM52 2013).

Although several factors affect thermal comfort or discomfort, overheating is usually attributed to high temperatures. In addition to these, overheating concerns conditions in which people experience thermal disturbances and cannot be adequately identified by a single measurable temperature value. Temperature increase rate, duration

of high temperature are all important factors (CIBSE-TM52 2013). For example, a very rapid increase in temperature will result in a higher degree of thermal discomfort and thus a more gradual increase in temperature and an overheating sensation.

Thermal comfort also depends on climate conditions. The Köppen-Geiger classification is a simple system that separates only four basic types. This classification is based on the nature of human thermal problems (Szokolay 2012).

As people adjust to changing conditions, the comfort temperature in the non-air-conditioned buildings will change according to the outdoor temperature and person to person. In recent studies, it is considered that due to climate change, a significant change in the outside air temperature may occur in a much shorter period than the monthly intervals, as some of the sudden hot spells have occurred over recent springs and summers. For this reason, comfort temperature is evaluated according to the recent average outdoor temperatures.

"Overheating as the condition when the actual indoor temperature for any given day exceeds the upper limit of the comfort temperature band for that day by enough to make people feel uncomfortable (CIBSE-TM52 2013).*"

If an example is given according to this definition; In a room temperature where the upper limit of the daily average comfort temperature is 26°C, it can be disturbing that the indoor temperature, which is 28°C for most of the day, rises to 30°C in a very short time.

Lai et al. (2018) investigated natural and mechanical ventilation systems in China. This study addressed the effect of thermal comfort on ventilation behavior. They monitored the apartments for a year according to environmental parameters: indoor air temperature, relative humidity, CO_2, $PM_{2.5}$, VOCs in different climate regions. As a result, thermal comfort directly influences ventilation behavior. A mechanical ventilation system causes less thermal discomfort than natural ventilation.

Sassi (2017) studied thermal comfort in super-insulated housing with natural and DVS (decentralized ventilation systems) s in the south of the UK. Eight decentralized and naturally ventilated, highly insulated homes were monitored for one year according to air pollutants and environmental parameters in line with the adaptive thermal comfort model, such as CO_2, CO, NO_2, VOCs, and relative humidity and temperature etc. As a result, centrally mechanical ventilated buildings are not providing personal control of the indoor temperature. And, in decentralized systems, the occupants have the benefit of being able to change their indoor environment to make it comfortable. With these systems, the room-

controlled heating/ cooling sources provide a different thermal zone within an apartment that responds to different users' requests.

Baranova et al. (2017) researched the correlation between energy efficiency and thermal comfort on natural and mechanical ventilation strategies. They compared indoor air overheating and energy consumption which depends on ventilation types. The results show that mechanical ventilation is an effective north-facing room with a 50% window-to-wall ratio.

This information influences thermal comfort by temperature, relative humidity, and perceived air quality (National Research Council 2007). Therefore, for thermal comfort, the operation of buildings systems for heating, ventilation, and air conditioning (HVAC) must consider (Albatayneh et al. 2019).

2.2. International Standards and Local Regulations

IAQ, lighting, acoustics, and thermal comfort are important for mental and physical well-being to create good indoor environmental quality. Although indoor air quality in buildings can be affected by outdoor air pollution, some other factors adversely affect indoor environments and the health of occupants of the building. Many national organizations and international bodies have set new building standards, rules, policies, regulations, and guidelines to provide good indoor environmental quality. These standards provide thermal comfort in indoor environments and ensure that people exposed to these indoor environments are healthy.

2.2.1. Indoor Air Quality Requirements

Poor IAQ is detrimental to health and comfort and can adversely affect office, school, and healing performance in healthcare settings (Albatayneh et al. 2019). There are worldwide recommended concentration guidelines and standards specifically for indoor air pollutants. The research on IAQ was undertaken based on the regulations and standards provided in different countries. Table 2.2 shows the global distribution of deaths from outdoor air pollution, annual CO_2 emissions, and the relative percentage contribution of publications in some countries IAQ field European Union including, Australia, Canada, China, Japan, India, Norway, Singapore, South Korea, Switzerland,

Russia, Turkey, United Kingdom and the United States and their regulations are also included. The table shows the share of annual deaths attributed to outdoor air pollution worldwide. These data show between 1990 and 2017. Most of the deaths due to outdoor air pollution occur in India, Turkey ranked 2. with 36%, China is in 3, with a 30% increase (OurWorldInData 2016). And also, this table has the growth of global emissions from the mid-18th century through 2018. The highest absolute change emissions of CO_2 in 9.84 billion tons in China and followed the United States with 5.27 billion tons of emissions today.

Referring to Turkey's result, there has been a change with 425.18 million tons of CO_2 emissions, of 283% increase. The contribution to literature about IAQ, a search using the keyword "indoor air quality" in the Scopus literature database, resulted in a total of 12.200 publications between 2012 and 2021. (Search executed on 15 January 2021). Looking at the table, the highest contribution was made by the United States 25.09% and China 14.05%, while the United Kingdom, Canada, and South Korea followed with 5.13%, 4.58%, 4.31%. Also, Turkey contributes the publication 0.77%.

Table 2.2. Comparison shares of deaths, outdoor air pollution, Annual CO_2 emissions tons and, Contributions to the total amount of publications on IAQ according to the given countries (Source: OurWorldInData 2016).

Country	Share of deaths from door air pollution (person)			Annual CO₂ emissions tonnes			Contributions to the total amount of publications on IAQ		National/ International bodies involved in setting air quality guidelines and standards
	Start in 1990	End in 2017	Relative Change %	Start in ~1800s	End in 2018	Relative Change %	2012-2021	%	
Austria	5.16	4.31	-16	168,544 t.	68.87 m.t.	40,762	63	0.54	
Australia	4.33	2.86	-34	62,288 t.	417.04 m.t.	669,637	285	2.42	NHMRC
Belgium	6.20	4.65	-25	6.40 m.t.	97.56 m.t.	1,425	124	1.05	AIVC, SHC
Bulgaria	6.52	5.78	-11	0 t.	44.51 m.t.		9	0.08	
Canada	4.13	2.84	-31	3,664 t.	571.14 m.t.	15,587,751	**507**	**4.31**	Health Canada
China	7.59	9.85	30	0 t.	9.84 b.t.	9.84 b.t.	**1652**	**14.05**	AIVC, SQSIQA, SEPA
Croatia	5.26	5.30	<1	5.23 m.t.	18.60 m.t.	255	9	0.08	
Cyprus	7.36	6.55	-11	267,472 t.	7.49 m.t.	2,701	26	0.22	

(cont. on next page)

Table 2.2. (cont.)

Czechia	7.37	5.74	-22	92.87 m.t.	105.95 m.t.	14	95	0.81	
Denmark	5.76	4.43	-23	135,568 t.	34.81 m.t.	25,577	342	2.91	DICL
Estonia	3.01	2.22	-26	32,976 t.	19.56 m.t.	59,213	29	0.25	
Finland	3.72	2.03	-45	36,640 t.	46.99 m.t.	128,145	279	2.37	FISIAQ
France	4.31	3.31	-23	2.24 m.t.	337.91 m.t.	14,994	**478**	**4.07**	ANSES, OQAI
Germany	6.03	4.44	-26	468,992 t.	759.00 m.t.	161,737	**409**	**3.48**	UBA
Greece	6.45	5.84	-9	168,544 t.	73.89 m.t.	43,738	164	1.4	AIVC member
Hungary	4.76	5.17	9	113,584 t.	49.86 m.t.	43,794	50	0.43	
India	4.39	8.26	88	0 t.	2.46 b.t.		346	2.94	NAAQS, ISHRAE
Ireland	5.53	3.59	-35	395,712 t.	38.93 m.t.	9,738	27	0.23	HSE WELs, AIVC
Italy	5.85	4.78	-18	29,312 t.	338.03 m.t.	1,153,103	**476**	**4.05**	
Japan	4.93	3.67	-26	10,992 t.	1.16 b.t.	10,571,053	**405**	**3.45**	MHLW
Latvia	5.39	4.58	-15	10,992 t.	7.19 m.t.	65,317	26	0.22	
Lithuania	6.40	4.90	-23	11.95 m.t.	13.55 m.t.	13	33	0.28	
Luxembourg	5.30	3.85	-27	25,648 t.	9.58 m.t.	37,258	2	0.02	
Malta	6.76	5.46	-19	245,488 t.	1.58 m.t.	545	7	0.06	
Netherlands	6.26	4.49	-28	2.87 m.t.	161.62 m.t.	5,534	209	1.78	NSL
Norway	4.06	2.78	-32	10,992 t.	44.33 m.t.	403,160	80	0.68	NIPH
Poland	6.48	5.71	-12	406,704 t.	343.54 m.t.	84,369	223	1.9	
Portugal	3.59	3.72	4	21,984 t.	50.93 m.t.	231,548	**352**	**2.99**	
Romania	4.69	4.47	-5	0 t.	74.06 m.t.		98	0.83	
Russia	6.65	5.43	-18	852.61 m.t.	1.71 b.t.	101	24	0.2	
Singapore	7.31	6.69	-8	1.73 m.t.	40.58 m.t.	2,246	150	1.28	NEA
Slovakia	7.62	5.74	-25	29.69 m.t.	36.03 m.t.	21	64	0.54	
Slovenia	4.91	4.31	-12	3.98 m.t.	14.43 m.t.	262	26	0.22	
Spain	4.68	4.11	-12	3,664 t.	268.23 m.t.	7,320,692	181	1.54	AIVC member
South Korea	5.77	5.9	2	3,664 t.	640.58 m.t.	17,483,114	**539**	**4.58**	KOC
Sweden	3.70	2.44	-34	32,976 t.	41.03 m.t.	124,314	221	1.88	IVL
Switzerland	5.45	3.60	-34	146,507 t.	36.87m.t.	25,059	103	0.88	
Turkey	**7.43**	**10.12**	**36**	**150,2 t.**	**428.1m.t.**	**284,927**	**91**	**0.77**	AQAMR
United Kingdom	5.85	4.08	-30	9.35 m.t.	379.04 m.t.	3,954	**603**	**5.13**	HSE WELs, AQS, COMEAP
United States	4.93	3.84	-22	0 t.	5.27 b.t.		2949	25.09	ASHRAE, ACGIH, EPA

17

There are many standards for IAQ in the world. National regulations and international standards have been used in some countries. In some countries, air quality guidelines have been developed or suggested as an alternative for national use. Generally, European Community follows the same regulations, such as WHO and EPA. According to WHO indications, this constant and increasing attention to IAQ has shown, over time, a fundamental cultural change to develop and increase sanitation actions (Settimo, Manigrasso and Avino 2020). At the European Community level, the resolution of 13 March 2019 advocates clean air for all (Mitova et al. 2020). It is of great concern to government, regional and worldwide health organizations because of its impact on human health. In this respect, the European community has invited member states to take and implement measures to struggle with air pollution. Also, many countries' national organizations and World Health Organizations (WHO) have stipulated standards and guidelines. These standards and guidelines are applied to limit human exposure to certain breathing air pollutants (Ahmed Abdul–Wahab et al., 2015). International organizations that establish the air quality guides and standards are listed in Table 2.3. The standards and guidelines of the indoor air contaminants are summarized in this table. For the IAQ, WHO and the different organizations globally have suggested different limit values for indoor air pollutants. In IAQ, CO_2 is of great importance and is also used as a proxy ventilation rate (Fisk 2017). IAQ acceptability, air exchange rates, and whether sufficient fresh air is provided to the indoor area in buildings are indicated by CO_2 concentrations (Apte 2000). So, the concentration of CO_2 level in an indoor environment for ASHRAE is no more than 700 ppm (mg/m^3) above outdoor concentration and 600 ppm (high level of comfort), for OSHA 600-1000 ppm (preferred), for EPA 800 ppm (acceptable), for CIBSE 1000 ppm and WHO 1000 ppm (2005).

Table 2.3. The primary IAQ standards and guidelines are stipulated by WHO and some national agencies.

Organization
American Society of Heating, Refrigerating and Air Conditioning Engineer (ASHRAE Standard-55)
Occupational Safety and Health Administration (OSHA)
US Environmental Protection Agency (EPA)
Chartered Institution of Building Services Engineers (CIBSE)
World Health Organization (WHO)

2.2.2. Thermal Comfort Requirements

Providing comfort conditions depends on certain factors that influence the perception and experience of thermal comfort of the occupants. Air temperature, relative humidity, mean radiant temperature, and air velocity parameters affect indoor thermal comfort. Furthermore, these parameters are coupled with two personal factors: the clothing of the occupants (i.e., thermal resistance) and the level of activity (i.e., metabolic rate). Some organizations and institutions are studied on thermal comfort. And they have focused on defining commonly accepted criteria and parameters that have been different international standards. ISO 7730 Standard in Europe, ASHRAE Standard 55 (2010) in the USA, and CIBSE (2013) from the UK have guided the thermal comfort (Table 2.4).

Table 2.4. The primary Thermal Comfort standards and guidelines.

Organization
International Organization for Standardization Ergonomics of the thermal environment (ISO 7730)
American Society of Heating, Refrigerating and Air Conditioning Engineer (ASHRAE-55)
Chartered Institution of Building Services Engineers (CIBSE)

ISO 7730 is a standard that moderate thermal environments and determination of the PMV (Predicted Mean Vote) and PPD (Predicted Percentage of Dissatisfied) -were developed from Fanger in (1970) indices and specification of the conditions for thermal comfort. Iso thermal comfort standards are valid, reliable, and usable data with sufficient practical application. The aim of the ISO 7730 is comfort evaluation in moderate environments. For airspeeds greater than 0.2 m/s, the PMV calculations employ the elevated airspeed method, which calculates and reports the cooling effect of the air movement ASHRAE Standard-55 (2010). PMV is calculated based on four measurable quantities (air velocity, air temperature, mean radiant temperature, and relative humidity) and two expected parameters (clothing and metabolism rate) (Gilani, Khan and Pao 2015). According to these standards, PMV is kept between ranges of ±0.5 for a good standard of comfort. A score that corresponds to the Thermal Sensation Scale is given by the PMV equation (Table 2.5) (Olesen and Parsons 2002).

Table 2.5. The Thermal Sensation Scale of the PMV and PPD index.

Category	Thermal state of the body as a whole	
	PPD (%)	PMV
I	<6	-0.2<PMV<+0.2
II	<10	-0.5<PMV<+0.5
III	<15	-0.7<PMV<+0.7

In this table, these categories of buildings are defined according to occupants' level of expectations. Category I is the high-level expectation, Category II represents the normal level of expectation, and Category III is an acceptable, moderate level of expectation (Grignon-Massé, Adnot, and Rivière 1993).

The ISO 7730 and ASHRAE-55 (2010) include a diagram to estimate the air velocity required to offset any increase in temperature (Fountain and Ares 1993). The operative temperature is a simplified measure of human thermal comfort derived from air temperature, mean radiant temperature, and air velocity. According to the comfort-adaptive approach, the comfort limits for operative temperature are based on an indoor air velocity of 0.2 m/s. And according to ISO 7730, the operative temperature is 24.5°C in the summer and 22°C in the winter. The relationship between air velocity and operating temperature upper limit is shown in Figure 2.2. It has been observed that the increase in operative temperature cannot be above the comfort zone values of 3.0°C, and the rising air velocity should not be greater than 0.8 m/s (Abdeen et al. 2019).
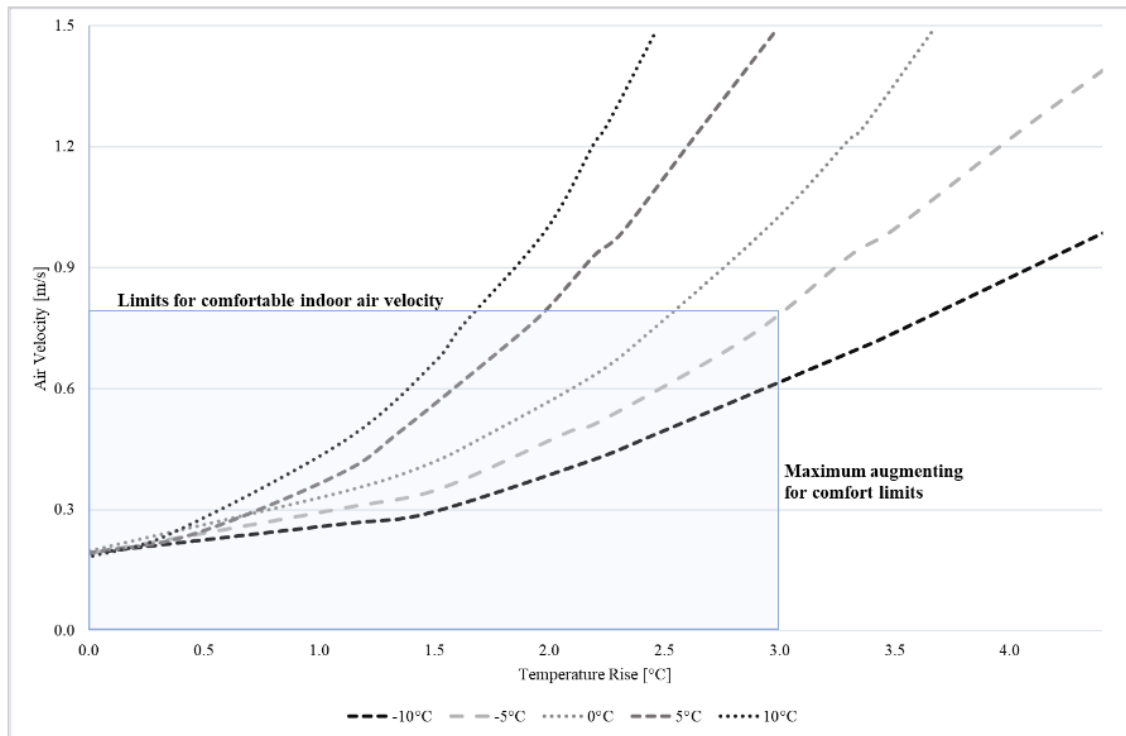
Figure 2.2. Air velocity is required to offset the increase in temperature.
(Source: ASHRAE Standard-55 2010; Olesen and Parsons 2002)

The purpose of ASHRAE Standard-55 (2010) is to determine acceptable thermal environmental conditions for 80% or more of those living in an indoor environment. Here, temperature, thermal radiation, humidity, and air velocity are examined as environmental factors, while personal factors are activity and clothing (Markov 2003).

Figure 2.3. shows the comparison of adaptive thermal comfort standards like equations, envelopes, boundaries, and limits of applicability (Lomas and Giridharan 2012). According to adaptive comfort theory, the ideal indoor operative temperature for occupants who can interact with the building and its equipment is determined by outdoor environmental conditions (Carlucci et al. 2018). The three standards present very similar envelopes of thermal acceptability shown in Figure 2.3. The first is the CIBSE TM36 standard (2005) for climate change and the indoor environment, published by the Chartered Institution Building Services Engineers (CIBSE). This standards' subsequent one is the CIBSE TM52 (2013) points out that the operative temperature of predominantly mechanically ventilated rooms in summer should not exceed 26°C. The other is the CIBSE TM59 (2017), which states that between 10:00 p.m. and 7:00 a.m., the operative temperature in bedrooms should not exceed 26°C. The ANSI/ASHRAE Standard 55

(2010), on the other hand, specifies the acceptable operative temperature ranges for natural conditions. The last one is the European Standard EN 15251 (2007), the maximum indoor temperature for residential mechanically cooled buildings is 26°C (Guo et al. 2020). In this figure, the calculated maximum running mean (T_{rm}) temperatures for the derived typical and extreme years fall in June, July, or August and are, for the Test Reference Year (TRY) and Design Summer Year (DSY) are for 2005 19.5°C and 22.9°C; for the 2030s–21.1°C and 24.4°C; for 2050s–21.5°C and 26.6°C; for 2080s–22.6°C and 28.6°C (Lomas and Giridharan 2012).
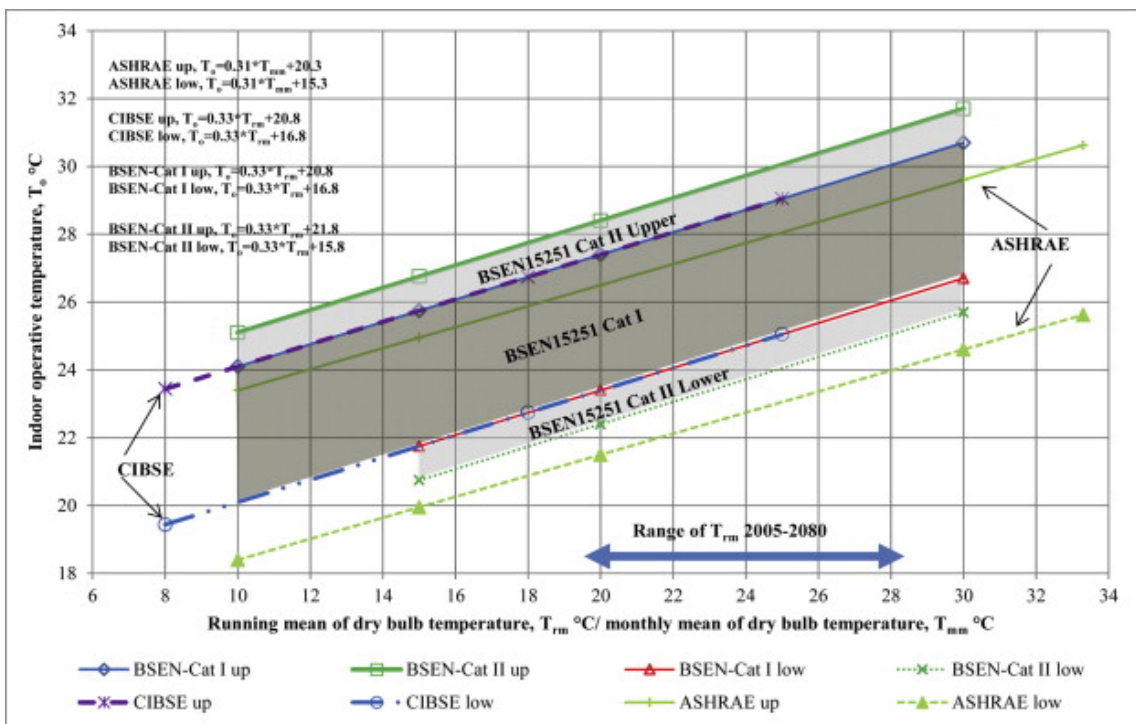
Figure 2.3. Thermal comfort and overheating criteria.
(Source: Lomas and Giridharan 2012)

The ASHRAE 55 standard (2010) defines internal thermal conditions for normal healthy adults. The method is applicable when the occupants are free to adapt their clothes. There are conflicts with the situation of some of the patients here. The method allows an internal operative temperature envelope with upper and lower bounds increasing with average monthly ambient air temperature. The CIBSE Guide provides an envelope acceptable indoor operative temperature, increasing with the daily running mean of the mean ambient air temperature. Also, it is stated that the envelope is related

to normal healthy individuals. The new European Standard BSEN15251 (2007) offers a more holistic approach to other methods. The most important difference is, the standard's scope includes hospitals and methods for a long-term evaluation of the indoor environment, and the envelope width depends on the category of the space under consideration.

2.2.3. Energy Recovery Requirements

In recent years, zero energy buildings, energy efficiency, and sustainability have become the agenda of the building industry worldwide. Most countries have adopted new building standards, codes, policies, regulations, and guidelines (Table 2.6). For instance, the Energy Performance of Buildings Directive (EPBD) (2010) was adopted to improve the energy performance of buildings, emphasizing the development of a common framework for energy savings in the construction sector across Europe. According to this directive, the annual energy balance of buildings is expected to be zero by using low primary energy and producing energy and selling excess energy they produce. Many countries have developed building design standards by setting different guidelines.

Table 2.6. The building energy performance directive, standards, and guidelines from some national/international agencies.

Directives	Country	References
Energy Performance of Building Directive (EPBD)	European Union	(EPBD 2010)
Energy Performance of Building Directive (EPBD)	United Kingdom	(EPBD 2010)
Association for Environment Conscious Building (AECB)	United Kingdom	(AECB 2015)
Building Research Establishment Environmental Assessment Method (Breeam)	United Kingdom	(BREEAM 2015)
Passivhaus	Germany	(Passivhaus 2008)
Leadership in Energy and Environmental Design (LEED)	USA	(LEED 2020)
Basic Energy Plan (BEP)	Japan	(BEP 2011)
Greenhouse and Energy Minimum Standards (GEMS)	Australia	(GEMS 2012)
The Ministry of Housing and Urban-Rural Development (MOHURD)	China	(MOHURD, n.d.)
Building Energy Performance (BEP-TR)	**Turkey**	**(BEP-TR 2008)**

Also, standards have been introduced for residential and non-residential uses, setting minimum standards for energy efficiency of building components, including building envelope, heating, ventilation, HVAC systems. All these policies, standards, and tools will encourage building design and services to use energy-efficient building materials, adopt new technologies, and at the same time ensure that adequate ventilation systems are considered to save energy (Ahmad and Riffat 2020).

2.3. HVAC Systems

Heating, Ventilation, and Air Conditioning (HVAC) systems provide comfortable conditions in homes, offices, and commercial facilities by controlling indoor air throughout the year. When HVAC systems are properly controlled, they make human lives healthier and more efficient. In some countries, residential, institutional, commercial, and industrial buildings have a controlled environment with HVAC systems throughout the year.

The energy used in HVAC systems is a major proportion of the total energy used in Europe (Teke and Timur 2014). The energy usage of a building is related directly to the HVAC system's energy demands. Research shows that air conditioning is responsible for 10% to 60% of overall building energy usage, depending on the building type (Ellis and Mathews 2002). HVAC systems have the largest final energy use in both the residential and non-residential sectors. According to studies conducted in developed countries, HVAC systems are the most energy-consuming devices and constitute approximately 10-20% of energy use (Pérez-Lombard, Ortiz and Pout 2008). In buildings, HVAC systems dominate the total energy consumption. The indoor environment conditioning is the cause of most of the total energy use, but still provides an important possibility for reducing energy use with new technologies. For an efficient HVAC system, all components must work effectively and efficiently. Therefore, decisions regarding the selection and design of HVAC systems are extremely important for overall energy savings (Ali 2013).

2.3.1. Classification of HVAC Systems

HVAC systems are classified as centralized and decentralized systems. These systems centralize the entire building as a whole or condition a specific building area. Table 2.7 compares centralized and decentralized systems according to selection criteria (Seyam 2018).

Table 2.7. Comparison of Centralized and Decentralized Systems.

Criteria	Centralized System	Decentralized System
Temperature, humidity, and space pressure requirements	Fulfilling any or all of the design parameters	Fulfilling any or all of the design parameters
Capacity requirements	-Considering HVAC diversity factors to reduce the installed equipment capacity -Significant first cost and operating cost	-Maximum capacity is required for each piece of equipment -Equipment sizing diversity is limited
Operating cost	-More significant energy-efficient primary equipment -A proposed operating system that saves operating cost	-Less energy efficient primary equipment -Various energy peaks due to occupants' preference -Higher operating cost
Reliability	Central system equipment can be an attractive benefit when considering its long service life	Reliable equipment, although the estimated equipment service life may be less
Flexibility	Selecting standby equipment to provide an alternative source of HVAC or backup	Placed in numerous locations to be more flexible

To regulate the temperature inside the room, centralized or decentralized HVAC systems can choose. However, when choosing the HVAC system, space requirements, capacity, operating cost, reliability, and flexibility are decisive parameters (Table 2.7).

2.3.1.1. Centralized Systems

A central HVAC system can condition one or more indoor environments, and its main equipment is located in a convenient central location outside the service area, inside,

on top, or adjacent to the building (ASHRAE Standard-55 2010). Indoor environment mediums with their equal thermal load must be conditioned by centralized systems. As seen in Figure 2.4, the zones used in the control system to provide thermal energy sub-classify the central HVAC system (Seyam 2018).
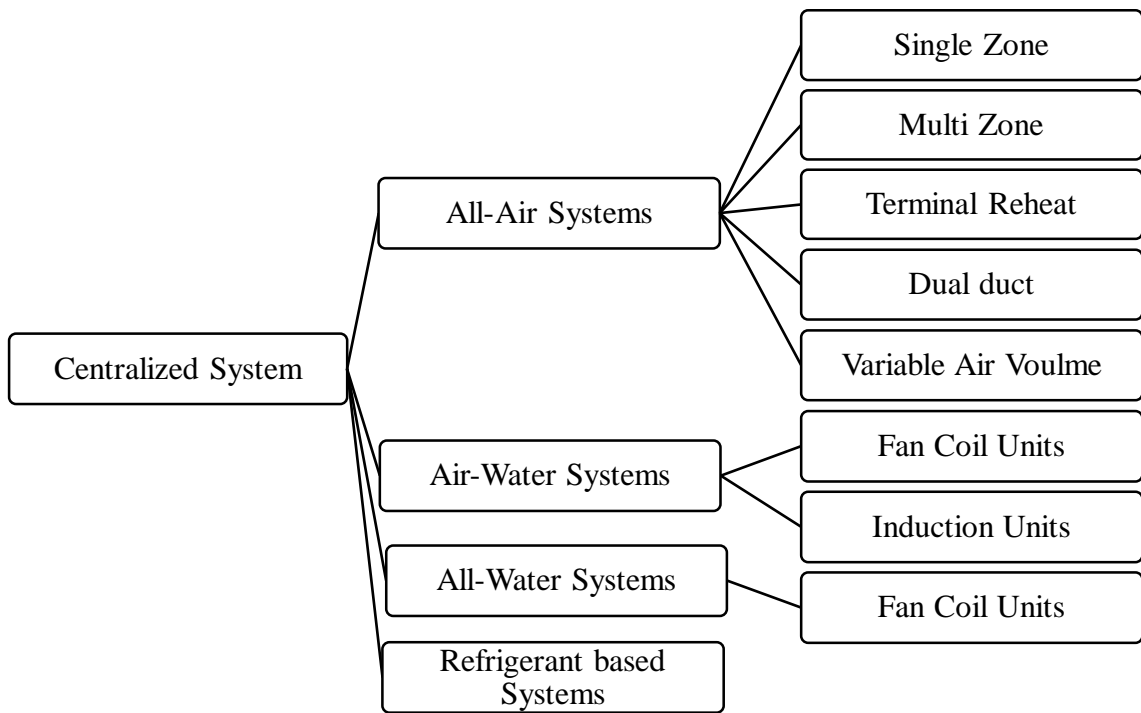
Figure 2.4. Classification of Centralized Systems.
(Source: Seyam 2018)

2.3.1.1.1. All-air Systems

HVAC equipment is centrally located. All air systems are cooled by sending the cooled and dehumidified air to the conditioned room, and heating is done by sending the heated air to the conditioned room. All air systems can filter air and provide fresh air (Figure 2.5).
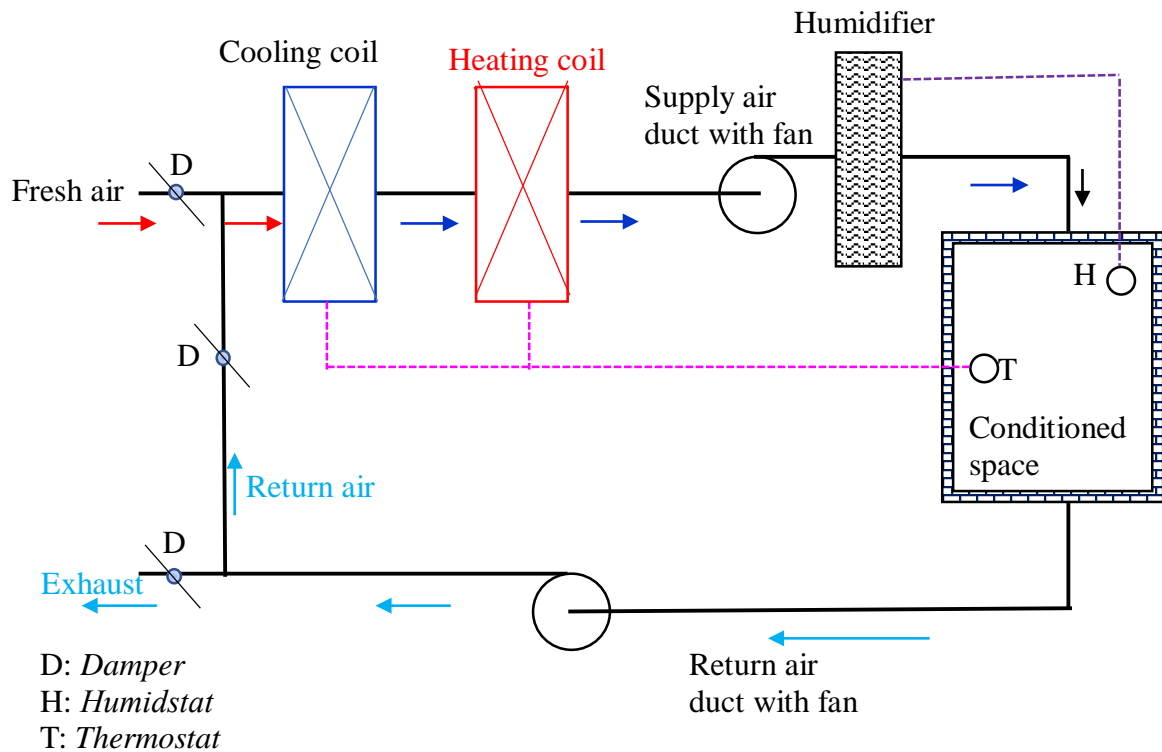
Figure 2.5. Schematic diagram of all air systems.
(Source: Seyam 2018; Goetzler et al. 2016)

The all-air systems have some advantages and disadvantages. It usually includes the cheapest equipment, but due to the size of ducting required and the cost of installation, it is not always easy or cheap to install in a building. It can be difficult to maintain proper temperature control, and the system may be inefficient. These systems can be adapted to all air conditioning systems for comfort. And it is applied in schools, hospitals, laboratories, hotels, etc., which require individual control of room conditions. The essential distinctiveness is to supply fresh air. AHU always supplies adequate fresh air to maintain IAQ. Here, the return air is balanced in proportion by the rule Supply Air = Return Air + Fresh Air.

2.3.1.1.2. All-water Air Conditioning Systems

These systems are completely water systems (Figure 2.6). Hot water and cold water prepared in one center are sent to fan-coil devices distributed in the building. Hot water is supplied by a hot water boiler, while cold water is produced in the cooling (chiller) group. Fan-Coil devices are devices containing a fan and coil. Heated or cooled

air is taken from the room with the help of the fan and passed over the serpentines, and is given to the room again. If cold water passes through the coil, cooling takes place, and if hot water passes, heating takes place. The pump is used for water circulation. These systems are usually hotels, hospitals, and offices. Fan-Coil units are usually placed in front of windows or suspended ceilings (Seyam 2018; Yılmaz 1997; Zhang Wright and Hanby 2006)

PRV: *Pressure Reducing Valve*
FCV: *Flow control valves*
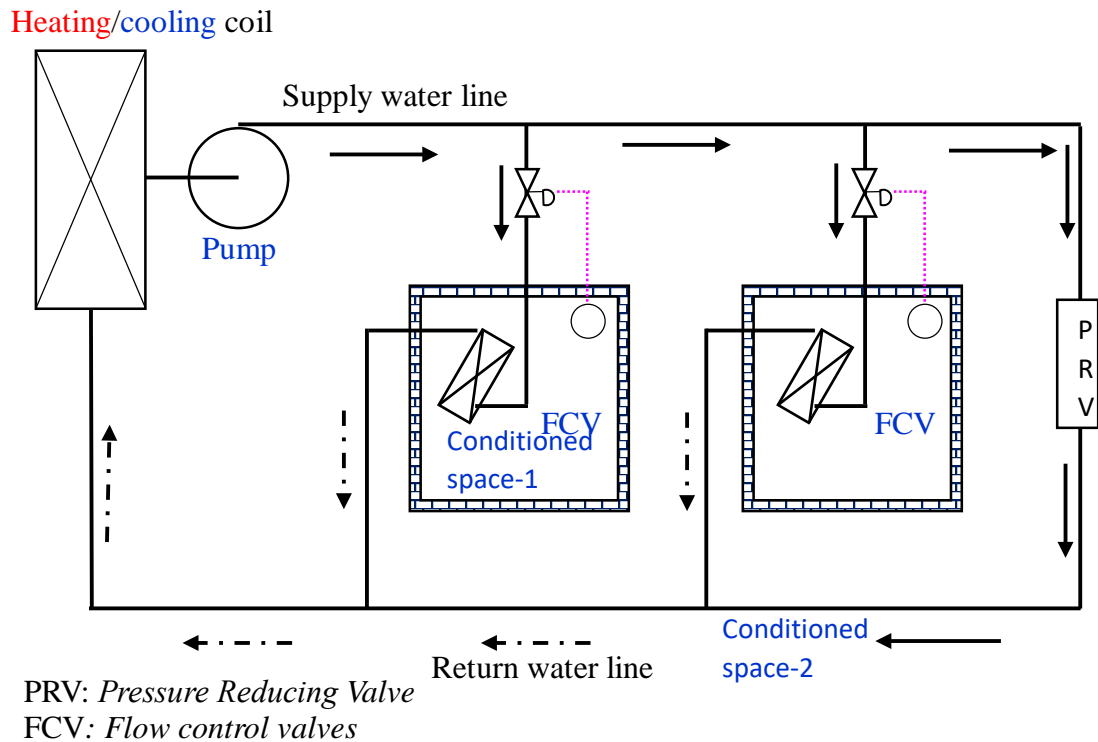
Figure 2.6. Schematic diagram of all water systems.
(Source: Seyam 2018; Goetzler et al. 2016)

2.3.1.1.3. Hybrid (Air-Water) Air Handling Units

There is no ventilation in conventional fan-coil systems in these systems (Figure 2.7). Only heating and cooling are done. In these fan-coil systems, fresh air deficiency is eliminated by applying different applications. One of the applications; each of the fan-coil units is supplied with fresh air from the outside via its duct connection. And the fresh air with heat recovery and pre-conditioning, the quantity determined by the automation system, is provided with the central air conditioning system (Seyam 2018; Yılmaz 1997; Zhang Wright and Hanby 2006).
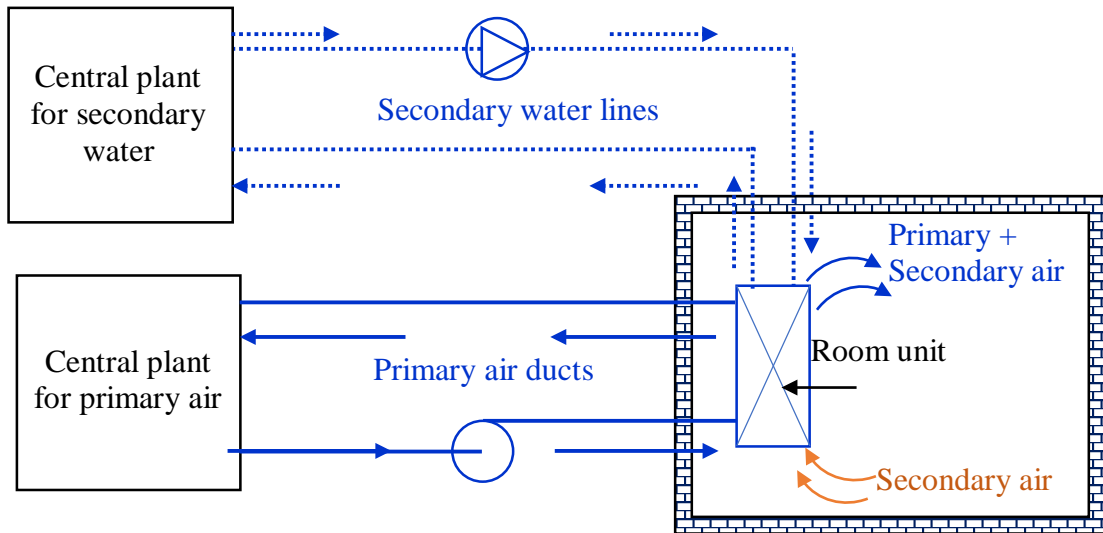
Figure 2.7. Schematic diagram of air-water systems.
(Source: Seyam 2018; Goetzler et al. 2016)

With this system, much space is saved, and heating and cooling are possible. As air-water systems require relatively low air flow rates, the cross-sectional areas of the required air supply and extract ducts are reduced considerably. The air supply is generally constant volume and provides outside clean air for ventilation.

2.3.1.1.4. Refrigerant-based Systems

All air conditioning systems are designed to offer thermal comfort to building occupants. A broad range of air conditioning systems are available, from basic window-fitted units to small-split systems, medium-scale package units, large-chilled water systems, and, most recently, variable refrigerant flow (VRF) systems. These systems use refrigerants to create cool air compared to a typical HVAC system that uses water to cool air. VRF systems come from a central heat exchanger-compressor unit and associated internal units. With its advanced automation features, many interior units can be operated in different comfort conditions for summer and work as heat pumps in winter to meet their heating needs. Each interior unit of the energy recovery type systems can independently operate in heating or cooling mode in the same season (Seyam 2018; Goetzler et al. 2016). There is a heat recovery system that can be installed for that purpose.

Besides these types of Air Conditioning Systems, The Air Handling Units are the devices that can perform the air conditioning processes such as ventilation, heating,

cooling, humidification, dehumidification, filtering, and heat recovery under the control of automation (Küçüka 2005).
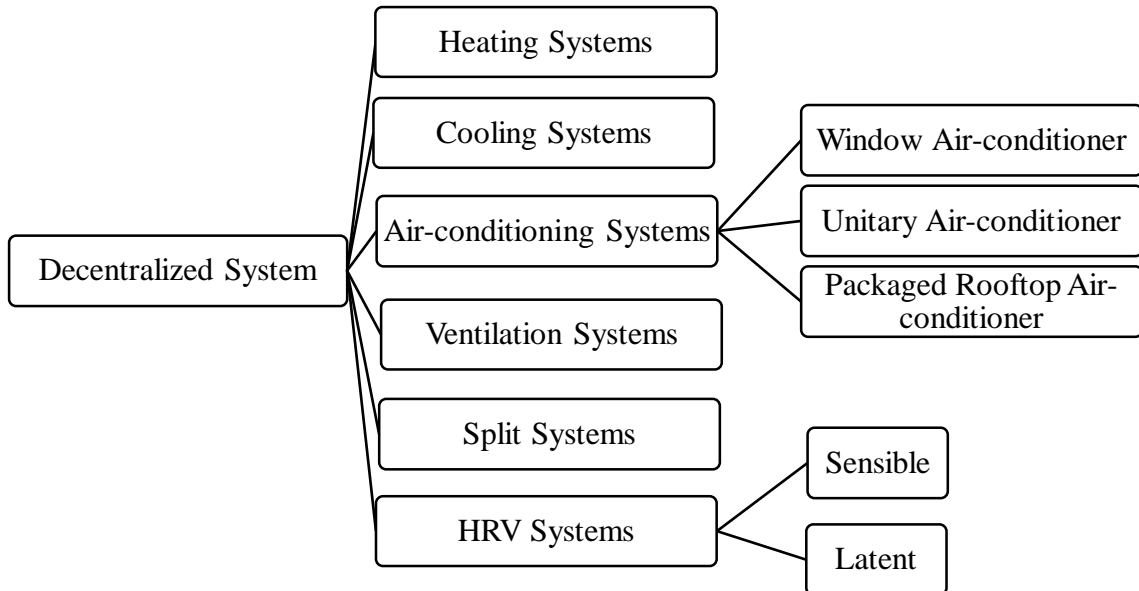
Figure 2.8. Decentralized HVAC System types.
(Source: Seyam 2018)

2.3.1.2. Decentralized Systems

It is applied for small projects without a central plant with low initial cost and simplified installation. These systems are also installed in office buildings, shopping malls, schools, health facilities, hotels, apartments, research labs, computer rooms, and other multi-person residences (ASHRAE Standard-55 2010). Decentralized systems are connected to a refrigeration cycle, heating source and one or more individual HVAC units with direct or indirect outdoor air ventilation Components of these units consist of a package containing fans, filters, heating source, cooling coil, refrigerant compressor (s), controls, and condenser (ASHRAE Standard-55 2010). There are many decentralized systems, as represented in Figure 2.8 (Seyam 2018).

2.3.1.3. Decentralized Ventilation and Centralized Ventilation Systems

Choosing the best system is essential for practical reasons and ensuring the people's comfort in the building. Choosing a centralized and decentralized system is the main issue in selecting air conditioning systems for buildings. Higher energy efficiency and improved load-management capabilities are two major advantages of centralized air conditioning systems. It's also less difficult to maintain. On the other hand, a decentralized air conditioning system offers lower initial costs. It has minimum installation and space requirements. Also, the most essential distinction is that decentralized systems have separate zone controls allowing users to change the IAQ easily.

In this section, DVS, according to different climatic conditions, are compared with centralized systems, and as a result, it has been determined that DVSs can cause lower pressure losses, and these systems provide much more energy savings. These articles have been examined experimentally and numerically (Merzkirch et al. 2016; Mikola, Simson and Kurnitski 2019; Zemitis et al. 2016; Baldini, Kim and Leibundgut 2014; Mahler and Himmler 2008) and numerically (Bonato, D'Antoni and Fedrizzi 2020; Carbonare et al. 2019; Manz et al. 2000) according to different climatic conditions (Bonato, D'Antoni and Fedrizzi 2020; Zemitis et al. 2016) or building usage types offices (Carbonare et al. 2019; Mahler and Himmler 2008) and residential building (Murgul et al. 2014; Berkel et al. 2014).

Merzkirch et al. (2016) compared CVS and DVS and presented the findings of a comprehensive field study on ventilation systems in residential buildings. They examined 20 CVS and 60 DVS in Luxembourg, and they discussed differential pressure, specific fan power, and heat recovery efficiency. As a result, the heat recovery efficiency of DVS is determined to be higher than CVS.

Mikola, Simson, and Kurnitski (2019) simulated pressure differences using field measurements and IDA-ICE software to evaluate the performance of DVS units and analyze pressure differences in a multi-story building in Estonia. The laboratory measured the recuperative and regenerative performances of two types of ventilation units, and their indoor air changes were evaluated with simulations. Thus, by using wall integrated units, correct design recommendations can be given by determining the pressure differences to provide a satisfactory thermal comfort and heat recovery.

Bonato, D'Antoni, and Fedrizzi (2020) examine the performance of the DVS unit integrated into the facade and its potential to reduce HVAC energy consumption in office spaces located on the perimeter of the building. Numerical simulations with TRNSYS software were analyzed according to the climatic conditions of three European countries. As a result, based on the analyzed climate and building, it has been concluded that DVS can effectively reduce energy consumption and save 65% electricity compared to CVS, while cooling demand can be reduced by 35% -70%.

Carbonare et al.'s (2019) study is simulation-based research examining DVSs. A demand-controlled ventilation scheme was studied with a co-simulation method, using EnergyPlus and Modelica programs, and a mathematical approach to user comfort (i.e. quadratic for relative humidity and exponential for CO_2). As a result, while thermal comfort has increased, 10% energy saving has been achieved.

Zemitis et al. (2016) evaluated ventilation solutions for nZEB (near-zero energy buildings) multi-story buildings in three European geographic clusters. The concept of geographic cluster indicates transnational areas with strong similarities in climate, culture, construction typologies, and other factors. Studies have been conducted for Denmark, Estonia, Latvia, and Portugal, and technical and economic comparison of ventilation systems for nZEB buildings in these countries has been made. Within the scope of the H2020 project, it has been concluded that heat recovery mechanical supply and exhaust ventilation units are economically efficient.

Baldini, Kim, and Leibundgut (2014) examined the performance of DVS for hot and humid climates such as Singapore. DVSs, which have great potential to reduce pressure losses, can reduce exergy loss and energy savings with radiant cooling. A modified design of a DVS unit including a 3-stage heat exchanger is examined in detail in this study.

Murgül et al. (2014) conducted a study on DVS, which are applied especially in residential buildings. It has been shown that an effective way to reduce energy losses due to heating and ventilation in residences can be achieved by applying DVS with heat recovery units to achieve thermal balance.

Berkel et al.'s (2014) article review the existing residential ventilation by focusing on three main areas. These; distribution systems, ventilation control, and energy recovery technology. Wall-integrated heat recovery ventilation systems, which are a new concept especially for DVS, were also mentioned, and potential applications for residential ventilation were evaluated.

In the experimental study of Mahler and Himmler (2008), DVSs were evaluated for office buildings, and the long-term results were obtained; air temperature and humidity measurements, airflow measurements, noise emission, and user surveys are also included in this study.

Manz et al. (2000) investigated the effect of air leaks on the performance of DVS units with heat recovery. According to the numerical study, it has been observed that air leaks can significantly reduce the performance of ventilation units in terms of ventilation efficiency, and as a result, it is seen that energy savings are achieved with these systems.

2.3.2. Ventilation

Today, in many countries, the ventilation of buildings is a challenge. In COVID-19, the importance of good IAQ is once more emphasized (Afshari 2020). It can control ventilation, air temperature, relative humidity, and pollutant concentrations. A ventilation system must be sized adequately to meet the welfare needs of the owners. For this reason, ventilation and well-being are closely linked to each other. Modern technologies enable us to build more heat-insulated buildings with airtight casing effectively. However, the buildings become unlivable when there is no proper ventilation system due to the low IAQ. With the increased atmospheric pollution in our cities, opening only the window does not provide a good solution. Because there is no control over the concentration of pollutants in the room by the amount of renewed air by natural ventilation, for this reason, ventilation systems are often the most appropriate solution. Natural ventilation of buildings is achieved by creating openings in the building's exterior: chimneys, windows, and openings in the roof, atriums, and ventilation towers, etc. In old buildings, low U value windows provide renewal of the inside air, while new buildings are known to have much more restricted airflow due to the more efficient windows used to reduce thermal losses. Natural ventilation has many disadvantages (Gheorghe and Ion 2011):

- The amount of regenerated air cannot be controlled,
- Energy losses in cold seasons,
- The weather is very hot in summer and very cold in winter,
- There is more noise in the room due to opened windows,
- No control of the quality of the air taken in (pollution),
- Regional high air velocity

Therefore, mechanical systems are becoming widespread to provide adequate indoor air requirements. To provide good airflow control - which lacks natural ventilation - a mechanical air handling system can be designed to ensure proper ventilation. In such systems, the airflow is provided by one or more fans, ducted or not. Systems without ducts consist of one or more fans on the walls or ceiling. The simplest solution is to use one or more extraction fans and several openings to allow fresh air to enter the room. This solution is common in industrial environments. In residential and commercial environments, duct systems are preferred, the fans can be placed in a remote location, which removes noise from the room. Mechanical ventilation systems have the following advantages (Mardiana-Idayu and Riffat 2011):

- Controlled air flows,
- Controlled air streams,
- No external noise and limited running noise,
- Controlled air quality,
- Reduced thermal losses,
- Optional energy recovery using heat exchangers.

With a better understanding of indoor pollutants, new and effective measures have been developed, including the development of indoor air filters (Sublett 2011). Air filtration is often proposed as a component of environmental control measures. However, while HVAC systems offer an opportunity for all indoor filtration, poorly maintained or contaminated systems can increase the risk of asthma and other allergic symptoms. These filters grouped under "air conditioning" or HVAC are the primary means of improving IAQ. As a major element in air conditioning systems, the air filter plays a significant purpose. The addition of a proper air filter to an air conditioner is a perfect solution for removing 98% of airborne contaminants (Elsaid and Ahmed 2021). It is now believed that "sick building syndrome" is a possible air conditioning problem that can be improved with better filtration (Sutherland 2008). Different filtration systems remove airborne particles from supply air systems and enclosed spaces. Filter panels are placed in front of blower fans in HVAC systems and ventilation units (AHU) in heating and cooling systems. According to Elsaid and Ahmed (2021), appropriate ventilation, good air filtration technologies, humidity adjustment, and temperature control enhance the indoor air quality for airborne infectious illnesses, including COVID-19.

HEPA air filters in air conditioners should be replaced with nanofibrous air filters or enhanced electrostatic air filters, according to the findings of this study. These panes may include glass, cellulose, or polymeric fibers ranging in diameter from 1 to 100 μm. Filter mats vary in density and depth, with pores ranging from 70 to 99%. Due to differences in fiber diameters and mat densities, the filters differ in their ability to capture airborne particles (Godish and Fu 2019). Filters designed for the treatment of air fall broadly into three categories (Table 2.8) (Sutherland 2008).

Table 2.8. Filter Types.
(Source: Godish and Fu 2019, El Fouih et al. 2012)

Filter Categories	Efficiency	Size	Air Velocity Features	Materials
Dry-type panel filters	High porosities and low dust spot efficiencies.	Collect large particles (5-10 microns in size)	Capable of working with relatively high airflow velocities	Fiberglass, open-cell foams, nonwoven textile cloths, and cellulose fibers.
Extended-surface dry-type filters	Finer media for trapping and retaining finer particles.	Collect smaller particles (0.5-5 microns in size)	Air velocities are generally low, of the order of 0.12 m/s or less.	Cellulose, glass fiber, wool felt.
Viscous-media panel filters	Ultra-fine or final stage filters yield very high efficiencies.	Collect sub-micrometer particles (99.95% or better).	Air velocity, in this case, is limited to about 0.03 m/s.	Different fabrics of synthetic fibers.

Indoor air pollution is among the top five environmental health risks (EPA 2018). The best way to address this risk is to control or eliminate the sources of pollutants and ventilate an indoor with clean outdoor air. However, the indoor air should be limited by weather conditions or undesirable contaminants in outdoor air with natural ventilation. Also, these methods are insufficient, so a mechanical system is useful for the indoor environment.

2.3.3. Heat Recovery System Solutions

The heat recovery ventilation (HRV) principle is to recover the heat from the exhaust air and transfer it via a heat exchanger into the supply air. With the increasing

share of ventilation, heating/cooling loads, heat recovery through mechanical ventilation systems reduces heat losses and saves energy (El Fouih et al. 2012).

Heat recovery systems are necessary for designing air conditioning systems with minimum energy consumption (Yılmaz 1997). These systems are divided into two main groups: Recuperative and Regenerative systems.

2.3.3.1. Recuperative Systems

Plate Heat Recovery the conditioned air is passed through a heat exchanger so that the fresh air is not mixed with the heat exchanger.

2.3.3.2. Regenerative Systems

Run Around Heat Recovery conditioned return air and fresh air through two separate heat exchangers with water inside to provide heat recovery.

Heat Pipe Heat Recovery is a type of heat recovery by utilizes the principle of evaporation and condensation of the refrigerant in a single two-part heat exchanger placed in the conditioned air and fresh air.

Rotary Drum Heat Recovery with the help of a rotary type of heat exchanger, heat recovery between fresh air and indoor air with temperature and humidity difference is performed (Yılmaz 1997).

In this context, all central air systems can be used in shopping malls, concert halls, etc., where many people are together, even though the initial investment cost is high and much space is occupied. On the other hand, in the case of all water air conditioning systems, the fresh air requirement can be met using heat recovery systems. Thus, heat recovery systems are more useful than all-air systems, with low initial investment cost, with efficient use in terms of IAQ and user comfort.

Many studies in the literature about ventilation systems, especially heat recovery systems. In residential buildings, ventilation losses, in general, can be 35-40 kWh/m²-year, and up to 90% of this can be recovered with HRV, depending on the buildings' airtightness and insulation (Tommerup and Svendsen 2006). Many studies have searched the effect of HRV on the energy use of buildings. Heat recovery ventilation systems ensure the efficient use of energy due to transferring the heat from exhaust air to the fresh

air supplied indoors (Cuce and Riffat 2015). These systems typically recover approximately 60% to 95% of the energy in the exhaust air and significantly improve the energy performance of buildings (Mardiana-Idayu and Riffat 2011). Although there are several studies on heat recovery systems, there are still shortcomings in the research and development of the use of recovery systems in building applications (Zeng, Liu and Shukla 2017; Van Berkel, Pressnail and Touchie 2014)

However, CVS requires large volume requirements within the space (Etheridge and Sandberg 1996). According to building typologies, many studies examine the performance and energy consumption reduction potential of the DVS unit integrated into the facade in office spaces (Mahler and Himmler 2008) and articles containing experimental and field study results on existing residential ventilation systems. Wouters, Barles and Blomsterberg 2001; Hekmat, Feustel and Modera 1986; Jokisalo et al. 2003). In several studies, wall integrated HRV systems, which are a new concept especially for DVS, was also mentioned, and potential applications for residential ventilation were evaluated (Merzkirch et al. 2016; Mikola, Simson and Kurnitski 2019; Van Berkel, Pressnail and Touchie 2014).

2.3.4. Review of Heat Recovery Systems

Some mechanical systems store latent heat in heat recovery ventilation and the studies that store sensible heat. The following publications are comprehensive reviews of heat exchangers, air conditioners, and solutions for building envelopes with latent heat storage and include experimental studies:

Xu Riffat and Zhang (2019) offer current developments in four heat recovery systems for residential applications. The systems are categorized as recuperative and regenerative. While recuperative systems are fixed plate and heat pipe, regenerative systems are run around and rotary drum types. The emphasis of this study is on pressure, air leakage, economic analysis, and combining heat pipe systems with other sustainable technologies. Consequently, the results show that the integration of regenerative heat recovery can achieve heat recovery ranging from 64.6% to 70%.

Balci, Ezan, and Turhan (2019) propose a new heat exchanger with PCM to recover waste heat from the flue gas of a boiler. The thermal energy recovered from the flue gas is stored in the heat exchanger for later use while the combi operates in central

heating mode. They also developed a mathematical model to examine the behavior of the PCM in detail. As a result, PCM increases the water temperature, and with the use of PCM, the efficiency of the boiler increases while energy consumption decreases.

Asker et al. (2018) integrate PCM on a wall to increase the energy efficiency of a building and examine the thermal behavior of this wall. They developed a time-dependent one-dimensional heat transfer model using ANSYS-Fluent software. They compared four different walls and found that a 1 cm PCM application was insufficient to keep the indoor and outdoor temperature at the desired temperature range. Yet, the heat transfer was significantly reduced by applying 2 cm PCM. Thus, the use of PCM in the building envelope is an option to reduce the energy consumption for air conditioning.

Alizadeh and Sadrameli (2016) focus on and review free cooling in residential and commercial buildings. They highlight the advantages and disadvantages of cooling systems. They study the cooling, technical, geographical, and economic differences and performance evaluation criteria and application of PCMs.

Soares et al. (2013) examine how and where PCMs are used in latent heat thermal energy storage (LHTES) systems. Besides, they explore the relationship between buildings solutions and their energy performance. They also investigated the integration of PCM into structural elements, methods to measure thermal properties, numerical modeling, and latent heat storage system containing PCM.

2.4. Thermal Energy Storage Using in Buildings

Thermal energy storage technologies have been commonly used during the past decades. Different type of thermal energy systems has been developed to facilitate the use of thermal energy in different needed scales. Storing energy and using it in-demand times is crucial in building energy efficiency. The stored energy, whether cold or heat, can reduce cooling or heating loads and reduce the temperature fluctuations in interior spaces (Konstantinidou 2010). External surfaces of the building are the link between the building as a thermodynamic organization, and external thermal loads include outdoor different climatic conditions, primarily temperature, wind, and solar radiation. And we can control the effect of outdoor conditions on indoor spaces by improving envelope thermal properties as a function of the capacity of the envelope and the building structures to store heat. Thermal energy storage in buildings mainly occurs through a change in the

internal energy of a material as sensible heat or latent heat or a combination of both. A diagrammatic overview of major techniques for thermal energy storage using solar radiation as the most potential infinite source of energy is shown in Fig. 2.9 (Malekzadeh 2015).
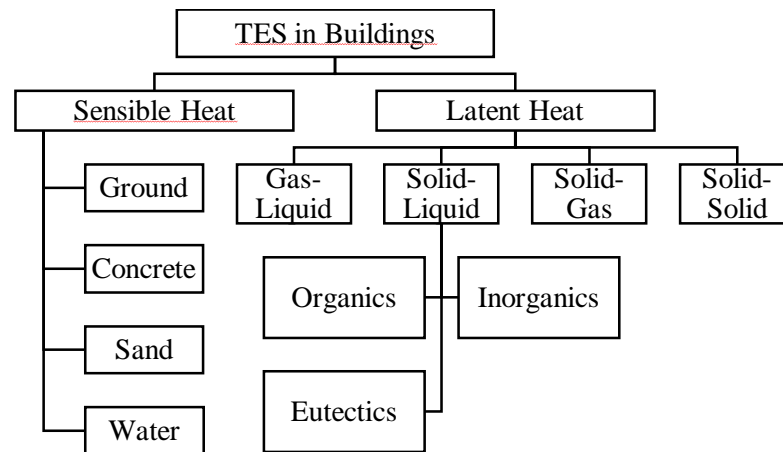
Figure 2.9. Different Types of Thermal Energy Storage.
(Source: Konstantinidou 2010)

2.4.1. Sensible Heat Storage

In the type of sensible heat storage, thermal energy is absorbed and stored with an increase in the temperature of solid or liquid material, in which the standard building materials such as bricks and concrete are used on the exterior/interior walls, on the floor. The heat capacity of the SHS materials is dependent on the specific heat, the temperature variations, and the amount of storage material, and as a result, the storage process is followed by an increase in the material temperature during the process (Lane 2018). Large-scale thermal energy storage is widely accepted as sensible heat. The choice of environment is usually dependent on the heat capacity of the environment, the range of temperatures that the store will operate, and the space available for it (Figure 2.10). Figure 2.10 shows the materials' specific heat, density, and thermal conductivity graphs, which are the main thermal properties of sensible heat storage materials. In particular, many studies use the sensible heat storage calculation method for the thermal insulation properties of walls (Pekdogan and Basaran 2017; Pekdogan 2015).
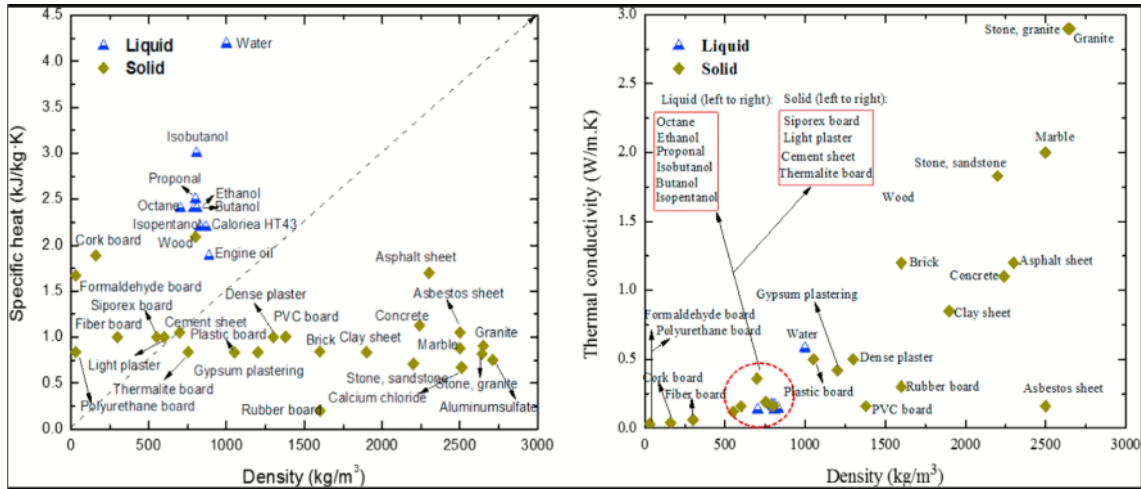
Figure 2.10. Heat storage as sensible heat leads to a temperature increase when the heat is stored (Source: Li 2016).

The heat capacity is given by the amount of material, volume, or mass. It is then called molar, volumetric, or mass-specific heat capacity. The specific heats of incompressible substances depend on temperature only. Therefore, the change in the internal energy of solids and liquids can be expressed as;

$$Q_d = m \cdot c_{avg} \cdot \Delta T \qquad \text{Eq. (2.1)}$$

As shown in Equation 2.1. The ratio of stored heat Q_d to the temperature rise ΔT, m is the system's mass, and c_{avg} is the average specific heat evaluated at the average temperature. To be effective as a thermal mass, we need materials with high heat capacity, moderate heat conductivity, medium density, and high emissivity (Çengel 2018).

2.4.2. Latent Heat Storage

Latent heat is the heat released or absorbed by a body or a thermodynamic system during a constant temperature process. The phase transition period is when the temperature of the system remains constant despite the system's absorption (or release) of heat. Latent heat storage can be obtained by solid-solid, solid-liquid, solid-gas, and liquid-gas phase changes (Shukla 2015). The material used to store the latent heat absorbed by the material during the phase change is called the "Phase Change Material"

(Konstantinidou 2010; Abhat 1983). LHTES material has substantially higher thermal energy absorption and spreading capacity than SHTES materials.

For this reason, by incorporating the LHTES system in a small amount, more heat storage systems are obtained instead of SHTES in the buildings. When a larger volume container is considered to create sufficient space for the phase change process, it results in melting and solidifying the storage material at a constant temperature. When the storage material absorbs heat during the melting process, the material temperature remains constant at the melting temperature, also referred to as the phase change temperature.

Figure 2.11 shows the relationship between the volumetric latent heat density and the market's melting temperature of commercially available PCMs. Sensible heat storage in water at different temperatures for heating and cooling is shown as a reference (yellow line). The volumetric latent heat density of commercially available inorganic materials in the area shaded in blue in Figure 2.11 ranges from 150 to 430 MJ/m^3. On the other hand, the red-colored area represents organic materials. These materials' volumetric latent heat capacity belongs to a lower range between 100 and 250 MJ/m^3. The water that can be used as a reference has a capacity ranging from 63 to 250 MJ/m^3 for sensible heat storage, cooling, and heating, respectively.
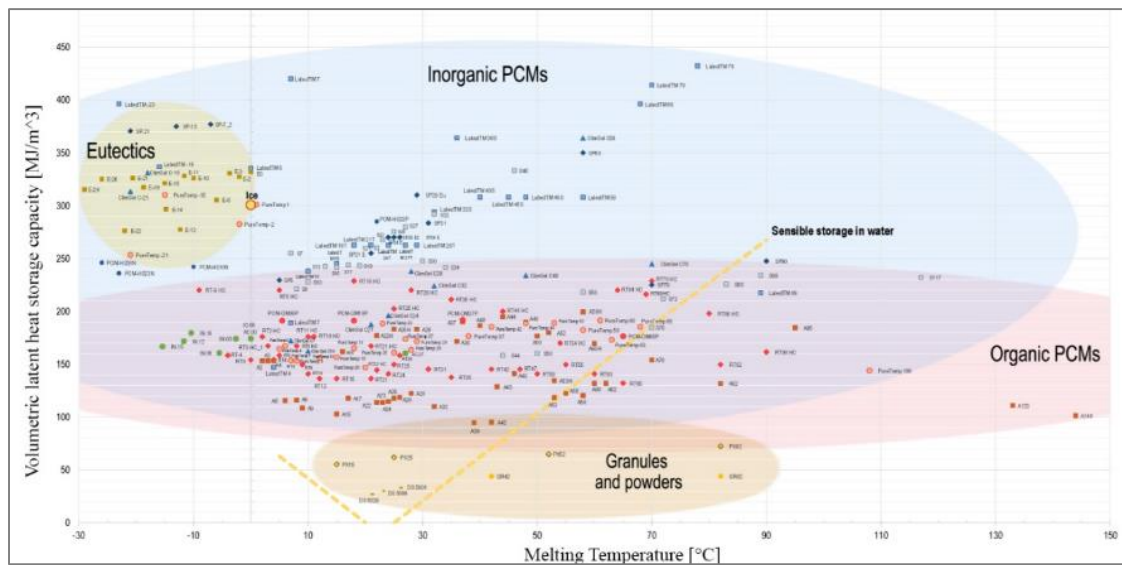
Figure 2.11. Commercially available PCMs and water volumetric heat storage capacity. (Source: Vakhshouri 2020)

Phase transformation happens when the temperature of the storage medium reaches the phase change temperature, as opposed to sensible heat storage. Until the storage medium absorbs a certain amount of thermal energy, its temperature remains at the phase change temperature. When the internal energy of the medium is increased by the value of the latent heat of fusion, the medium achieves a complete phase change (Dincer and Ezan 2018). It appears that the thermal energy absorbed or released by the unit phase change per mass is much higher than the energy stored by increasing the temperature. (Equation 2.2).

$$Q_g = m_{PCM} \, x \Delta h$$ Eq. (2.2)

As a result, latent heat is calculated from the enthalpy difference (*Δh*) between the material phases. In the case of solid-liquid phase change, it is called solid-liquid phase-change enthalpy, melting enthalpy, or heat of fusion (Çengel 2018).

2.4.2.1. Potential of Using Latent Heat Storage with Solid-Liquid Phase Change

First, the heat absorbance by these solid-liquid PCMs is similar to that of conventional SHS materials, increasing their temperature at their heat absorption. However, PCMs absorb and release thermal energy at a nearly constant temperature. Although the volume of the heat storage is small, the sensibility is higher than the heat storage capacity. The thermal storage capacities of the unit masses of these materials, called PCM, are quite high. They can store 5 to 14 times more heat per unit volume than SHS materials such as water, concrete, and rock (Abhat 1983; Buddhi and Sawhney 1994). For this reason, it can be said that latent heat storage is more advantageous than other energy storage techniques.

2.4.3. Sensible and Latent Energy Storage HRV Systems

In addition to these studies aimed at analyzing and solving problems related to fluid behavior by using algorithms such as CFD analysis through computer simulations, empirical analysis and important studies on CVSs and DVSs are also available in the

literature. The articles summarized below generally include sensible and latent energy storage heat exchangers as well as CFD analysis.

Zeng et al. (2017) review the recent development of air-to-air heat and mass recovery technologies. Extensive research was conducted on passive systems, mechanical ventilation systems, defrosting methods, dehumidification systems, and heat and mass exchangers integrated into the energy-efficient systems of buildings. The applications, advantages, disadvantages, and basic performance criteria of each system are detailed. As a result of this study, it was stated that the use of heat exchangers caused insufficient airflow. Also, heat and mass exchanger solutions can cause air losses and leaks in mechanical ventilation systems. Finally, there is an overheating problem during dehumidification in heat and mass exchangers.

Kim and Baldini (2016) compiled extensive research on energy analysis in a DVS compared CVS in European climatic conditions. As a result, DVSs cause lower pressure losses. The fan speed and airflow rate can be adjusted simply and effectively depending on indoor climate and thermal conditions. A radiant panel with a DVS was found to have the lowest energy consumption for heating, ventilation, and air conditioning.

In Cuce and Rıffat's (2015) study, information is given about applications related to the development of heat recovery systems. In general, terms describe heat recovery systems, their working principles, system components, and the typical heat recovery technologies, including building applications with theoretical, experimental, and simulation studies. In addition, the environmental impacts of heat recovery systems are also evaluated. According to this study, the highest efficiency is seen in rotary drum heat recovery systems. Besides, the results obtained from the literature show that heat recovery systems have the potential to reduce the energy demand of buildings and, therefore, greenhouse gas emissions in the atmosphere.

Culha et al. (2015) examine heat exchangers in wastewater source heat pump applications, classify wastewater heat exchangers in detail based on many features, including their utilization and construction methodology. According to these studies, they concluded that the prevention of biological contamination is an important area to be considered and that in most commercial applications, custom-designed shell and tube heat exchangers are used.

Russell and Sherman (2007) explore existing and potential ventilation technologies following the ASHRAE 62.2 Standard for residential buildings in the North American climate. Various mechanical systems, natural ventilation, and passive

ventilation systems are among the studied technologies. The main parameters related to each system include operating costs, installation costs, ventilation rates, and heat recovery potential.

As can be seen in the articles mentioned above, a wide variety of energy-efficient systems have been developed for buildings, and studies to recover waste energy of buildings are also considered within this scope.

2.4.4. Temperature Control

The thermal energy can be stored or released in a phase change material without significant temperature variation. For this reason, the use of PCM as heat storage material in building components can reduce temperature fluctuations within the building material and prevent high surface temperatures (Mehling and Cabeza 2008).

Figure 2.12 shows the different phases of a phase change process (Wang et al. 2007). Generally, phase-changing materials have four types: solid-solid, solid-liquid, solid-gas, and liquid–gas. (Akeiber et al. 2016). PCMs are substances that absorb or release large amounts of latent heat when they change phase. This phase change occurs in a heating or cooling process as soon as the material reaches the temperature of the specific phase change. During latent heat absorption or latent heat release, the temperature of the PCM remains constant. (Pause 2018). In this process, PCM has sensible and latent heat regions. In the initial phase, the heat transfer increases the temperature of the material until the melting temperature of the specific phase changes. In the melting region, PCM transforms into liquid without any temperature change. The solid material absorbs the latent heat of fusion to turn into a liquid. The reverse of this process occurs when the heat is rejected from the material again (Dincer and Ezan 2018).
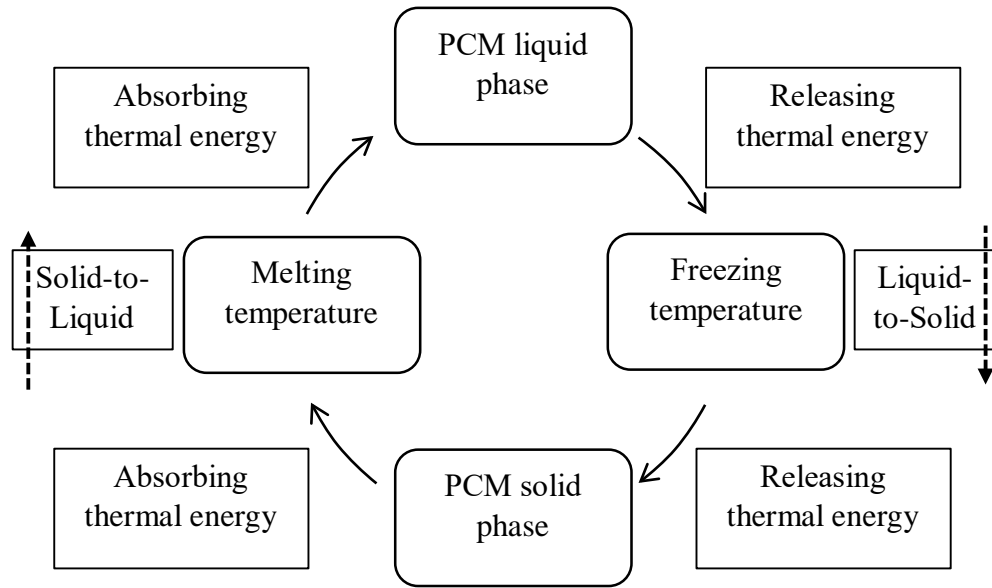
Figure 2.12. Working principle of the phase change of a PCM.
(Source: Malekzadeh 2015)

2.5. Phase Change Materials

"A suitable material is having all the desired properties of a phase change material and having its melting point in the required temperature range." (Shukla 2015). PCMs regulate temperature flows in a range defined by latent heat storage.

2.5.1. Classification

Depending on the phase change situation, PCMs are divided into solid-solid PCMs, solid-liquid PCMs, and liquid-gas PCMs. Among them, solid-liquid PCM's are the most suitable for thermal energy storage. PCMs are divided into three categories depending on their composition - organic PCMs, inorganic PCMs, and eutectic PCMs, as shown in Figure 2.13.
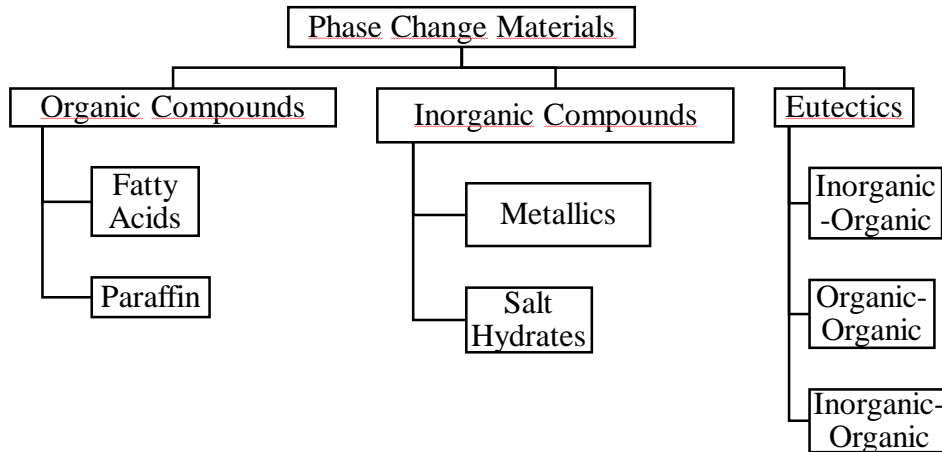
Figure 2.13. Phase Change Materials Classification.
(Source: Sharma et al. 2009)

Comparing these different PCM types is listed in Table 2.9 (Sharma et al. 2009). The main characteristics of each group of PCM are compared in this table. The advantages and disadvantages of these materials are shown in Table 2.9.

Table 2.9. Comparison of different kinds of PCMs.
(Source: Sharma et al. 2009)

Classifications	Advantages	Disadvantages
Organic PCMs	Availability in a large temperature range	Low thermal conductivity
	The high heat of fusion	Relatively large volume change
	Good compatibility with other materials	
	No supercooling	
Inorganic PCMs	High thermal conductivity	Supercooling
	Low volume change	Corrosion
	Availability in low cost	
Eutectics	Sharp melting temperature	Lack of currently available test
	High volumetric thermal storage density	

2.5.2. Potential of PCMs Applications

With the development of PCM technology, applications are common in both domestic and industrial applications. Some of these are the conditioning of buildings, the cooling of electricity and heat, transportation of blood and hot-cold therapies, waste heat

recovery, heating, and cooling water, incorporation of textiles for human comfort, solar energy facilities, spacecraft thermal systems, etc. In buildings, the addition of phase change materials to building elements and the provision of thermal comfort conditions using less energy is a wide working area (Agyenim et al. 2010) have been compiled and compared the heat transfer and phase change problem formulations used in latent heat storage applications in buildings and according to these studies, it is seen that it is generally realized between 0 and 60°C in buildings. The most commonly used phase change materials in this temperature range are paraffin and salt hydrates.

Thermal comfort can be defined by operating temperatures that vary at different times of the year. According to ASHRAE Standard-55 (2010), the normally recommended room temperature is 23.5-25.5°C in summer and 21.0-23.0°C in winter. PCMs with phase change temperatures (18-30°C) are preferred in building applications to meet thermal comfort requirements.

Another important advantage of utilizing PCMs is the ability to shift the amount of energy required at peak times from 14:00 to 17:00. And also, the indoor air temperature is reduced with the use of PCM. At this point, PCMs make more effective indoor climates with daily temperature fluctuations. The usage of PCMs can both reduce and shift the peak, as shown in Figure 2.14.
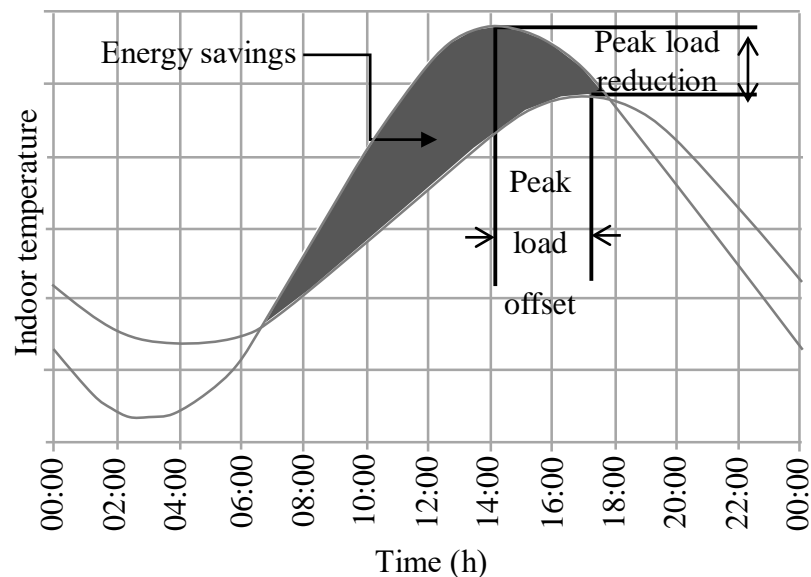
Figure 2.14. Illustration of peak load offset and peak load reduction.
(Source: Mehling and Cabeza 2008)

Also, this shows that PCM changes regular buildings into a regenerative organization that reuses excessive heat (during the day), which usually is removed using cooling systems at a time (during the night) it is needed. This time lag leads to efficient use of the cooling system in the nighttime when the outdoor temperature drops and the HVAC system runs more efficiently and reduces total building energy consumption (Kalnæs and Jelle 2015).

2.5.2.1. Use of PCM and LHTES with PCM

The articles above summarize the principles of using PCMs in ventilation and the advantages and disadvantages of such systems. Many studies calculate the performance of these systems and analyze them with computational fluid dynamics software, while some studies carry out experiments.

Hu et al. (2020) experimentally and numerically examined a solar air heat exchanger integrated PCM into a ventilated window. This system heated the fresh air with solar energy before ventilating the indoor environment. The system aimed to increase IAQ with solar energy storage and continuous air supply.

Metin et al. (2019) The effects of the inlet temperature and velocity of the heat transfer fluid on the system's performance in the spherical capsules in a row in the LHTES unit were analyzed with ANSYS-FLUENT software. The method applied was controlled by comparing it with the numerical results in the literature, and it was found that the deviation was less than 10%. Consequently, increasing the inlet temperature and air velocity is directly proportional to the melting time.

Ezan et al. (2018) worked on photovoltaic panels and PCM, and the difference that highlights this study in the literature is that the convection in the PCM is also analyzed using a numerical code. As a result, as the thickness of the PCM increases, the difference between conduction and convection models reaches 50%, based on photovoltaic panel temperature.

Stritih et al. (2018) conducted experimental and numerical studies on the use of latent heat storage with an air solar energy collector mounted on the facade of an office building in Ljubljana. They used the experimental results to validate the TRNSYS software. According to the required heat for covering ventilation losses without an additional system, the highest energy savings of the system were in April and October.

Tokuç et al. (2017) study the use of PCM on a roof to provide indoor comfort conditions. In this study, they evaluate the decrease in cooling load depending on the amount of PCM for four different climatic regions in Turkey and remark upon the significance of the relationship between melting-solidifying of PCM, climate, and PCM type.

Tokuç et al. (2015) studied the thickness of PCM in roof layers for Istanbul. This study includes experimental and numerical methods, and time-dependent simulations for summer conditions were evaluated according to Istanbul climate conditions. As a result, it has been observed that 2 cm of PCM thickness is suitable for flat roofs in Istanbul.

Yıldırım et al. (2017), in this study, 2D numerical analyzes of the flow module of an LHTES system were performed. The high-temperature water obtained from the solar collector flows over the spherical capsules in the storage tank, and the PCM inside the capsule's melts. The time-dependent change of the PCM in the capsule was analyzed using ANSYS-FLUENT software. As a result, significant differences were observed between the sphere close to the inlet and the other spheres in heat transfer rate.

Fiorentini et al. (2015) presented an experimental analysis of a new solar-powered HVAC system designed for UOW (University of Wollongong Australia) Solar Decathlon House, the winner of the Solar Decathlon China 2013 competition. This HVAC system consisted of an air-based photovoltaic-thermal system and a channel with PCM integrated with a heat pump. The focus was on the optimization of position-velocity-time modes and the discussion of results from experimental tests. As a result, the system's efficiency was relatively higher than a commercial air conditioning system.

Murray et al. (2015) aimed to experimentally develop a small capacity fan coil unit with heat recovery. The unit consists of two rotor-type sensible and latent heat exchangers, cooling coil, supply, and exhaust fans. It is designed for air conditioning in the Singapore climate. Consequently, the heat recovery wheel provided latent cooling for space rather than the sensible loads.

Weinlader et al. (2014) studied a ceiling cooling system with PCM. The experimental results indicate that this system has achieved a temperature drop of up to 2°C compared to the control group that does not have a cooling system.

Arkar and Medved (2007) conducted experimental and numerical research on the cooling efficiencies of two systems in a low-energy building. One system used mechanical ventilation with two latent heat storages to cool the fresh supply air and the

recirculated indoor air. Thus, they determined the most suitable PCM melting temperature for free cooling for Ljubljana, Slovenia.

2.5.2.2.Performance of LHTES Systems Containing PCM

Experimental and numerical studies examine the heat recovery performance in ventilation systems with latent heat storage using PCM in the literature.

Promoppatum et al. (2017) conducted controlled laboratory experiments by placing PCMs with different melting temperatures in a real-size heat exchanger consisting of staggered tubes. They created a mathematical model of the system with the ANSYS-Fluent software and extensively examined the PCM's time-dependent temperature and liquid percentage changes in the pipe for the store/reuse cycles.

Diallo et al. (2017) presented a numerical investigation of the energy performance of an energy-efficient ventilation system that can be integrated into a building facade. The system has a modular heat recovery unit with latent heat storage. The performance calculations using TRNSYS software examined five different climate conditions in Europe. Hence, the energy savings using this system was in the range of 16.5–23.5%.

El Mankibi (2015) presented experimental and numerical study results of a heat exchanger with PCM designed to provide IAQ. Numerical simulations were carried out for one month in winter to investigate the most suitable design criteria by changing the heat exchanger dimensions, the amount of PCM, and PCM properties.

Liu et al. (2017) designed a heat recovery unit containing PCMs with different melting temperatures and numerically examined the effect of this unit's operation and design parameters on energy consumption.

Stathopoulos et al. (2017) characterized different PCMs for use in a heat recovery device containing PCM capsules in the form of a rectangular prism. The model was compared with experimental data and accurately predicted the heat exchanger unit performance under different air flow rates and inlet air temperature.

Although many scientific studies on the PCM heat recovery application of ventilation systems, O'Connor et al. (2016) emphasized a lack of commercial products. In this study, O'Connor et al. (2016), who made a brief introduction of the heat recovery system with PCM produced by the Cool-Phase company, emphasized that this product has the potential to reduce energy consumption by up to 90% compared to conventional

HVAC systems. As a result, more thermal energy storage capacity can be provided in a more compact geometry than the ceramic solution by using less amount of material with the use of PCM.

El Fouih et al. (2012) used the TRNSYS software to model and characterized the annual performance of a heat recovery unit in residential and low-energy commercial buildings. The model also compared the unit's performance with a standard ventilation system. Thus, the dependencies for the efficiency of the heat recovery ventilation system were the heating load, ventilation device characteristics, and building type.

To have IAQ, thermal comfort, and also to provide heat recovery, correct design suggestions can be given with wall embedded units. It is seen that with this approach, the energy consumption of ventilation units can be effectively reduced. In addition, wall-integrated DVSs can be minimized the amount of volume.

2.6. Market Research for Decentralized HRV

To control the IAQ and sufficient ventilation, appropriate filters should be used in the system, and the airflow should be controlled. These systems generally consist of an air supply grill, an air filter, an axial fan, and a ceramic HRV unit, from outdoors to indoors. These products can provide different fresh air flow rates depending on their fan capacities and the selected control levels. There are many different wall integrated heat recovery systems on the market. Table 2.10 summarizes the features of commercially available wall integrated DVS. Here, the product information is compiled from the catalogs of the companies. In particular, 25 heat recovery systems belonging to 15 companies that store sensible energy have been examined according to airflow rate, size, alternative cycle, and speed control modes. In general terms, it is seen that the flow rate range of the products is a minimum of 8 m^3/h, a maximum of 115 m^3/h. However, on average, it is within the range of 15-50 m^3/h. The fans usually work in one direction for 70 seconds. The number and placement of units inside a space depend on the size of the space to be ventilated, the desired air change rate, and the homogeneous fresh air distribution. In addition to giving aesthetic value to architectural designs, these DVSs are easier to control and generate less noise than CVSs. However, the proper design, selection, and implementation of energy-efficient ventilation systems require a holistic approach to the buildings and the users.

The most important factor when calculating the fan capacity is the calculation of the room volume and the desired air change per hour. According to the report of the European Commission, the minimum accepted air change rate is determined as 0.5-1 ACH (Air Change per Hour) on average. As seen in Table 2.10, the products vary in airflow rates depending on the fan performance. Considering the airflow rates depending on the speed control modes, it is seen that it is generally 15-50 m³/h. The products selected in Table 2.10 on the market vary between 2 and 5 modes for all products.

Table 2.10. Commercially available wall integrated decentralized heat recovery ventilation systems and their features.

Firms	Products	Airpower level (m³/h)	Casing dimension HxWxD	Fan Reverse Cycle (sec)	Control level
Ventomaxx (Ventomaxx, 2020)	Z-WRG Rondo IQ	17-43	200x200	70	
	Z-WRG RONDO PLUS LAW	15-75	280x218	70	5
	Z-WRG RONDO PLUS LAL		280x218	70	
AVE (AVE, 2020)	VNRD150EC		335x390		
Vortice (Vortice, 2020)	VORT HRW MONO	10-40			
Blauberg (Blauberg, 2020)	VENTO Expert	8-25	284x234	70	3
	Fresher 50	20-50			
STIEBEL ELTRON (Stiebel Eltron, 2020)	LT50	14-54			3
	VLR 70 S	10-70	285x360		3
envirovent (Envirovent, 2020)	HEATSAVA				
Inverter (Inverter, 2020)	iV14R/V	24-55			
Lunos (Lunos, 2020)	NEXXT K	15-115	510x510		4
	NEXXT G	15-90	510x510		4
	eGO	16-38			4
	e2	16,5-26		55-70	4
Orca (Orca, 2020)	pico 50	14-28-54			
PRANA (Prana, 2020)	PRANA 150	25-115	200	70	
SEVI (Sevi, 2020)	SEVI	17-21-29-41/90	210x210	70	4
RDZ (RDZ, 2020)	WHR 60	14-28-54			
Vents (Vents, 2020)	TwinFresh R-50	22-58		70	2
	TwinFresh S-60	35-58			2
	TwinFresh RA1-50	25-50		70	2
Fantini Cosmi/aspira (Fantini Cosmi, 2020)	ASPIRVELO AIR ECOCOMFORT	25-50		35-200	2
aiolos air (Aiolos air, 2020)	Smartair	16-22-30-43	190x214	50-70	4
	Pleasentair	18-28-38-46			4

CHAPTER 3

EXPERIMENTAL METHOD

Experimental research is the oldest form of quantitative research. Quantitative research is an approach to testing objective theories by examining the relationship between variables. This research approach begins with a theory (or hypothesis) that is tested to determine whether or not it is supported (Neuman 2013). These variables can typically be measured on instruments to analyze numbered data using statistical procedures. Quantitative purists have assumptions about testing theories deductively, controlling for alternative explanations, and generalizing and replicating the findings (Creswell 2003). They have a post-positivist worldview, experimental design, and pretest and posttest measures of attitudes. This research type deals with the objects of empirical research for achieving posterior knowledge by conducting three main steps: experimental design, testing measurement methods, implementation of experimentation of experiments for testing validity of hypothesis (Creswell and Guetterman 2019; Bernold and Lee 2010). The difference between experimental research in pure science and experimental research in social science is that research can be carried out in a laboratory where it is relatively easy to control the environment (Moore 2006).

The following sections introduce the experimental studies carried out as part of this work. The experimental testing validated the CFD analysis detailed in Chapter 4. This chapter provides an overview of the experiment design and the parameters of the experiment. The experimental methodology covered in the chapter detail the design of the heat recovery ventilation system, prototyping the test chamber and DVSs, and measurement of the experiment properties. Also, this chapter includes information about TES material, calibration, and uncertainty details.

3.1. Research Framework

The performance of the wall-integrated single-room ventilation units is studied. Firstly, the on-site measurements are performed in laboratory conditions. The next step is to calibrate the laboratory measurements according to the measured temperature, air

velocity, and pressure difference values. In experimental studies, uncertainties affect the accuracy of the data. So, the uncertainty calculations are made. Then the fan performance and heat recovery unit performance are calculated according to all calibrated and measured data. Following this, CFD models are produced.

3.1.1. Physical Model

The real-scale experiments were carried out in the Building Physics Laboratory of the Faculty of Architecture, Izmir Institute of Technology. An experimental chamber was previously used for the thermal study of a double-skin façade (Inan, Başaran and Ezan 2016; Inan, Basaran, and Erek, 2017; Başaran and Inan 2016) redesigned and prepared for this study. The experimental setup includes two spaces that simulate indoor and outdoor temperature conditions. An insulated aerated concrete wall separates them. Parametric studies have been carried out to determine the performance of two wall integrated HRV systems (Figure 3.1).

Figure 3.1. The experimental setup; I: aerated concrete wall, II: indoor environment, III: outdoor environment, VI: constant temperature bath, VII: cooling group.

3.1.2. Test Chamber

The experimental setup shown in Figure 3.2 consists of eight main parts: The aerated concrete wall (I) separates the simulated indoor (II) and outdoor (III)

environments. The simulated indoor environment (II) dimensions are 2.7 m depth, 1.5 m width, and 3 m height, and it has 10 cm thick insulated panel walls. The simulated outdoor environment (III) has 2 m depth, 1.5 m width, and 3 m height measurements. The experimental two HRV systems stored internal and latent thermal energy (IV) for individual experiments separately are mounted inside the two air ducts (V), which are positioned outside of the wall for being accessible while taking measurements inside the units the ducts insulated against heat transfer. The heating/cooling constant temperature bath (VI) with a flowmeter condition the indoor (II), while a cooling group (VII) and a thermostat-controlled heater (VIII) condition the outdoor (III) environment. The heating/cooling systems use wall-hung serpentines to condition the air, as shown in Figure 3.2. Thermocouples (shown as *T*) continuously measure temperatures from the points shown schematically in Figure 3.2.
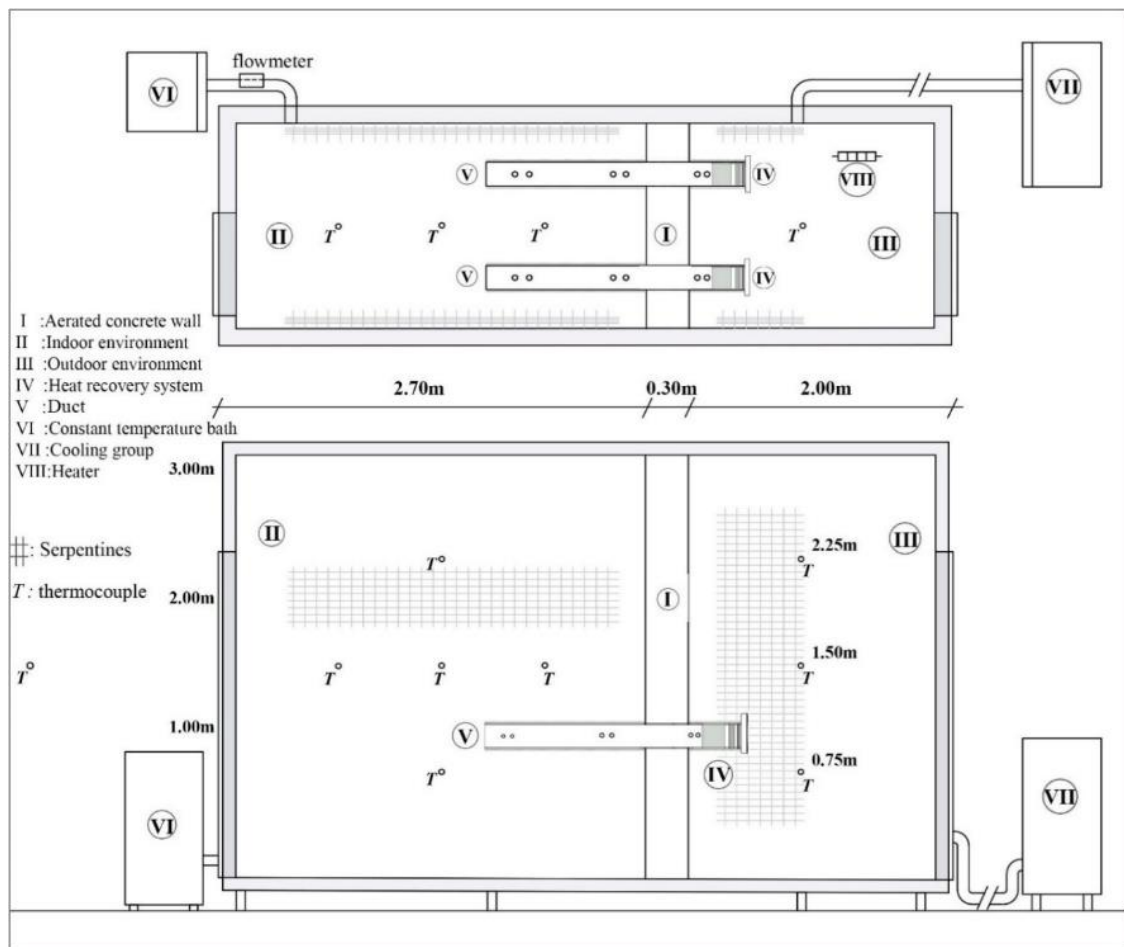
Figure 3.2. Plan and section of the experimental setup (not in scale)

3.1.3. Wall Structure

The outside of the experimental setup created within the scope of the project and both simulated rooms are given in Figure 3.3. In this study, the wall with a very low total heat transfer coefficient is considered to determine the wall thickness and material. The wall that separates the indoor and outdoor environments from each other consists of two layers of aerated concrete. For the externally insulated condition, a multi-layer wall structure is constructed with a 10 cm mineral-based aerated concrete heat insulation board as an insulation material on the 20 cm aerated concrete block wall as a body element (Figure 3.4).

Figure 3.3. I: aerated concrete wall, II: indoor environment, III: outdoor environment, V: air ducts

Aerated Concrete (0.2m)

Mineral-based Aerated Concrete Heat Insulation (0.1m)
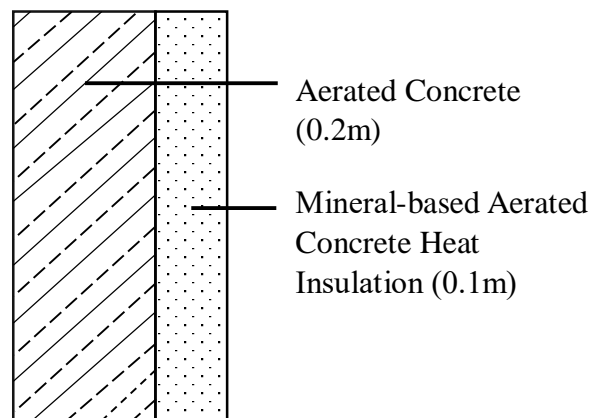
Figure 3.4. Externally insulated multilayer wall, which is numbered I in Figure 3.3.

According to TS-825 thermal insulation regulation, the total heat transfer coefficient of the wall composition separating the two conditioned environments in the experimental setup should be less than 0.25 W/m²K. The exterior wall overall heat transfer coefficient (U-value) described as the Silver Standard is 0.25 W/m²K. These U values were also considered in the heat loss and gain calculations, and the results were compared with each other (Olivier 2008). According to this recommendation, the U value of the wall in the experimental setup is 0.227 W/m²K.

3.1.4. Duct Setup

Two prototypes of the heat recovery ventilation systems in the air ducts are integrated into the aerated concrete wall that separates the indoor (a) and outdoor (b) environments. The Duct-1 and Duct-2 in Figure 3.5 are placed one meter above the ground and have a cross-sectional area of 0.175 m x 0.175 m. The air inside the ducts flows in opposite directions. While Duct-1 works in exhaust mode, Duct-2 works in supply mode. Fans work simultaneously in opposite directions to minimize the pressure imbalances in the rooms that represent indoor and outdoor environments. Thermocouples are placed within the ducts to monitor the temperature variations of air and the HRVs in the ventilation ducts.

a) indoor   b) outdoor
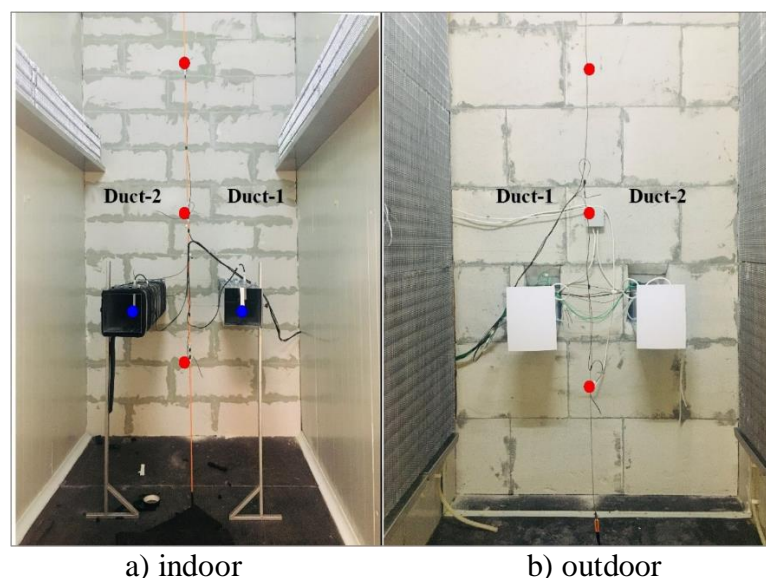
Figure 3.5. Ducts' location in simulation rooms with temperature (red dot) and velocity (blue dot) measurement points.

For all experiments, indoor and outdoor environment temperatures were monitored until the system reached representative temperature conditions while the inlet and outlet sections of the ducts were sealed with covers. A thermostat-controlled electric heater or direct expansion evaporator was used to stabilize the outdoor environment temperature. When the desired temperature was reached, the ducts cover was opened, and the experiments started. During the experiments, two systems installed at each duct worked in synchrony. While one system exhausted air from the inside, the other supplied fresh air from the outside through the ducts. Thermocouples within the ducts monitor air temperature variations and the ceramic unit and PCM in the tubes.

For the measurements, thermocouples located at the inlet and outlet constantly measure the temperature changes of the airflow inside the ducts, and a datalogger records these measurements. The duct section and measurement points are given in Figures 3.6a, which is the ceramic unit, and 3.6b, which is the tube bundle unit. Two air velocity transmitters which are shown in Figures 3.5a, 3.6a, and 3.6b, placed in the room that simulates the indoor environment measures air velocities in both ducts. Moreover, a differential pressure meter placed before and after the energy storage units records pressure drops for the exhaust and supply conditions of the units (Figure 3.6a, 3.6b). In the exhaust mode, laminar flow and hydrodynamically fully developed close to the outlet. Therefore, air velocity is measured close to the outlet from different points at the cross-section of the ducts. Meanwhile, the velocity measurement is taken from the specified point in supply mode. Besides, a thermocouple near the duct outlet measures the air temperature for calculating the mass flow rate of the air considering the density variation with temperature.

a. Duct setup and measurement points for ceramic (not to scale)

(b) Duct setup and measurement points for tube bundle (not to scale)
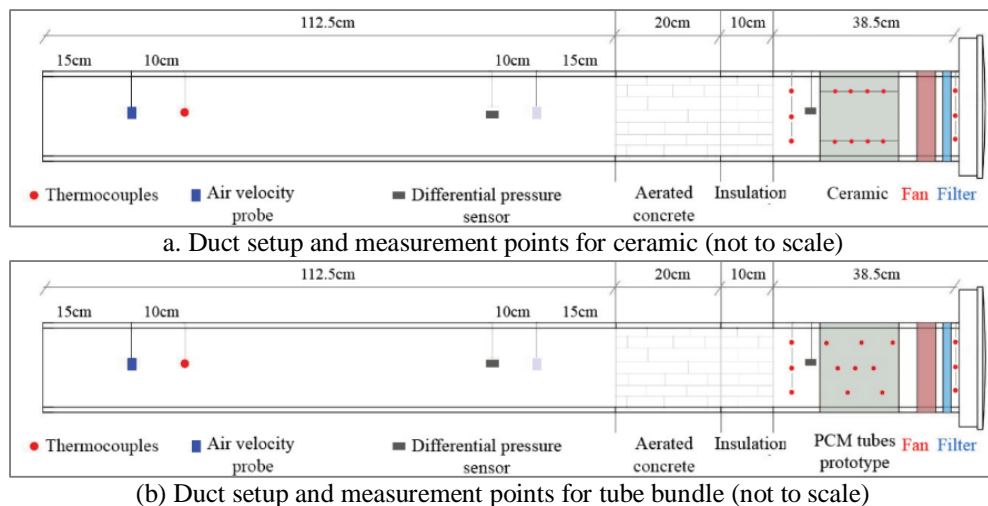
Figure 3.6. Duct setup with the HRV units for sensible and latent energy storage.

3.2. Ceramic Heat Recovery Ventilation System

To control the IAQ, proper filters should be used in the system, and the airflow should be controlled, in addition to adequate ventilation. These systems include an air supply grill, an air filter, an axial fan, and a ceramic HRV system from the outside to the indoors. These systems can provide different fresh air flow rates depending on their fan capacity and control settings. On the market, there are several wall-integrated heat recovery systems. In these experiments, the characteristics of the ceramic material have a relatively high specific heat storage capability and are closed-pore surfaces easy to clean, as shown in Figure 3.7.
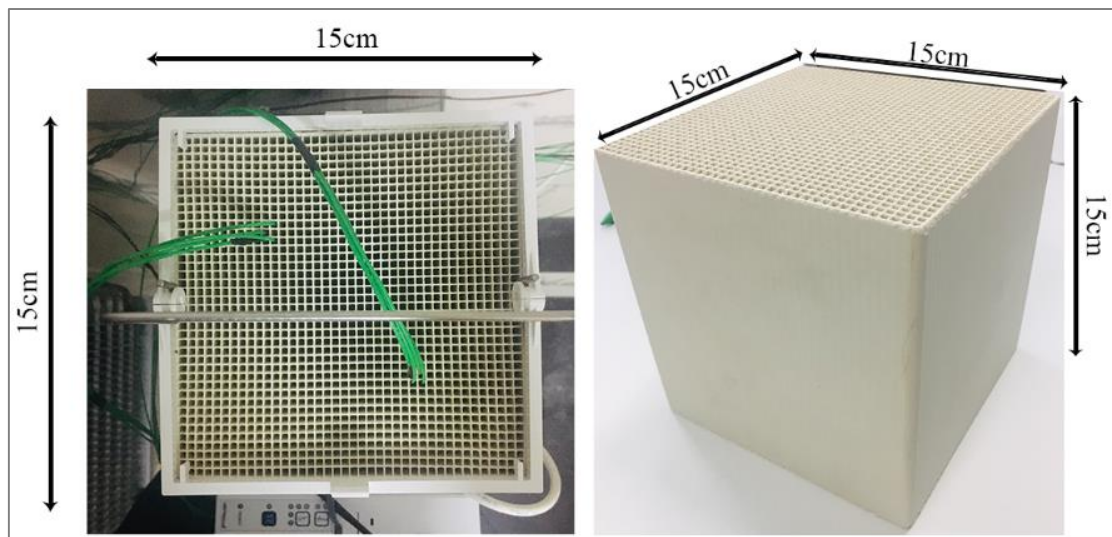
Figure 3.7. Overview of the ceramic material for sensible energy storage in HRV unit.

There are approximately 1600 cells in total in its 15 cm-by-15 cm structure (Figure 3.7). The dimensions of the cells are 4.3 mm on the outer line and 3 mm by 3 mm on the inner parts. The cell wall thickness is 0.6 mm. The outer wall is 2 mm (Figure 3.7). As seen in Figures 3.7 and 3.8, 8 thermocouples, 4 of each, are placed to give the average temperature of the ceramic material. Specific heat is the amount of heat required to change the temperature of a substance's unit mass, and the differential scanning calorimeter method is used to measure specific heat. This method measures the amount of energy absorbed or released while the sample taken from the ceramic material is heated and

cooled for a few cycles between 5℃ and 35℃. The specific heat value of the ceramic material was measured to have an average value of 0.725 kJ/kg℃.
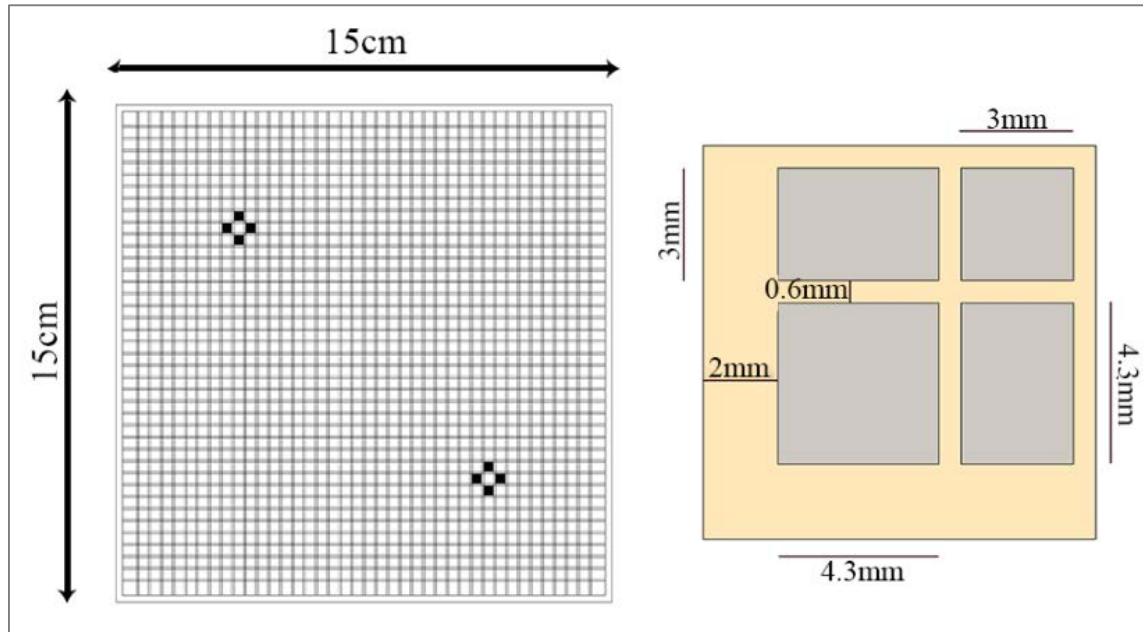
Figure 3.8. Thermocouple placement (mentioned with bold square) and geometric details of the ceramic unit.

Figure 3.9a shows the isometric view of the HRV system, and Figure 3.9b shows the front view of the ventilation system with a ceramic HRV unit consisting of covers for inside (1) and for outside (2), filter (3), fan (4), and HRV unit (5).
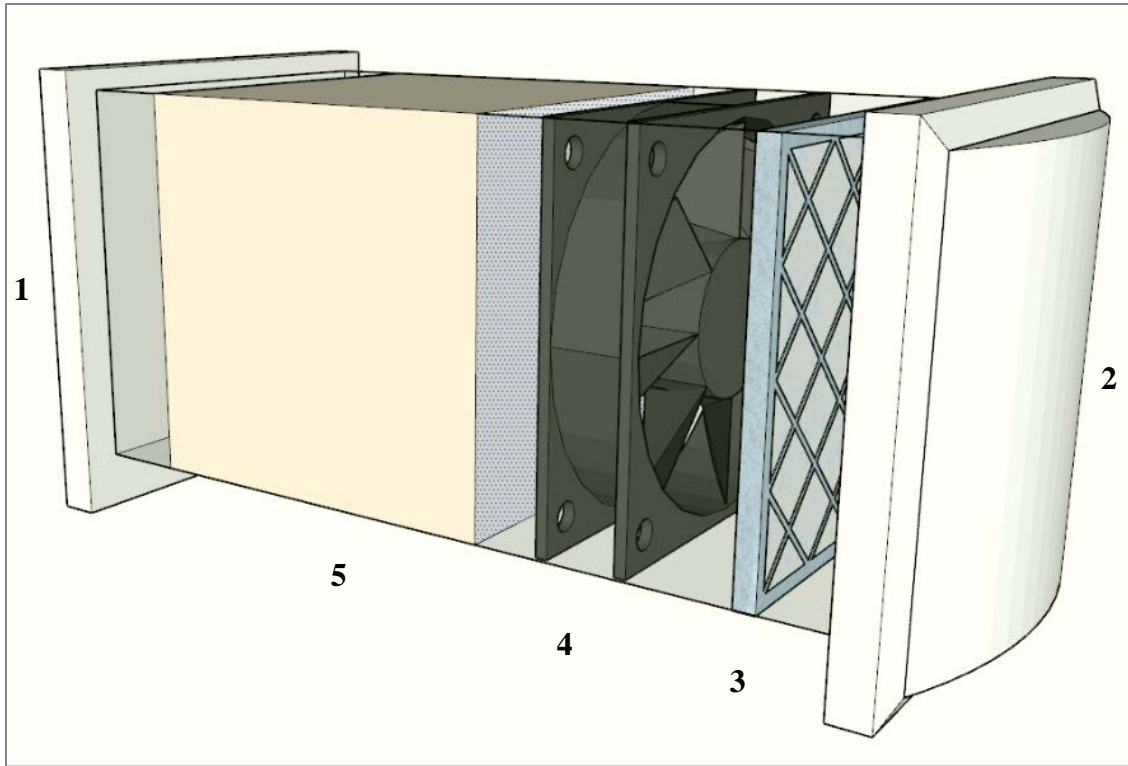
a) isometric view
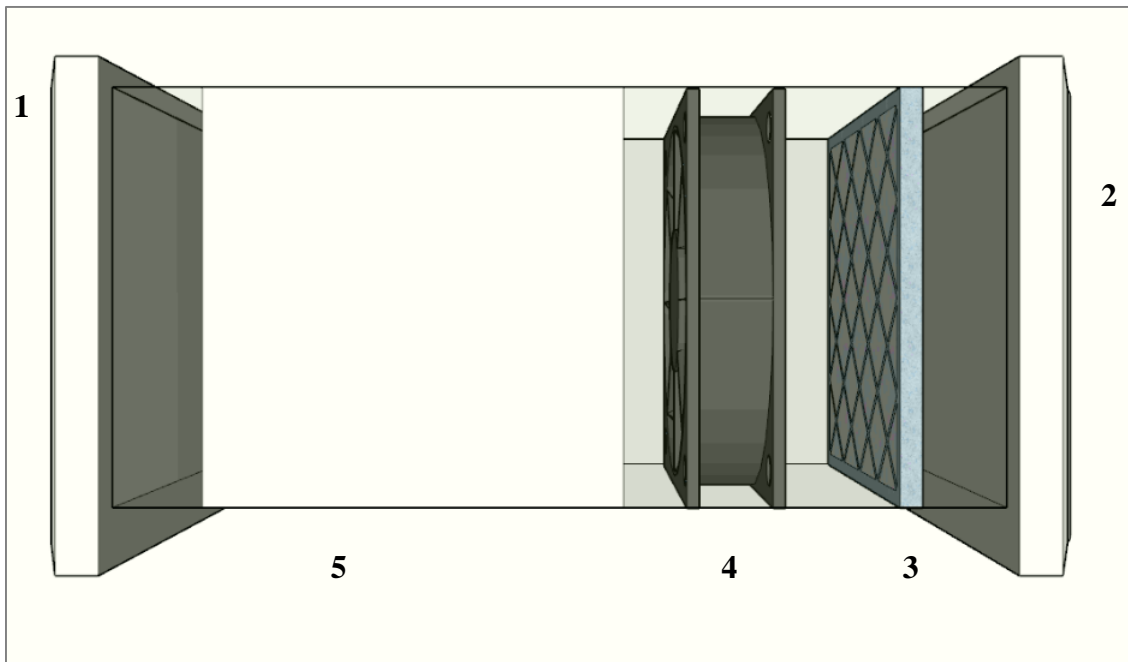
b) front view

Figure 3.9. 3D views of the ceramic heat recovery system.

3.3. Design of the Tube Bundled Prototype With PCM Heat Recovery Ventilation System

In literature, three different TES systems can be defined as sensible, latent, and thermochemical. Thermal energy is stored in sensible heat as a result of the change in temperature of the storage material, while latent heat is stored as a result of the phase change process of the storage material, and in thermochemical storage as a reversible chemical reaction between the two substances (Gasia et al. 2017). Sensible TES systems, as mentioned in Chapter 2, have a disadvantage: To obtain enough thermal storage capacity, significant changes in the temperature of the system are necessary because of the low heat capacity of the materials (Campos-Celador et al. 2020). However, LHTES has high storage densities and narrow operating temperatures (Mehling and Cabeza 2008).

Mehling and Cabeza (2008) studied design criteria for sensible and latent heat storage systems. And in this study, four main LHTES systems are compared to each other. These are direct contact, modular, slurry, and HRV unit. All units are filled with PCM. As a result, the HRV system has a high storage density.

Shröder et al. (2014) investigated the different types of HRV units, which are double pipes, shell-and-tube HRV units with baffles in stretched and U-shape alignment, and plate HRV units. As a result, according to energy efficiency, investment costs, and cleaning purposes, U-shaped shell and tube HRV units are preferred.

Permana et al. (2019) compared the heat transfer coefficient between a single tube and a multi-tube with the same heat transfer surface. The single-tube dimension is 40 cm in length and 9.5 cm diameters, while multi tubes HRV unit consists of ten tubes which are 40 cm length 0.95 cm diameters. The ambient temperature, outlet, and inlet air are recorded via a T-type thermocouple. As a result, the heat transfer coefficient of a multi-tubes HRV unit is 26.6% higher than a single tube HRV unit.

In the light of these studies, a tubular HRV unit is designed in this study. The experimental, decentralized ventilation unit with heat recovery uses an HRV unit to transmit heat from the exhaust air to the supply air and can be installed directly on a facade. Figure 3.10 shows the overview of the tube bundle prototype. The tube bundle consists of 100 copper staggered tubes in its 15 cm-by-15 cm structure filled with PCM at the airflow direction.
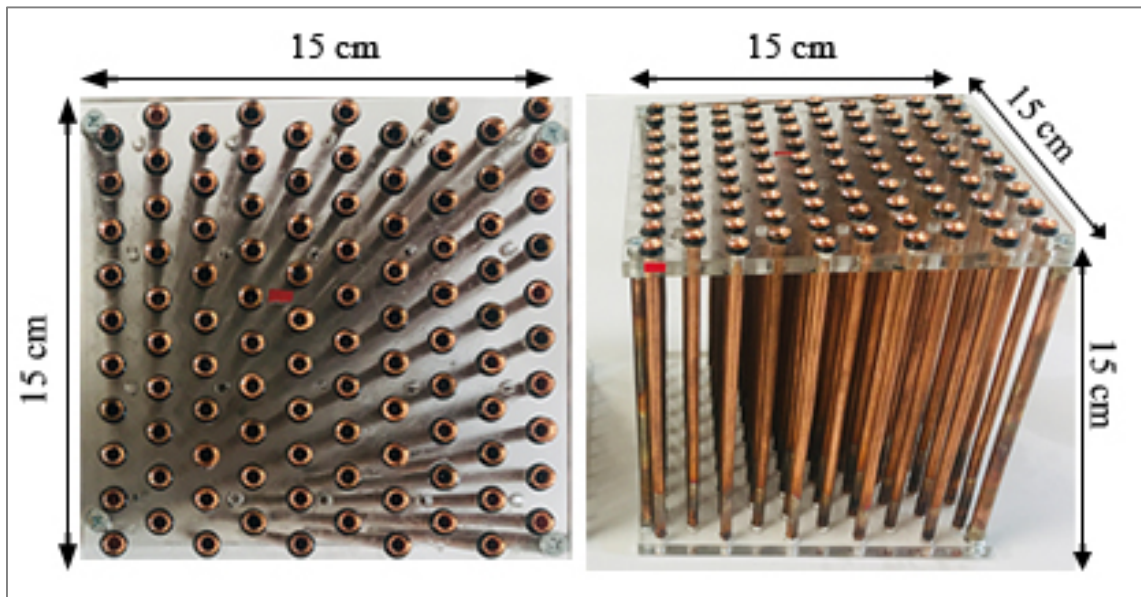
Figure 3.10. Overview of the tube bundle unit for latent energy storage in HRV unit.

The height of one tube is 15 cm, and its outer diameter is 4.76 mm. Liquid PCM was poured into the tubes having 0.3 mm wall thickness. The tube arrangement in the bundle is designed as 1.4 cm for the transverse pitch and 1.4 cm for the longitudinal pitch. The prototype measured the diagonal pitch between tube centers is measured as 1.565 cm in the prototype (Figure 3.11).
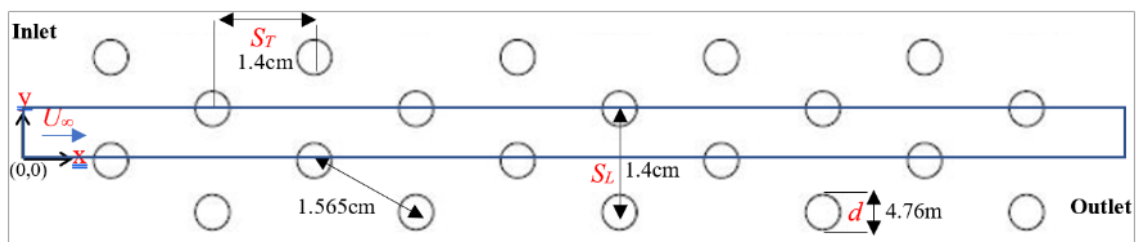
Figure 3.11. Section of the tube bundle prototype.

Figure 3.12a shows the isometric view of the HRV system, and Figure 3.12b shows the front view of the ventilation system with a tube bundle prototype, which consists of covers for inside (1) and for outside (2), filter (3), fan (4), and HRV unit (5). The air taken from outside passes through the filter before reaching the indoor environment.
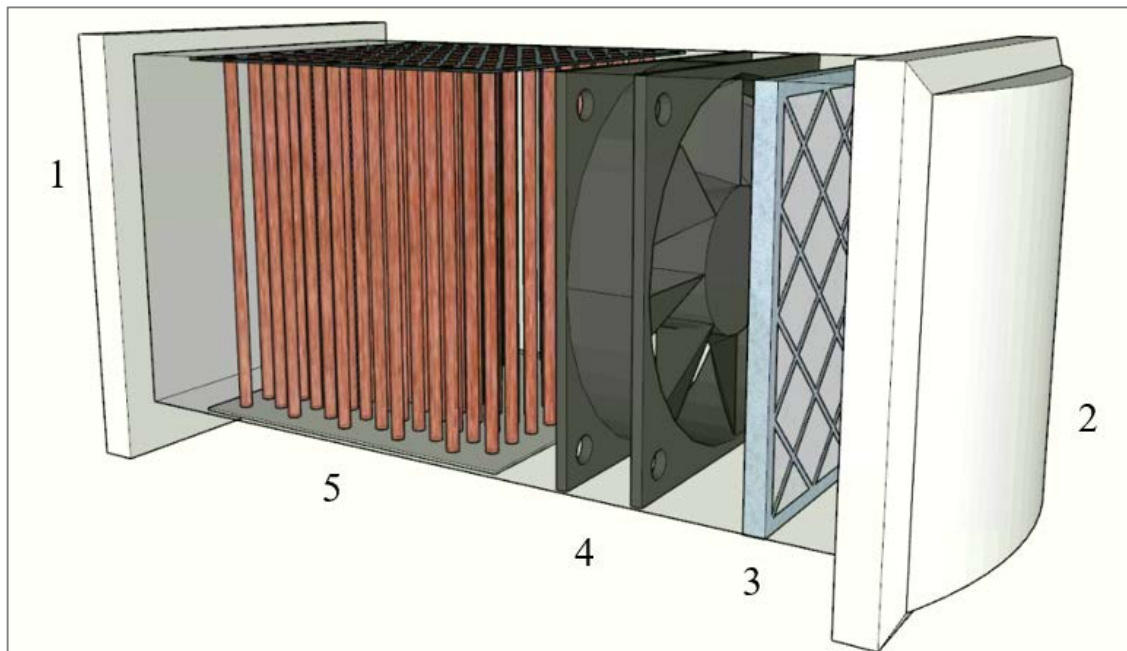
a) isometric view
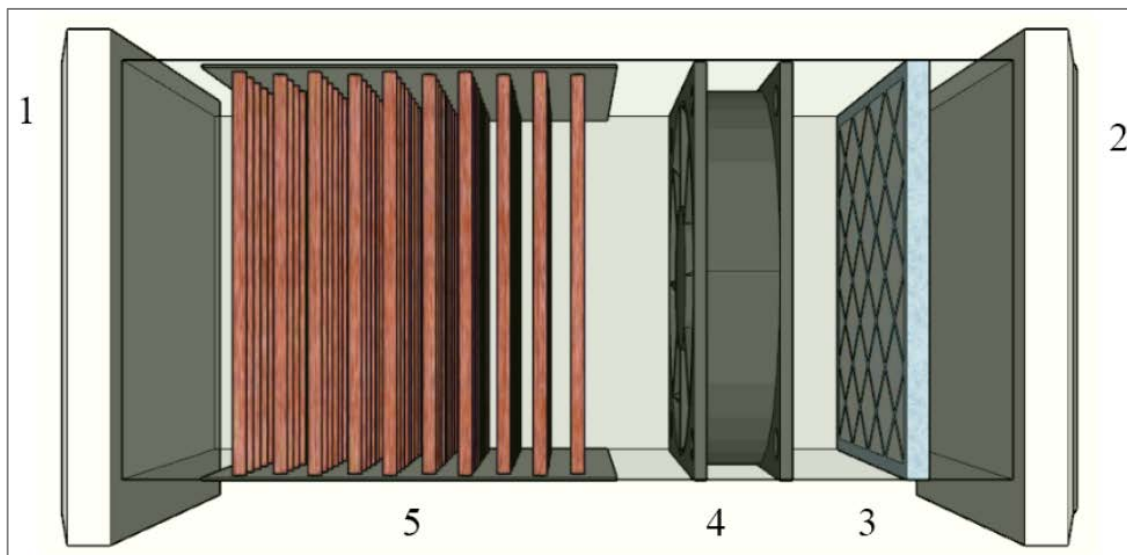
b) front view

Figure 3.12. 3D views of the tube bundle heat recovery system.

3.4. Experimental Procedure

The experimental procedure is divided into three processes: the preparation process, the data collection process, and analyzing and interpreting the data process.

(1) The preparation process is to reach and maintain the representative temperature conditions for the inlet and outlet sections of two HRV systems that are closed during this period by controlling the temperature of the indoor and outdoor rooms.

- For sensible HRV system which is the ceramic unit; (22±1°C) and outdoor (35±1°C) room for summer condition and indoor (20±1°C) and outdoor (5±1°C) for winter condition.

- For latent HRV system which is tube bundle unit (22±1°C) and outdoor (35±1°C) room for summer condition.

Indoor and outdoor temperature values were chosen based on the thermal comfort condition (ASHRAE Standard-55 2010) and Turkish State Meteorological Service 1991-2020 measurements as the average temperatures maximum 33.2°C and minimum 5.7°C in İzmir (MGM-TR 2021).

(2) After adjusting the system, two HRV units (ceramic and tube bundle) are used alternatively in exhaust/supply modes in certain periodic cycles. The thermal energy stored by the units is monitored during these periodic cycles. Throughout the experiments, indoor and outdoor temperatures, temperatures at the inlet and outlet sections of the units, temperature changes in the units, air velocity at the ducts where units integrated, as well as the pressure differences between indoor and outdoor environments and between inlet and outlet sections of the units are measured (Table 3.1). These experimental data measured by the instruments (mentioned in Table 3.1) are recorded with a datalogger in time steps of 5 seconds during the experiments. During the experiment, this 64-duct data logger, temperature, air velocity, and differential pressure measurements taken from different points of the experimental setup are recorded.

(3) The reliability of the test results is determined by the uncertainty analysis given in the following section. Using the measurement results, the thermal energy storage capacity of HRV systems is calculated for different operating times.

Table 3.1. Information of test instruments.

Test parameters	Test instruments	Test instrument places	Number of the test instrument
Temperature	T-type thermocouples	Indoor and outdoor environments	5 indoor 3 outdoor
		Inlet and outlet sections of the HRV units	3 both sections (twice for Duct 1 and 2)
		In the HRV units	8 (twice for Duct 1 and 2)
Air velocity	Blitz Sens VS-C2-1-A Air velocity transmitter	Inlet and outlet sections of the ducts	1 (twice for Duct 1 and 2)
Differential pressure	HK Instruments DPT-R8 Analog manometer	Indoor and outdoor environments	1 instrument for 2 points differentials
		Inlet and outlet sections of the HRV units	1 instrument for 2 points differentials

3.5. Experimental Setup Measurement Devices

For calculating and describing the variation of the experimental setup, ambient temperature, air velocity, pressure drop measurements play a decisive role in significantly determining temperature, flow rates, and pressure differences changes. The air velocity measurement and pressure drop results are also important factors for the fan characteristics. In this section, air velocity and pressure drop measurement devices and their results are explained under the sub-heading of evaluation of fan characteristics.

These data are stored in the HIOKI LR 8402-20 datalogger for evaluation throughout all experiments. During the experiment, these measurements taken from different points of the experimental setup are recorded with this datalogger with 64 channels. Figure 3.13 shows the HIOKI LR 8402-20 datalogger and control checkpoint.
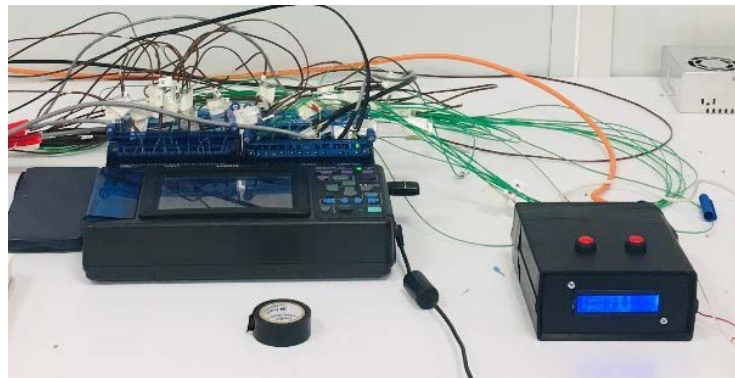
Figure 3.13. HIOKI LR 8402-20 datalogger overview.

3.5.1. Temperature Measurements

Nickel-based thermocouples (K type thermocouples) and copper constantan thermocouples (T type thermocouples) are used for temperature measurements from many points of the experimental setup. Measurement ranges for these thermocouple types are -200 to + 1200°C for K type and -200 to + 350°C for T type (Goodfellow and Wang 2021).

The positions of thermocouples inside the test rooms are shown in Figure 3.5. The number and placement of thermocouples are as follows; one thermocouple measures the laboratory environment, in which the experimental setup is placed, five thermocouples

provide the temperature values of the indoor environment, and three thermocouples represent temperature for the outdoor environment. In the indoor environment, one thermocouple is placed at the midpoint of the exit sections of the two ducts to measure the air temperature inside the duct for determining the air density. In the outdoor environment, for each duct, three thermocouples measure the system inlet temperature in front of the filter, and three thermocouples measure the system outlet temperature (Figure 3.6).

There are two different installations of thermocouples for two different HRV units stored sensible and latent energy. As shown in Figure 3.16, a total of eight thermocouples are placed in the ceramic HRV units to investigate the sensible energy storage in each duct to measure temperature changes along the ducts and mean temperatures of each ceramic material. Thermocouple positions within the ceramic HRV units are indicated as Group 1 and Group 2 and numbered from 1 to 4 for Duct-1 and Duct-2, respectively.
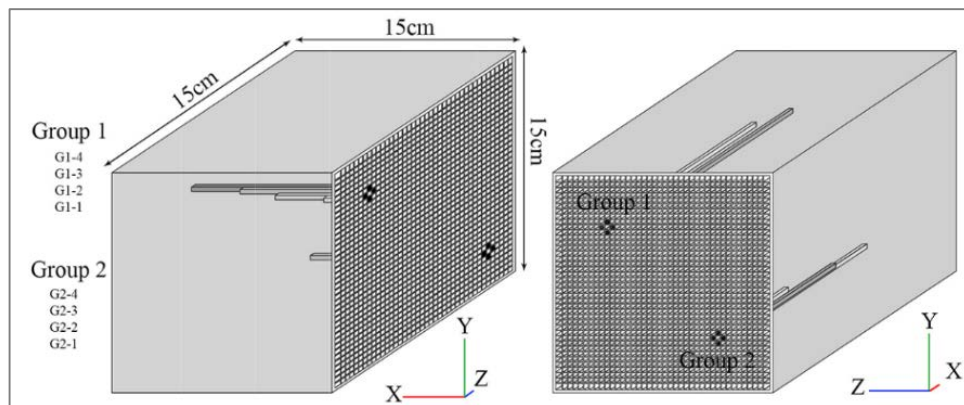
Figure 3.14. Thermocouple layout inside the ceramic material (not in scale).

For the experimental studies of the heat stored latent energy, the critical measurements in the system are the determination of the solid and liquid phases (Ezan, Ozdogan and Erek 2011). The temperature measurements of the medium are used for monitoring the melting and solidification process. Besides this measurement, eight thermocouples are placed in the tube bundle prototype with PCM in each duct. Their placement is shown in Figure 3.16. These locations are selected to give the average temperature gradient in the PCM. And these thermocouples are placed into the tubes in the direction of flow to the depth of 3.5 cm, 7 cm, and 10.5 cm from top to bottom, as shown in Figure 3.17.
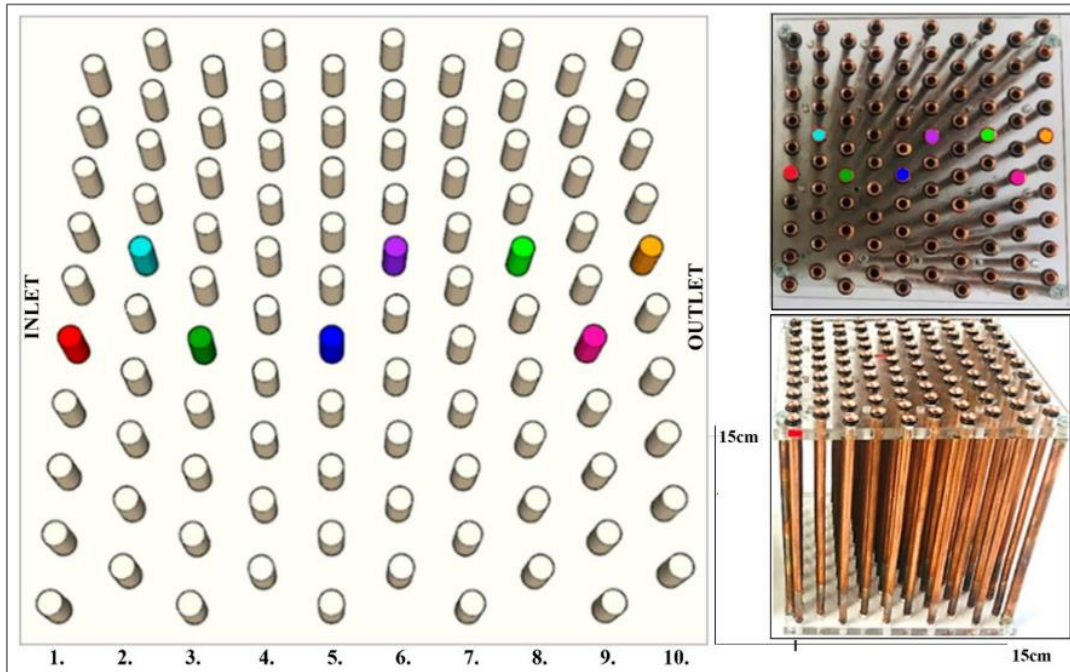
Figure 3.15. Thermocouple placement inside the prototype of the decentralized HRV system with PCM

3.5.2. Evaluation of the Fan Characteristics

The axial fan, installed inside the ventilation unit, can work in two flow directions. The fans of commercial products have limited speed, and their exhaust-supply times are also limited. Therefore, a fan control system is developed in the current study. This interface controls the fans' desired velocity and working period on the heat recovery system. The capacity of fans to produce a needed air volume flow rate against an expected system resistance to flow, or pressure, is taken into account while choosing them. Fans for wall-integrated ventilation systems available in the market have limited speeds and directions and charging-discharging times. This study selects the most suitable fan for the system, and the fan characteristics are investigated in this section. The air velocity measurement and pressure drop results are also important factors for the fan characteristics.

3.5.2.1. Air Velocity Measurements

One of the key parameters to evaluate the functional capacity of an HVAC system is the volumetric flow rate of air. A parabolic velocity profile occurs inside the duct

section due to the viscous fluid flow within the ducts; therefore, measurement of air velocity at a single point is not sufficient to determine the mean velocity value of the duct's cross-section. Different standards can be used to measure the airflow rate accurately. DIN EN 12599 is used in Germany, and most of Europe; DIN EN 16211 and ASHRAE Standard-111 (2008) can also be used. The common point of all these standards is that measurement points must be distributed inside the cross-section of the duct. DIN EN 12599 recommends using the Trivial linear equation solution method while measuring the air velocity in these air ducts. According to this method, the first step is to divide the velocity field in the duct section into equal-sized measurement areas. Then, measurements are taken from the midpoint of each section, and finally, the resultant arithmetic means value represents the result.
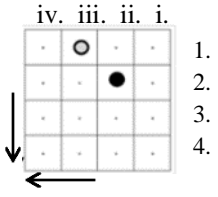
Blitz Sens VS-C2-1-A air velocity transmitter (Figure 3.16) is used to measure the air velocity inside the ducts at specified positions. The measurement range of this device is 0-1m/s. This thermal anemometer, also called a velocity meter, works to measure the airspeed and volumetric flow via heating and cooling of the sensor by electricity (Goodfellow and Wang 2021). Its highly precise thin-film sensor is 180 mm long and produced in narrow spaces. The air velocity measurement probe, Blitz Sens VS-C2-1-A air velocity transmitter, was calibrated in a wind tunnel by a comparison method in which the reference sensor and the test instrument were placed in the test section of the tunnel. The uncertainty of the measurement value of the test instrument was calculated by using 5 data in a series measured in 30 seconds. Detailed calibration result for air velocity transmitter is in appendix 1.

Figure 3.16. Blitz Sens VS-C2-1-A air velocity transmitter and in-channel measurement
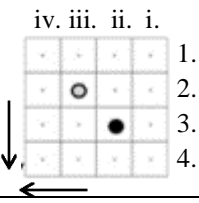
According to the measurement results of the ceramic HRV unit, the points that gave the closest values to the average were determined, and the measurements were taken from those points at the cross-section of the duct (shown in Table 3.2) during the experimental studies. The average supply air velocity results are 0.215 m/s, and the exhaust velocity is 0.165 m/s. These average values were measured at two different positions in the ducts due to the airflow direction and providing a fully developed flow. Tables 3.2 and 3.3 represent the characterization test results for supply (out to in) and exhaust (in to out) values of Duct 1 by the Trivial method (DIN EN 12599 n.d.).

Table 3.2. Duct 1 fan supply (out to in) and exhaust (in to out) characteristic test results for air velocity in m/s for ceramic HRV unit.

		iv. Column	iii. Column	ii. Column	i. Column	Avg.
Supply	1. Line	0.15	0.11	0.10	0.18	0.22
	2. Line	0.20	0.19	**0.21**	0.27	
	3. Line	0.25	0.28	0.27	0.32	
	4. Line	0.26	0.31	0.32	0.32	
Exhaust	1. Line	0.14	**0.16**	0.16	0.15	0.16
	2. Line	0.18	0.20	0.19	0.14	
	3. Line	0.15	0.23	0.20	0.18	
	4. Line	0.15	0.21	0.16	0.11	

In Table 3.3, velocity measurements are taken along the duct cross-section for exhaust and supply from 16 different points, than the average velocity values in the duct sections are calculated to determine the airflow rates for LHTES. In Duct 1, the average velocity for supply air is 0.344 m/s, and the average for exhaust air is 0.282 m/s for tube bundle HRV prototype. The points that provided the nearest values to the calculated average velocity values were selected to represent the average velocity (marked in Table 3.3). The following velocity measurements were taken from these points during experimental studies to determine the mean velocity and volumetric and mass flow rate.

Table 3.3. Duct 1 fan supply (out to in) and exhaust (in to out) characteristic test results for air velocity in m/s for tube bundle HRV unit.

iv. iii. ii. i.		iv. Column	iii. Column	ii. Column	i. Column	Avg.
Supply	1. Line	0.270	0.341	0.320	0.350	0.344
	2. Line	0.306	0.345	0.371	0.403	
	3. Line	0.280	0.380	0.38	0.415	
	4. Line	0.271	0.300	0.35	0.370	
Exhaust	1. Line	0.390	0.252	0.199	0.242	0.282
	2. Line	0.395	0.251	0.225	0.278	
	3. Line	0.306	0.225	0.282	0.281	
	4. Line	0.270	0.281	0.283	0.347	

3.5.2.2. Pressure Drop Measurements

The differential pressure measurement is monitored with an analog manometer from two points in the experimental setup. Two separate measurements are taken to measure the pressure difference between the indoor and outdoor environments and the pressure difference between the systems on the two ducts with fans working in exhaust and supply modes. HK Instruments DPT-R8 Differential Pressure Transmitters (Figure 3.17) are used for these measurements. This transmitter is mainly used in HVAC systems to control and monitor the fan airflow and pressure. This differential pressure measurement system is arranged to operate in the range of 0-25 Pa. The data are stored for evaluation in the HIOKI LR 8402-20 datalogger.

Figure 3.17. HK Instruments DPT-R8 Differential Pressure Transmitter.

Figure 3.18 shows the pressure difference values between the indoor and outdoor environment of the ceramic units, which is operated for 1-minute, 2-minute, 5-minute, and 7.5-minute in winter conditions. The system, which works during specified times, first operates Duct 1 exhaust, while Duct 2 supplies and then works in the opposite direction. Respectively, in the system running for 1-minute, the fan produces an average pressure difference of 4.82 Pa, 4.90 Pa in 2-minute, 5.10 Pa when it runs for 5-minute, and 4.82 Pa when it lasts for 7.5-minute.
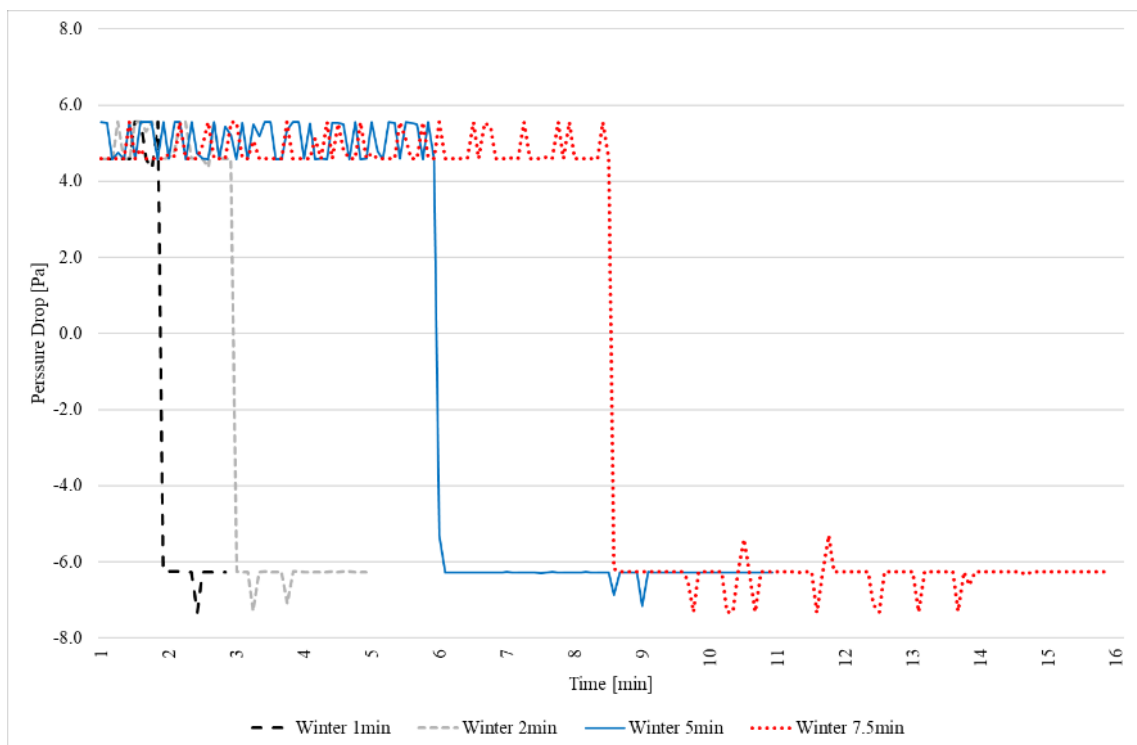
Figure 3.18. The pressure difference at the inlet and outlet of the systems while the fan operates in exhaust and supply modes for different running times for the ceramic unit

Figure 3.19 shows the cases when the fan is working in exhaust and supply mode for cycles of 15-minute, 20-minute, and 30-minute. While Duct 2 operates in the exhaust mode, Duct 1 is in supply mode. When the system runs for 15-minute, the fan produces an average pressure difference of 8.20 Pa. A difference of 8.07 Pa is the average value when moving air from inside to outside for 20-minute. Meanwhile, the fan-produced average pressure difference is 8.02 Pa for both units running together for 30-minute. During the airflow from the outdoor to the indoor environment, the pressure difference

between two fans for 15-minute, 20-minute, and 30-minute is 9.74 Pa, 9.78 Pa, and 9.57 Pa, respectively.
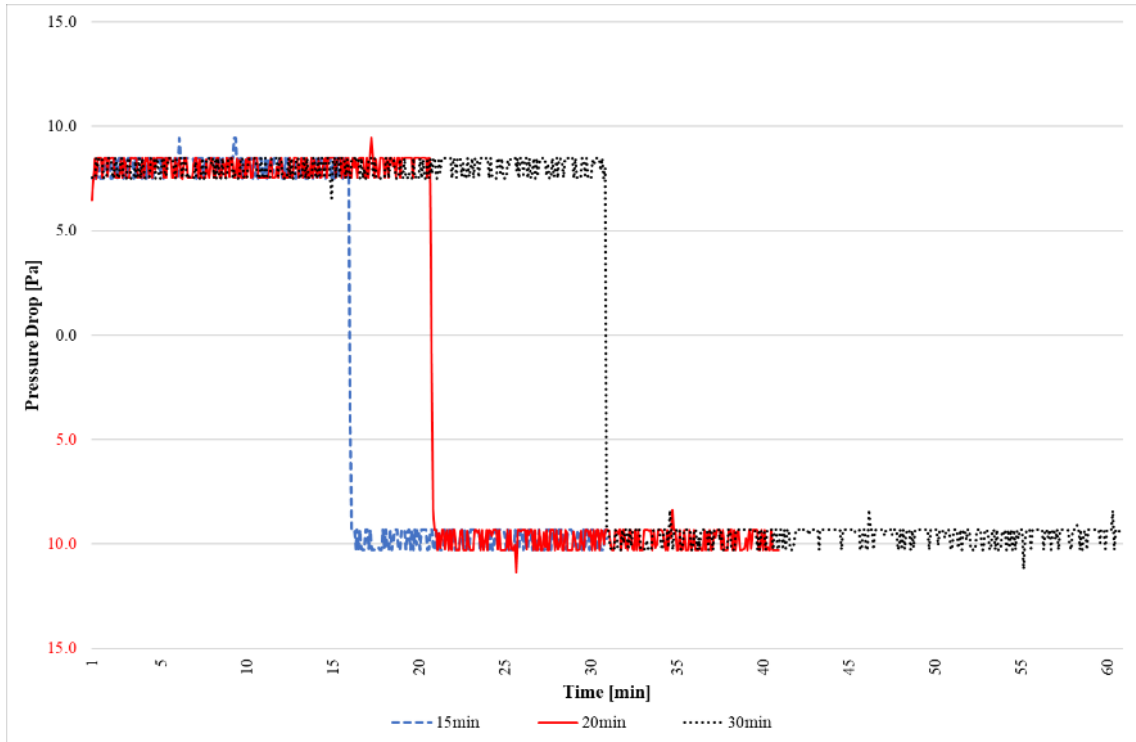
Figure 3.19. The pressure difference at the inlet and outlet of the systems while the fan operates in exhaust and supply modes for different running times for the tube bundle unit

Koper, Palmowska and Myszkowska (2020) measured airflow rates for different pressure drops, namely 0, 4, and 7 Pa, using a single room decentralized heat recovery unit in winter conditions. For 7 Pa, the volume flow rate was 22 m^3/h in supply mode and 6 m^3/h in exhaust mode. A regenerative heat exchanger effectiveness was calculated experimentally in the study of Zemitis et al. (2016). The results showed that for a 10 Pa differential pressure, fresh air deviations could range from 30% to 100% for the nominal flow rate of 30 m^3/h. Regarding these references, for the current experimental setup, the average pressure loss in this system is approximately 10 Pa (Figure 3.19), and the volume flow rate is 28 m^3/h in supply mode and 22 m^3/h in exhaust mode. So, the fan performances of the current study were quite better than the other studies (Zemitis et al. 2016; Koper, Palmowska and Myszkowska 2020) for the same and similar pressure drops.

And also, the tube structure affects the pressure drop. Kumar and Prabu (2015) compared the three different tube bundles for HRV units. The first is the smooth tube, the second is a micro fin-tube, and the last is a corrugated type of tube. According to pressure drop results, the smooth tube is better than the others. However, according to effectiveness results, the corrugated tube bundle gives more effectiveness. So, the pressure drop is related to the structural consideration.

3.5.2.3. Fan Characteristics

Before running the experiments, the fan characteristic of the system is obtained, and the common points in the direction of supply and exhaust are determined according to the normalized air velocity and the pulse width modulation (PWM). Also, it is seen that from Figure 3.20, the fan operates with 47% efficiency. The manufacturer fan characteristics result in appendix 2.
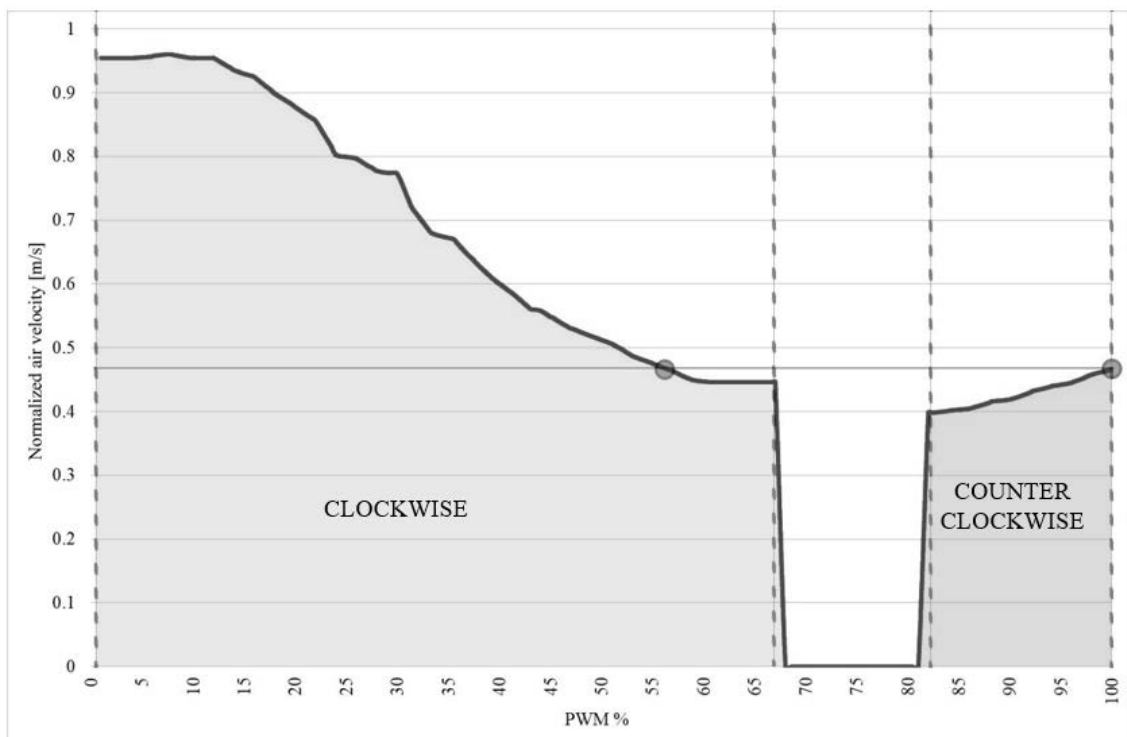
Figure 3.20. Calculated normalized air velocity

3.6. Usage of Thermal Energy Storage Material in Prototype

The most common PCMs are paraffin and salt hydrates. Phase change materials (PCM) are widely used in LHTES applications, and several studies have been conducted in the literature to review the applications of TES systems containing PCM in different applications (Dardir et al. 2019). Because of their high storage densities and latent heat properties, PCMs are frequently used for more energy storage in many applications for residential buildings (Bland et al. 2017). Pagkalos et al. (2020) compared the sensible heat storage and a latent heat storage medium with CFD. It was found that PCM can store 4.1 times more energy than water for the same volume of the storage tank. And the charging process duration of PCM is 3.9 or 3.0 times longer than water for the same volume of the storage tank, also depending on the tube length (Pagkalos et al. 2020).

All these studies are taken into account, in this experimental study, the tubes in the LHTES unit are filled with PCM to store thermal energy better for the same volume of the sensible energy storage unit. According to the climatic conditions of the experiment, RT27 is chosen. RT27, which is paraffin that changes phase at around 27°C, was placed in copper tubes in liquid form. The tube bundle consists of 100 copper staggered tubes filled with PCM at the airflow direction. Liquid PCM was poured into the tubes. The inner volume of a tube is 2.04 cm^3, and the total empty weight of the tube bundle is 906 grams. When the copper tube bundle is filled with liquid PCM, it weighs 1065 grams and 1062 grams when the PCM solidifies due to the difference in solid-liquid density. Therefore, on average, 1.6 grams of RT27 PCM (2016) can be added into a tube. The properties of the RT27 injected into the tubes and the physical properties of the air and copper are shown in Table 3.4. Studies by (Tokuç, Başaran and Yesügey 2015; Durakovic and Torlak 2017) are taken as the reference for the physical properties of PCM, and values for air and copper refer to (ASHRAE Standard-55 2010) for Table 3.4.

Table 3.4. Physical properties of RT27 (Tokuç, Yesügey and Başaran 2017; Rubitherm Technologies 2016), air, and copper (ASHRAE Standard-55 2010).

Name	Unit	RT27	Air	Copper	Ceramic
Density, Solid-phase (15°C)	kg/m^3	880	1.188	8900	~2200
Density, Liquid-phase (40°C)	kg/m^3	760	-	-	-
Specific Heat	kJ/kgK	2.4	1.0064	0.386	0.725
Latent Heat	kJ/kg	184	-	-	-
Thermal Conductivity	W/mK	0.2	0.024	400	1.4-1.5

3.7. Calibration Process

All thermocouples with datalogger used in the experimental setup are calibrated in the calibration laboratory of the Izmir Chamber of Mechanical Engineers. Thermocouple calibration was carried out in a constant temperature bath at 0°C, 7°C, 14°C, 21°C, 28°C, 35°C, and 42°C, considering different ambient conditions. Temperature measurement devices are calibrated by comparing a thermometer under calibration with a reference thermometer. The most common method for calibrating temperature sensors is to immerse the temperature sensors in a calibration bath (Figure 3.21). The calibration is performed by immersing the temperature sensors (Figure 3.22) (including a reference sensor). The temperatures measured by the calibrated sensor and the reference thermometer are taken as the basis, and the results of each thermocouple's measurements are fit to the base to ensure high accuracy.

Figure 3.21. Constant temperature bath.

Figure 3.22. Thermocouples with datalogger

The calibration process consists of reference instruments, test instruments, deviation, and uncertainty mean.

Reference instrument: To obtain correct measurement results, it is important to compare the devices with a fixed reference value with the constant case. A reference instrument is the same conditions as the system to be calibrated.

Test instrument: Represents the device to be calibrated.

Deviation: The value shows how much the measurement results deviate from the reference instrument measurement. This value is calculated using various statistical model methods. Table 3.5 shows the calibration results performed by comparing the temperature values measured from the reference instrument's measurement values with test instrument measurement values.

Table 3.5. Measurement results at 42°C.

Measured Unit	Reference°C	Test°C	Deviation°C	Uncertainty°C
UNIT-1-1	42.00	42.10	0.10	0.17
UNIT-1-2	42.00	42.20	0.20	0.17
UNIT-2-1	42.00	42.24	0.24	0.17
UNIT-2-2	42.00	42.15	0.15	0.17
UNIT-4-1	42.00	42.07	0.07	0.17
UNIT-4-2	42.00	42.19	0.19	0.17

Uncertainty: It refers to the measurement range by the test device. For instance, If the uncertainty of a test system calibrated at 42°C is ±0.17°C, we expect this system to measure 42°C between 41.83°C and 42.17°C. Measurement uncertainties are given in Table 3.5. The uncertainties with confidence probability value represent the standard uncertainty multiplied by the coverage factor k=2 providing about 95% confidence interval for the normal distribution. Detailed calibration results for thermocouples are in appendix 3.

3.8. Uncertainty Analysis

In experimental studies, some uncertainties affect the accuracy of the data. Uncertainty calculations were made within the scope of the method followed by Holman (2012) and Tokuc et al. (2015), which is also provided in ISO "Guide to the Expression of Uncertainty in Measurement" as the uncertainty analysis method for errors caused by an experimental set and measurement tools (Willink 2013). For a measurement with n variables, the result R is a function of the independent variables x_1, x_2, x_3...x_n, whereas w_1, w_2, w_3...w_n are uncertainties in the independent variables. R-value is expressed based on independent variables as

$$R = R(x_1, x_2, x_3 \dots x_n)$$

Eq. (3.1)

If w_R is defined as the uncertainty value in the result, the uncertainty of all independent variables are given with the same odds, then Eq. (3.2) is used;

$$W_R = [\left(\frac{\partial R}{\partial x_1}w_1\right)^2 + \left(\frac{\partial R}{\partial x_2}w_2\right)^2 + \left(\frac{\partial R}{\partial x_3}w_3\right)^2 + \cdots + \left(\frac{\partial R}{\partial x_n}w_n\right)^2]^{1/2}$$

Eq. (3.2)

For the experimental studies, the uncertainty analysis of the mass flow rate (Eq. (3)) and heat transfer rate (Eq. (4)) in the duct were calculated. Accordingly;

$$\dot{m} = \rho_a A_c V_a$$

Eq. (3.3)

$$\dot{Q} = \dot{m}c_p\Delta T$$

Eq. (3.4)

The uncertainty in Eq. (3.3) is caused by the density of the air (ρ_a), the cross-sectional surface area through which the air passes (A_c), and the average velocity of the air (V_a). The heat transfer rate uncertainty value in Eq. (3.4) depends on the mass flow rate ($\dot{m}$), the specific heat of air at constant pressure (c_p) and temperature difference (ΔT). Accordingly, parameters affecting the mass flow rate and the heat transfer rate for the air in the equations are defined as

$$\dot{m} = f(\rho_a, A_c, V_a) \qquad \text{Eq. (3.5)}$$

$$\dot{Q} = f(\dot{m}, c_p, \Delta T) \qquad \text{Eq. (3.6)}$$

The uncertainty values of each independent variable are given in Table 3.6. The uncertainty of the mass flow rate is calculated according to the parameters defined in Eq. (3.5). For the measured air velocity values obtained in the experiments, the uncertainty value was taken from the catalog value of the manufacturer. And later, it was determined to be approximate ~5.94% by interpolation. The uncertainty of the mass flow rate of air calculated for each independent variable given in Table 3.6 is ~6.27%.

Table 3.6. Uncertainty values of each independent variable measured in the experimental studies.

Variables	Value	Uncertainty	Specifications
Air density, ρ_a	1.184kg/m^3 @25°C	±0.02%	
Air velocity, V_a	0-1m/s	±5.94%	Manufacturer: BLITZSENS, Type: VS-C2-1-A, (2pcs)
The cross-sectional area which the air passes, A_c	0.0225m^2	±2%	
Temperature, T	0-42°C	±1%	Datalogger manufacturer: HIOKI, Type: LR8402-20 (K/T), (37pcs of Thermocouples)
Specific heat of air, c_p	1007 J/kgK @25°C	±0.02%	

The uncertainty of heat transfer rate during the experiments is calculated based on the parameters defined in Equation 3.6. The total uncertainty value of thermocouples with

datalogger was evaluated in accordance with the uncertainty of the devices used during the calibration. And the uncertainty of heat transfer rate is calculated as ~6.35% based on the mass flow rate, specific heat, and temperature uncertainty values.

3.9. Summary

This chapter presents the experimental methods of wall integrated HRV Systems. Firstly, the on-site measurements are represented. The next step is to calibrate the laboratory measurements according to the measured temperature, air velocity and pressure difference values. Also, in this chapter, the uncertainty values for measurement tools are detailed. The real-scale experiments were carried out in this study. The experimental setup consists of 8 main parts, which are the aerated concrete wall, simulated indoor and outdoor environments, HRV systems are integrated inside the two air ducts, and the heating/cooling constant temperature bath with a flowmeter condition the indoor, while a cooling group and a thermostat-controlled heater condition the outdoor environment. Air velocity, pressure drop, and temperature data play a critical role in estimating and characterizing the variation of the experimental setup flow rates, pressure differences, and temperature changes. This chapter also shares the procedure of these measurements, measuring devices used, and the uncertainty results. The average supply air velocity results are 0.215 m/s, and the exhaust velocity is 0.165 m/s for the ceramic unit. And the average velocity for supply air is 0.344 m/s, and the average for exhaust air is 0.282 m/s for tube bundle HRV prototype. For the SHTES, the fan produces an average pressure difference of 4.9 Pa, for the LHTES, 9.7 Pa. The total uncertainty of thermocouples with dataloggers was calculated using the devices' uncertainty during calibration. Based on the mass flow rate, specific heat, and temperature uncertainty values, the heat transfer rate uncertainty is ~6.35%.

CHAPTER 4

NUMERICAL ANALYSES

Numerical studies of the heat recovery units with phase change material (PCM) and ceramic material are carried out with the help of the ANSYS-FLUENT package program. Within the scope of the numerical study, temperature distributions and flow analysis in three-dimensional and two-dimensional flow geometries are investigated depending on time. The heat recovery units' geometric variables and operating parameters are differentiated, and design alternatives are created in this context. In addition, the system has been evaluated considering constraints such as thermal performance and pressure drop. Details of the numerical studies conducted are shared below.

4.1. Theory and Background

Fluid mechanics is a fundamental field that is the basis of many important industry and research topics, and fluid flow is studied experimentally, analytically, and numerically (Zhai 2006). In recent years, computational fluid dynamics (CFD) has been used frequently in research to predict the flow numerically developed by the analytical base. Besides, the advantage of experimental analysis is to it provides good resources to verify and validate different theories and models. However, most physical experiments can be expensive to implement, and limited data can be collected. On the other hand, most theoretical analysis in fluid mechanics can only be done for simple or simplified cases such as steady and one-dimensional problems. Numerical analysis solves complicated problems and equations. This approach has many advantages to solve the problems. The analysis with the computer takes a short period of time. And it can be simulated as real conditions. Also, the cost of the CFD is almost negligible when compared experimental approach. However, the most important disadvantage of this method is accuracy. It is very important to determine the boundary conditions for the accuracy of the results of the problems.

Along with the governing equations for velocity, the solution of mass, momentum, energy conservation equations, and 2D and 3D scales are also used in CFD programs.

CFD is used for many industrial areas such as HVAC, electronics, chemicals, etc. In the last years, CFD has played an important role in building designs, energy efficiency, indoor air quality, and thermal comfort in the built environment (Averfalk, Ingvarsson and Persson 2014). Thermal comfort and indoor air quality are affected by operating conditions, control strategies of HVAC systems. With CFD, the HVAC systems' efficiency can study by changing system control, supply, and exhaust air conditions. Also, the CFD can assist the natural ventilation strategies by modeling and optimizing building sites and indoor layouts (Zhai 2006).

4.2. CFD Modeling Procedure

The most important element in CFD, abstracting, simplifying from the real world into the simulation model with accurate solutions. To a successful CFD model, it is important to define sufficient details. When defining the problem, the flow characteristics to be simulated (steady/unsteady flow, laminar or turbulent flow, etc.) should be determined based on specific simulation goals and interests. After defining the problem, the material's physical properties are specified in CFD software. And then, boundary and initial condition setup is an important step in the simulation. To model fluid flow motions for momentum, mass, and energy transfer, the discretization and grid generation of the domain can give an adequate solution to the problem. Before running the CFD engine, the numerical control parameters specification such as convergence criteria and iteration number allowed maximum residues before running the CFD engine. Figure 4.1 shows the overview of the computational solution procedure for CFD problems (Ezan 2011).

Governing partial differential equations (mass, momentum and energy) & Boundary and initial conditions

↓

Discretization approaches (finite volume or finite differences)

↓

Basic derivations of finite volume or finite difference equations

↓

System of algebraic equations

↓

Numerical methods

↓

Approximate solutions of field variables
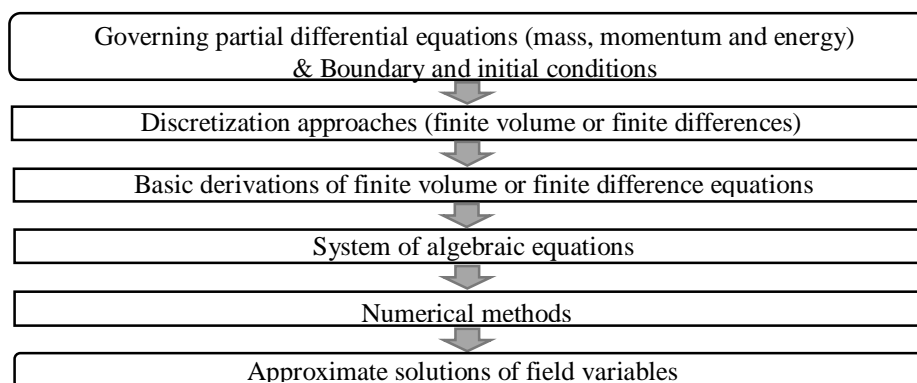
Figure 4.1. Schematic of CFD solution process.
(Source:Averfalk, Ingvarsson and Persson 2014)

4.3. Governing Equations

CFD programs generate solutions that apply to different flow elements for partial differential equations. The equations characterize the fluid flow with pressure, temperature, density, and velocities. These equations are known as the Navier-Stokes set of equations and the equation of state. The equations presented here are taken from the (Çengel and Cimbala 2018). For the unsteady laminar flow of a viscous, incompressible Newtonian fluid without free-surface effects, the equation of motion is the continuity equations (Çengel and Cimbala 2018).

In this study, the following main assumptions are considered:

- The fluids for two systems - which are SHTES' fluid is air, LHTES' fluid is PCM and air - are Newtonian and incompressible,

- The melting/solidification flow are time-dependent,

- The coordinate system is 2-dimensional Cartesian,

- No-slip conditions are valid for wall surfaces, and

- Viscous dissipation and radiation effects are neglected.

For the case of unsteady, incompressible, laminar flow of a Newtonian fluid with constant properties and without free-surface effects, the motion equation is to be resolved by CFD. A 2D Cartesian system of coordinates is used.

There are five equations and can be expressed as:

For continuity:

$$\frac{\partial(\rho)}{\partial t} + \frac{\partial(\rho u)}{\partial x} + \frac{\partial(\rho v)}{\partial y} = 0 \qquad \text{Eq. (4.1)}$$

For x-momentum:

$$\frac{\partial(\rho u)}{\partial t} + \frac{\partial(\rho u^2)}{\partial x} + \frac{\partial(\rho uv)}{\partial y} = -\frac{\partial \rho}{\partial x} + \left[\mu \frac{\partial^2 u}{\partial x^2} + \mu \frac{\partial^2 u}{\partial y^2} \right] \qquad \text{Eq. (4.2)}$$

For y-momentum:

$$\frac{\partial(\rho v)}{\partial t} + \frac{\partial(\rho uv)}{\partial x} + \frac{\partial(\rho v^2)}{\partial y} = -\frac{\partial \rho}{\partial y} + \left[\mu \frac{\partial^2 v}{\partial x^2} + \mu \frac{\partial^2 v}{\partial y^2} \right] \qquad \text{Eq. (4.3)}$$

For energy:

$$\frac{\partial(H)}{\partial t} + \frac{\partial(uH)}{\partial x} + \frac{\partial(vH)}{\partial y} = \frac{\partial}{\partial x}\left(k\frac{\partial T}{\partial x}\right) + \frac{\partial}{\partial y}\left(k\frac{\partial T}{\partial y}\right) \qquad \text{Eq. (4.4)}$$

x and y are the horizontal and vertical coordinates, and the velocities are u and v, respectively. ρ is the density, k is the thermal conductivity in equations. An enthalpy-porosity technique is used in ANSYS-FLUENT for modeling the solidification/melting process (ANSYS-Fluent, 2021). In this technique, the regions where such liquid and solid fraction of material coexist is called mushy zone. The liquid fraction lies between 0 and 1 in mushy zones. In the mushy zone, the porosity of 0 indicates the material is fully solidified, whereas 1 indicates the material is melted. The energy equation for PCM converted enthalpy definitions into the temperature-based form for LHTES. In Eq. 4.5, the H is the total volumetric enthalpy value. Total volumetric enthalpy is the sum of sensible and latent heat of the PCM, which is;

$$H = h + \rho_L f h_{sf} \qquad \text{Eq. (4.5)}$$

where h is the sensible enthalpy, ρ_L is the density of liquid PCM, f is the melting fraction and h_{sf} is the latent heat of fusion.

$$h = h_{ref} + \int_{T_{ref}}^{T} \rho c \, dT \qquad \text{Eq. (4.6)}$$

The sensible enthalpy' components are the density of PCM is ρ, specific heat which is c and dT is the temperature of the PCM (Ezan 2011).

4.4. Physical Domain

The geometry used for flow analysis has to be generated and imported for processing using CFD tools. This step in this current study is the 3D modeling step of the heat recovery system with ceramic and PCM tube bundle. The geometric model includes the design of the whole system with the other apparatus. In the "Design Modeler" tool of

the ANSYS program, firstly, the geometry is drawn in 2D, and the model is made 3D after. ANSYS Design Modeler is a tool for creating a geometry that connects directly to CFD meshing and analysis. However, one of the main reasons for using 2D modeling while analyzing the study is that the system flow geometry can be followed better and accurately and obtain the best convergence results. In addition, with this 2D model, temperature distribution and flow profiles are determined by monitoring the change in units to time-dependent, and pressure drops for different operating conditions of the system are analyzed. The geometry represents solid, physical objects, the fluid volume must be defined for CFD analysis (Calautit and Hughes 2014).

4.5. Mesh Generation

The grid generation is the most important step for the CFD solution: the cells on which variables are calculated throughout the computational domain (Çengel and Cimbala 2018). Many CFD simulations can run structured or unstructured grids. A structured mesh requires substantially less memory than an unstructured mesh with the same number of elements, as neighbor connectivity can be specified implicitly by array storage. And also, this grid generation can save time. The distinction between structured and unstructured meshes usually applies to the elements: quadrilaterals are typically used for two-dimensional structured meshes, while triangles are used for unstructured meshes. (Bern and Plassmann 2000).

In simple geometries, the structured grid is more applicable. In complex geometries, the unstructured meshes are allowed flexibility to define irregular shapes. The structured grids are more rapidly converged and more accurately than the unstructured grid for the CFD codes. It should be noted that regardless of the type of grid chosen (structured or unstructured, quadrilateral or triangle, etc.), the quality of the grid is most critical for accurate CFD solutions. (Çengel and Cimbala 2018). In this study, for the ceramic heat recovery system mesh structure is applied structured, for the tube bundle heat recovery system with PCM is applied to unstructured meshes.

4.6. Mesh Quality

Mesh quality is a key point for the accurate results of numerical simulation. Given a discrete boundary, the mesh is defined as an item judged to be reasonable in size and

quality (shape). The size relates to the greater or lesser thickness of the boundary discretization and continues to be properly defined within the domain. Quality is related to element aspect ratios (Borouchaki and George 2000).

Skewness is one of the main methods of measuring the quality of the mesh. Compared to an idealized cell, either triangular or quadrilateral, skewness measures the accuracy of a cell. The Fluent Meshing User's Guide (2020) defines the skewness of how close to ideal (equilateral or equiangular) a face or cell is (Figure 4.2). Highly skewed faces and cells are unacceptable, as the equations assume that cells are relatively equilateral/equiangular.

Equilateral triangle   Highly skewed triange

Equiangular quad   Highly skewed quad
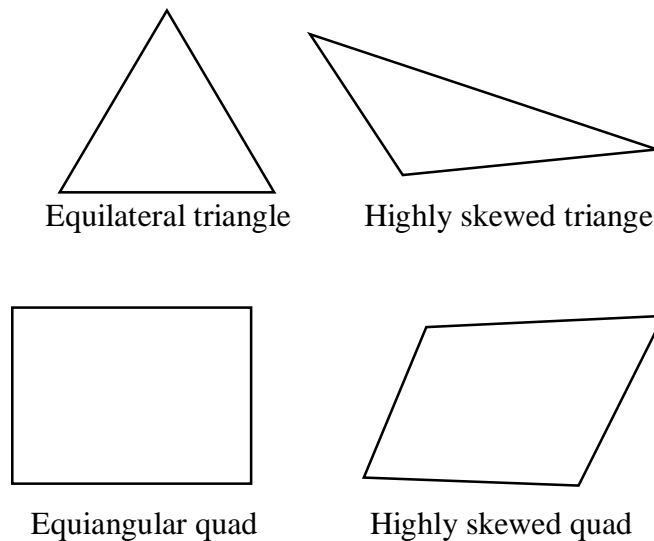
Figure 4.2. Ideal and Skewed Triangles and Quadrilaterals.
(Source: Borouchaki and George 2000)

Two methods can be used to measure skewness; the first is based on the equilateral volume, which is only for triangles and tetrahedral, and the second is based on the deviation from a normalized equilateral angle, which is for pyramids and prisms. In the equilateral volume deviation method, skewness is defined as Eq.4.7.

$$Skewness = \frac{Optimal\ Cell\ Size - Cell\ Size}{Optimal\ Cell\ Size} \qquad \text{Eq. (4.7)}$$

According to The Fluent Meshing User's Guide (2020), for mesh quality, the skewness value is approximately 0.1 for 2D and 0.4 for 3D. Table 4.1 shows the range of skewness values and corresponding cell quality. When between 0.25 and 0.5 is good quality mesh according to the skewness range, the 0-0.25 is excellent, and the 0.75-0.9 range is considered fair. 0.9 and above values are classified as poor and bad quality. As the equations assume that the cells are equilateral, cells are classified as bad, and degenerate are unacceptable.

Table 4.1. Range of skewness values and corresponding cell quality.

Value of Skewness	Cell Quality
1	Degenerate
0.9-<1	Bad
0.75-0.9	Poor
0.5-0.75	Fair
0.25-0.5	Good
>0-0.25	Excellent
0	Equilateral

4.7. Simulation Details of the HRV Units

The CFD model is designed according to a real-scale laboratory experiment. This CFD model is analyzed as the same room and equipment and indoor and outdoor environmental conditions. In the CFD model, the dimensions of all parts of the HRV units and duct in the experimental setup are designed the same. This part includes problem identification, mesh generation, mesh quality and mesh verification, and boundary conditions for the CFD model.

4.7.1. Problem Identification

In Chapter 3, the experimental setup of the system and the experiments for two separate HRV systems are in detail. In CFD, the duct has the same dimensions as the experiments. The duct has a fully developed laminar flow area of 1.5 meters after the HRV unit to the outlet. A 15 cm by 15 cm HRV unit is placed inside this duct, which has

a section of 15 cm by 15 cm. The distance between the unit and the inlet is 0.06 m. As seen in the experimental setup, there is a filter and a fan. However, filter and fan are not defined in the CFD model, and only boundary conditions are assigned to the surfaces. Figure 4.3 shows the CFD model in general terms. In the simplified drawing, there are general dimensions of the model. First, experiments were carried out with the ceramic system available in the market in the area reserved for the HRV unit, and then experiments and CFD analyzes were carried out on the prototype. As shown in Figure 4.3, the system consists of 3 main parts. In the system design, area I is the inlet section where the fresh air will be transferred to the indoor environment, area number II is the tube bundle where the HRV unit is located, and number III is the conditioned air outlet transferred to the indoor environment.
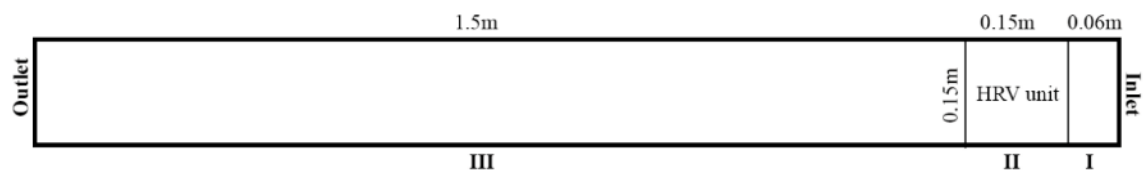
Figure 4.3. Simplified section for duct and dimensions.

4.7.1.1. Ceramic System for Sensible Thermal Energy Storage

The project shown in Figures 4.4a and 4.4b are 2D and 3D images of ceramic heat recovery systems modeled in the Design Modeler tool. While the area I have seen in Figures 4.4a and 4.4b represents the region from the outlet to the HRV unit, the area where the ceramic HRV unit is located is indicated as II. Simulations to be made will continue over only one cell ceramic.

a)

b)
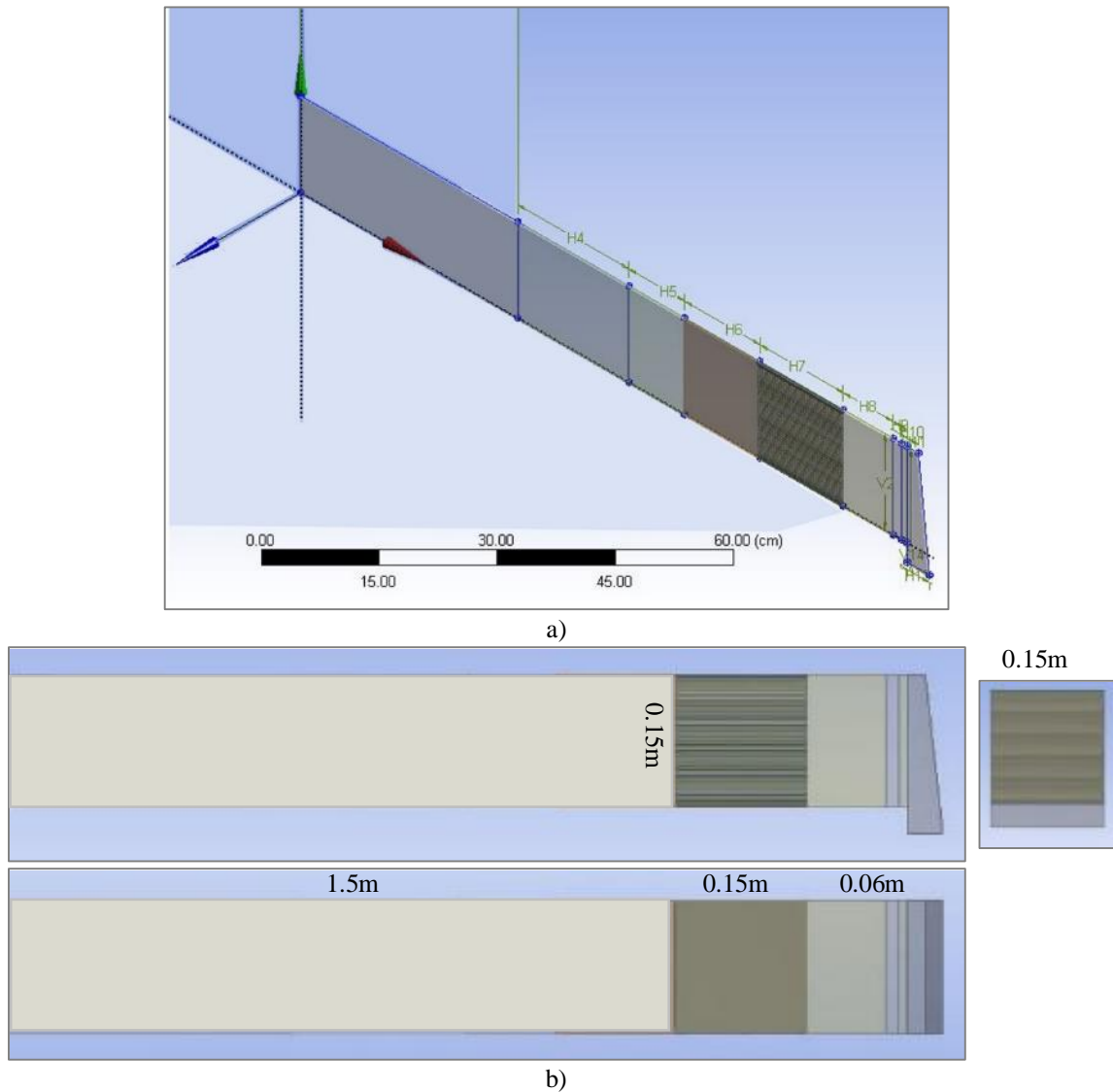
Figure 4.4. a) Overview of the 3D ceramic heat recovery system and b) 2D views designed in the Design Modeler module

4.7.1.2. Tube Bundle System for Latent Thermal Energy Storage

Tube bundle system placed in the duct in the area indicated in figure 4.5. The project shown in Figures 4.5a and 4.5b is 2D and 3D images of the tube bundle system designed in the Design Modeler tool. As seen in Figure 4.5b, a symmetrical region which name is the computational domain, has been chosen in the 2D model to be simulated. Future analysis will continue through this zone. The 0.135 m represents the area in the middle of the 5th and 6th tube from the inlet indicated in this figure. Grid convergence and static pressure, as well as velocity values calculated in the following sections, are detailed on this surface.
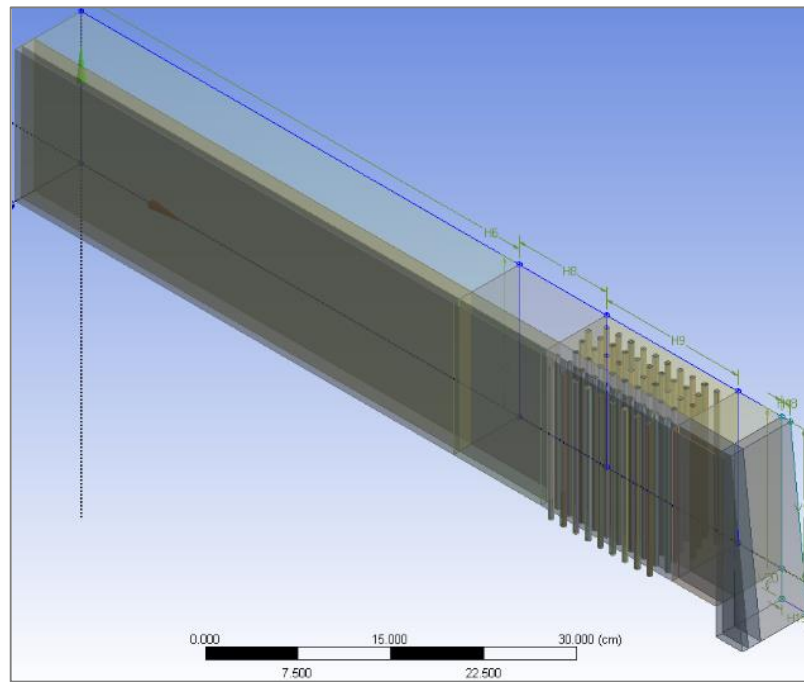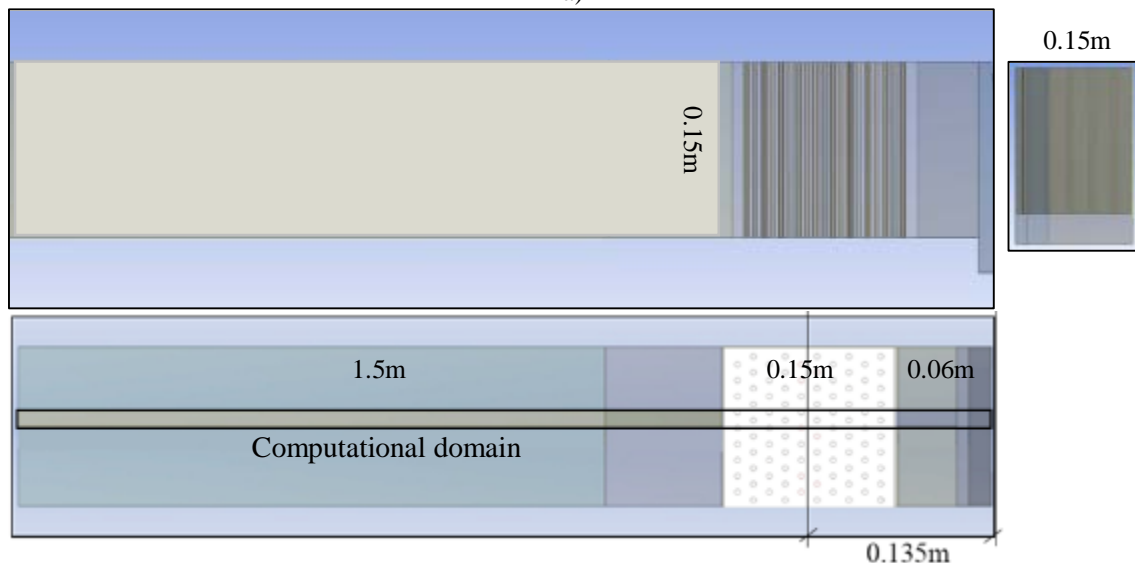
Figure 4.5. a) Overview of the 3D tube bundle heat recovery system and b) 2D views designed in the Design Modeler module

4.8. Numerical Approach

CFD is a computer-based engineering method and a numerical approach in which detailed calculations can be done (Karaçavuş and Aydın 2017). CFD is performed to investigate the heat transfer performance and fluid flow characteristics. First, the model is primarily divided into mesh within the Fluent program. Then, flow analysis is obtained with the ANSYS-Fluent tool.

4.8.1. Mesh Generation

For the study of the CFD model, the generation of the computational mesh from the fluid volumes is provided. In defining the accuracy of a solution, mesh quality is an important factor, and thus many designers spend a considerable amount of time ensuring that the mesh is suitable for the simulations. For each geometry, the individual mesh is to be created before simulations. With the system's design, a mesh structure is created, regions are defined as solid and liquid, and boundary conditions are determined. There are some points to be considered in defining mesh. The size and type of the elements are important to obtain the most accurate result. Because the use of more elements causes both excessive calculation time and an increase in error rate. The boundary layer is a thin region that is close to the fluid. And to accurate results would be placed as many gird points as possible to the wall. Also, attention should be paid to deformities that may occur in the elements. It is important not to exceed the 0.9 value given as the maximum value for the coefficient of skewness not to give calculation errors in the FLUENT program. The automatic mesh generation should not be done when analyzing complex geometries.

A few other analytical analyses need to be done before generating the meshes. It is controlled according to grid independence on the specified plane's residuals and temperature, pressure, and velocity values. The total number of cells is determined in three different models: coarse, medium, and fine grids, and the results are compared. If the residues reach a certain value and no longer change, we assume it converges (Werner 2016).

4.8.1.1. Grid Independence Study

The mesh resolution can affect the result of a CFD simulation. A grid independence study is performed in the study. Besides the mesh resolution, convergence can influence the result as well. Accordingly, mesh independence is obtained with the grid convergence index. The term grid convergence index (GCI) compares the numerical results of the same problem belonging to different mesh structures. Different mesh sizes are based on the same boundary conditions as all other models (Roache 1994). A grid convergence study is a necessary test in any CFD simulations (Zhao and Su 2019). The solution is in the asymptotic range of convergence when the GCI value for the meshes

used in the simulation is small. The mesh is refined at least three times, each time solving and getting results until an asymptotically converged solution is obtained.

Many cases estimate meshes for the GCI method in the literature (Roache 1994; Hirt and Nichols 1981; Karimi et al. 2012). Celik and Hu (2004) demonstrated an error transport equation to quantify the discretization error. To calculate the GCI, there are three steps to define this value.

Step 1. First, the mesh size "h" (Eq.4.13) assigned to the 2-D geometry is calculated on the representative cell.

$$h = [\frac{1}{N} \sum_{i=1}^{N} (\Delta A_i)]^{1/2}$$

(Eq. (4.13)

where ΔA_i is the area of the ith cell and N is the total number of the cells.

Step 2. After the defined grid refinement factor between specified meshes, the second step is to calculate the apparent order p of the method using the expression. p is the formal order of accuracy of the algorithm, and which can be computed using Eq 14.14

$$p = \frac{1}{\ln(r_{23})} \ln \left[\frac{(r_{23}^p - 1)e_{12}}{r_{12}^p - 1)e_{23}} \right]$$

Eq. (4.14)

where r_{23} and r_{12} represent ratios of the h value of the meshes. The third grid is the "coarse" mesh size, the second grid is the "medium" mesh size, and the first grid is the "fine" mesh size. Here, e is the analysis result for the specified variables, and e_{12} and e_{23} represent the differences between variables. The variables used in this calculation are pressure, temperature, and velocity for the specified plane, which is 13.5 cm from the inlet.

Step 3. The third step is the calculation of GCI along with the apparent order p. (Gümüş, Seven and Şimşek 2020).

$$GCI_{23}^{fine} = F_s \frac{|E_{23}|}{r_{23}^p - 1}$$

Eq. (4.15)

where E_{23} expresses the fluid's velocity, pressure, and temperature values at the point determined in fine mesh resolutions 1, medium mesh resolutions 2, and coarse mesh resolutions 3. And the F_s is a safety factor. Roache (1994) recommended a range of 1.25 $\leq F_s \leq 3$ for the safety factor. This factor is a statistical analysis for a large number of samples based on analytical or numerical benchmarks (Xing and Stern 2010). Also is used to convert the best error estimate into a 95% confidence interval, uncertainty estimate. The selection of the magnitude of this factor depends on the intended accuracy (Karimi et al. 2012). In this calculation, the safety factor is taken as 1.25.

In light of this information, mesh independence studies for ceramics and tube bundle systems are shared in this section. Six different meshes have been simulated for ceramic and tube bundle systems.

4.8.1.1.1. Ceramic System Mesh Structure Decision

Three different modules have been generated on the ceramic unit's mesh tool, shown in Figure 4.6. These are fine, medium, and coarse modules. This figure shows the boundary layer effect on the ceramic edges; an appropriate mesh density is preferred in these areas. In this study, a mesh structure is created using quadrilateral elements with edge sizing and face meshing features.

The ceramic system boundary condition is the same with experiments. For ceramic systems, the outdoor temperature is 5°C, and the indoor temperature is kept 20°C. According to air velocity measurements, the average supply air velocity results are 0.215 m/s. In this study, six different grid densities of unstructured quadrilateral grids are generated for ceramic HRV units with 7204, 31812, 55944, 88000, 136136, and 264660 nodes, respectively shown in Figure 4.7. All the parameters for the six simulation runs are kept the same.
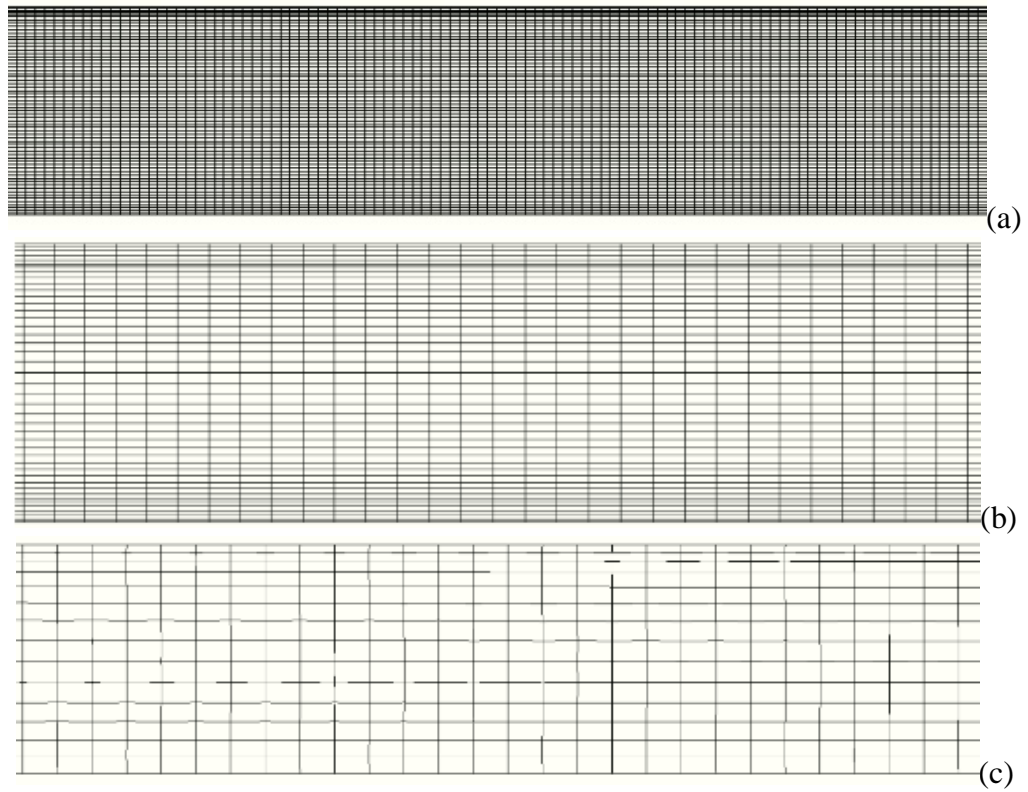
Figure 4.6.   Three different modules for meshes (a) fine, (b) medium, (c) coarse for ceramic unit
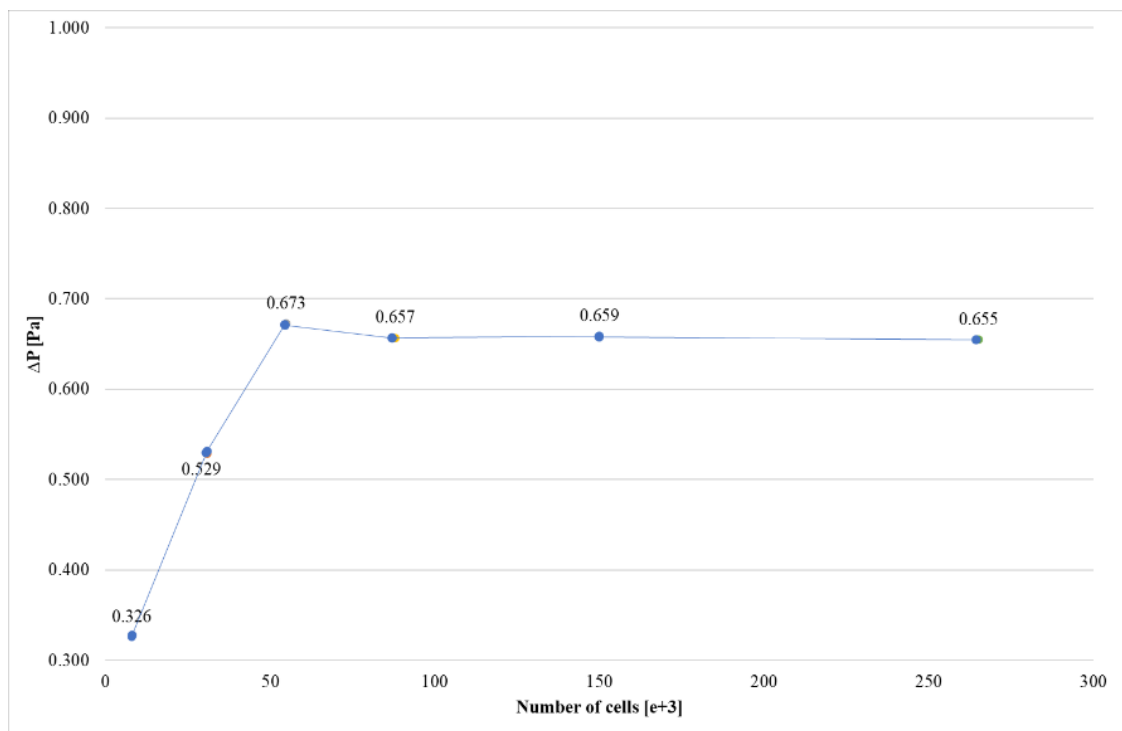
Figure 4.7. Calculated pressure as a function of the number of cells at the x=13.5 cm

The mesh convergence index is calculated on the coarse mesh resolutions with 7204 cells, the medium mesh resolutions with 55944 cells, and the fine mesh resolutions with 264660 cells (Table 4.5).

Table 4.2. Mesh properties.

	Mesh	Type	No. of cells
1	Fine	quadrilateral	264660
2	Medium	quadrilateral	55944
3	Coarse	quadrilateral	7204

The values found by the grid convergence method are given in Table 4.6. As shown in this table, there are three different variables for calculation. The results are obtained in the table when the analysis is made at 13.5 cm. Looking at the velocity, temperature, and pressure values, the GCI value is -9E-08%, -3E-03%, and -2E-04%, respectively. The computational accuracy is shown to be independent of the mesh density.

Table 4.3. Grid convergence index results for x=13.5 cm.

	Velocity (m/s)	Temperature (K)	Pressure (Pa)
h_1	0.095	0.095	0.095
h_2	0.031	0.031	0.031
h_3	0.021	0.021	0.021
e_1	0.320	306.820	0.327
e_2	0.320	306.940	0.660
e_3	0.320	306.919	0.655
p	-1.463	3.580	0.895
GCI (%)	-9E-08	-0.0029	-0.0002

4.8.1.1.2. Tube Bundle System Mesh Structure Decision

For this model, one case is determined. In Table 4.3, pressure change, temperature, and velocity are given at 35°C. These data are calculated according to S_T is 0.014 m,

velocity is 0.345 m/s as a measured value in experiments. The height of one tube is 15 cm, and its outer diameter is 4.76mm. Liquid PCM is poured into the tubes having 0.3 mm wall thickness. Those calculations are solved according to Zukauskas's (1972) Method. And according to this velocity, the Reynolds number is 152.472. It can be seen that the assumption of laminar flow valid is here. The geometry is created according to these values. Three different modules have been generated on the mesh tool, shown in Figure 4.8. As shown in Figure 4.8, since the boundary layer effect will occur on the tube walls, an appropriate mesh density is preferred in these zones. The sensitivity of the solution has been increased by using a mesh structure in the zone where the tubes where the PCM is located. This type of mesh structure is extremely important for the accuracy of the solution results. In this study, a mesh structure is created using triangle and quadrilateral elements.
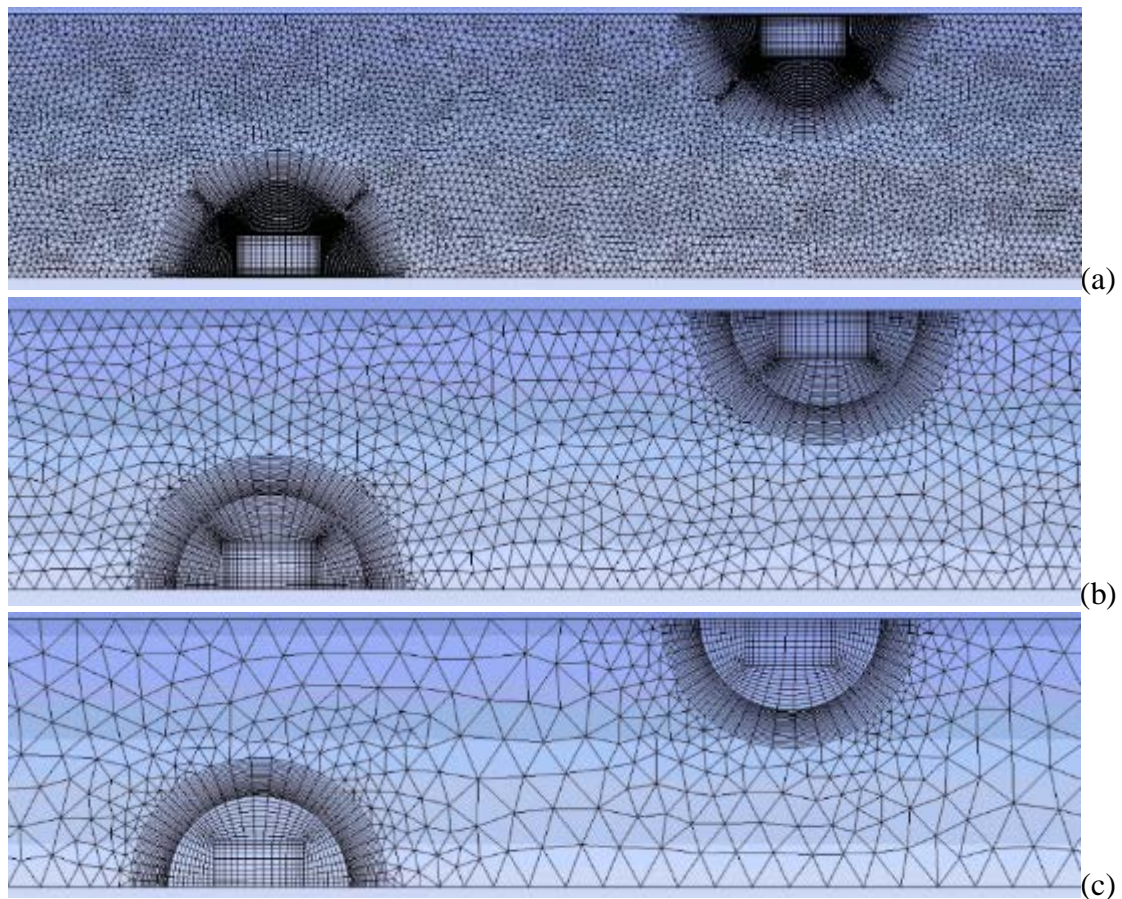
Figure 4.8. Three different modules for meshes (a) fine, (b) medium, (c) coarse for tube bundle unit.

Before calculating the grid convergence index, many cases have compared each other according to a calculated static pressure value. Many mesh structures have been analyzed, and these can be classified as very coarse, coarse, medium, fine, very fine, ultra-fine. Figure 4.9 is the calculated static pressure x=13.5 cm (the middle of the HRV unit) from the inlet in the Fluent analysis program. The various grid resolution cases in the entrance flow region of duct flow function of the number of cells. The number of cells Case 1 is 5×10^3 the data for pressure is 0.2045 Pa, Case 2 is the 20×10^3 which is 0.1739 Pa, Case 3 has 50×10^3 cells, and for this case, the result is 0.1778 Pa, Case 4 is the $200 \times 10^{3,}$ and the result is 0.1802 Pa, Case 5 has 250×10^3 cells, Case 6 has 300×10^3 cells, and the calculated data are 0.1801 Pa and 0.1808 Pa, respectively.
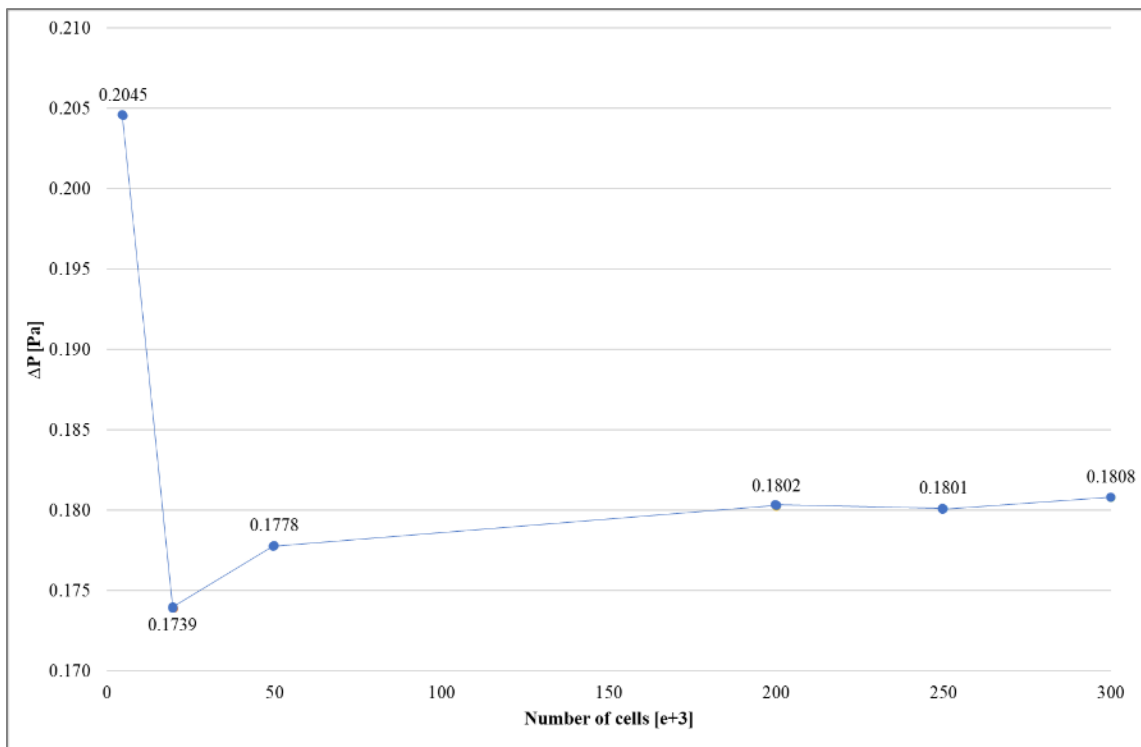
Figure 4.9. Calculated pressure as a function of the number of cells at the x=13.5 cm.

The mesh convergence index is calculated on the coarse mesh resolutions with 22781 cells, the medium mesh resolutions with 54185 cells, and the fine mesh resolutions with 189539 cells (Table 4.7).

Table 4.4. Mesh properties.

	Mesh	Type	No. of cells	Max_skewness
1	Fine	quadrilateral, triangle	189539	0.81769
2	Medium	quadrilateral, triangle	54185	0.62852
3	Coarse	quadrilateral, triangle	22781	0.50002

The values found by the grid convergence method are given in Table 4.8. Here are the results obtained from 3 different mesh structures. The results are obtained when the analysis is made at 13.5 cm in the table. Looking at the velocity, temperature, and pressure values, the GCI value is 0.0002% in the velocity analysis, -0.000042% in the temperature analysis, and 0.0097% in the pressure differences for 13.5 cm from the inlet. As a result, it is concluded that the computational accuracy is independent of the mesh density. The fine mesh is chosen for the study as it is accurate enough and more efficient.

Table 4.5. Grid convergence index results for x=13.5 cm.

	Velocity (m/s)	Temperature (K)	Pressure (Pa)
h_1	0.029	0.029	0.029
h_2	0.024	0.024	0.024
h_3	0.018	0.018	0.018
e_1	0.346	307.990	0.174
e_2	0.344	307.990	0.178
e_3	0.343	308.000	0.180
p	7.598	-19.683	3.591
GCI (%)	0.0002	-0.000042	0.0097

4.8.2. Boundary Conditions

The next step in generating the mesh is to determine the appropriate limits of initial boundary conditions for the surfaces affecting the fluid flow to complete the effective simulation and solution of a CFD model. The boundary conditions of this study should also represent the experimental conditions. Computational domain, boundary, and initial conditions used in numerical modeling are given in Figures 4.10a and 4.10b. As seen in these figures, there are physical boundaries of inlet, outlet, symmetry, and wall. The symmetry condition prevents flow from crossing the boundary but allows the flow to move along the boundary (Albatayneh, Alterman and Page 2018). The experiment determines the horizontal velocity component as the inlet boundary condition, and the

uniform velocity inlet is defined as 0.34 m/s for the tube bundle and 0.21 m/s for the ceramic, while the vertical velocity component is taken as 0. All simulations for ceramics were made on one cell. However, here, unlike the velocity value measured at the duct inlet, the velocity value for a single cell is recalculated over the flow rate, and the air velocity flow through a single cell is 0.32 m/s.

a)

b)
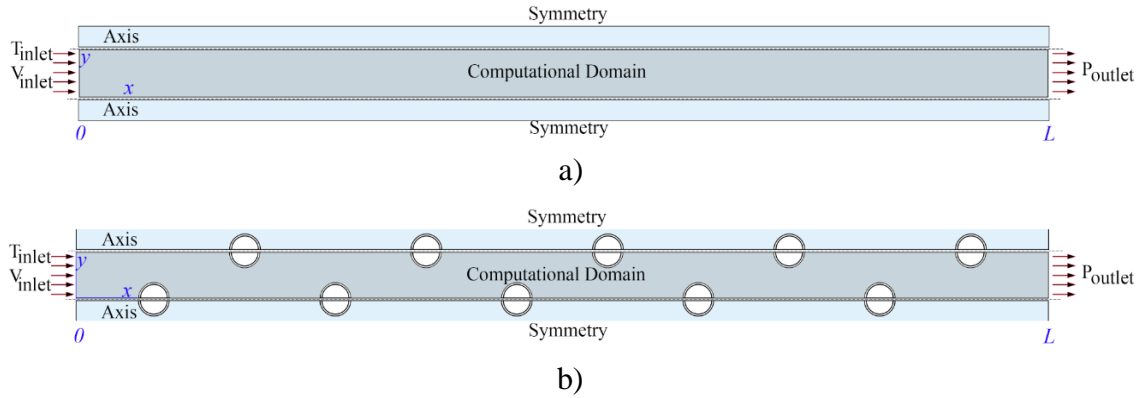
Figure 4.10. Computational domain and boundary conditions of a) ceramic and b) tube bundle system.

The required boundary conditions are shown in Table 4.9. The physical boundaries comprise inlet, outlet, symmetry, and wall. It is assumed that the whole domain is initially at the ambient temperature. Temperature and velocity are fixed values at the inlet and the tube wall during initialization. There is a no-slip condition for walls to achieve realistic velocity profiles close to walls. And on the symmetry the velocity component and the gradients are zero (Maheshwari, Chhabra and Biswas 2006).

Table 4.6. Boundary definitions.

Inlet	Velocity Inlet	$x = 0 \rightarrow T = T_{inlet}$
		$x = 0 \rightarrow v_x = U_{inlet}$
		$x = 0 \rightarrow v_y = 0$
Outlet	Pressure	$x = L \rightarrow P_{outlet} = 0$ (gage)
Body surfaces	Symmetry	$\partial T/\partial_y = 0$
		$v_y = 0$
		$\partial v_y/\partial y = 0$
		$\partial v_x/\partial y = 0$
Tubes	No-slip	$v = 0$

4.8.3. Solution Method

The Ansys Fluent software has 2 different solvers: the pressure-based and density-based coupled solver. For the tube bundle prototype, the pressure-based solver can be used for forced flow conditions included melting and solidification problems (Al-Abidi et al. 2013). This solver uses an algorithm in which the conservation of mass of the velocity field is obtained by solving a pressure equation (Chorin 1968). Also, the first-order upwind, power-law and second-order upwind schemes are widely used for solidification and melting problems. Convective terms in momentum equations, energy equations are discretized using a second-order upwind interpolation scheme, and turbulent equations are first-order upwind interpolation schemes. The SIMPLE algorithm does the pressure-velocity coupling for interpolation. The material physical properties are related to the problem, and the materials' density, heat capacity, thermal conductivity, viscosity can be changed. The user can define individual component properties (Chapter 3-Table 3.2).

Convergence is obtained when the residual of the continuity, momentum, and energy equations are reduced to less than 10^{-6}, $10^{-6,}$ and $10^{-8,}$ respectively, and the iteration number used is 1000 for each time step to generate better convergence criteria (Gürel 2020; Driels and Shin 2004) The time step is set as 0.1s for tube bundle and ceramic heat recovery system. In this study, these HRV units LHTES and SHTES are solved in a 2D plane. All solution methods are the same for tube bundle and ceramic heat recovery systems.

4.8.4. Model Verification and Validation

In this work, the flow model replicates the computer and experimental models to identify and eliminate errors. For the verification process, the model is implemented of the computer model. This model is a numerical procedure for solving equations prescribed in the mathematical model with a computer code.

4.8.4.1. Verification of Method with Reference Study

In Figure 4.11, the analysis of Reynolds and Nusselt number results are compared to find the accuracy of the Fluent settings and mesh structure in a single sphere on the duct. In this analysis, water is used instead of air, and the accuracy of the established Fluent and mesh structure is compared with the reference study (Yıldırım et al. 2017; Maheshwari, Chhabra and Biswas 2006). Nusselt number changes obtained in numerical and reference studies are compared for a single sphere. In these analyzes, the Reynolds number is taken as 1, 5, 10, 50, and 100. As a result, it is seen that the Nusselt number increases while the Reynolds number increases. In other words, Re and Nu numbers increase in direct proportion. The Nusselt numbers obtained in the present study and the values in the reference article, and the numerical data are coherent (Maheshwari, Chhabra and Biswas 2006). To calculate the Nusselt number, the total surface heat flux value is taken from simulation results and Eq. 4.9 is applied. While calculating the Reynolds number, the inlet velocity is important.
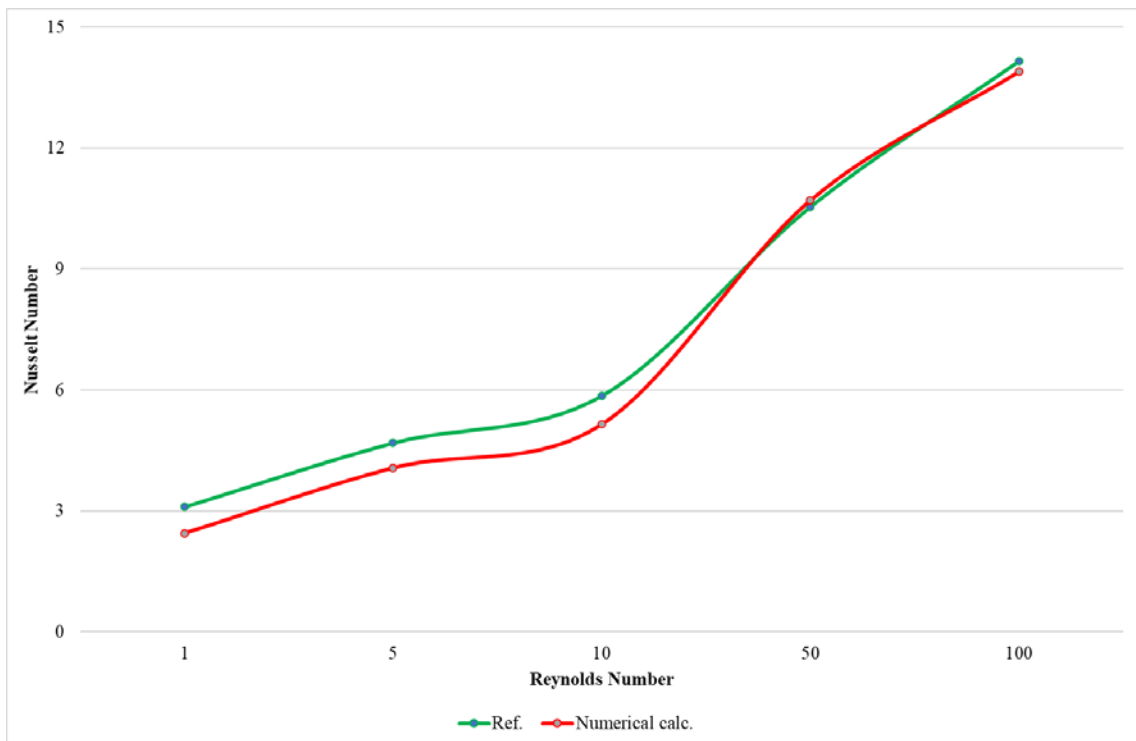
Figure 4.11. Verification of the method for a flow analysis of the numerical calculation results and the reference study (Source: Yıldırım et al. 2017; Maheshwari, Chhabra and Biswas 2006).

4.8.4.2. Validation of Model for Ceramic Heat Recovery System

After verifying the numerical method of the model, experimental validation outcomes and numerical outcomes have compared each other. Time-dependent variations of computed temperature and experimental results are compared in Figure 4.12 and Figure 4.13. For validation, a physical experiment is conceived and designed. The study is solved in a 2D plane. Figure 4.12 is the verification of the method for a flow analysis of the experimental results for ceramic HRV units. As shown in this figure, the charging and discharging process is 2-minute. The experimental data measured by the instruments are recorded with a datalogger in time steps of 5 seconds during the experiments. In CFD, the time step size is 0.1 s. According to this figure, the average temperature values standard deviation for the charging process is 0.65%, for the discharging process, it is 1.59% compared with CFD and experimental study results.
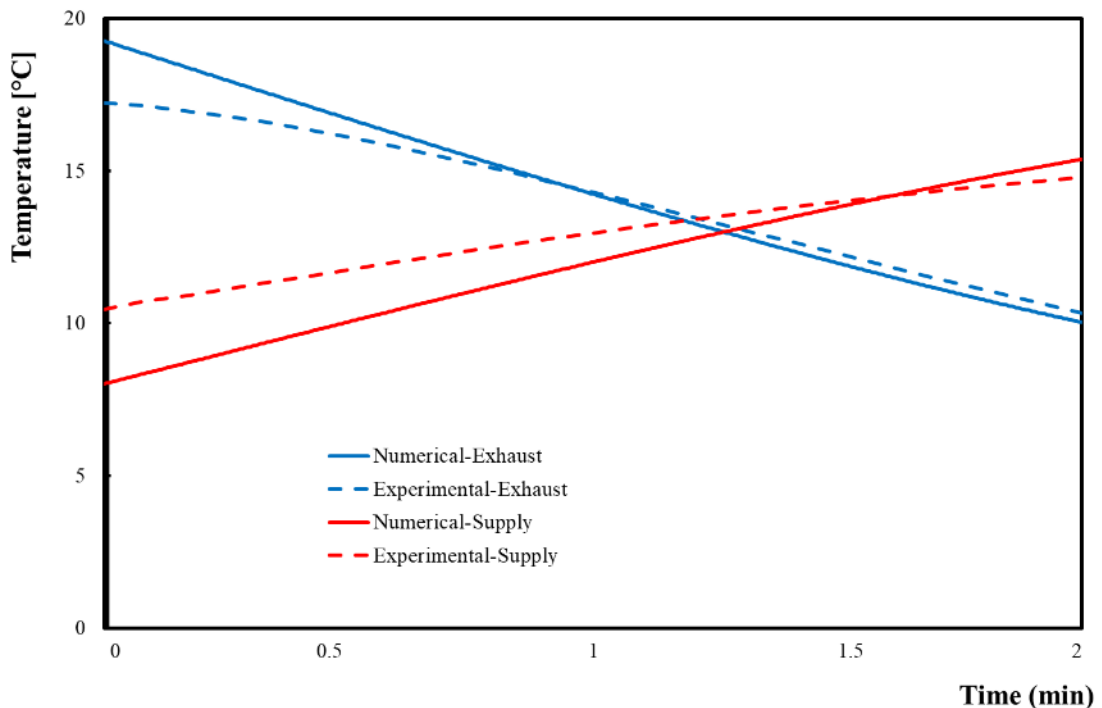
Figure 4.12. Verification of the method for a flow analysis of the experimental results and numerical calculation results for ceramic system.

4.8.4.3. Validation of Model for Tube Bundle Heat Recovery System

The other verification study for the tube bundle system. The experiments are conducted with LHTES HRV units using RT27 for the PCM and air for the HTF. Figure 4.13 has a charging and discharging process for both analysis models for 15-minute results. During the charging and discharging process in the experiment, the data is recorded at 5-second intervals. For the numerical analysis time, the step size is 0.1. The information about the measured points is given in Chapter 3, and the average temperature of the tubes and the result obtained from the numerical study are compared in this graph. As a result, while the average temperature values standard deviation for the charging process is 1.32%, for the discharging process, it is 1.38% compared with numerical solutions and experimental study results. In this study, it has been shown that the numerical model can be used to examine melting and heat transfer in LHTES systems with different geometries.
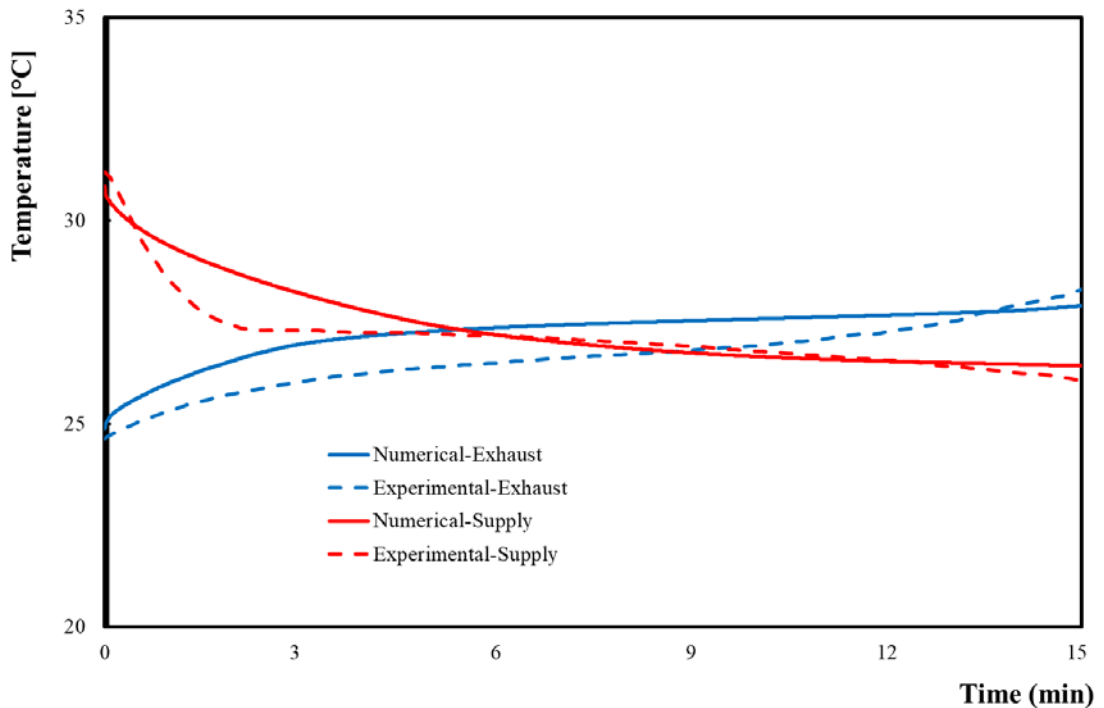
Figure 4.13. Verification of the method for a flow analysis of the experimental results numerical calculation results for tube bundle system

4.9. Summary

This chapter is provided the theoretical background of the CFD for modeling and simulation. The geometry modeling, mesh structure, solvers, and equations used for CFD model results to be accurate and reliable are mentioned. The GCI is calculated according to pressure change, temperature, and velocity to accurate results. And also, before calculating the grid convergence index, many cases have compared each other according to a calculated static pressure value to minimize the effect of such errors and uncertainties.

Using the knowledge gained from the CFD analysis, many different configurations of tube bundle heat recovery systems with PCM are modeled and analyzed. Their boundary conditions and some of the geometries are changed. Each system is modeled and analyzed with varying tubes, inlet, and outlet temperatures. The flow properties of the two types of heat recovery systems, especially the prototype heat recovery system, are investigated by reproducing the conditions observed in the experiments with the CFD model.

CHAPTER 5

RESULTS AND DISCUSSION

The following chapter details the experimental results and CFD simulations results for decentralized heat recovery systems with two different concepts of TES. The decentralized HRV systems store

- sensible energy into ceramic material and
- latent energy into the tube bundle containing PCM.

The boundary conditions are defined for the CFD according to experimental measurements. The CFD simulations are validated using the results of the experiments given in Chapter 4. Therefore, the accuracy and reliable solutions of the numerical analysis are suitable for different arrangements and configurations.

In the context of this study, the thermal energy storage performance of the HRV systems is firstly evaluated by the experiments. Two decentralized HRV systems work in synchrony one by one during the experiments. At the same time, one system exhausts air from the inside, the other supplies fresh air from the outside.

This chapter contains 4 subtitles. The first section is the experimental results, the second section is the numerical results, the third section is the refinement of the tube bundle HRV system, and the fourth section is the simulations made in different climates. In this chapter, the charging and discharging results are shared for both experiments and numerical studies. In addition, after the experiments and numerical studies, different refinement cases are simulated for the LHTES HRV unit, and the results are examined. Besides these refinement simulations, analyzes are made in different climatic conditions the energy performance of the tube bundle prototype is produced.

5.1. Experimental Results

Experimental setup detailed in Chapter 3, the real-scale experiments are carried out in the Building Physics Laboratory of the Izmir Institute of Technology, Faculty of Architecture. Controlled parametric studies are carried out experimental testing of the ceramic HRV unit and the tube bundled HRV unit. During these experiments, the systems

placed in the two ducts work synchronously. In one experimental set, HRV units with SHTES and in another set of HRV units with LHTES are experimentally investigated under different operating conditions. In this section, the results are shared in detail.

5.1.1. Charging and Discharging Experiments for SHTES

In this study, seven experiments are detailed for two decentralized heat recovery units operating simultaneously, the duct and the simulation rooms were monitored until steady-state conditions were attained before recording measurements for each experiment. For the simulation of summer conditions, the indoor environment is kept at around 20°C, and the outdoor environment is kept at approximately 35°C, while in winter conditions, the indoor environment is kept constant at around 20°C and the outdoor environment approximately at 5°C. The heat recovery units were operated for specific cycles of; 1-minute, 2-minute, 5-minute, 7.5-minute, and 10-minute, as given in Table 5.1.

Table 5.1. Experiments and conditions.

Investigated Parameter	Conditions		Constant Parameters	Variables
Time	Winter	1-minute	-Indoor Temperature (20°C) -Outdoor Temperature for winter (5°C), for summer (35°C) -Supply Velocity (0.21 m/s) -Exhaust Velocity (0.16 m/s)	-Duct Inlet Temperature - Duct Outlet Temperature -Ceramic Temperature - Pressure Difference -Velocity
		2-minute		
		5-minute		
		7.5-minute		
		10-minute		
	Summer	7.5-minute		
		10-minute		

The depths of the thermocouples are coded as follows; 1-1 and 2-1 represent the thermocouples at 12 cm, while 1-2 and 2-2 at 9 cm, 1-3 and 2-3 at 6 cm, 1-4, and 2-4 represent the thermocouples at 3 cm depth for D1 and D2, respectively, in Figures 5.1. These four thermocouples are also mentioned as two groups numbered G1 and G2 separately. T_{inside} and $T_{outside}$ given in Figures 5.1 are indoor temperature and outdoor temperature, respectively. The average of the three thermocouples placed before the filter in the unit and the average of the three thermocouples placed after the ceramic HRV unit is coded as D_{1Tin} and D_{2Tin}, $D_{1Tout,}$ and D_{2Tout}, in D1 and D2, respectively (Figure 5.1).
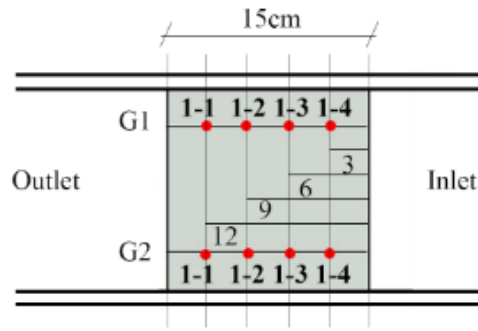
Figure 5.1. Ceramic thermocouple placement (in cm).

The temperature measurements of thermocouples in ceramics are given in Figures 5.2-5.8. The graphs on the left side of Figures 5.2-5.8 belong to Duct 1 (D1), and the graphs on the right side belong to Duct 2 (D2). These graphs show the temperature distribution when two units are operated simultaneously for different time periods defined above. Values from the thermocouples placed in 3cm, 6cm, 9cm, and 12cm depths inside the ceramic material show a temperature gradient inside the HRV unit during the experiments. Figure 5.2 shows the temperature data taken from the thermocouples in the ceramic HRV units from the two ducts for the experiment conducted in simulated winter conditions operating for 10 minutes with 1-minute cycles. In other words, each 1-minute, the operating direction is changed via the fan controller interface. During the experiment, the indoor average temperature (T_{inside}) was measured from five points and was kept around 20°C, while the outside average temperature ($T_{outside}$) was calculated at approximately 3°C by using data from three thermocouples. Average air temperatures measured by the three thermocouples placed at the inlets (T_{in}) and the outlets (T_{out}) of the heat recovery system fluctuated by as much as 3°C during the experiment because of the thermal inertia of the ceramic HRV units. Ceramic materials were heated by indoor air, and their temperatures increased between 1°C and 3°C, depending on the position of the thermocouples in the ceramics. Temperatures of the inside part of the ceramic materials close to the indoor environment had a relatively higher temperature increase, therefore they stored more thermal energy. On the other hand, temperatures of the outer part of the material were close to the outside temperature, and their fluctuations were about 1°C, with less thermal energy storage, yet all of the energy stored in the system was discharged at the end of each cycle.
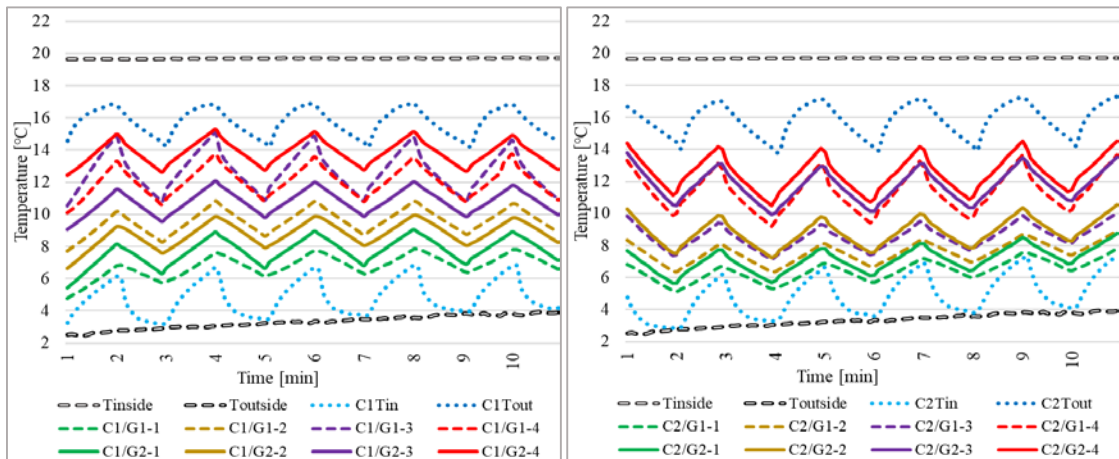
Figure 5.2. Heat recovery system operating for 10 minutes with 1-minute cycles in simulated winter conditions for Duct 1 and 2.

Figure 5.3 gives the results for the simulated winter conditions, and the values of the units working for 6 minutes with a 2-minute cycle can be seen. Inside and outside temperatures were almost constant during the experiment, and the two ventilation systems worked synchronously but with different airflow directions. Since the working period was changed to a 2-minute cycle, temperatures of the ceramic materials increased by up to 7°C, depending on the measurement positions. The material temperatures were close to the outside temperature at the outer part of the ceramic, and the temperature fluctuations were less than the inner part of the ceramic. The 2-minute cycles also showed that the thermal energy-charged could be discharged from the ceramic material.
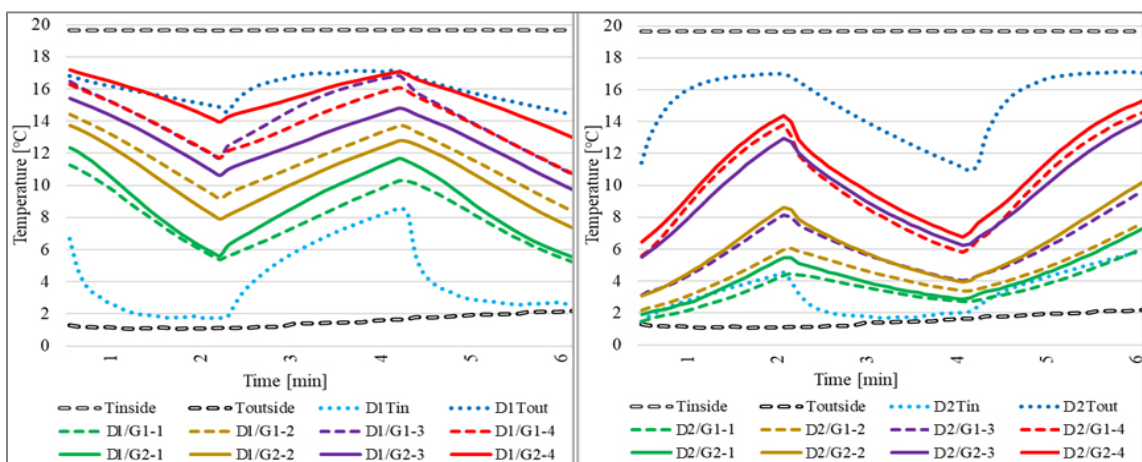
Figure 5.3. Heat recovery system operating for 6 minutes with 2-minute cycles in simulated winter conditions for Duct 1 and 2.

Figure 5.4 shows 5-minute cycles in simulated winter conditions for a total of 20 minutes. In general, the indoor environment remained constant, and there was a fluctuation of approximately 1°C at the outdoor temperature. When the system was operated for 5-minute, the temperatures at the inner part of the ceramic became close to the indoor temperature. Besides, depending on the thermocouple locations, a temperature difference of 10°C inside the ceramics.
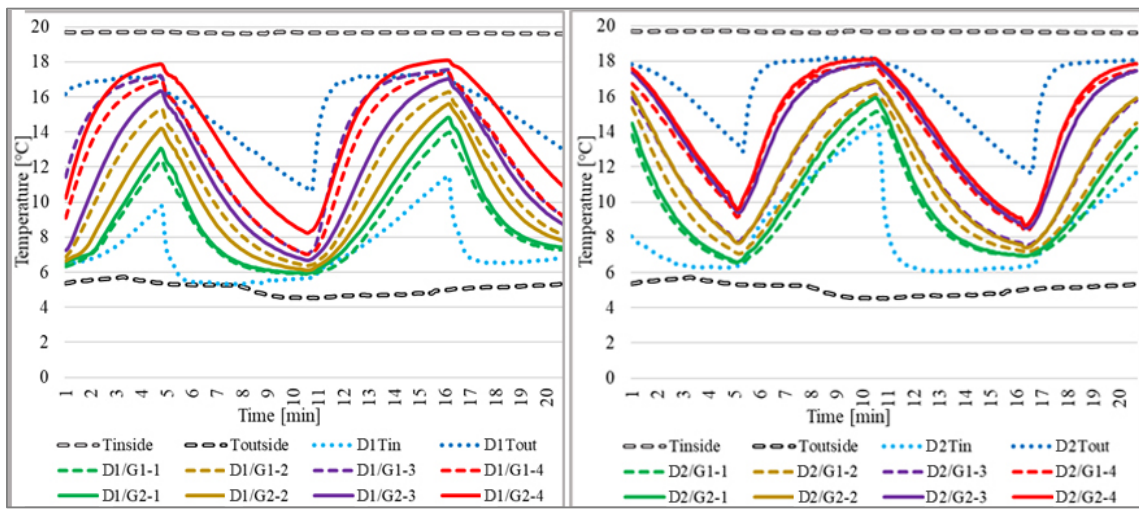
Figure 5.4. Heat recovery system operating for 20 minutes with 5-minute cycles in simulated winter conditions for Duct 1 and 2.

In Figure 5.5, there are 2 cycles of 7.5-minute, in total 15 minutes in simulated winter conditions, and units are operated by changing direction after each cycle. This experiment shows a fluctuation up to 2°C at the outdoor temperature. Besides, when the system is operated for 7.5-minute, the ceramic temperatures near the indoor and outdoor sides are approximately equal to indoor and outdoor temperatures at the end of the cycle. The results shown in Figure 5.6 belong to Duct 1 and 2, two cycles are shown for the 7.5-minute cycle of simulated summer conditions. When the outdoor temperature remain constant at approximately 34°C, the indoor environment was stable at 23°C. The temperature values at the inside of the ceramics increased to around 8°C. When the system was operated in the opposite direction, the thermocouple values reached the indoor temperature approximately at the end of the cycle.
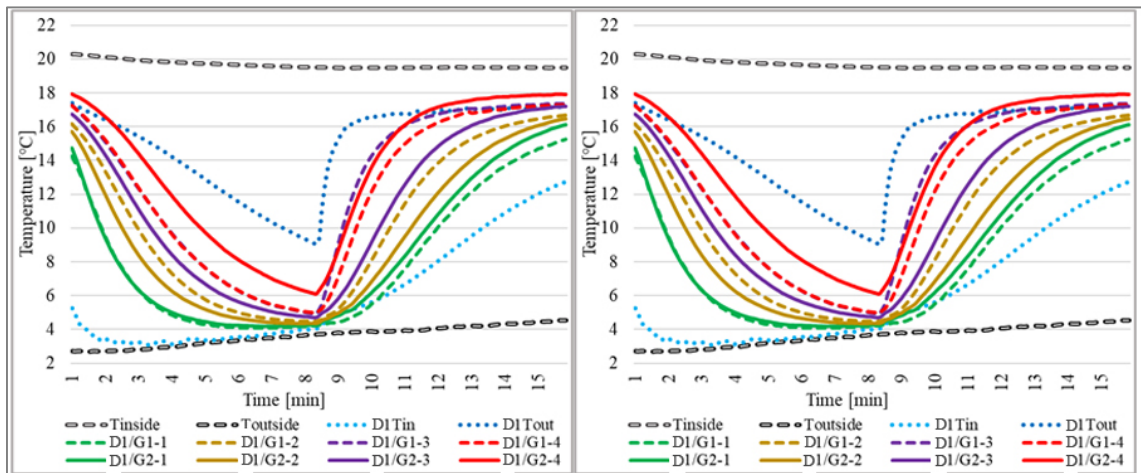
Figure 5.5. Heat recovery system operating for 15 minutes with 7.5-minute cycles in simulated winter conditions for Duct 1 and 2.
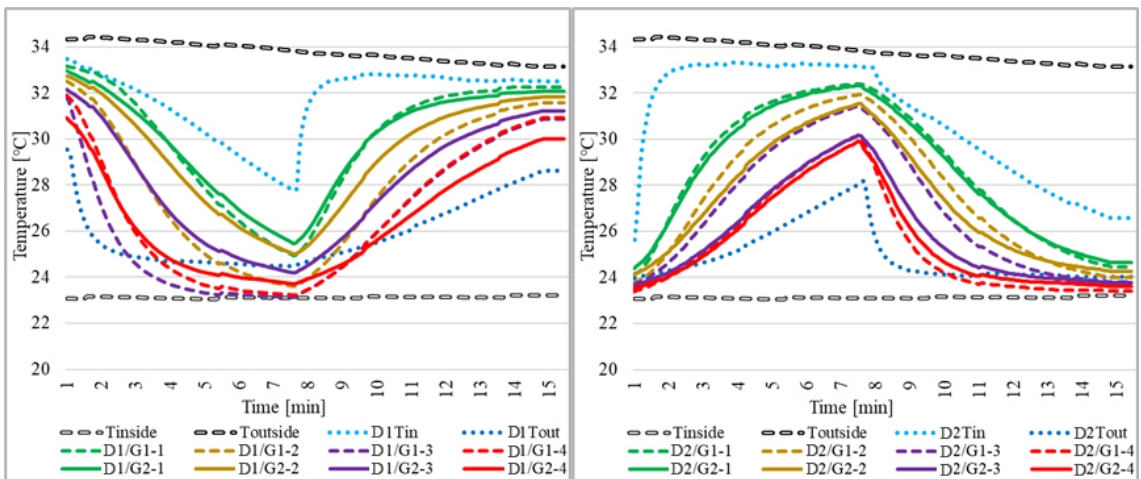
Figure 5.6. Heat recovery system operating for 15 minutes with 7.5-minute cycles in simulated summer conditions for Duct 1 and 2.

In Figures 5.7 and 5.8, the units were operated for 10-minute, in simulated winter and summer conditions, respectively. The indoor environment is generally stable at 20°C and the outdoor environment varies between 3°C to 5°C in Figure 5.7. Considering temperature distribution inside the ceramic at the end of the cycle process, almost all the temperature values are equal to the outdoor or indoor temperature, depending on the airflow direction. Figure 5.8 shows that the outdoor temperature fluctuates up to 2°C, and the indoor temperature is generally stable at 21°C. There is a decrease or increase of approximately 12°C in the ceramic's temperatures during the 10-minute cycles. Temperature values at the ceramics change significantly in the first part of the periods. After that, there were no

remarkable temperature alterations in the ceramic material, indicating that the thermal energy storage rate decreased gradually during a 10-minute cycle.
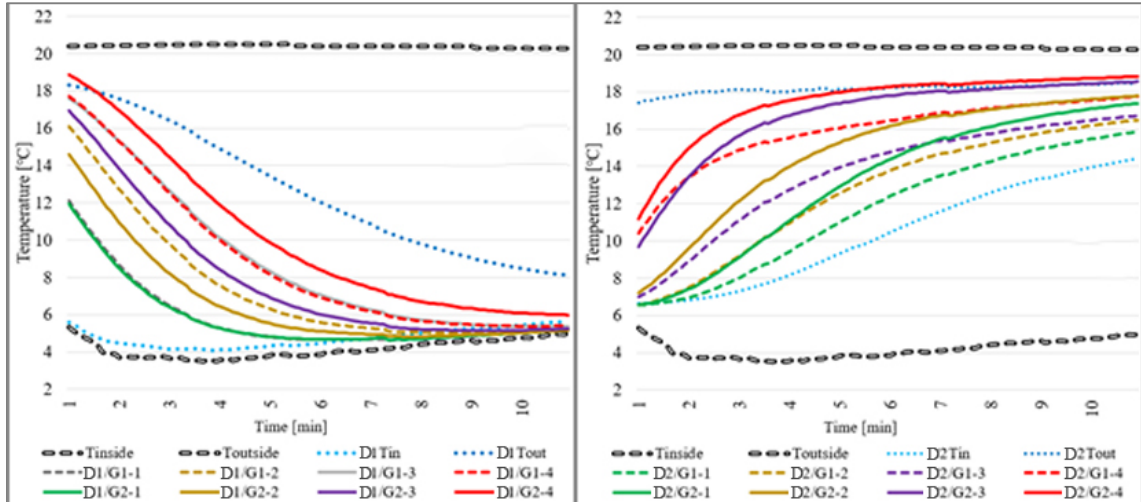
Figure 5.7. Heat recovery system operating for 10-minute in simulated winter conditions for Duct 1 and 2.
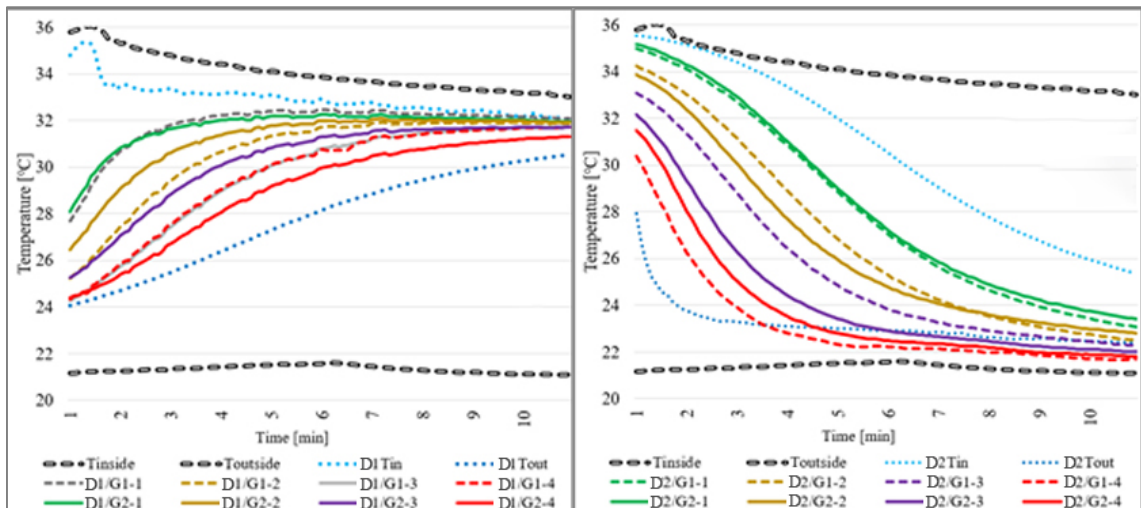
Figure 5.8. Heat recovery system operating for 10-minute in simulated summer conditions for Duct 1 and 2.

5.1.2. Charging and Discharging Experiments for LHTES

The experiments were conducted for the two DVS tube bundle prototypes with PCM that operate simultaneously. At the start of each experiment, the duct and the indoor environment were monitored until the system reached steady-state conditions. After that, two HRV units installed at two ducts were used alternatively in the exhaust and supply modes in a certain periodic cycle to achieve charge and discharge conditions for the thermal energy storage of the units. Experiments continued for 15 min, 20 min, and 30 min cycles given in Table 5.2. For the simulation of summer conditions, the indoor environment temperature is maintained at around 22°C, and the outdoor environment is kept at approximately 35°C.

Table 5.2. Experiments and conditions.

Investigated Parameter	Conditions		Constant Parameters	Variables
Time	Summer	15-minute	-Indoor Temperature (22°C) -Outdoor Temperature (35°C) -Supply Velocity (0.34m/s) -Exhaust Velocity (0.28m/s) -PCM Melting Temperature (27°C)	-Duct Inlet Temperature - Duct Outlet Temperature -Ceramic Temperature - Pressure Difference -Velocity
		20-minute		
		30-minute		

Temperature gradients in the tubes in the two ducts depend on the outdoor and indoor environment temperatures, as shown in Figures 5.9-5.11. For the figures below (Figure 5.9-5.11), D1 represents Duct 1, and D2 represents Duct 2. The placement of the thermocouples is coded by the number of rows in which they are located to represent the temperature individually. Duct inlet and outlet temperatures are specified as DTin and DTout, respectively. In addition, the phase change at 27°C for PCM is indicated in all figures. In addition, all graphs contain direction indicators. These direction indicators represent the characterization test results for supply (inlet to outlet) and exhaust (outlet to

inlet) of ducts. Meanwhile, Tinside and Toutside are indoor temperature and outdoor temperature, respectively.

The experiment in Figures 5.9-5.11 is for the simulated summer conditions. Temperature changes when both units run simultaneously for Duct 1 (D1) and Duct 2 (D2). Thereby, the charging and discharging of the PCM can be monitored by following the temperature change in the thermocouples. The system operates for 15 min in one direction, then, afterward it operates in the opposite direction for another 15 min (Figure 5.9).

Duct 1 first takes supply air from the outside, and the PCM melts between 26°C and 28°C. Later, the solidification process begins when the system operates in the reverse direction (Figure 5.9-D1). Temperature fluctuations occur in the outdoor environment due to the thermostat of the experimental setup. When the ambient temperature rises above or sinks below ±1°C, the thermostat activates and either stops or starts the heating system. Since the outdoor environment has a smaller volume, heat losses have a higher impact and cause faster cool down.
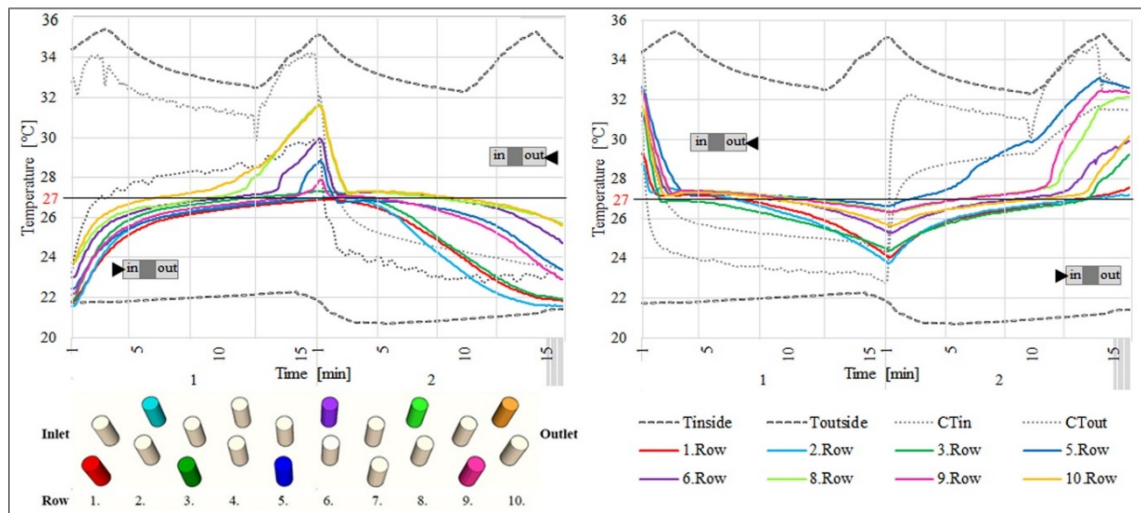
Figure 5.9. Heat recovery system operation for 30 min, with 15 min cycles in summer conditions for Duct 1 (D1) and Duct 2 (D2)

Thus, the fluctuation in the outdoor environment occurs mainly due to the thermostat-controlled heater. As seen in Figure 5.9, when the systems in Ducts 1 and 2 are operated for 15 min, the PCMs in the temperature trend inside the tubes of the first three rows do not reach 27°C, thus they are not fully melted. The other measured rows

have temperatures higher than 27°C, which shows that the PCMs are melting, and the fastest melting tube rows are the 8th and 10th. Duct 1 and Duct 2 work in opposite directions. Duct 2 is in the exhaust, while Duct 1 is in the supply. In Duct 2, the fastest solidifying tube row is the PCMs inside the first two tubes. So, this figure shows that there is not enough time to stabilize the temperature distribution of the PCMs inside all the tubes. For this reason, the system must operate for a while for the PCM to melt or solidify. Hence, the system was operated for different operation times, and Figures 5.10 and 5.11 give the results.

Figure 5.10 shows the results of 20 min of operation for summer. At the beginning of the experiment, while the fan in Duct 1 supplies air, the fan in Duct 2 exhausts air from the indoor environment. The average indoor temperature is 22°C, and the outdoor temperature is around 35°C. While one cycle duration is 40 min, Figure 5.10 shows two 20-min exhaust and supply modes for D1 and D2. The figure shows that the melting and solidification process sufficiently occurs in the PCM tubes. Looking at the rows one by one, the ones with the lowest temperatures in exhaust mode are the first two rows in D1. In the supply mode, in D2, the fastest melting row is the 5th and 9th. Then it is 8th, 10th, 6th, 3rd, 1st, and 2nd, respectively. Moreover, when the system operates for 20 min, the temperature increases inside the tube bundle, and the melting and solidification process of the PCM performs better than the 15 min cycle presented in Figure 5.9.
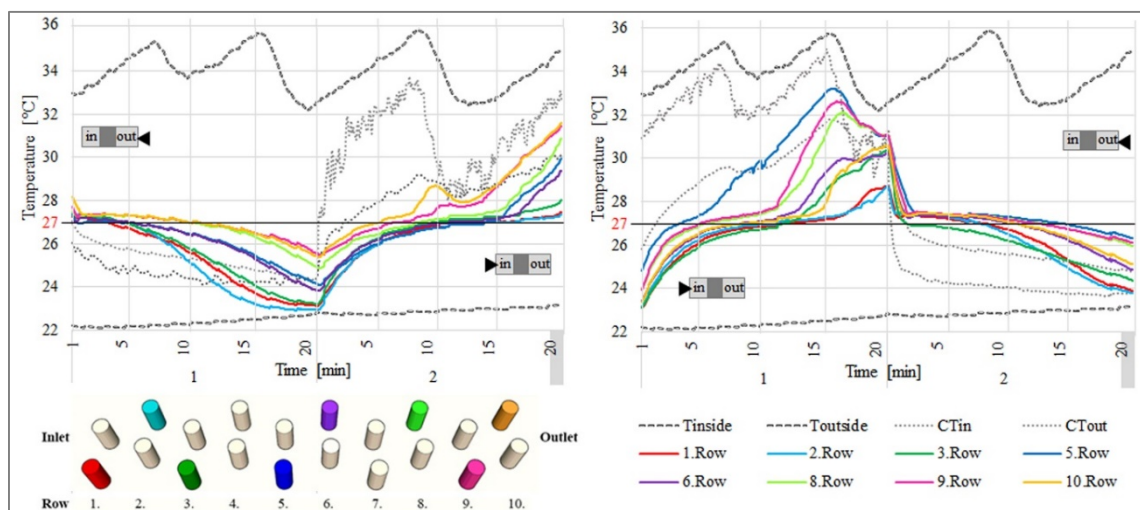
Figure 5.10. Heat recovery system operating for 40 min with 20 min cycles in summer conditions for Duct (D1) and Duct 2 (D2).

Figure 5.11 gives the results of operation for 30 min of exhaust and 30 min of supply modes. Thus, the cycle is 60 min in total. On average, the indoor temperature is $21\pm1°C$, while the outdoor temperature is around $33°C$. As can be seen, PCM completely melts in Duct 2 and completely solidifies in Duct 1 in 30 min. Then, the temperatures of the thermocouples increase. This indicates that sensible heat storage follows LHTES. Thus, the temperatures of these thermocouples get very close to the indoor or outdoor environment when the system operates for 30 min.

When Duct 1 is in exhaust mode, the first two rows solidify first. And then 3rd, 9th, 5th, 6th, 8th, and 10th are solidifying, respectively. While Duct 2 operates in supply mode, the first row of melting tubes is the 5th and 9th row. Then the rows of tubes 8th, 6th, 3rd, 10th, 1st, and 2nd, are melted, respectively.
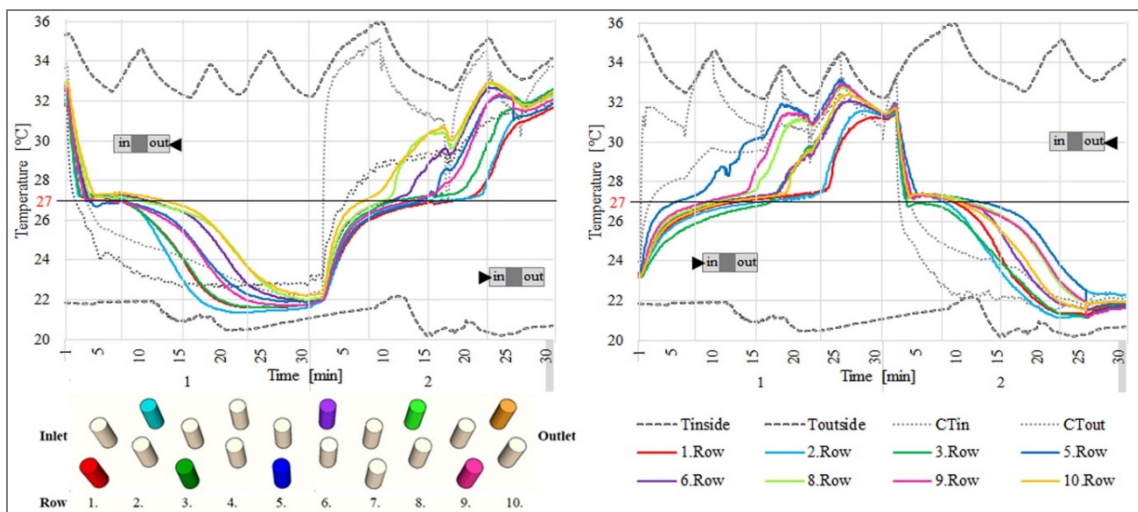
Figure 5.11. Heat recovery system operating for 60 minutes with 30-minute cycles in summer conditions for Duct 1 (left) and Duct 2 (right)

Figure 5.12 shows the melting process of the PCM inside the tubes while working in the supply mode. This color chart represents the temperatures measured in the tubes from blue to red. Red is the $35°C$ which is the row of tubes with the highest temperature, while blue represents $27°C$ is the row of tubes that have not completely melted, which is the mushy zone. When the system operates for 15 min, the first three rows are not fully melted. And in all operation time, the last three rows have the highest temperature.
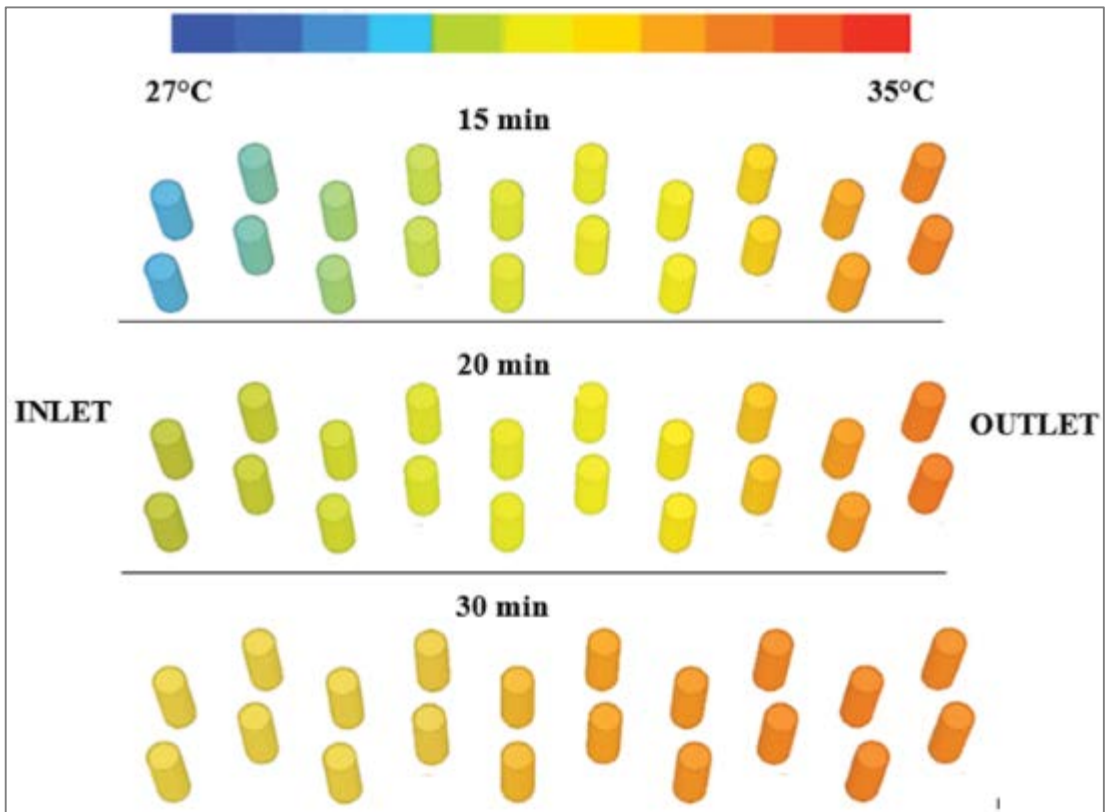
Figure 5.12. Temperature distribution for rows at the end of an operation cycle in supply mode

5.1.3. Data Reduction

In this section, calculations have been made based on the data obtained in the experiment, first for the ceramic HRV unit (SHTES) and then the examination of the tube bundle HRV unit with PCM (LHTES) is presented.

5.1.3.1. Data Reduction for SHTES

The amount of heat stored in/released from the ceramics embedded in the decentralized heat recovery systems of the experimental setup is calculated by using Eq. (5.1),

$$Q = mc_p dT \qquad \qquad \text{Eq. (5.1)}$$

where Q is the thermal energy (J), m is the mass of the ceramic (kg), c_p is the specific heat capacity of the ceramic (J/kg°C), and dT is the change in temperature (°C) of the ceramic material. Specific heat is the amount of heat required to change the temperature of a substance's unit mass, and the differential scanning calorimeter method is used to measure specific heat. This method measures the amount of energy absorbed or released while the sample taken from the ceramic material is heated and cooled for a few cycles between 5°C and 35°C. The specific heat value of the ceramic material was measured to have an average value of 0.725 kJ/kg°C.

The heat recovery ventilation system results with a ceramic HRV unit for D2 are tabulated in Table 5.3. These results are for a working cycle when the system operated from the indoor to the outdoor environment and from the outdoor to the indoor environment. Table 5.3 indicates that the result of the air energy change obtained from the weighted averages of D2-T_{in} and D2-T_{out} data and air velocity data measure during different time steps.

Table 5.3. Air energy change of the unit on Duct 2 for different cycles.

	Time [min]	D2-T_{in_Avg} [°C]	D2-T_{out_Avg} [°C]	D2-Air_Vel [m/s]	Std. Dev. of Velocity	Energy Change [kJ]
Winter	1	16.22	4.87	0.27	0.055	5.098
	2	13.76	2.15	0.27	0.023	10.607
	5	16.52	6.63	0.26	0.049	20.732
	7.5	16.97	8.91	0.29	0.013	29.281
	10	17.64	6.69	0.28	0.003	36.532
Summer	7.5	24.45	29.09	0.21	0.044	12.556
	10	23.09	30.58	0.25	0.005	30.855

The maximum possible heat transfer capacity, Q_{max}, is defined in Table 5.4 for the given set of operating conditions, and it is calculated by using Eq. (5.2) as;

$$Q_{max} = (\dot{m}\Delta t)c_p dT \qquad\qquad \text{Eq. (5.2)}$$

where $\dot{m}$ is the mass flow rate of air (kg/s), c_p is the air specific heat capacity (J/kg°C), dT is the temperature change of air (°C), and the dt is the cycle period in second. Table 5.6 gives the results for the thermal energy storage in the ceramic and the energy from the fan and the maximum energy values that can be stored. According to the Ebm-papst fan

manufacturer's catalog data, power consumption is 3.4 Watt when the nominal voltage is 12.0 Volts. Therefore, there is an energy gain/loss of approximately 0.2-2 kJ from the fan during a cycle period. When the data from Duct 2 are calculated, while the system is operated in winter conditions for 1-minute from outdoor environment to indoor environment, 4.478 kJ heat release occurs, when it is operated for 2-minute, 10.762 kJ energy is released.

Table 5.4. Total heat capacity of the unit on Duct 2 in certain periods at different time steps

	Time [min]	T_{inside_Avg} [°C]	$T_{outside\_Avg}$ [°C]	D2-in to out [kJ]	D2-out to in [kJ]	Fan [kJ]	Q_{max} [kJ]
Winter	1	19.69	4.32	4.478	4.240	0.20	7.142
	2	19.66	2.76	10.762	10.583	0.41	15.451
	5	19.72	6.26	21.832	20.682	1.02	29.819
	7.5	19.50	5.08	23.853	22.711	1.53	51.762
	10	20.39	4.75	24.120	21.520	2.04	73.571
Summer	7.5	23.10	34.16	17.730	16.890	1.53	27.699
	10	21.32	34.08	24.552	21.855	2.04	52.134

As seen in Table 5.4, as the system's operating time increases, heat transfer also increases. However, when looking at the storage per unit time, the best performance can be seen by operating the system for 2-minute. When the fan runs for a long time period, the cost of electrical energy increases. The fan is more advantageous when the system operates in a short period.

5.1.3.2. Data Reduction for LHTES

Table 5.5 shows the results of the tube bundle HRV system with PCM obtained from experimental data and calculations. In sensible heat storage systems, the variables that determine the amount of energy stored are the amount of material used, the specific heat of the material, and the temperature change during the heat storage. The amount of heat stored in/released from the PCM to the air is calculated by using Eq. 5.3;

$$Q = \dot{m}c_p dT dt \qquad \text{Eq. (5.3)}$$

where $\dot{m}$ is the mass flow rate of air (kg/s), c_p is the air specific heat capacity (J/kg°C), dT is the temperature change of air (°C), and dt is the running time period (s). The results of the experiments are presented in Table 5.5. The air energy change is obtained according to the weighted averages of three thermocouples (Tin) placed before the filter in the unit and the average of the three thermocouples (Tout) placed after the prototype and air velocity data measurements during specified time steps.

Table 5.5. Air energy change of the latent HRV prototype.

Time [min]	Direction [*in*: inlet, *out*: outlet]	D2-T_{in_Avg} [°C]	D2-T_{out_Avg} [°C]	D2-Air_Vel [m/s]	Std. Dev. of Vel.	Energy Change [kJ]	Avg. Storage Rate (Watt)
15	*in* to *out*	32.10	29.85	0.35	0.025	16.12	17.9
	out to *in*	26.02	24.29	0.30	0.010	14.68	16.3
20	*in* to *out*	30.46	28.34	0.32	0.056	27.24	22.7
	out to *in*	25.56	23.97	0.29	0.012	22.13	18.4
30	*in* to *out*	32.01	30.05	0.35	0.025	34.12	19.0
	out to *in*	24.17	23.39	0.32	0.027	19.88	11.0

The PCM, which is RT27, can store latent heat and is used in the prototype to add more energy storage capacity according to the temperature and phase changes in the material. So, when calculating the internal energy change in the PCM during the experiment, both the physical processes of heat storage, sensible heat and latent heat occur and need interpretation. Sensible heat is related to the temperature change of a substance, while latent heat depends on the phase change of the material, namely liquid to solid or solid to liquid phases in this study. Since phase change enthalpy is used to overcome the molecular attraction of particles, it has many times more energy storage capacity than sensible heat (Rubitherm Tech 2016).

Furthermore, air energy changes shown in Table 5.5 are used to investigate the performance of the heat recovery system. The storage rate per unit time is an important parameter for evaluation rather than the actual running period of the system. According to Table 5.5, when the system operates for 20 min, the system performs better than 15 and 30 min. Also, when looking at the calculation of the average storage rate per unit time, the best performance can be seen by operating the system for 20-minute. The thermal energy stored in the system from the previous cycle or waiting for the time

variations between the cycles are the reasons for the difference in supply and exhaust values for heat transfer rates.

5.1.4. Comparison of Mean Heat Transfer Rate

According to the mean heat transfer rates in Figure 5.13, the best result was observed when the system was operated for a 2-minute cycle for the ceramic system. The reason for the difference in the exhaust (in to out) and supply (out to in) values for heat transfer rates is due to the thermal energy stored in the ceramic from the previous cycle or waiting for the time differences between the cycles. According to the tube bundle HRV system in supply and exhaust mode, a 20-minute cycle gives the best result according to the mean heat transfer rate value. In addition to these, when the fan runs for a long period, electrical energy cost increases. So, the fan is more advantageous when the system operates for a short period. The calculations are based on air energy changes depending on Tables 5.3 and 5.5.
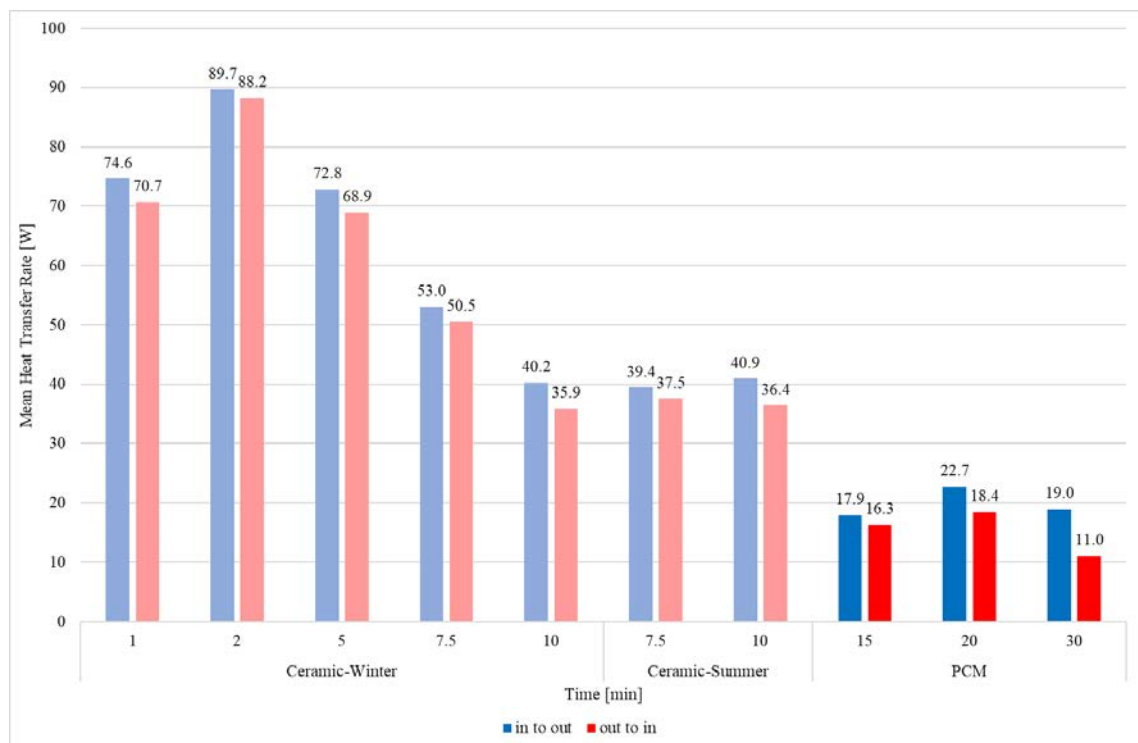
Figure 5.13. Comparison of mean heat transfer rates of ceramic and tube bundle systems

5.1.5. Calculation of Heat Recovery Efficiency

In literature, there are many studies about heat recovery efficiency. And some of these are decentralized heat exchanger systems. According to Merzkirch et al. (2016), the heat recovery efficiency is reduced 8-22% because of the wind or stack effect. According to this study, the heat exchanger unit's efficiency is dependent on the pressure difference. And the result is, if the pressure differences are 10-20 Pa, the efficiency is between 20-50%. Filis, Kolarik and Smith (2021) validated an average of 62% sensible heat recovery efficiency with simulations at a 5.2 Pa negative pressure difference. In addition, the present study provides 25%-55% efficiency compared to a place where this system is not used at all.

The best possible thermal efficiency cannot always be achieved due to experimental uncertainties and errors, and poor setup or breakdown during operation. To obtain the efficiency of the unit, it is calculated according to the following procedures described in European Standard EN 13141-8:2014 for non-ducted units to measure the temperature ratio on the supply air side. The heat recovery efficiency rate used in the calculations is the supply air side temperature ratio (Eq. 5.4).

$$\eta = \frac{1}{t_{cycle}} \left[\int_{t}^{t_{cycle}} \left(\frac{T_{21} - T_{22}}{(T_{21} - T_{22}) + (T_{22} - T_{11})} \right) dt \right] x\ 100 \qquad \text{Eq. (5.4)}$$

where;

T_{21} = supply inlet temperature (°C)

T_{22} = supply outlet temperature (°C)

T_{11} = inside temperature (°C)

η defines the effectiveness of a decentralized heat recovery prototype. The values of the supply operating regime period have been calculated by calculating each measurement point. The measurements are measured at 5-second intervals (dt), and t_{cycle} represents the specified operating time. For ceramic HRV, there are five winter condition results and two summer condition results included. In winter condition; 1-minute, 2-minute, 5-minute, also in winter and summer condition; 7.5-minute and 10-minute. For tube bundle HRV unit, 15-minute, 20-minute, and 30-minute cycles and efficiencies are calculated according to specified operating time.

According to Eq. 5.4, for the ceramic HRV unit, the supply efficiency for 2-minute operation time is 82%, 5-minute result is 76%, the 7.5-minute result is 73%, and the winter condition average result is 77%, and exhaust efficiency is 65%. For summer conditions, the unit is operated 7.5-minute, the supply efficiency result is 89%, and the 10-minute exhaust efficiency result is 45%.

For the tube bundle HRV unit, the supply efficiency results are 51.6% for 15 min, 54.9% for 20 min, and 46.7% for 30-minute. And exhaust efficiency results are 23.3%, 29.8% and 24.6%, respectively. Figure 5.14 shows the efficiency results according to different time steps.
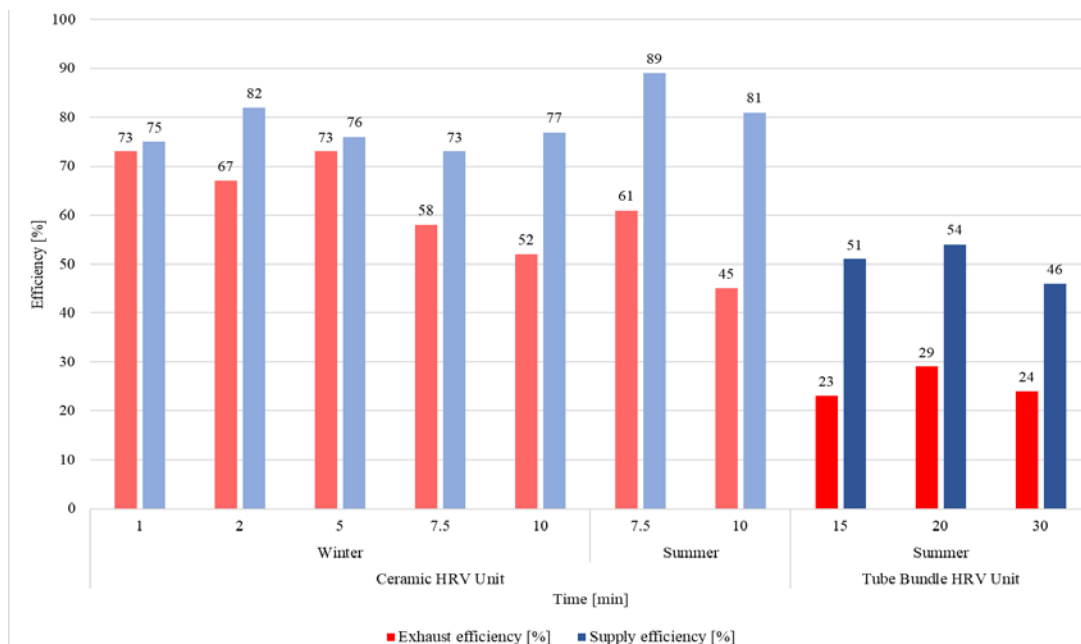
Figure 5.14. Efficiency results for heat recovery systems according to different time steps

Comparing the studies mentioned above, different combinations, tube bundle designs, and PCMs that melt at different temperatures should be simulated. And it should be considered that the efficiency of the tube bundle HRV unit should be increased with different design solutions. To obtain total internal energy per unit time, it will be possible to shorten the melting/solidification time and achieve the ceramic system's heat transfer rate. And to develop the system, parametric analyses are simulated with ANSYS Fluent. In the next section, the studies in the CFD results and the experimental analysis results are compared.

5.2. Simulation Results

As alluded to in the previous chapter, the simulation of HRV systems investigated and tested the potential to identify temperature, liquid fraction issues. In these simulations for this study, the ceramic and tube bundle systems are simulated in FLUENT. ANSYS is used to simulate the control system, provide the necessary boundary conditions required by the FLUENT model, and calculate the energy requirements of the systems. With these results, simulations of operating conditions are examined, and the ability of a building simulation tool to provide modeling and performance prediction of these systems is tested.

Many boundary conditions affect the results of the CFD model. One of them is the wall boundary conditions. The k-omega models (std and sst) are available as low Reynolds number models. To ensure that the predicted temperature changes are not affected by the initial temperature distributions, the analysis has been analyzed with at least 50 consecutive cycles. In this way, a cyclical behavior regarding temperature changes is obtained. The reason for doing this loop is to achieve a cyclic steady-state and eliminate boundary condition effects by providing airflow from the outlet and inlet. While the system operates from outdoor to indoor and from indoor to outdoor, stability has been achieved in cycles, and the difference between the last two cycles is only 2%.

5.2.1. Simulation Results of SHTES

The CFD simulations are modeled according to a real-scale laboratory experiment. These are analyzed as the same room and equipment and at the same indoor and outdoor environmental conditions. In the CFD model, the dimensions of all parts of the HRV units and duct in the experimental setup are designed the same. The simulations are detailed on one cell of the ceramic unit, which is explained in detail in Chapter 4. In transient state simulation, two operating phases are considered charging and discharging phases. During the charging phase, it is considered that the ceramic is subjected to the thermal influence of the cooling heat transfer fluid in winter conditions. And discharging process, the ceramic is subjected to the heating heat transfer fluid in winter conditions. Discharging of ceramic storage material is initiated by exhausting heat transfer fluid (HTF) through the discharging tubes at 5°C. Also, the charging of ceramic is initiated by

supplying HTF through the charging ceramic at 20°C. The temperature of the storage material varies with time.

Variation of volume average ceramic and air temperature with time is shown in Figure 5.15. It is seen from this figure that initially, the rise in the volume average temperature of ceramic and air is rapid and decreases with time. This is because of the higher driving force for conduction during the initial period of the charging cycle, and this driving force reduces with time as the ceramic is fast due to the high capacity and low thermal conductivity. In this figure, the charging and discharging process takes 1-minute cycles. 1-minute operation time is not enough to charge and discharge processes.
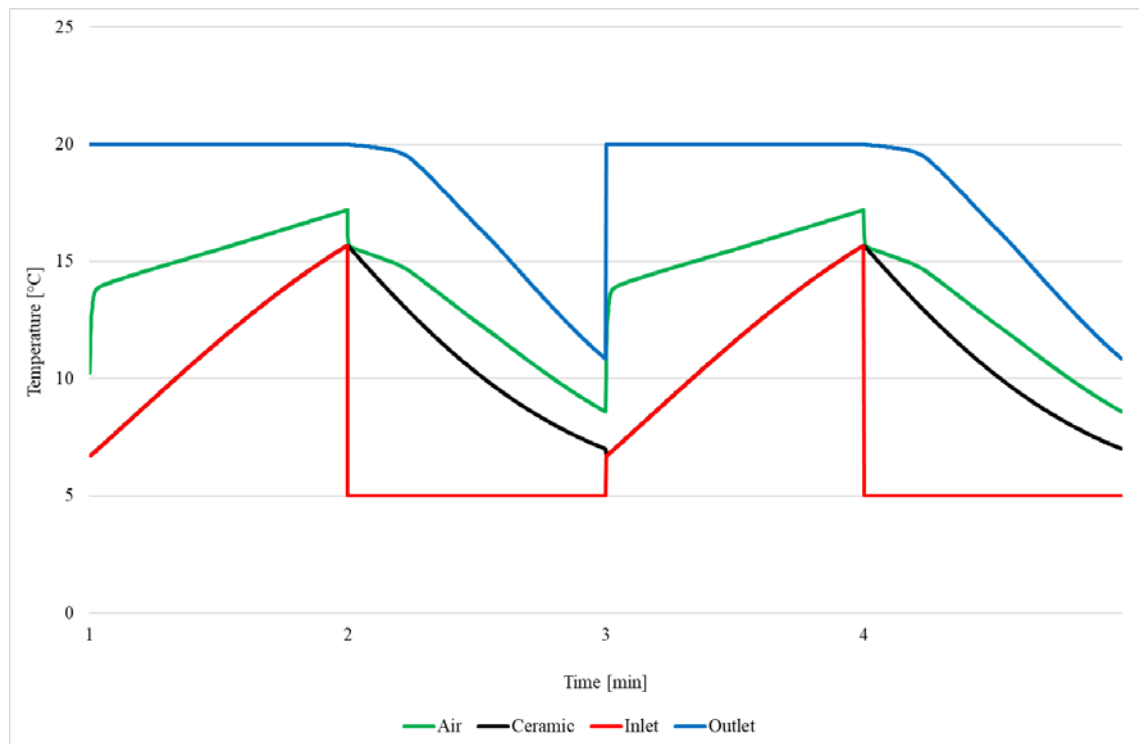
Figure 5.15. Cyclic results for 1-minute operating time for winter condition.

Figure 5.16 shows the charging and discharging cycle of the ceramic system. The inlet temperature is 5°C, and the outlet temperature, which is indoor temperature, is 20°C. At the same time, the inlet temperature rises to a maximum of 17°C, the fluid inside the ceramic and ceramic rises to 19°C. The outlet temperature drops to 6°C while the system operates from outdoor to indoor.
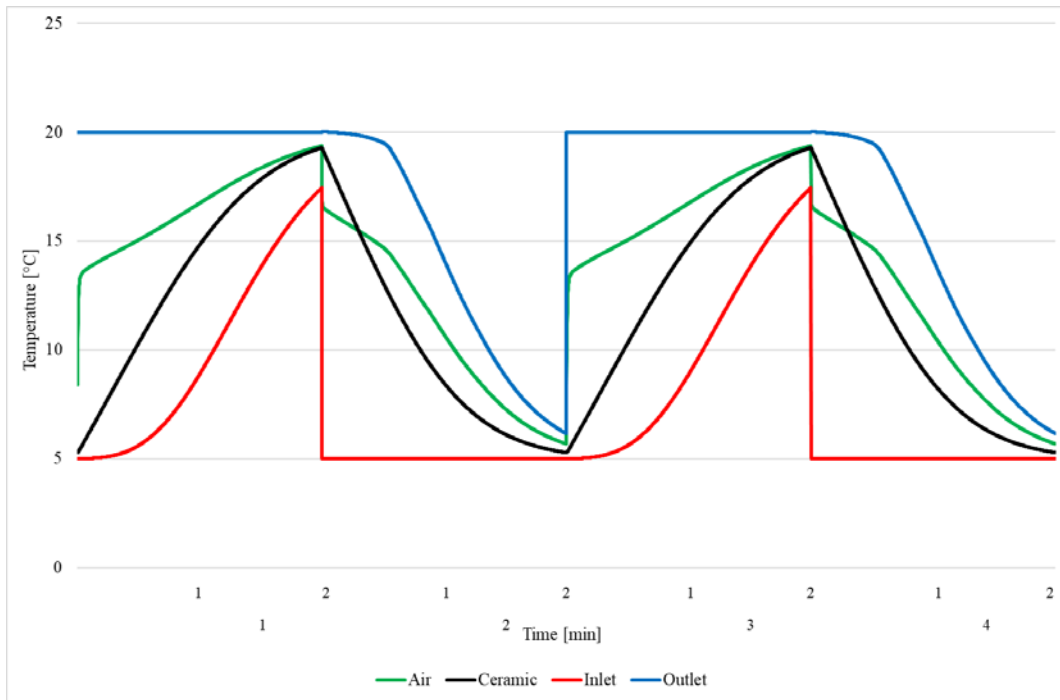
Figure 5.16. Cyclic results for 2-minute operating time for winter condition.

Figure 5.17 represents the 5-minute operating time for the winter condition of the ceramic system. Discharging process and charging process follow each other. It can be noticed that the temperature rise of ceramic is rapid first 150 s due to the high driving force for conduction and discharging curve becoming flat as time progresses after the 150 s. HTF receives the heat from the charged ceramic resulting in the decrease of the ceramic temperature and increase of HTF temperature along with the system.

Figure 5.18 through the temperature contours at different intervals of the charging and discharging cycle. The total charging and discharging in these figures are 150 s. In charging, the material's temperature reaches a definite rise in temperature ΔT. Here, the temperature distribution is seen throughout the 15 cm ceramic cell.

In winter conditions, with a temperature of 5°C from the outside environment, the system reaches the same temperature as the outdoor temperature in the 150s when the system is in the exhaust. The same is recognized for supply. Ceramic stores heat with the air absorbs into the system at 20°C from the indoor environment. As time increases, the temperature also increases during charging, through which energy is getting stored in the SHS ceramic. And also the amount of thermal energy recovered from the ceramic at the particular discharging time. As time increases, the temperature decreases during the discharge process, and energy is recovered from the SHS ceramic.

125
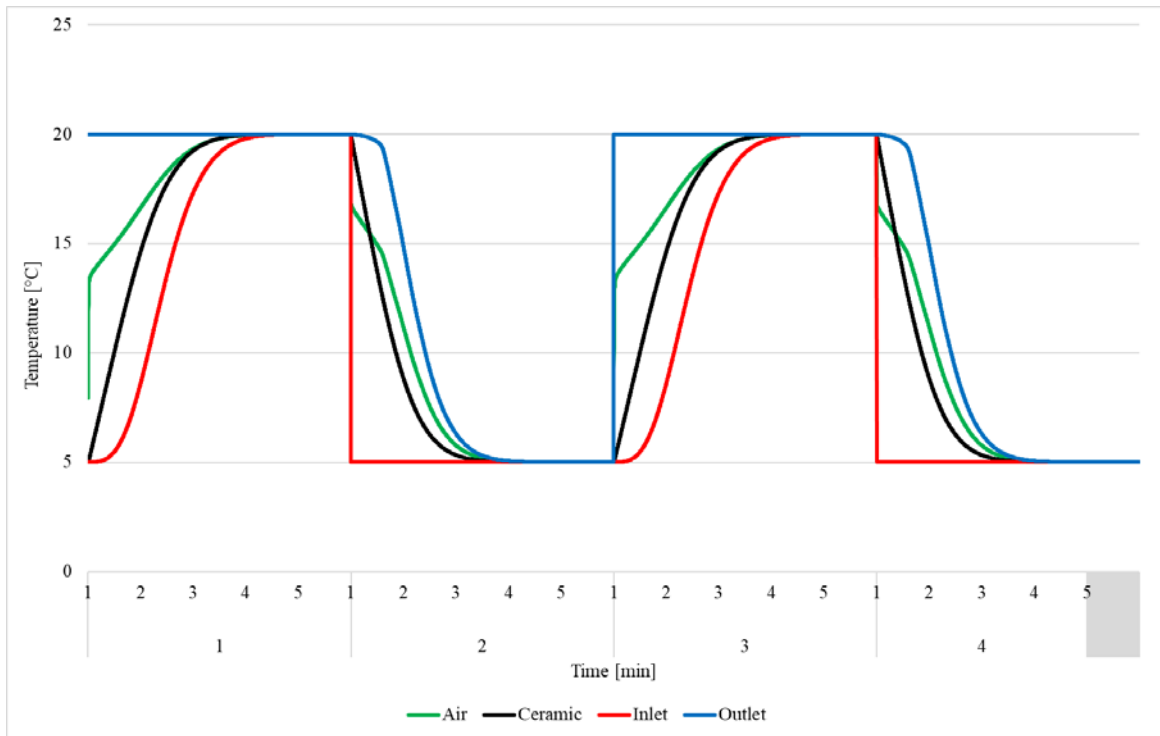
Figure 5.17. Cyclic results for 5-minute operating time for winter condition.
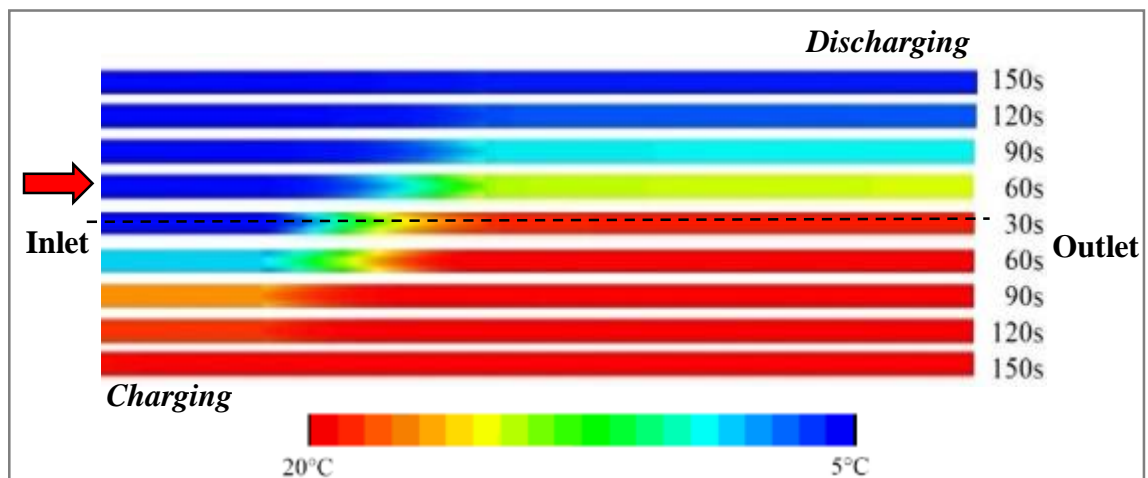
Figure 5.18. Temperature change in the system for 150 s operating time in a different time step charging and discharging processes.

The cyclic results for the 7.5-minute operating time for winter condition of the ceramic HRV unit are seen in Figure 5.19. Here, after the 150s, the charging and discharging curve becomes flat. The average system temperature reaches the inlet and outlet temperature in discharging and charging process.
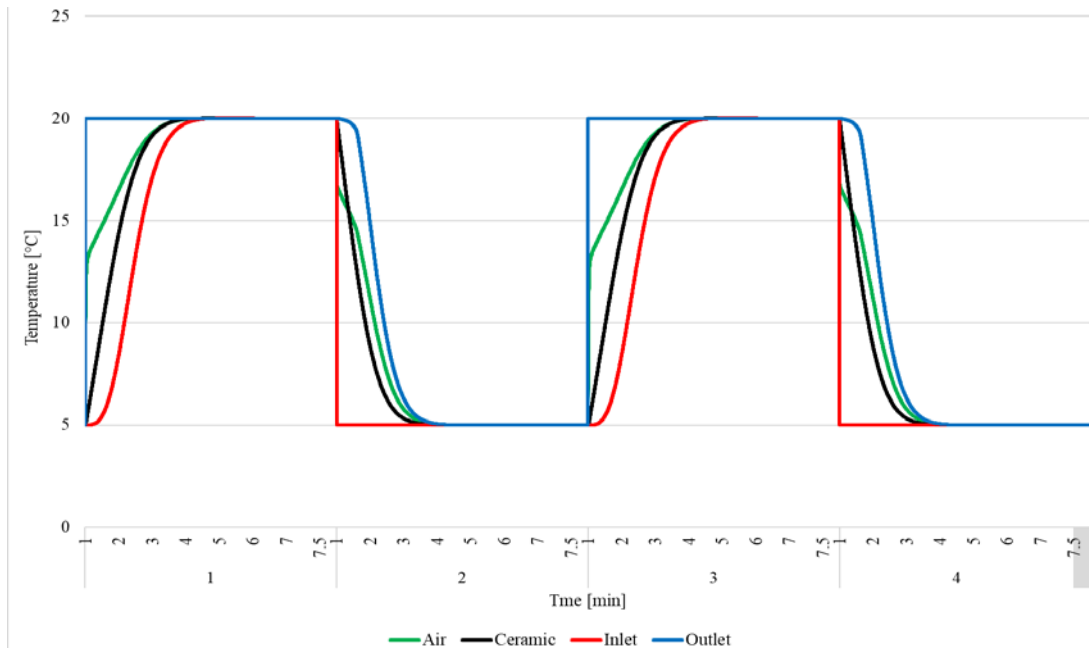
Figure 5.19. Cyclic results for 7.5-minute operating time for winter condition.

Figure 5.20 is related to cyclic results of the 10-minute operation time for the ceramic system. After the 150s, there were no differences in ceramic and HTF temperature. Because the system reaches the thermal balance, in this graph, in system, there are no remarkable temperature alterations in storage material.
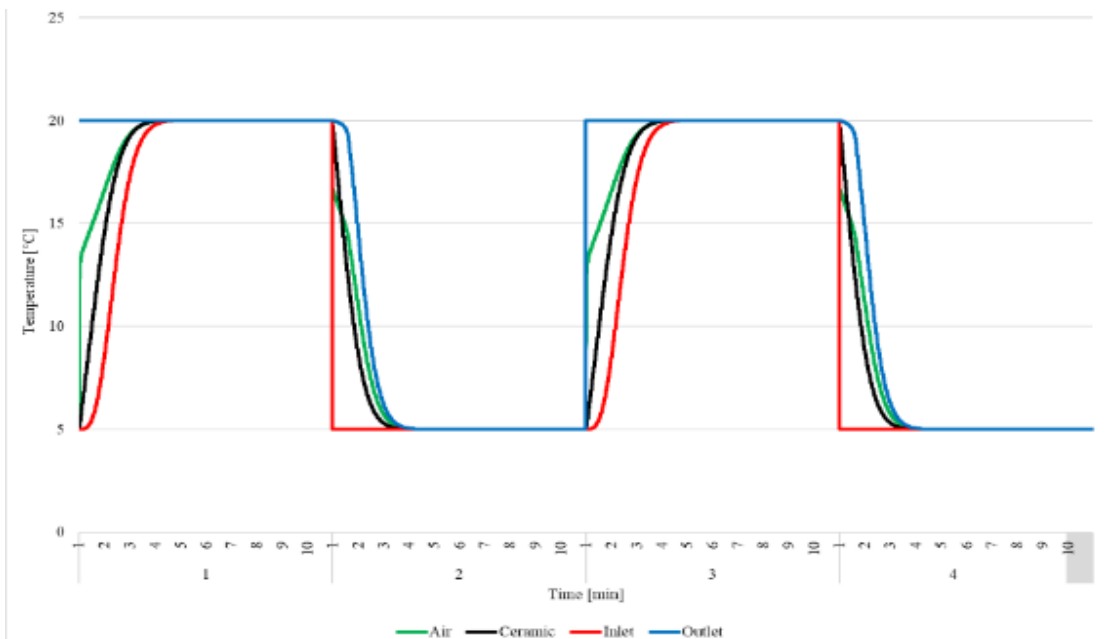
Figure 5.20. Cyclic results for 10-minute operating time for winter condition.

Figure 5.21 belongs to the ceramic system cycle for 7.5-minute of summer condition. When the outdoor temperature is 34°C, the indoor environment is stable at 20°C. At the end of the cycle process, the temperature distribution inside the ceramic is almost equal to the outdoor or the indoor temperature, depending on the airflow direction.
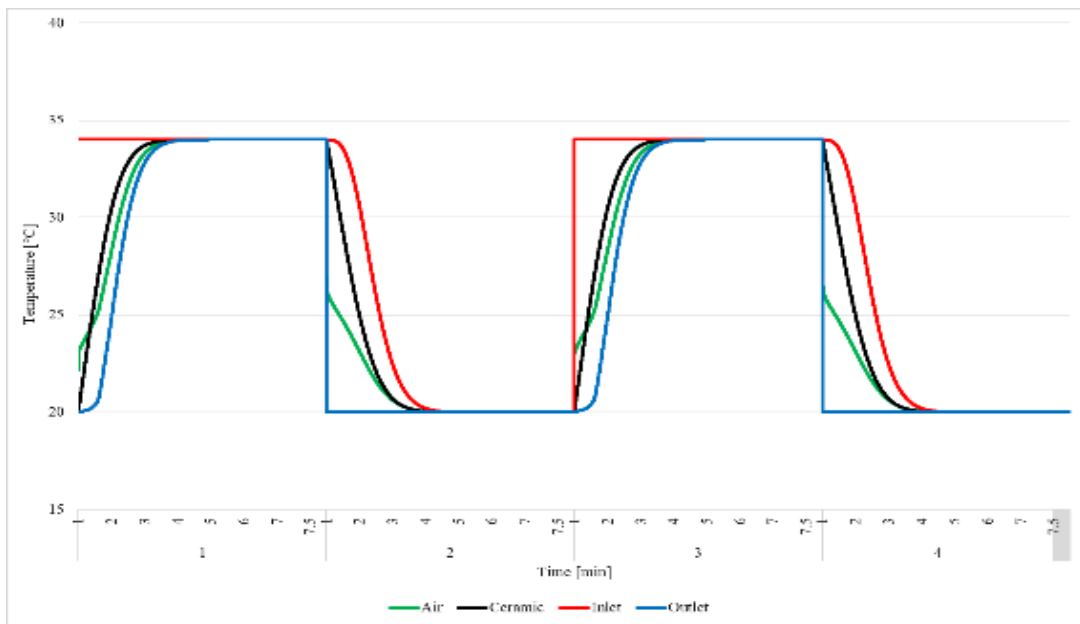
Figure 5.21. Cyclic results for 7.5-minute operating time for summer condition.

In figure 5.22, there are 2 cycles of 10-minute, in total 20 minutes in simulated summer conditions, and units are operated by charging and discharging processes. The indoor and outdoor temperatures remained constant at 20°C and 34°C, respectively. There is a decrease in discharging increase for charging approximately 14°C in the ceramic temperature during the 10-minute cycles.
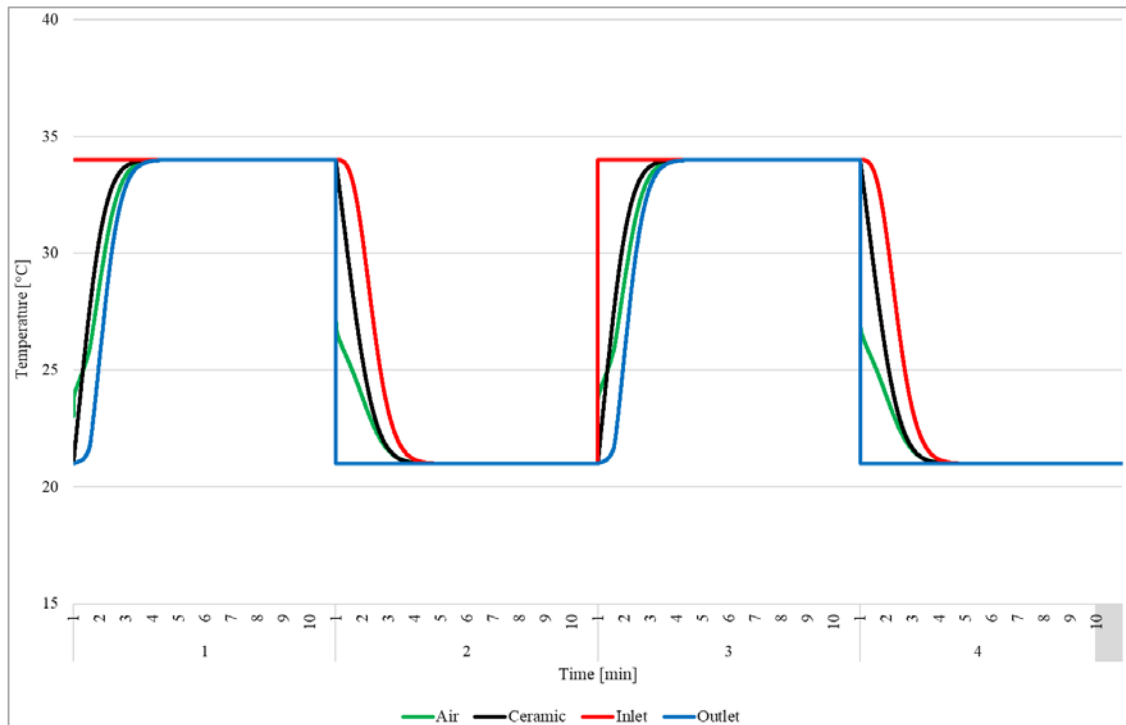
Figure 5.22. Cyclic results for 10-minute operating time for summer condition.

5.2.2. Simulation Results of LHTES

In Chapter 3, the experimental setup of the system and the experiments for two separate HRV systems are given in detail. In CFD, the duct has the same dimensions as the experiments explained in Chapter 4. CFD is performed to investigate the heat transfer performance and fluid flow characteristics. First, the model is primarily divided into mesh within the Fluent program. Then, flow analysis is obtained with the ANSYS-Fluent tool. According to the verification and validation process, the simulations are employed in this part.

The simulated model is correlated with the experimental temperatures measured by thermocouples. The simulation results that surface temperature increases when the discharge current increases. As shown in related figures, the difference was observed by operating the system for 15-minute, 20-minute, and 30-minute. It was observed that the PCMs inside the tubes close to the outlet melted later. Figure 5.23 shows the cycle results for the system with PCM operating in the last 2 cycles for 60 minutes. By keeping the indoor and outdoor temperatures constant, the temperature changes of the PCMs inside the tubes are observed. In this Figure, the inlet temperature is 34°C, and the outlet

temperature, which is indoor temperature, is 21°C. As can be seen in this graph, in the exhaust mode, the PCMs inside the tubes close to the inlet reaches the outside temperature faster and cannot reach after the 5th tube.
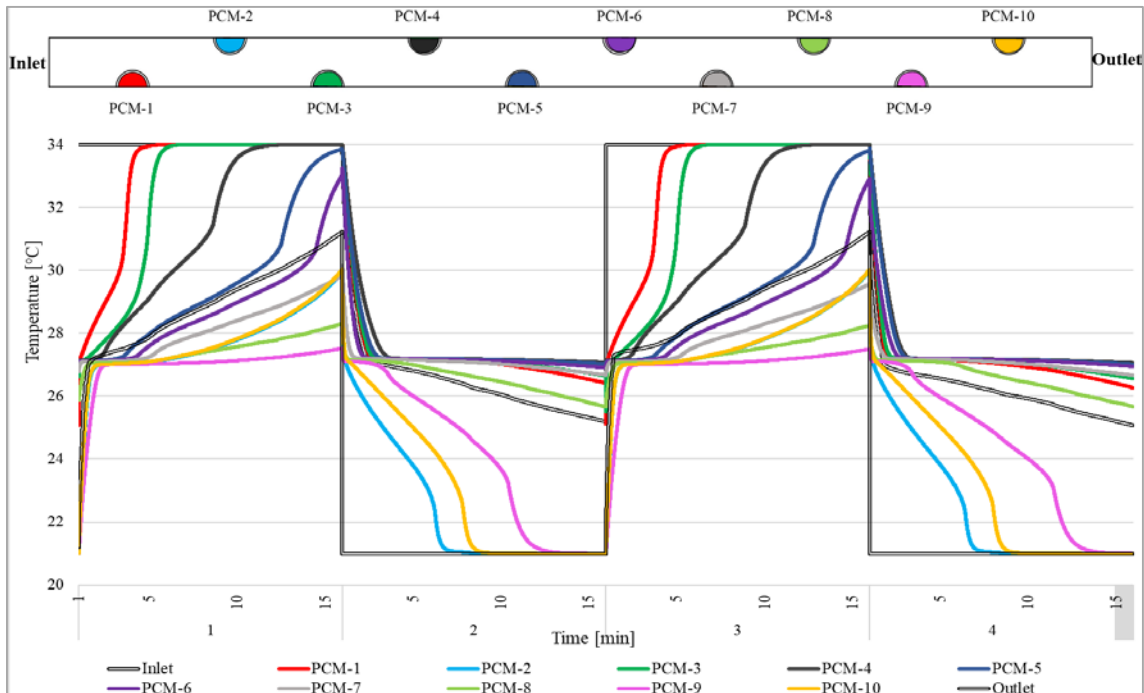
Figure 5.23. Cyclic results for 15-minute operating time.

Figure 5.24 represents the time-related melting and solidifying graphs for 15-minute operating. In addition, when the PCM tube bundle is compared with the experiments, it is seen that the PCMs inside the tubes close to the inlet are melted first. And also, while the 1st, 2nd, 3rd, 4th, 5th tubes completely melted and, in the 6th, 7th, 8th, 9th, and 10th tubes, complete melting is not observed. In addition, the solidification process works have a reverse situation. The tubes that solidified first are 10th, 9th, 8th, and the remaining tubes are not completely solidified.
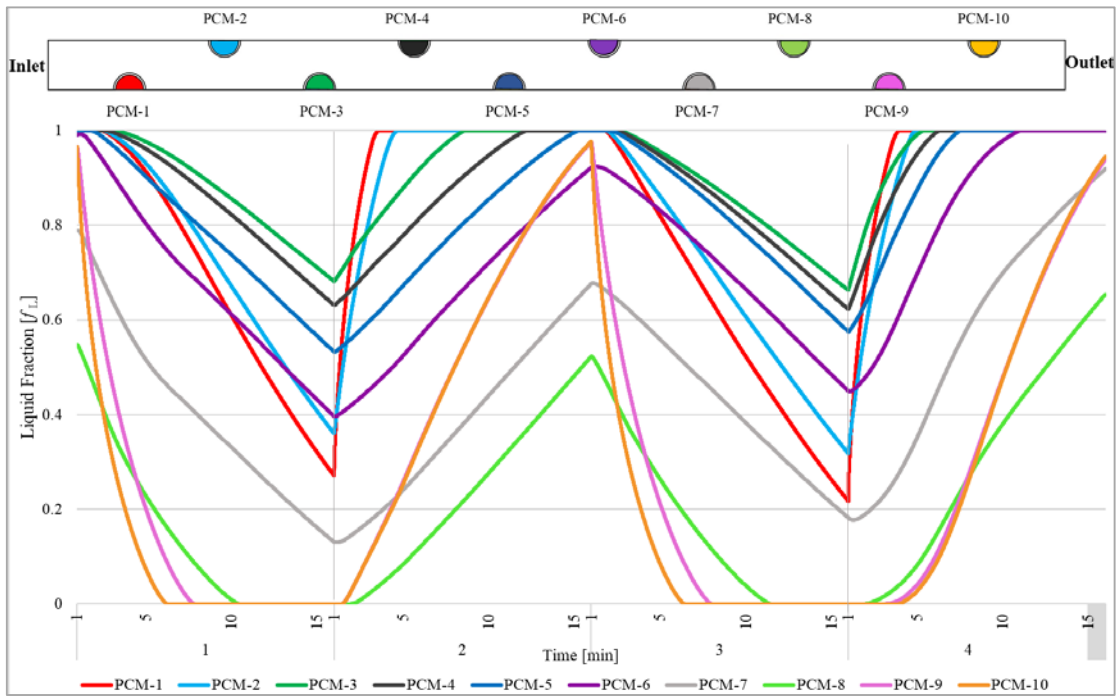
Figure 5.24. Melting/ solidification results for 15-minute operating time.

Figure 5.25, which is created based on Figure 5.24, shows the temperature distribution at 1.5 min., 3 min., 5 min., 7 min., 9 min., 11 min., 13, and 15 min. This figure shows the exhaust mode for the HRV system operating for 15-minute.
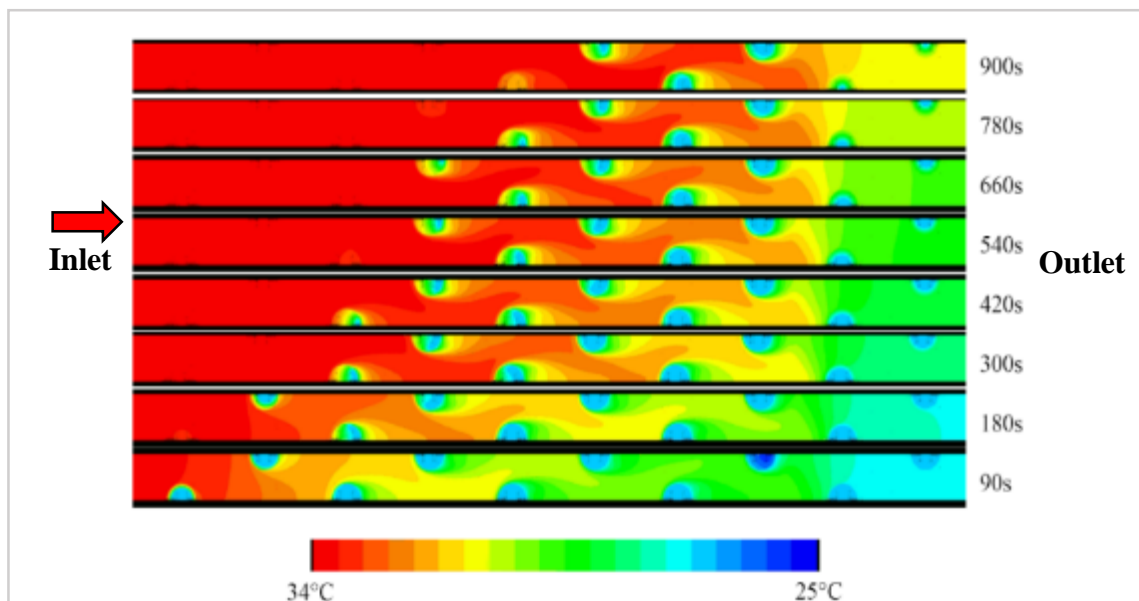
Figure 5.25. Temperature change in the system for the 15-minute operating time in a different time step.

Figure 5.26, 5.27, and 5.28 belongs to the 20-minute operating time for the tube bundle HRV system. Figure 5.26 shows the cyclic results of the tube bundle system. Here, the outdoor environment is 34°C, the indoor environment is 21°C. And while the PCMs in 4 tubes reached outdoor temperature, the others remained below this value. In supply mode, only 3 tubes reached the indoor temperature. Tube-8 remained at 27°C, the melting point of PCM. Tube-7 could only rise to 28°C. However, compared to 15-minute, it is seen that all tubes exceed the melting temperature of 27°C after 15-minute. In supply mode, the remaining tubes, except for 1st, 7th, 8th, 9th, and 10th, did not drop below the melting temperature.
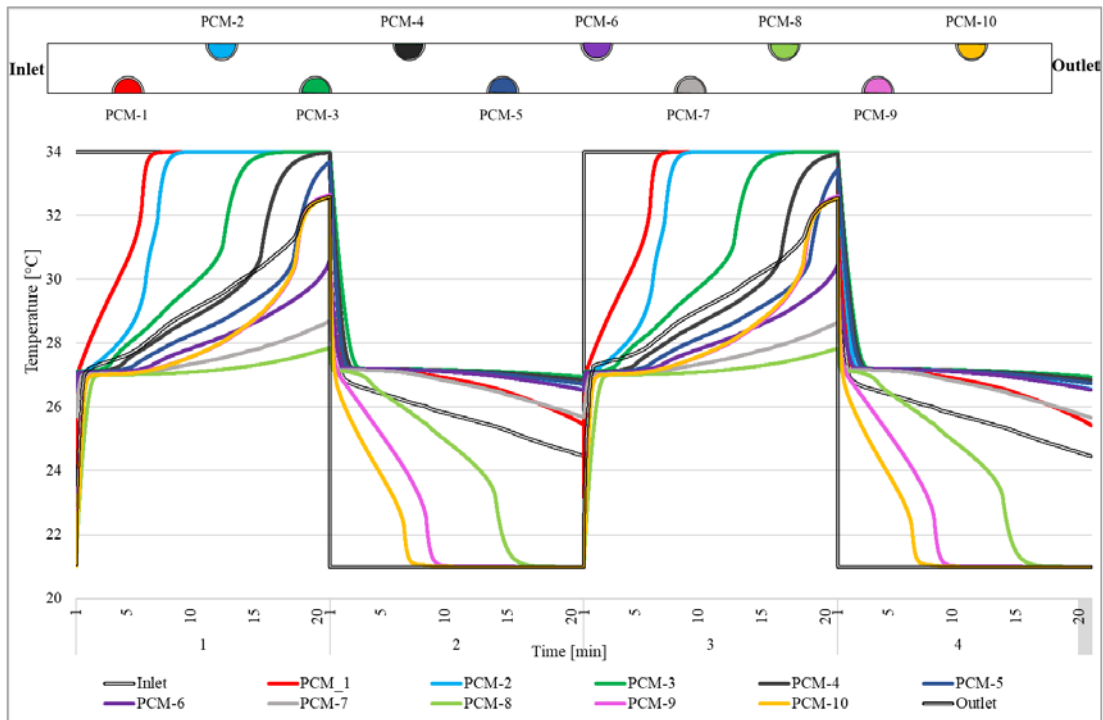
Figure 5.26. Cyclic results for 20-minute operating time.

Unlike the results of 15-minute, PCMs in all tubes melt and solidify except for only 2 tubes. These are Tube 7 and 8. According to supply mode, the solidification process is not completely occurred. When the fan operates indoor to the outdoor environment, the 8th, 9th, and 10th tubes are completely solidified. Looking at the 3rd, 4th, 5th tubes, it is seen that only half of them are solidified (Figure 5.27).
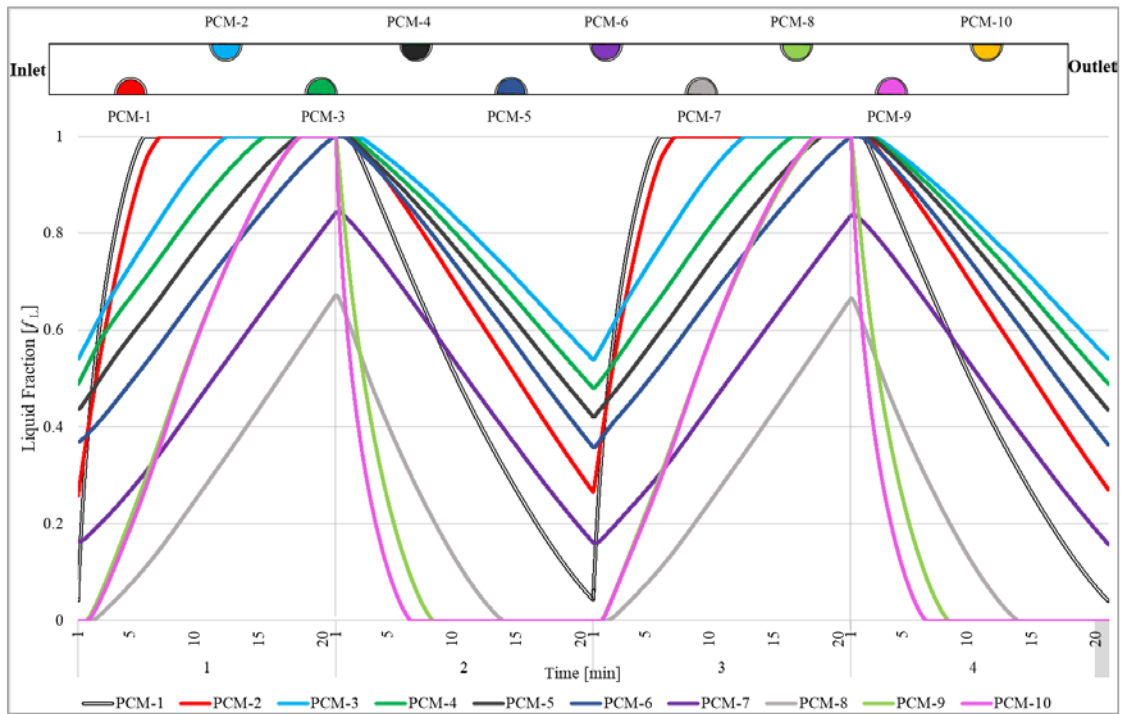
Figure 5.27. Melting/ solidification results for 20-minute operating time.

Figure 5.28 defines the system temperature change for 20-minute of operating time. In this figure, 1.5 min., 3 min., 5 min., 7 min., 9 min., 11 min., 13 min., 15 min., 18- and 20-min. results are found. The red color represents 34°C, while the blue color represents 25°C. In the system operating in exhaust mode, almost all tubes melted in the 20th minute. Only 3 tubes are not completely melted, and the 6th 7th, and 8th tubes also reached the melting temperature of 27°C.
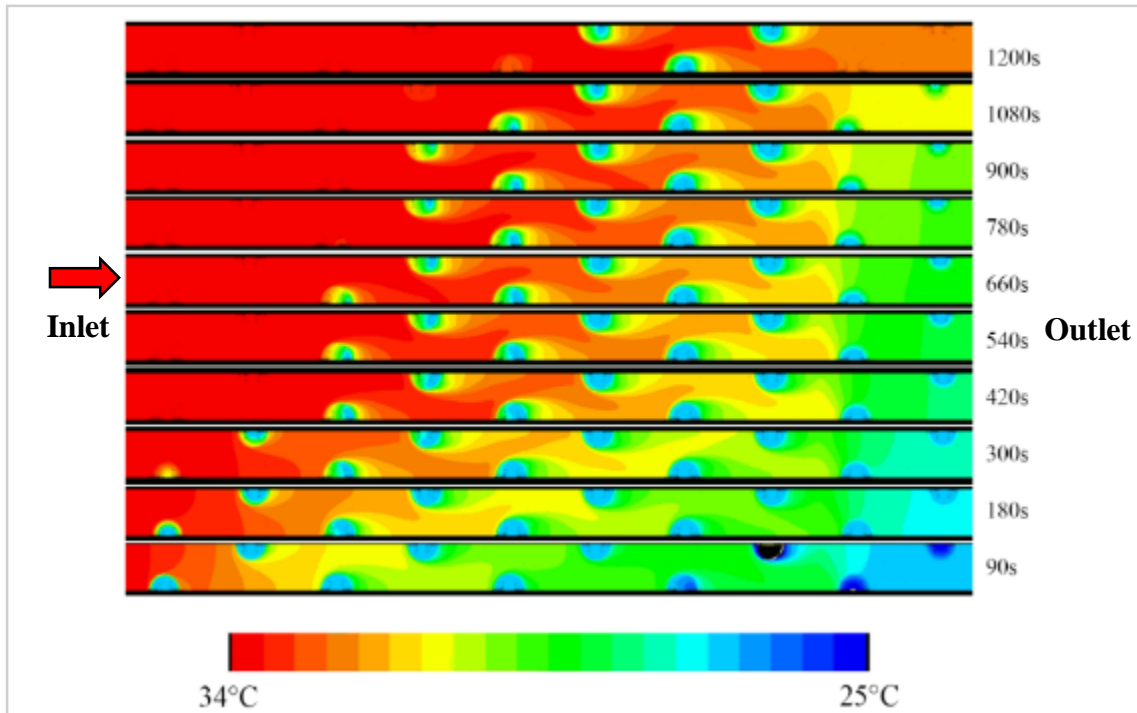
Figure 5.28. Temperature change in the system for the 20-minute operating time in a different time step.

Figures 5.29, 5.30, and 5.31 refer to the 30-minute operating time for the tube bundle HRV system. Figure 5.29 shows all-tube PCM in each tube melts and solidifies. Almost all tubes reach the outdoor temperature of 34°C, and only the 7th tube remains at 30°C. The phase change temperature of 27°C is exceeded by PCM in all tubes.

Figure 5.30 presents the 30-minute operation time liquid fraction and time graph. All PCM melted in the system. However, not all tubes solidify completely in case of solidification. The graph shows that the 4th tube solidifies 80% while the 2nd, 3rd, and 6th tubes solidify 90%.
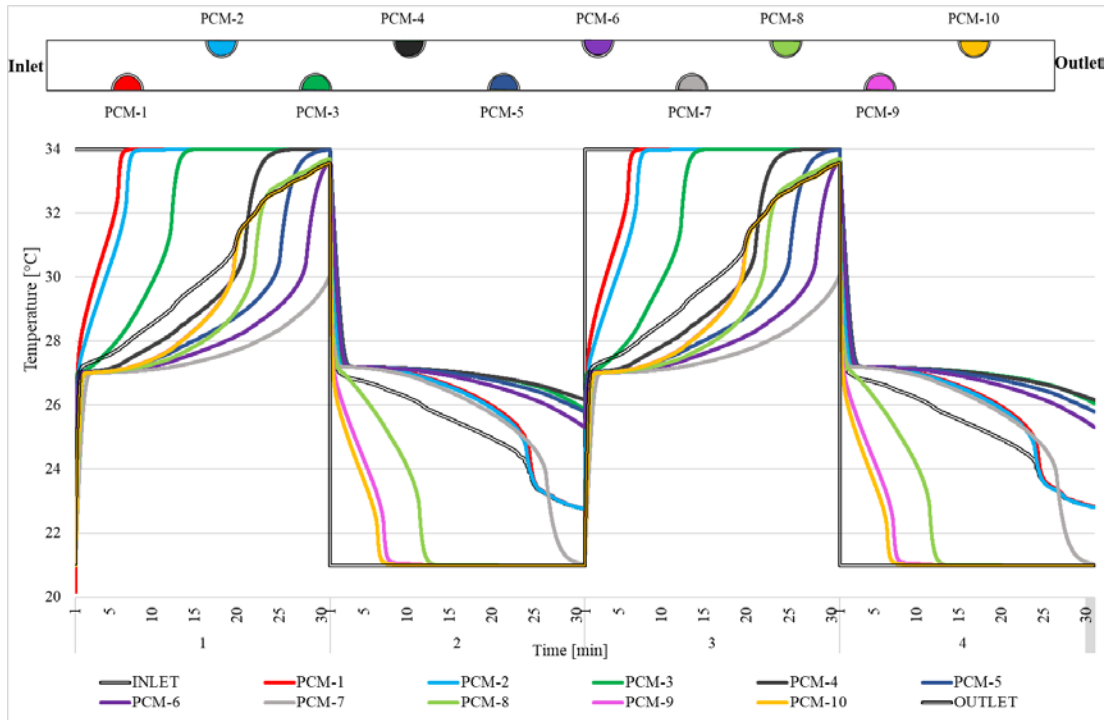
Figure 5.29. Cyclic results for 30-minute operating time.
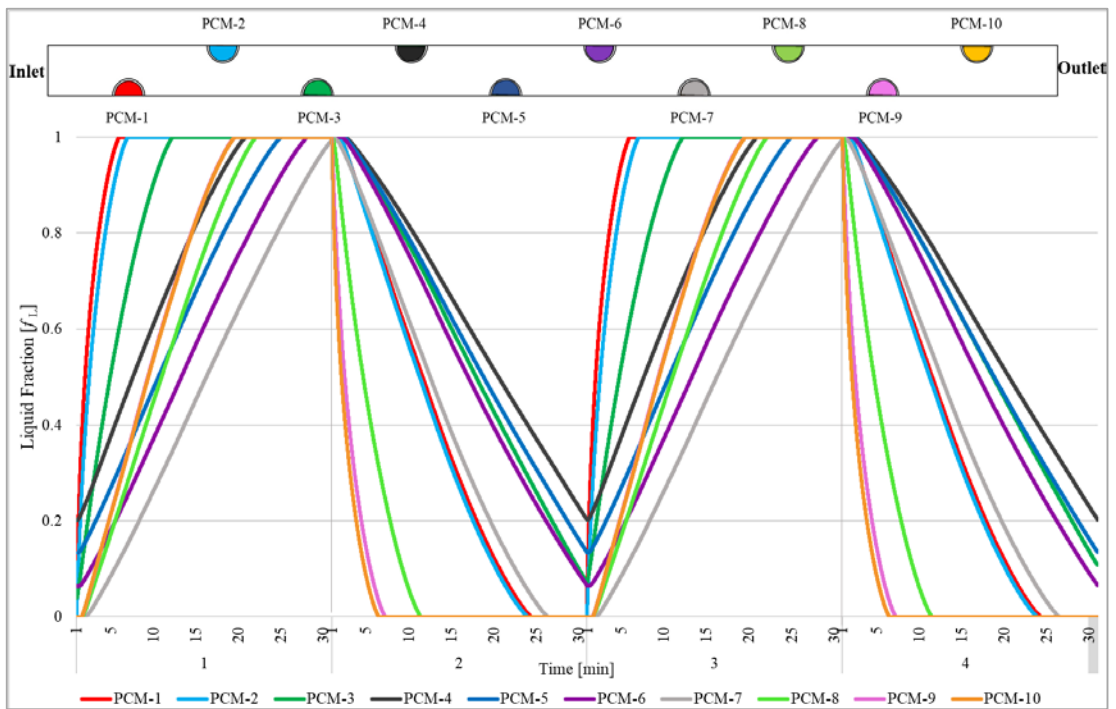
Figure 5.30. Melting/ solidification results for 30-minute operating time.

Figure 5.31 shows the temperature change of the tube bundle system at specific times. For 30-minute, the system was observed periodically. The indicator below shows the values of the colors. Here, blue represents 25°C which is indoor temperature, and red represents 34°C which is the outdoor temperature. As can be seen, all the tubes reached the outside temperature, only the internal temperature of the 7th tube could not reach 34°C completely.
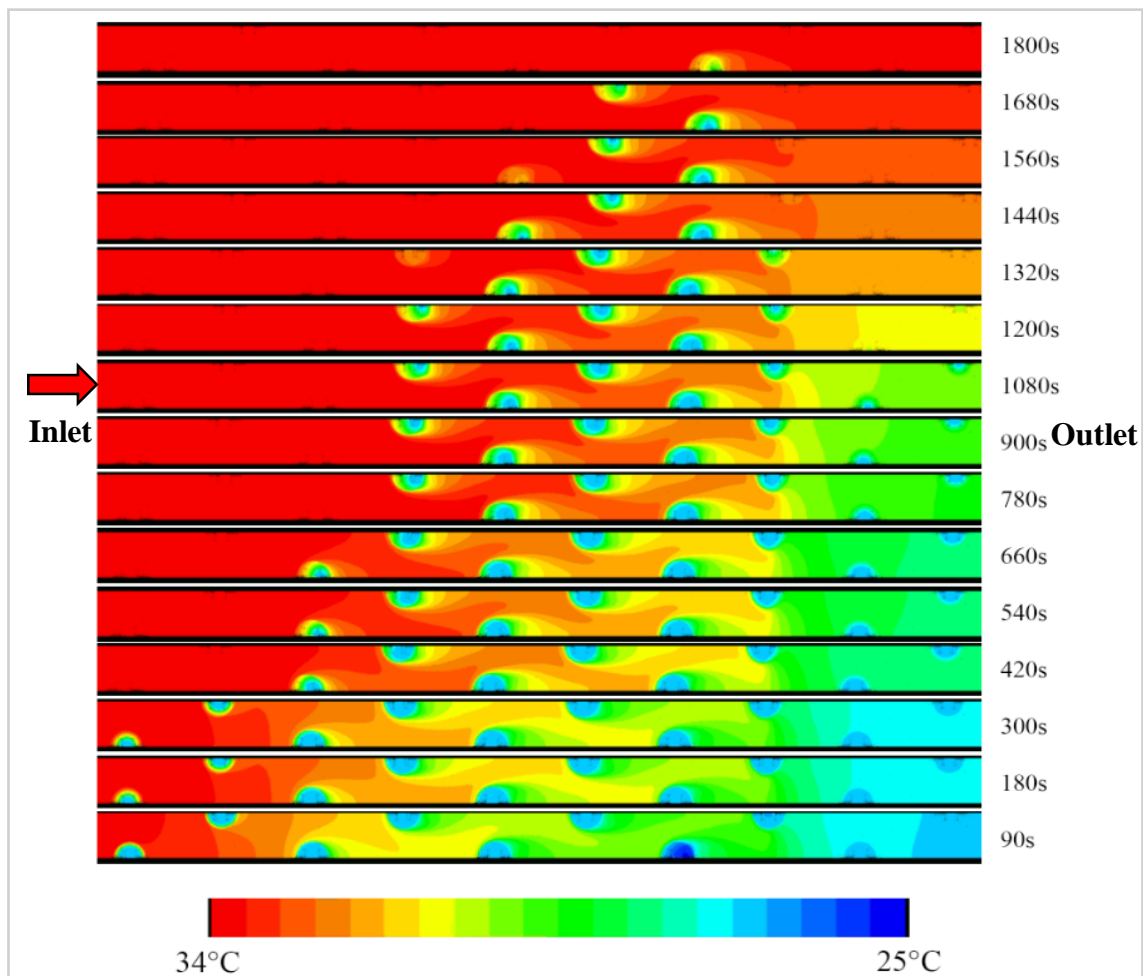
Figure 5.31. Temperature change in the system for the 30-minute operating time in a different time step

5.2.3. Data Reduction for Simulation Results

Sensible heat storage and Latent heat storage units' thermal models for charging and discharging characteristics have been developed with ANSYS Fluent software. The

number of charging and discharging has been optimized according to experimental data. The predicted results matched well with the data of the SHS and LHS units' experiments. The simulation results are summarized in Table 5.6, here air domain, PCM average temperature, ceramic temperature, inlet, outlet temperature, and HRV materials stored released energy results in terms of kJ. For the ceramic HRV unit 1-min., 2-min., 5-min., 7.5-min., and 10-min. cyclic results and for tube bundle units 15-min., 20-min., and 30-min. cyclic results have been shown.

The air energy change in the ceramic unit is given in Table 5.3 above, and the air energy change for the tube bundle is given in Table 5.5. Table 5.6 shows the results obtained from the simulations. Here, the energy changes in the units are shared, and there is a difference of 1-10% on average from the experimental results.

Table 5.6. Energy changes in the units according to simulations.

Time	Air_temp	Ceramic_temp	Inlet	Outlet	Ceramic (kJ)
1min	15.11	10.40	6.25	20.00	5.11
2min	16.57	13.73	9.66	20.00	10.32
5min	18.57	17.42	15.63	20.00	21.20
7.5min	19.11	18.44	17.41	20.00	30.91
10min	19.33	18.83	18.05	20.00	34.22
7.5min	32.22	32.01	34.00	28.67	16.14
10min	32.90	33.08	34.00	32.36	29.66
	Air_temp	PCM_temp	Inlet	Outlet	PCM (kJ)
15min	30.67	29.45	34.00	28.90	25.94
20min	30.87	30.00	34.00	29.05	34.82
30min	31.45	30.14	34.00	30.15	41.94

Figure 5.32 represents the mean heat transfer rates of the SHTES and LHTES HRV unit results related to Table 5.6. According to the results, the 1-minute and 2-minute mean heat transfer rate results are very close to each other for ceramic HRV units. Also, according to the tube bundle HRV system, 15-minute cycle and 20-minute cycle mean heat transfer rate results are very similar. In addition to these, when the fan runs for a long period, electrical energy cost increases. So, the fan is more advantageous when the system operates for a short period.
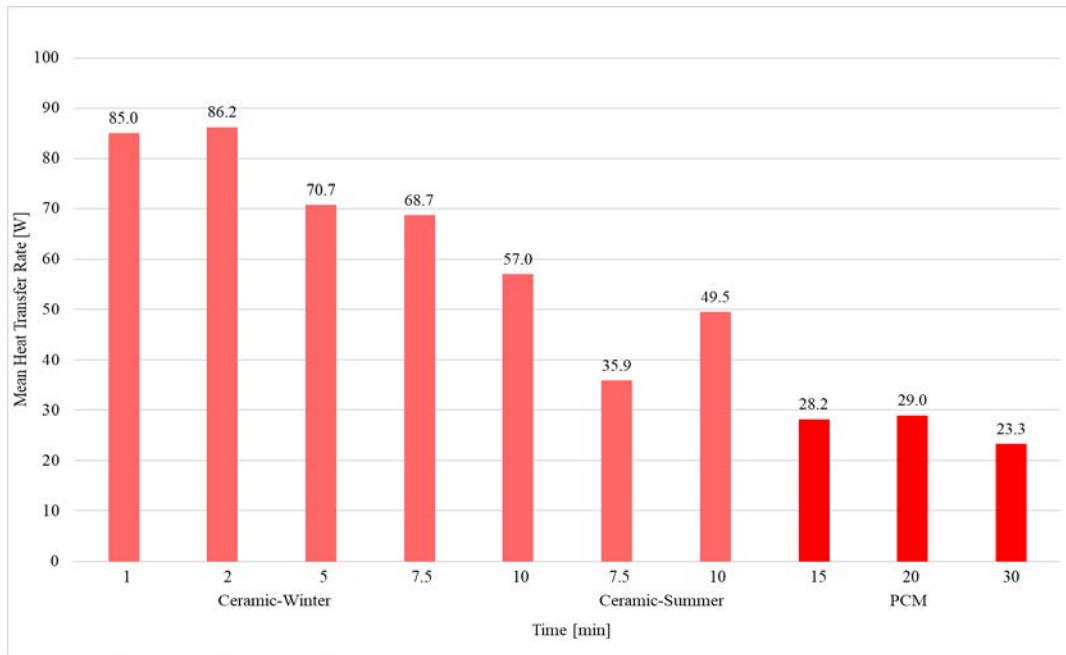
Figure 5.32. Comparison of mean heat transfer rates of ceramic and tube bundle systems

5.3. Refinement of the Tube Bundle Prototype Facade Unit

In this section, the changes of the CFD simulations for tube bundle decentralized heat recovery systems with six different concepts of alteration of the HRV units were investigated. As noted in this system's experimental and numerical results, the melting/solidifying results show that a 20-minute operation time gives the best thermal performance. Therefore, all simulations for tube bundle refinement are done in a 20-minute operation time. A numerical study of the charging and discharging process of the system validated experimental data that examined the performance of a tube bundle prototype LHTES.

The HRV unit design is very complex and considers different parameters such as the size of the HRV unit, heat transfer rate, pressure drop, long-term performance, and economic aspects. Various techniques have been applied to increase the heat transfer rate. Performance studies have been usually carried out by making changes in the size. The performance of the HRV unit is essential to reduce the size of the system and make the system more compact, and the performance depends on the heat transfer rate. A wide variety of experimental measurements and numerical studies (CFD) have been carried out in the literature (Kakaç 2020).

According to the literature, heat transfer can be enhanced with many different modifications of the HRV unit by using a tube bundle which is the object of this thesis. To obtain the best performance from the PCM tubes, the diameter of the tubes, pitch size of the tubes, different PCM solidification/melting temperature, tube shape, air velocity is studied through the CFD simulations (Figure 5.33). This model of the ANSYS-Fluent 19.0 package is used to develop the system. In this figure, the S_T means transverse pitch size, and S_L means longitudinal pitch size. For the 3mm tube, the transverse pitch size has been taken as 14 mm, and the longitudinal pitch has been changed. For 4.76 mm, both longitudinal pitch and transverse pitch sizes have been altered. And for the tube shape, air velocity, PCM combination, and case combination cases, the experimental setup tube bundle system is simulated separately, as shown in Figure 5.33.
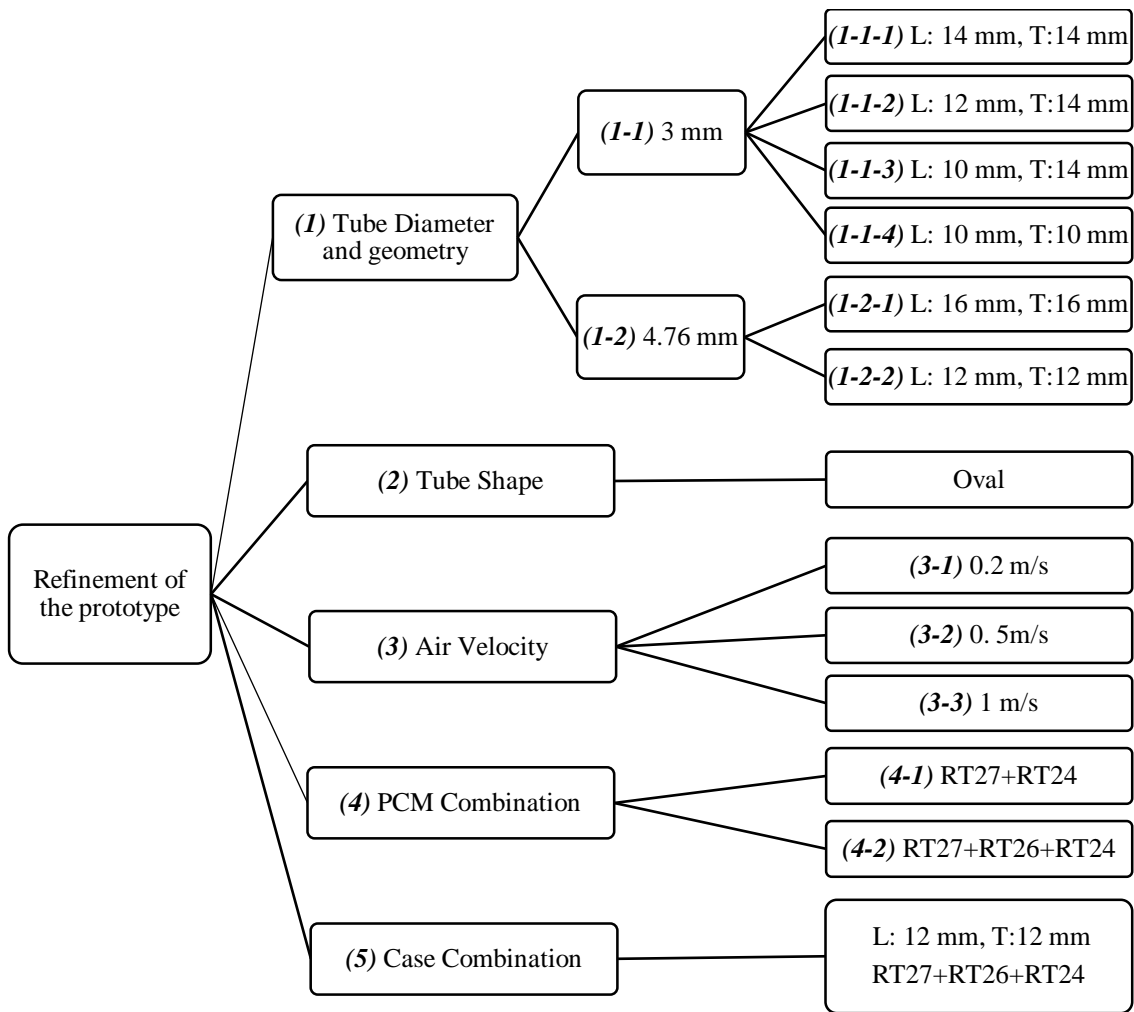
Figure 5.33. Refinement of the prototype classification.

In the light of these cases, a tubular HRV unit is changed in the following studies. Figure 5.34 shows the overview of the ventilation system with a tube bundle prototype. The numbers represent the covers for inside (1) and for outside (2), filter (3), fan (4), and HRV unit (5). In this decentralized ventilation unit with a heat recovery system, different simulations were made by changing the tube bundle dimensions [case *(1)*], changing the shapes of the tubes [case *(2)*], changing the fan speed [case *(3)*], and changing the PCM material used [case *(4 and 5)*].
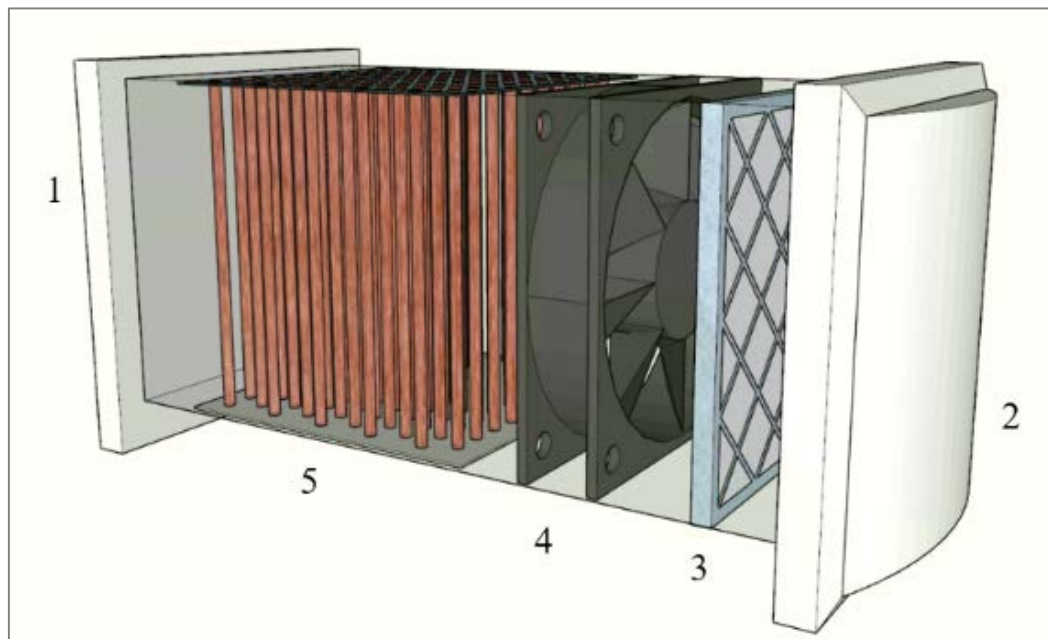
Figure 5.34. Overview of the tube bundle heat recovery system.

5.3.1. The prototype of the decentralized HRV system with PCM

The experimental studies of the HRV unit, introduced in Chapter 3, have 10 by 10 rows and consist of 100 copper staggered tubes filled with PCM, and this system is investigated under defined simulation conditions in this subsection. This tube bundle unit occupied with PCM acts as an HRV unit made up of copper tubes. This prototype consists of 100 copper staggered tubes filled with PCM at the airflow direction. The units' outer diameter is 4.76 mm. The tube arrangement in the bundle is designed as 1.4 cm for the transverse pitch and 1.4 cm for the longitudinal pitch. The prototype measured the diagonal pitch between tube centers as 1.565 cm in the prototype.

Figure 5.35 present the schematic diagram of the plan of the tube bundle system. The air is taken from outside (inlet), passes through the tubes and reaches the indoor environment (outlet).
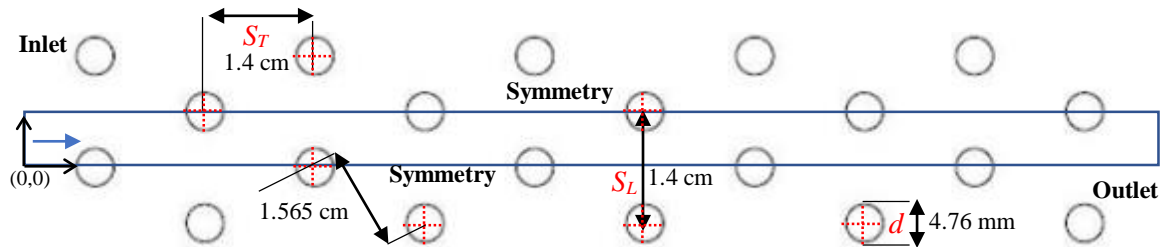
Figure 5.35. The prototype tube bundle system geometry.

This computational domain is given in Figure 5.35, with boundary and initial conditions are used in numerical modeling. The physical boundaries for this domain, inlet, outlet, symmetry, and wall. In this case, temperature and velocity are fixed values at the inlet and the outlet's reverse situation. In Figure 5.35, each row has 1 or 2 full tubes. Half tubes are alternately placed along the top and bottom walls of the test model to simulate an infinite tube bundle and reduce the wall boundary layer. The coordinate system and important geometrical parameters are also shown in this figure. The origin of the coordinate system is determined at the center of the row's middle tube. The transverse and longitudinal directions are denoted by x and y, respectively. The direction pointing out is given to the z-axis, which is not displayed. The 2D modeling of the computational domain has been performed in ANSYS FLUENT 19.0. CFD programs generate solutions that apply to different elements of the flow for partial differential equations. The equations characterize the fluid flow with pressure, temperature, density, and velocities. The geometry that may be utilized for flow analysis must be created and imported before CFD tools can process it. The geometric model covers the overall system design and the other equipment. The geometry is initially created in 2D in the ANSYS program's "Design Modeler" tool. The important thing for utilizing 2D modeling to analyze the research is that the system flow geometry can be followed more precisely, producing the best convergence results. Furthermore, by monitoring the change in units to time-dependent, this 2D model determines temperature distribution and flow profiles, and pressure drops for various operating conditions are studied.

Indoor and outdoor temperatures have been kept constant, and the indoor temperature is 21°C, and the outdoor temperature is 34°C. According to the melting/solidifying findings for the tube bundle system, 20-minute of operating time provides the optimum thermal performance for maintaining a comfortable indoor temperature with the least amount of energy consumption according to the storage rate. For this reason, 20-minute was taken as a reference for subsequent simulations.

According to most of the earlier experimental and numerical studies on flows in the tube bundles, focused on making changes in the dimensions of the tubes, the shape of the tubes, the system inlet air velocity, the PCM combinations used in the system. In the present study, the impact of the changes in the system is simulated and modeled, and the results are shared in this section.

5.3.2. (*1*) The Alteration of Tube Diameter and Geometry

Many studies have been done in the literature by changing tube sizes and pitch sizes, and according to these studies, the tube bundle has been simulated by making changes in the system 1, 3, 5, 6, and 7 are studied pitch ratios. Also, 1, 2, 3, and 4 are analyzed by changing the tube arrangement. Besides these, 1, 2, 3, 4, and 6 are worked numerically. 3rd and 7th studies set up the experimental setup for the tube bundle.

1 Erguvan and Macphee (2019) researched the energy and exergy analysis for tube banks. The CFD simulations are analyzed the different numbers of inline tubes, inlet velocity, pitch ratios. It was found that energy efficiency decreased with increasing pitch ratios. And increasing the number of inline tubes increased the energy efficiency because of high convective heat transfer.

2 Park et al. (2020) analyzed eight different tube arrays. The melting characteristics, energy density, liquid fraction and temperature distributions, heat transfer rate, and melting time are analyzed. The number of tubes affects the melting rate and the energy density. And also, the tube arrangements affect the required melting time.

3 Sakhaei et al. (2020) examined the effects of tube arrangement and pitch on the performance of a single-row tube bundle. This bundle arranges three different schemas, which are flat, inclined A, and V frames are investigated. Flat bundles showed greater pressure drops of up to 60% and heat transfer rates of 30% than their inclined counterparts.

4 Mahant et al. (2013) simulated flow performance with tube bundle, and the pressure drop of tube bundles with 30, 45, and 60° arrays are analyzed with ANSYS-Fluent. The results show that the pressure drop of the 60° array is less than at 45°.

5 Gugulothu et al. (2017) reviewed heat transfer enhancement techniques of heat exchangers. This research paper is to study the enhancement of heat transfer using passive techniques like Reynolds number, Nusselt number, friction factor, pitch ratio, pressure drop, and sizing, etc. in **6** Kongkaitpaiboon et al. (2010) study examined the pitch ratio and found that the heat transfer rate increases with the decreasing pitch ratio. **7** Bas and Ozceyhan (2012) experimented with twist ratios and clearance ratios. They investigated that heat transfer enhancement is greater for lower clearance ratio and lower twist ratio.

After the literature review, the heat transfer enhancement during charging and discharging of PCM is numerically analyzed according to the above studies. The tube diameter alteration parameters, size of the HRV unit, the boundary conditions, and the initial and final conditions of these cases are kept the same for performance comparison. At the starting of the charging, the PCM is considered a solid phase with a value of the liquid fraction of 0.00 at a temperature of indoor temperature, which is 21°C. On the other hand, liquid PCM will release thermal energy in discharge. In this case, the outer diameter is 3 mm. The tube arrangement in the bundle is designed as three different transverse pitches and longitudinal pitches. And then, for the 4.76 mm tube, the tube arrangement is changed as a 16 mm and 12 mm pitch size.

5.3.2.1. (*1-1*) 3mm Tube Diameter

In this tube bundle arrangement, the tubes in the system are replaced with tubes with a diameter of 3 mm. Four different pitch sizes are simulated with these 3 mm tubes, and the results are explained separately below.

The simulation results, which have been processed under subheadings, are given below, and the evaluation has been made according to the changed dimensions.

5.3.2.1.1. (*1-1-1*) 14mm Longitudinal and 14mm Transverse Pitches

The 3 mm diameter tubes are arranged 14 mm for the transverse pitch and longitudinal pitches. Figure 5.36 shows the 3 mm diameter tube bundle system. In this

arrangement, only the diameters of the tubes have changed, and the tubes that were previously 4.76 mm are 3 mm in this arrangement. However, the layout in Figure 5.36 remained the same as the pitch sizes experimental prototype.

Figure 5.36. 14 mm for the transverse and longitudinal pitches 3 mm tube diameter system cross-section.

Figures 5.37 and 5.38 illustrate the contours of temperature changes and liquid fraction of PCM for 20-minute of operation time starting melting. In this system, there are 100 tubes. The effect of pitch size and tube diameter on heat transfer enhancements of PCM varies with the distance between the tube arrays. Figure 5.37 shows the results of the temperature of tubes and inlet and outlet temperature. When looking at the 20-minute results, all PCMs are reached outdoor temperature, which is 34°C.
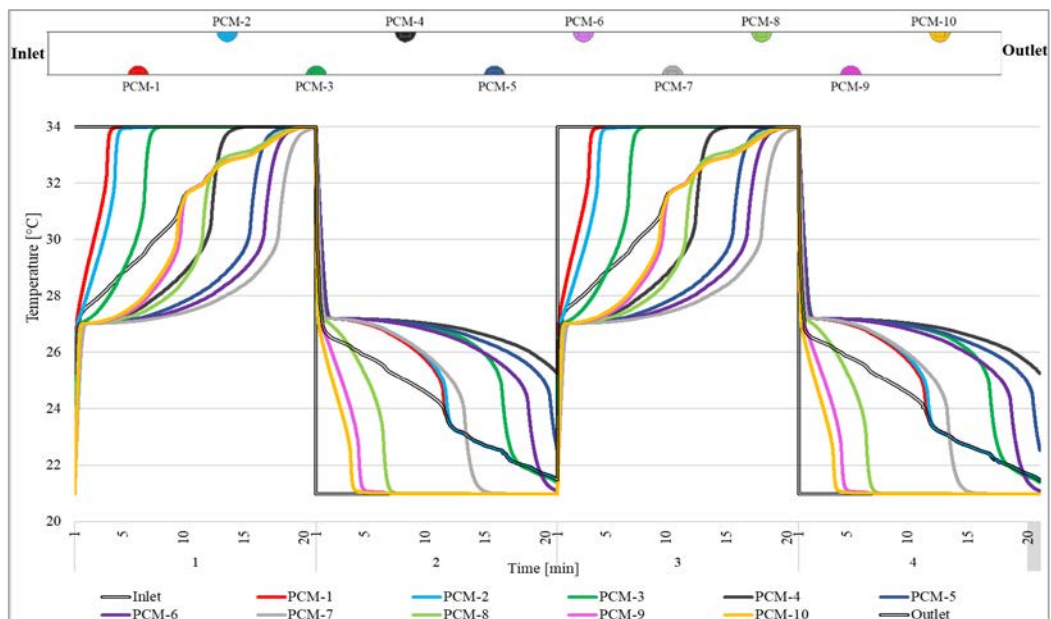
Figure 5.37. Cyclic results for Ø3 mm tube with 14 mm longitudinal, 14 mm transverse pitches.

144

Figure 5.38 illustrates the melting/ solidification of a 3 mm tube with a 14 mm pitch size of the prototype. Initially, the domain is fully occupied by the solid PCM, therefore, the value of the liquid fraction is zero (0.00), and this value increases as the charging time and decreases as the discharging time and becomes one (1.00) when the PCM is completely melted. All PCMs in the systems are completely melted; however, tube 4 is not completely solidified for 20-minute of operation time.
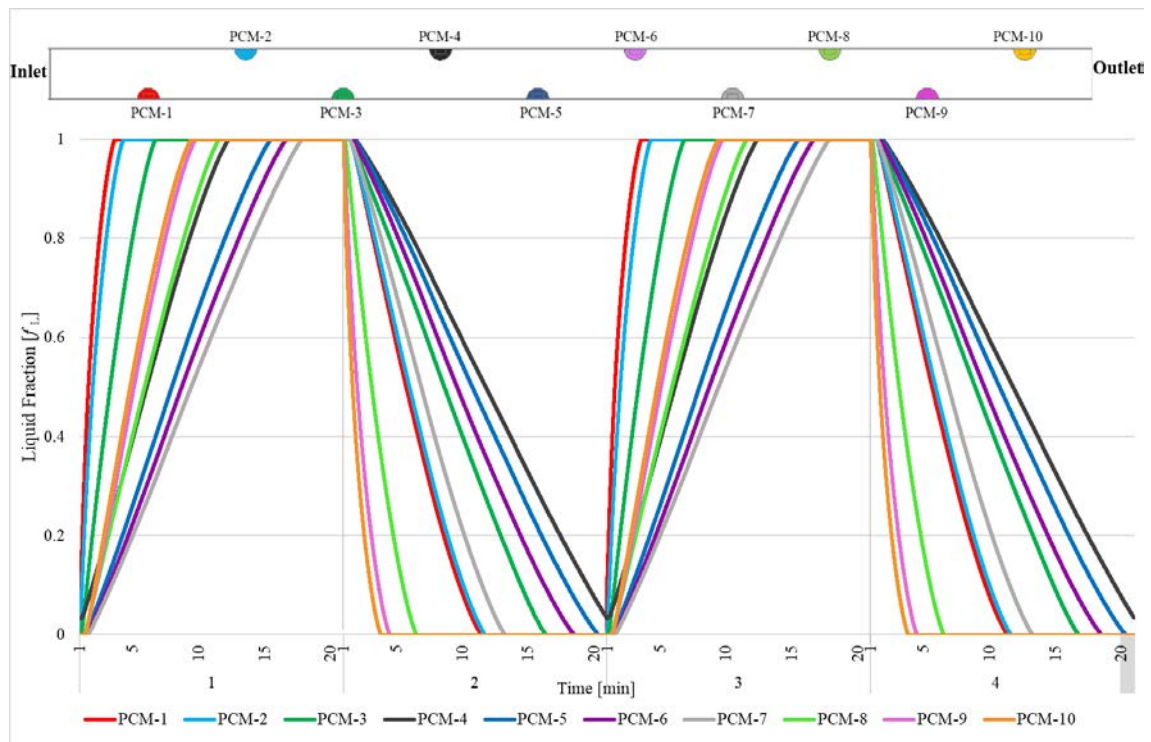
Figure 5.38. Melting/ solidification results for Ø3 mm tube with 14 mm longitudinal, 14 mm transverse pitches.

5.3.2.1.2. (*1-1-2*) 12 mm Longitudinal and 14 mm Transverse Pitches

The tube pitch size is 12 mm for 3 mm tube diameter in this arrangement. In this configuration, in the HRV unit, there are 120 tubes. And in one row, there are 6 tubes. Figure 5.39 shows the arrangement of the 3 mm tube. It shows the arrangement designed for the 3 mm tube. Here, unlike the above case, the tubes are multiplied by tightening the space between the tubes. And as seen in the figure, there are 12 tubes in a row in the flow direction.

145
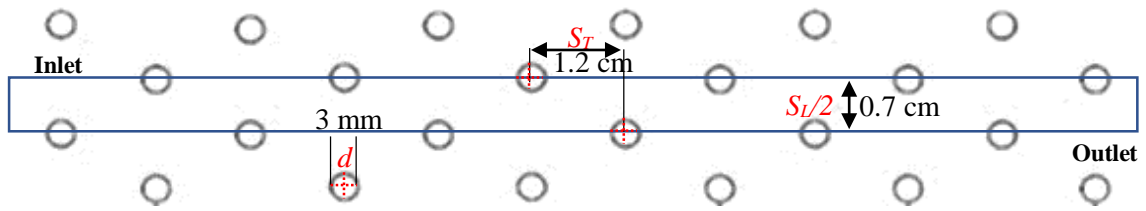
Figure 5.39. 12 mm longitudinal, 14 mm transverse pitches for 3 mm tube diameter system cross-section.

Initially, all PCMs are at 21°C in the solid phase. In 20-minute operation time, all PCMs are reached 34°C. In discharging process, the PCM inside the tubes acts as a heat source to melt the solid PCM. Figure 5.40 shows the contours of the temperature of tubes which increases and decreases. As a result, the solidifying process is not completely done after one cycle. PCM-5 and PCM-6 are not completely solidified.
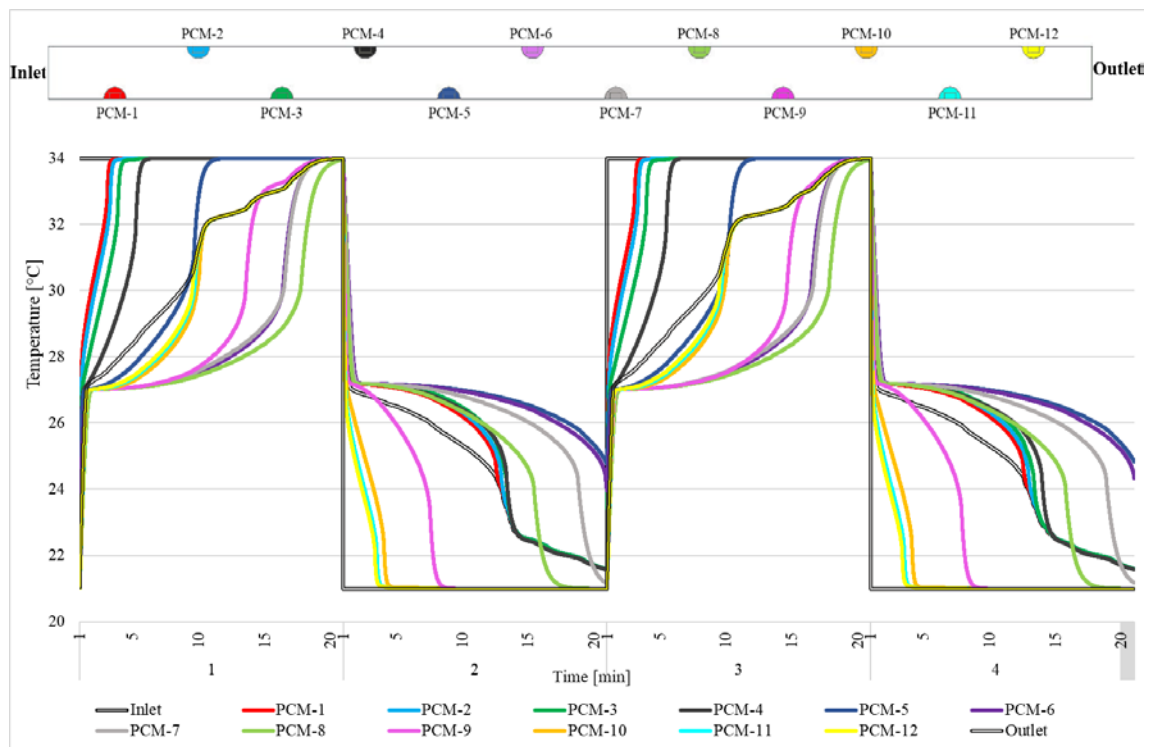
Figure 5.40. Cyclic results for Ø3 mm tube with 12 mm longitudinal, 14 mm transverse pitches.

The contours are shown in Figure 5.41, phase change from solid to liquid and liquid to the solid phase of PCM. It has been found that the value of liquid fraction at system becomes done (1.00) before 20-minute. The amount of PCM to be melted and solidified within an allowable time. But charging time and discharging time are different from each other. Charging time is shorter than discharging time in this arrangement. As a result, the 15 min. and 17 min. the liquid fraction became almost one for this case but solidifying process, all PCMs inside the tubes are not fully solidified.
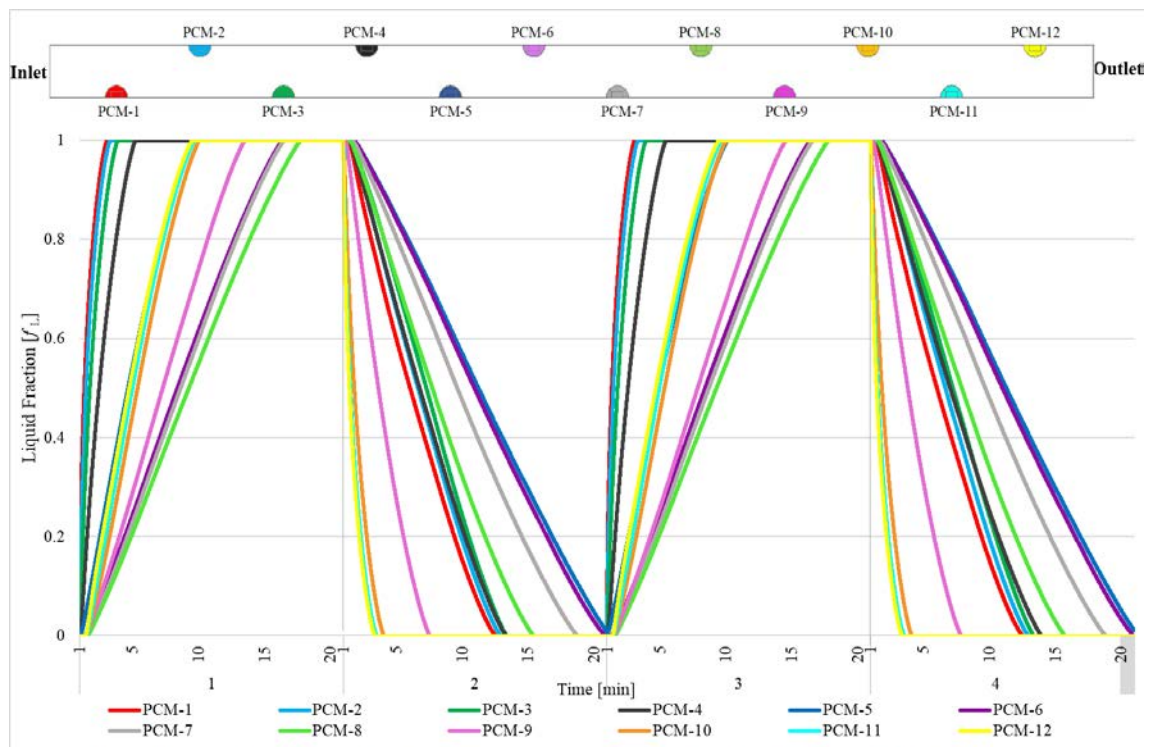
Figure 5.41. Melting/ solidification results for Ø3 mm tube with 12 mm longitudinal, 14 mm transverse pitches.

5.3.2.1.3. (*1-1-3*) 10 mm Longitudinal and 14 mm Transverse Pitches

With this arrangement, there are 140 tubes. In these cases, there are 14 rows of tubes in the streamwise airflow direction and 10 tubes per row in *y*, which is the spanwise direction. The longitudinal tube pitch (S_T) is 1 cm, and the transverse pitch size is (S_L) 1.4 cm. In Figure 5.42, the computational domain is taken as $S_L/2$ because of the geometric symmetry of the tube bundle HRV system.
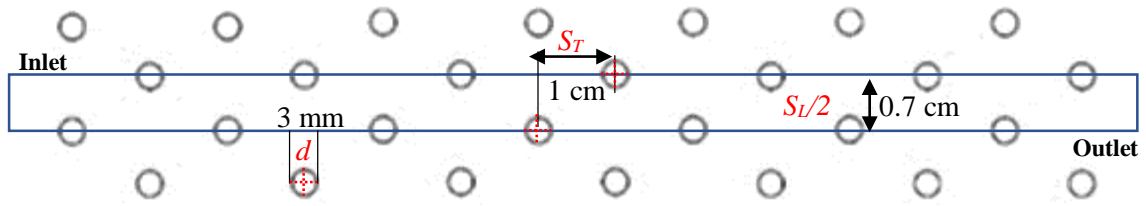
Figure 5.42. 10 mm longitudinal, 14 mm transverse pitches for 3 mm tube diameter system cross-section

In Figure 5.43, phase change takes place over a temperature interval. The phase change temperatures 27°C. Inlet air temperature is 34°C, and the indoor air temperature is 21°C. The temperature profile of each PCM node during 20-minute in the solidification and melting process is shown in Figures 5.43 and 5.44.
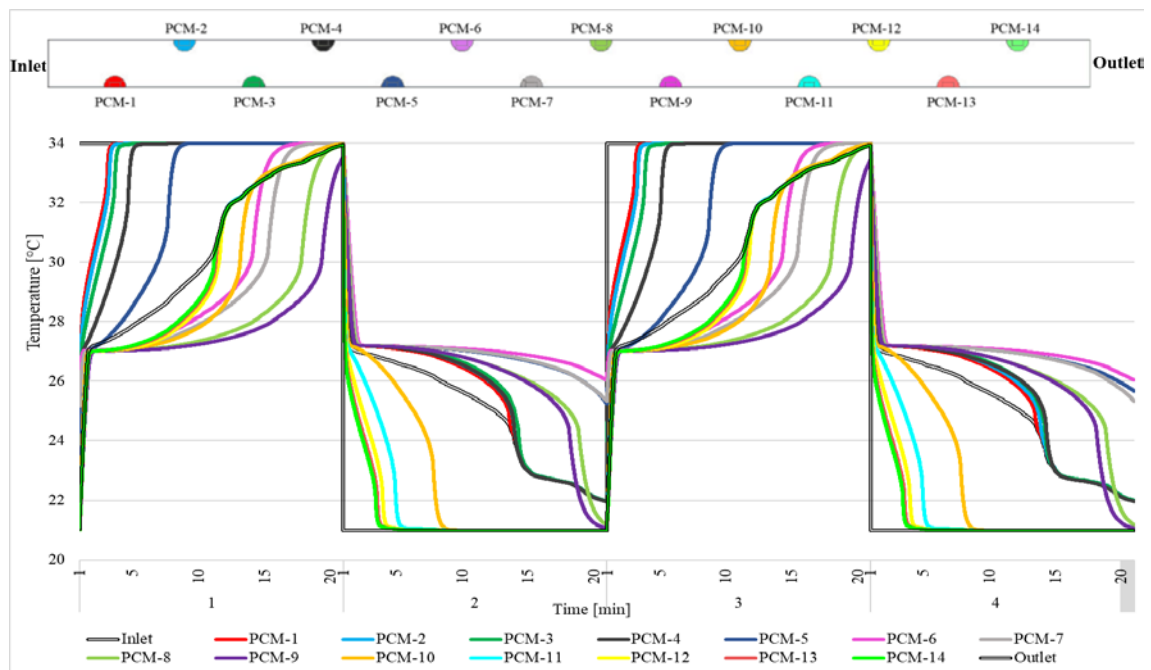
Figure 5.43. Cyclic results for Ø3 mm tube with 10 mm longitudinal, 14 mm transverse pitches.

The transient evolution of the PCM liquid-fraction profiles and the average temperature profiles are illustrated in Figure 5.44. It can be realized that all PCMs in the system are melted and solidified except the 6th tube. According to Figure 5.44, the best melting rate is that the PCM completes the melting before 20-minute.

148
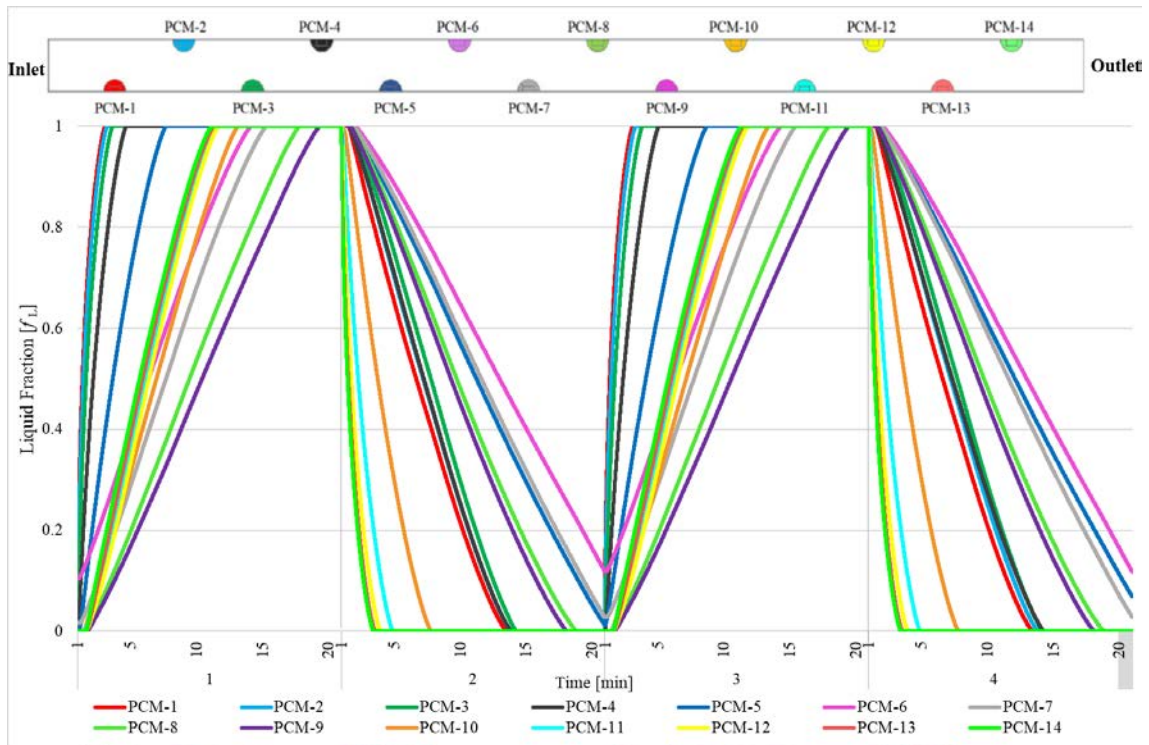
Figure 5.44. Melting/ solidification results for ∅3 mm tube with 10 mm longitudinal, 14 mm transverse pitches.

5.3.2.1.4. (*1-1-4*) 10 mm Longitudinal and 10 mm Transverse Pitches

In this case, there are 10 mm longitudinal and 10 mm transverse pitch sizes and a total of 3 mm diameter 196 tubes. Figure 5.45 shows the 10 mm-by-10 mm pitches size case for the tube bundle HRV system. The figure also shows the inlet and outlet of the model. In this case, $S_L/2$ is 0.5 cm.
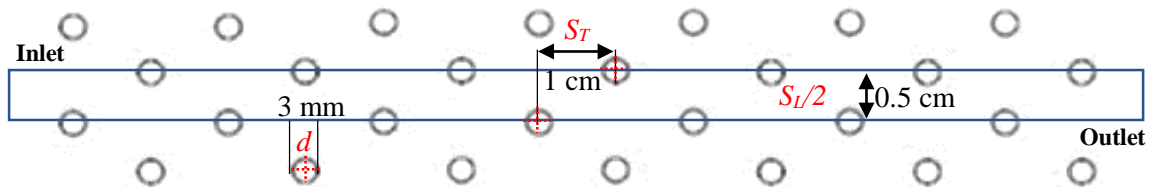
Figure 5.45. 10 mm longitudinal, 10 mm transverse pitches for 3 mm tube diameter system cross-section.

As in all simulations, in this case, the charging and discharging cycles of the system are simulated with 20-minute cycles. As seen in Figure 5.46, the temperature distribution of the thermocouples in 14 tubes can be seen. While the 14th tube reaches a maximum of 29°C, the 10 tubes of the system reach the outdoor temperature completely.
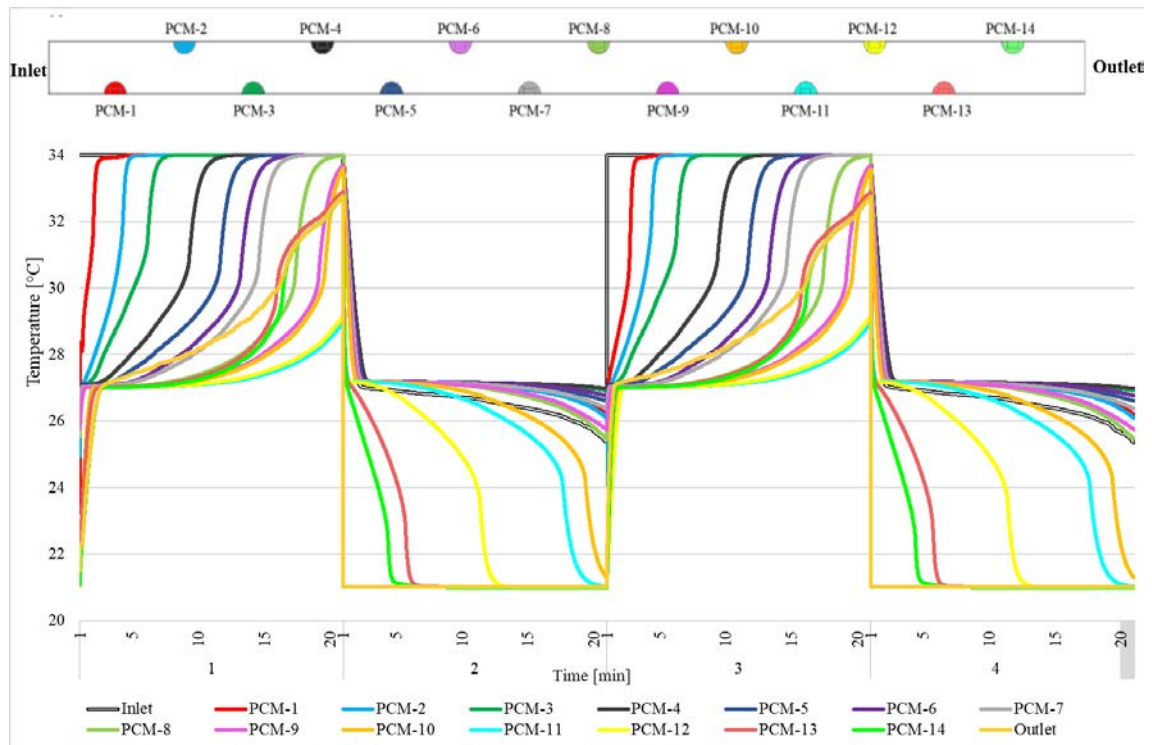
Figure 5.46. Cyclic results for Ø3 mm tube with 10 mm longitudinal and 10 mm transverse pitches.

Figure 5.47 represents the time-related melting and solidifying graphs for 20-minute operating. In addition, all PCM inside the tubes except the 11th and 12th tubes are completely melted. And the solidification process works have a reverse situation. The first solidified tubes were those close to the outlet. While the system is operating from indoor to outdoor environment, in supply mode since the measured air velocity in the experiments is less than the exhaust mode, there is no reaching the environment temperature as much as in the exhaust direction. However, the 5 tubes completely solidify and reach the indoor temperature in supply mode.
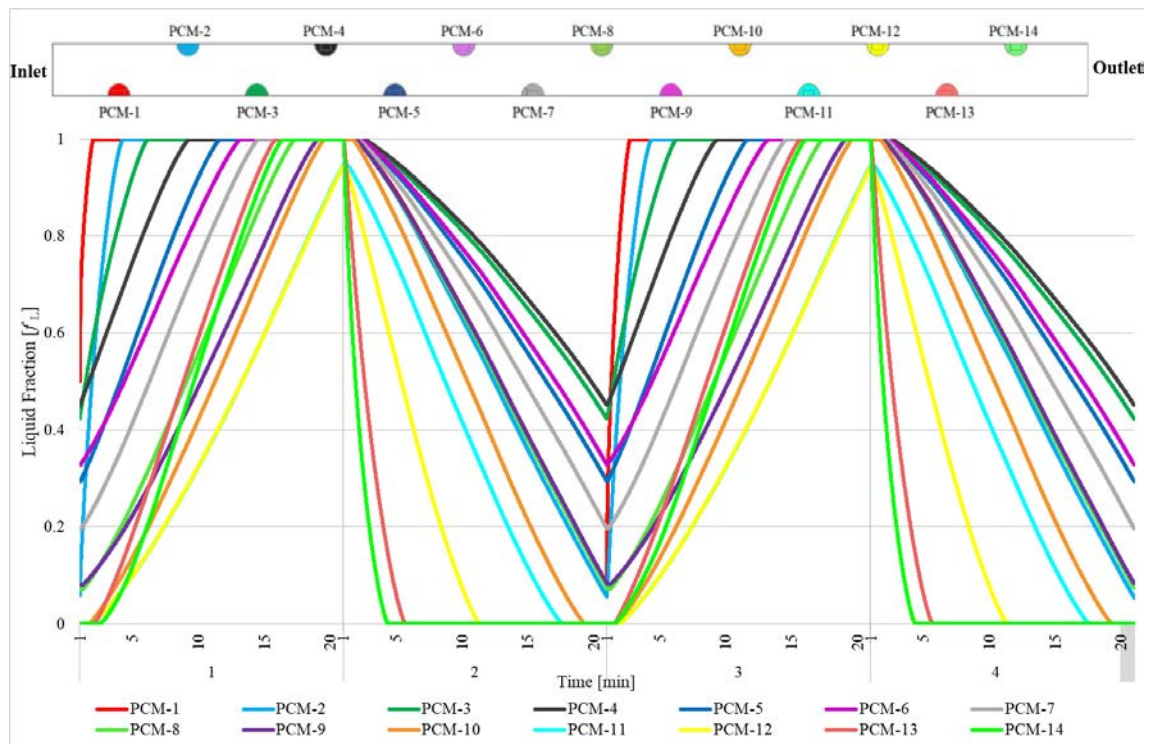
Figure 5.47. Melting/ solidification results for ⌀3 mm tube with 10 mm longitudinal and 10 mm transverse pitches

5.3.2.2. (*1-2*) 4.76 Mm Tube Diameter

In this case, the diameters of the tubes in the 15 cm system are fixed, and the longitudinal and transverse pitches of the tubes are changed. In this study, the results that can occur when the spacing of the 4.76 mm tubes is changed have been observed.

5.3.2.2.1. (*1-2-1*) 16 Mm Longitudinal And 16 Mm Transverse Pitches

In this case, 16 mm transverse and 16mm longitudinal pitch sizes were determined by changing the distances of the tubes between the tube bundle system used in the experiment. Figure 5.48 present the case for 4.76 mm. When tubes are placed in the system at 16 mm pitch size, there are 81 tubes.
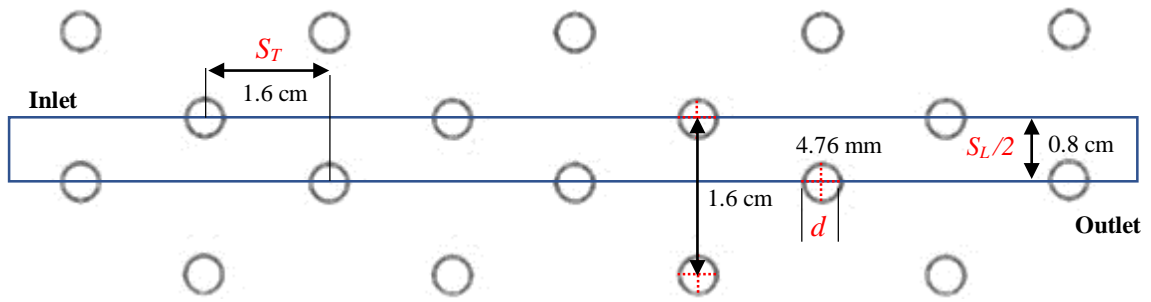
Figure 5.48. 16 mm for the transverse and longitudinal pitches 4.76 mm tube diameter system cross-section

Figure 5.49 shows the temperature distribution of 9 tubes. PCMs in all tubes, except for tube 6, reach outdoor temperature. The outdoor temperature is taken as 34°C, and the indoor temperature becomes 21°C during the solidification process. Only half of the PCMs can reach the indoor temperature of 21°C during the solidification process. As seen here, only 3 tubes reach the indoor temperature. These are the 7th, 8th, and 9th tubes.
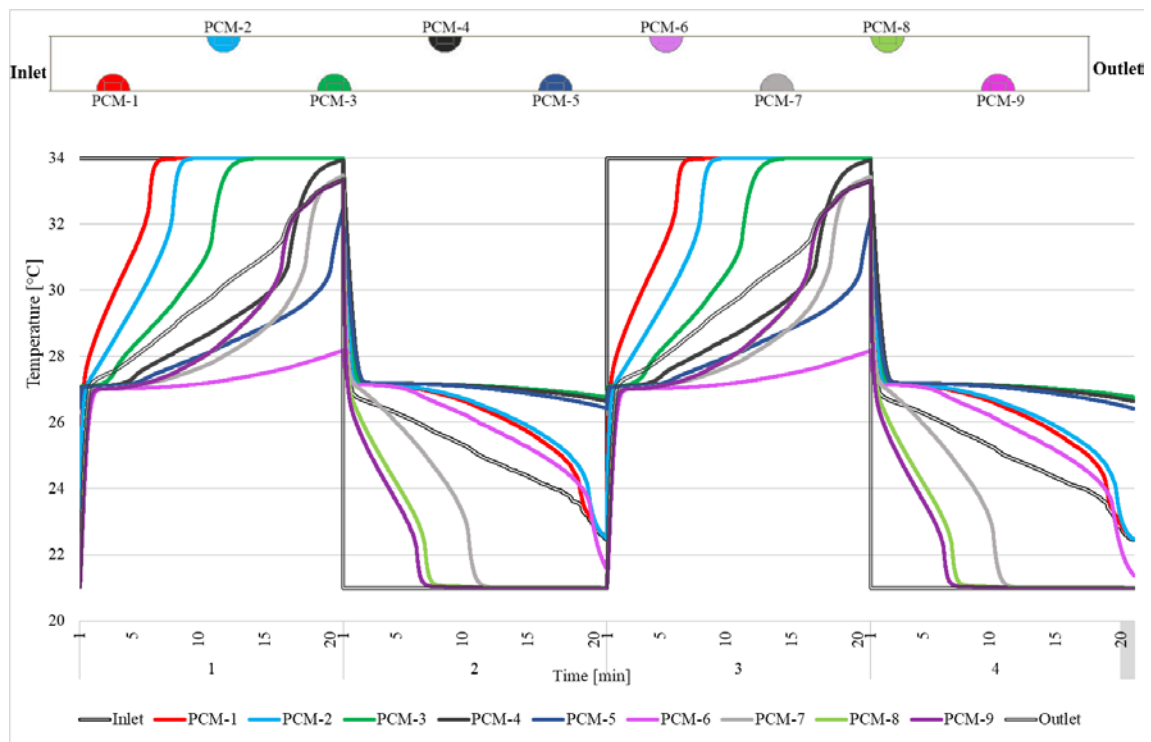
Figure 5.49. Cyclic results for ∅4.76 mm tube with 16 mm longitudinal, 16 mm transverse pitches

In Figure 5.50, the liquid fraction "f_L" can be evaluated on each tube to monitor the evaluation of the changing phase in the PCM enclosure. This figure gives the evaluation of the solid domain in 20-minute of operation time. The melting process begins from 1st to 9th except for the 6th tube. The solidification at the outlet shows the fastest rate. The rate of solidification 2nd, 3rd, and 4th rows is approximately 0.4. Only 60% of these tubes solidified.
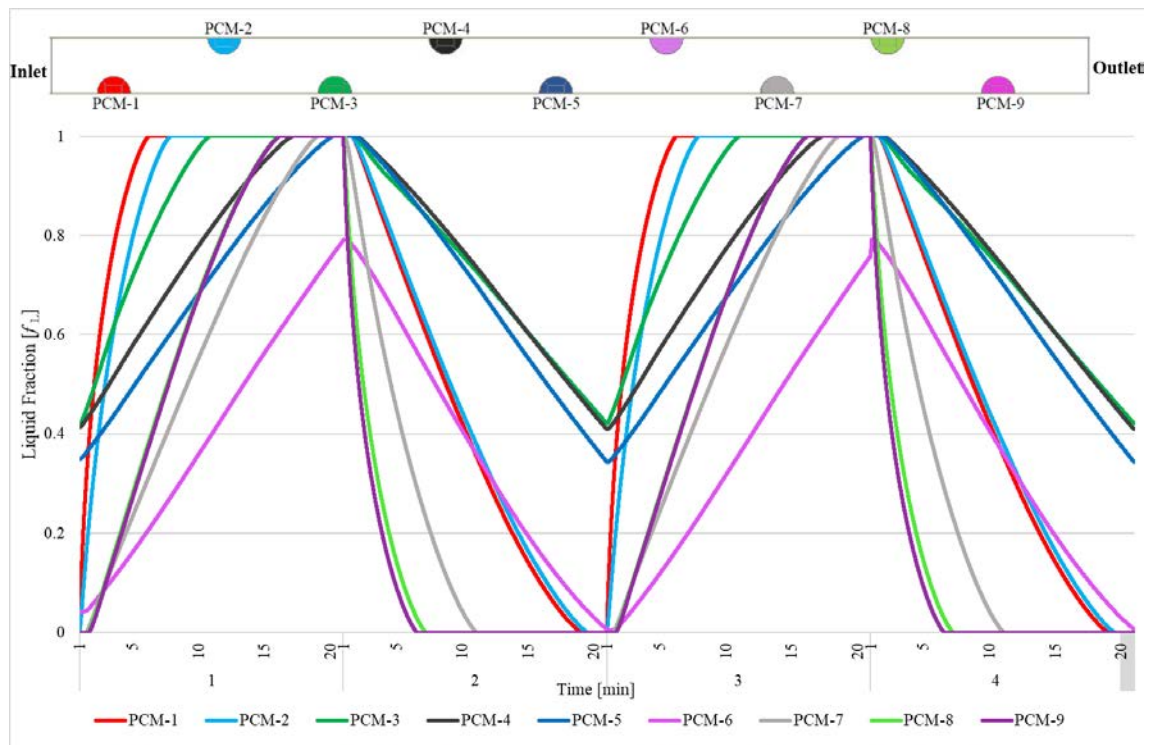
Figure 5.50. Melting/ solidification results for Ø4.76 mm tube with 16 mm longitudinal, 16 mm transverse pitches.

5.3.2.2.2. (*1-2-2*) 12 mm Longitudinal and 12 mm Transverse Pitches

In this case, the tubes have 12 mm longitudinal and 12 mm transverse pitches. The tubes diameter is 4.76 mm, and there are 144 tubes in the system. The arrangement of tubes for this case is present in Figure 5.51. In this case, the spacing between the tubes has decreased, and there are 12 tubes in each row, as seen in the domain.
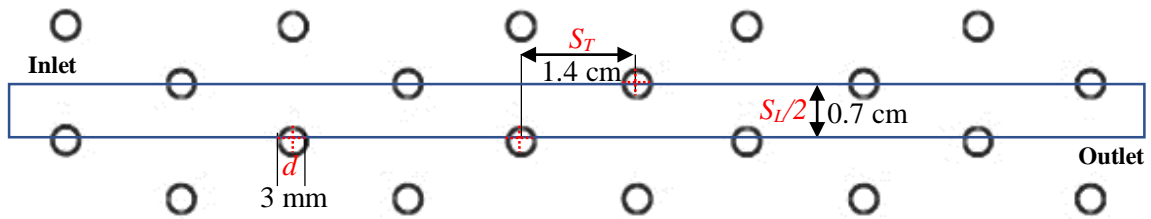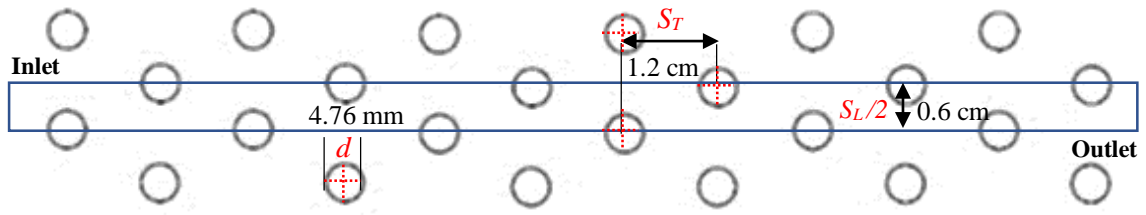
Figure 5.51. 12 mm for the transverse and longitudinal pitches 4.76 mm tube diameter system cross-section.

Figures 5.52 and 5.53 belong to 20-minute operating time for the tube bundle HRV system. Here, the outdoor environment is 34°C, the indoor environment is 21°C. And while the PCMs in 7 tubes reached outdoor temperature, the others remained below this value. In supply mode, only 4 tubes fully reached the indoor temperature.
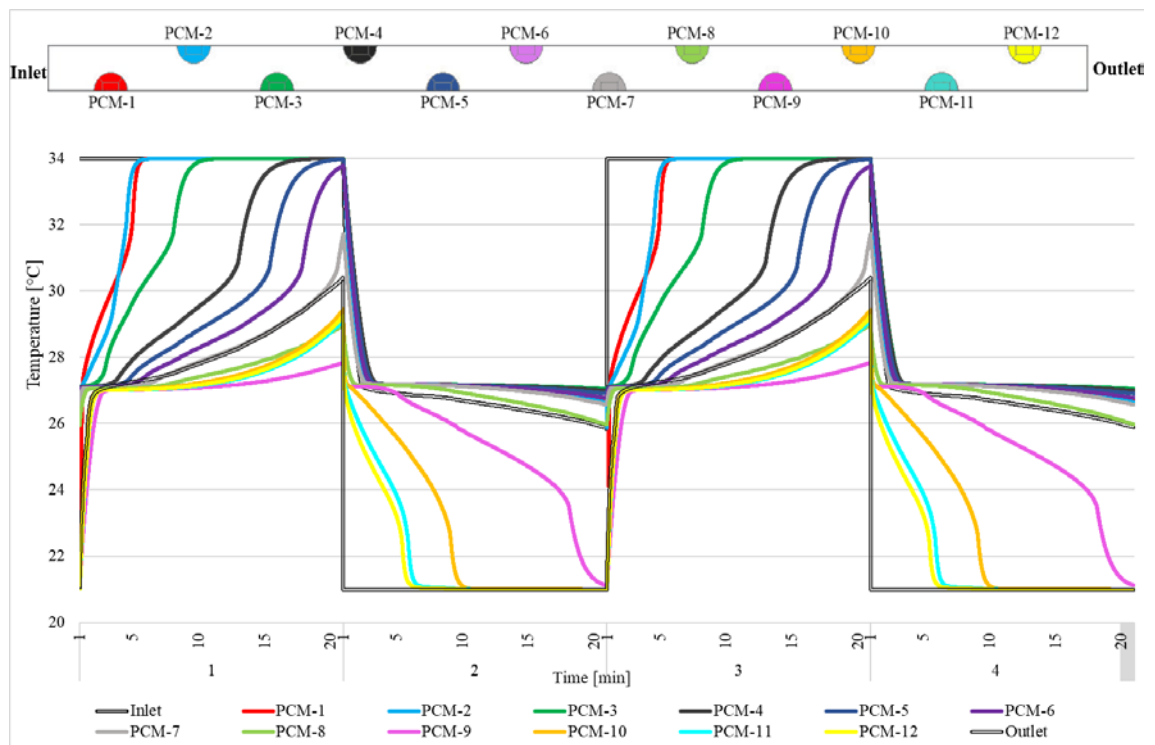
Figure 5.52. Cyclic results for Ø4.76 mm tube with 12 mm longitudinal, 12 mm transverse pitches.

Figure 5.53 shows the liquid fraction distribution of this system over time. In this figure, the charging and discharging process take 20-minute cycles. In general, 100%

melting is seen, while the 9th PCM melts at 60%, the PCM inside the 8th tube melts at 85%, the 10th, 11[th,] and 12th tube melts at 95%. HTF receives the heat from the charged PCM tubes resulting in the decrease of the PCM tubes temperature and increase of HTF temperature along with the system.
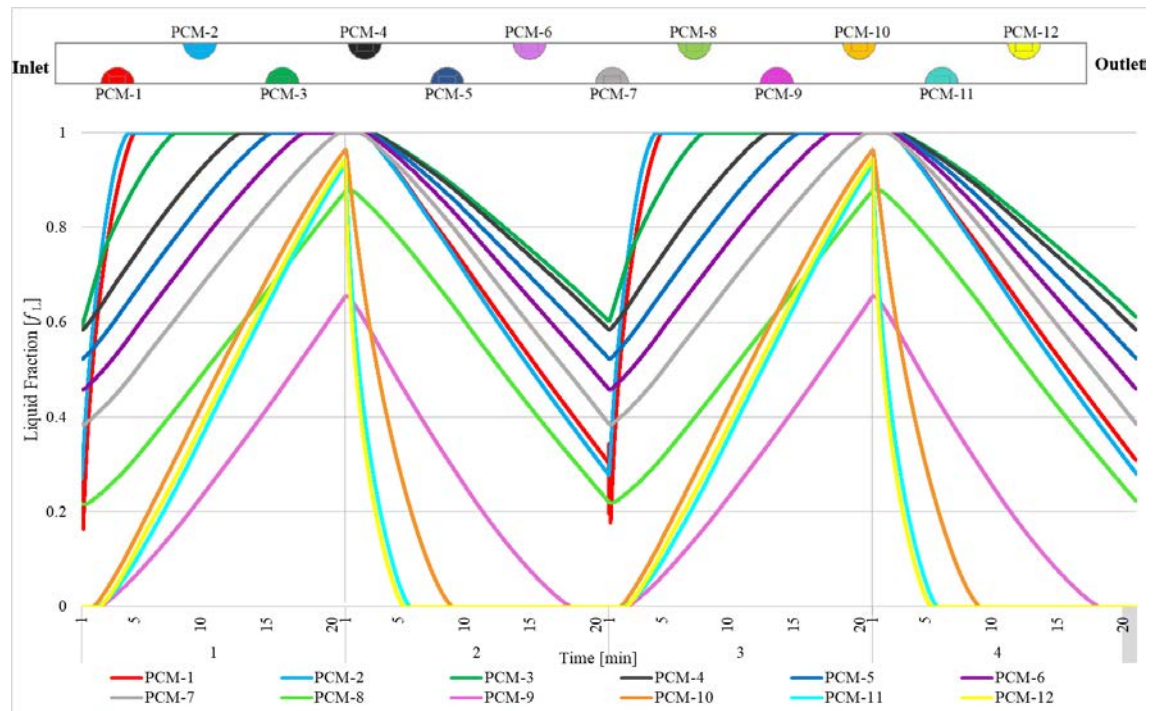
Figure 5.53. Melting/ solidification results for ∅4.76 mm tube with 12 mm longitudinal, 12 mm transverse pitches

5.3.3. (2) The Alteration of Tube Shape: Oval Tubes

There are several experimental and numerical studies available for oval tube shape as an alternative for round tube in the literature.

Myong et al. (2021) tested generic heat exchangers having oval tubes and round tubes for comparison. According to the findings of this research, the oval tube samples with a smaller diameter tube had the highest performance. Furthermore, the oval tube samples with a larger diameter tube had relatively low performance due to the significant pressure drops.

Li et al. (2018) studied experimentally heat transfer and pressure drop of the twisted oval tube bundle in crossflow with the staggered layout. The result is that the

performance of this twisted oval tube bundle is larger than that of the round tube bundle with the same layout. Also, the twisted oval tube bundle has an advantage in airside convection heat transfer over the round tube bundle with the same arrangement in crossflow.

Khan, Zou and You (2021) investigated the oval tube bundle with CFD. This study shows that the oval tube bundle provides better heat transfer enhancement with higher pressure drop than the traditional round tube.

Kim et al. (2014) investigated experimentally oval tubes and round tubes under wet and dry conditions. The experiments were conducted on sine wave fin and tube heat exchangers. According to the result of this paper, the heat transfer coefficients of oval tube samples are lower than the heat transfer coefficients of round tube samples. Oval tube pressure drops, on the other hand, are even smaller than round tube pressure drops.

Tan et al. (2013) investigated experimentally improving the heat transfer coefficient and decreasing the pressure drop with the twisted oval tube heat exchanger system. This study shows that the heat transfer coefficient of the twisted oval tube heat exchanger is higher, and the pressure drop is lower than the rod baffle heat exchanger. And the overall performance of the twisted oval tube Works more effectively at a low tube side flow rate and high shell-side flow rate.

According to these papers, in this case, the effect of the tube shape on the melting and solidifying process of PCM is presented. The charging-discharging process is observed by operating the system for 20-minute with oval copper tube bundles, which are confirmed to provide better heat transfer than the cylindrical copper tube. Figure 5.54 shows the oval tubes are the smallest copper tubes available in the market and which major axis is 4.5mm minor axis is 3mm. In this case, there are 100 tubes in the system.
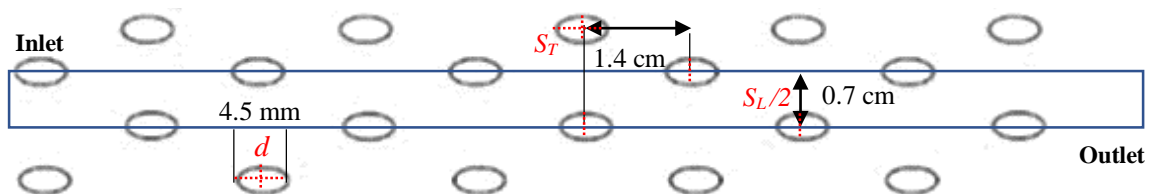
Figure 5.54. 14 mm for the transverse and longitudinal pitches 4.5 mm (major axis) tube diameter system cross-section

In this case, the charging and discharging efficiency are observed in Figures 5.55 and 5.56. When using oval tubes, the 5 tubes are completely melted in the charging process.
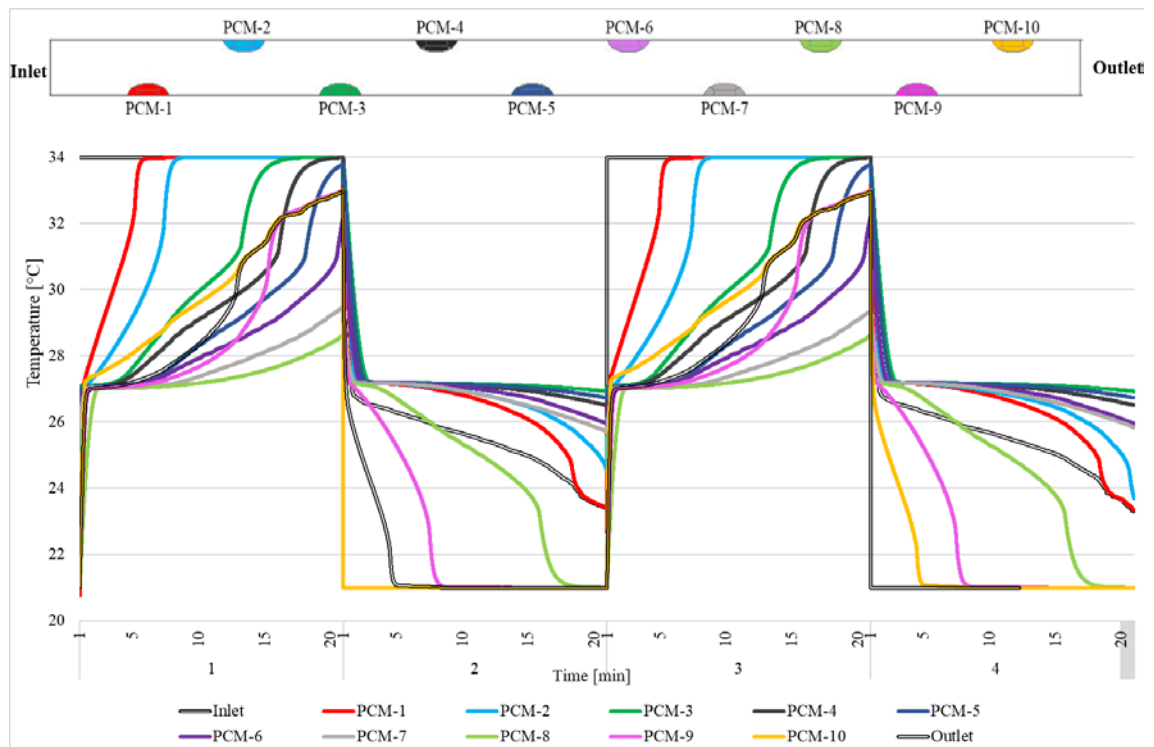
Figure 5.55. Cyclic results for Ø4.5 mm (major axis) oval tube.

Figure 5.57 shows the melting and solidification process of the oval tube case for the HRV system. The oval profile is found to be effective for the melting process except for the 8th and 7th tubes. While 80% of the 8th tube melts, 90% of the 7th tube melts. Looking at the solidification process, only 40% of the 3rd tube, 60% of the 2nd and 4th tube, and 80% of the 6th and 7th tubes solidify.
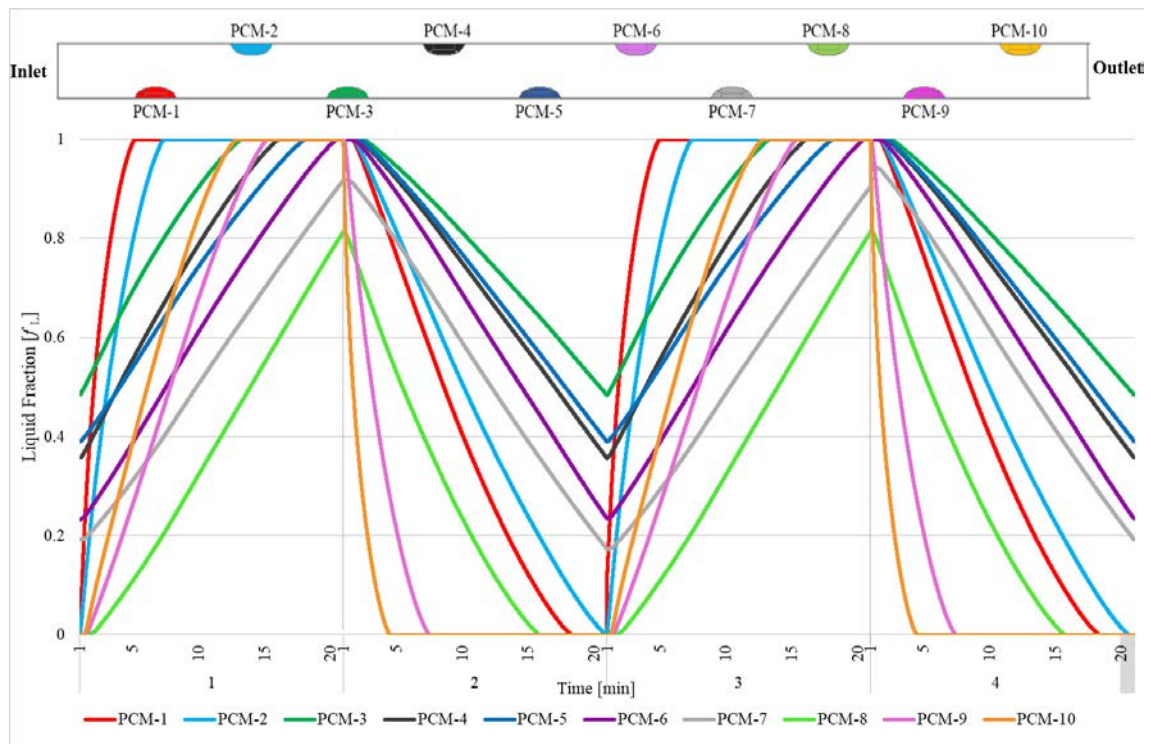
Figure 5.56. Melting/ solidification results for Ø4.5 mm (major axis) oval tube.

5.3.4. (*3*) Analysis of Changes of Air Velocity

The authors discovered that higher fluid velocity results in higher heat transfer, reducing associated irreversibility. Many researchers are interested in the performance of circular tube bundles and finned tube bundles.

Jang and Yang (1998) studied experimental and numeric ways for different values of inlet velocity ranging from 2 to 7 m/s. This paper showed that the average heat transfer coefficient of elliptic finned tubes is 35-50% of the corresponding circular finned tube having the same tube perimeter, while the pressure drop for elliptic finned-tube banks is only 25-30% of the circular finned-tube bank configuration.

Taufiq et al. (2007) present a second law analysis for the optimal geometry of fin array by forced convection. It has been shown that increasing the crossflow fluid velocity improves the heat transfer rate and reduces the irreversibility of heat transfer.

Erguvan and MacPhee (2019) investigated transient crossflow tube banks' first and second law efficiencies. The model was performed numerically. Because the thermophysical characteristics of the fluid are mostly dependent on the mean temperature, the inlet temperature of HTF was shown to have the highest effect on overall efficiency

158

in this study. In addition, because it depends on density and viscosity, the HTF's velocity varies as the temperature changes.

Jeebori (2008) studied to find the best tubes design regarding entropy generation. This study analyzes the effect of tube diameter, tube length, and pitch ratios. And the result showed that the higher air velocities and larger dimensionless pitch ratios improve the system performance. And small tube diameter is better performance for compact tube banks.

Most of the aforementioned studies focus on heat transfer, pressure drop, and flow velocity. To increase the system's overall performance, the authors optimized their design and increased or decreased some parameters like flow velocity. It was observed here that the system's performance increases with the increase of flow velocity. So, according to the literature, 0.2 m/s, 0.5 m/s, and 1 m/s case are simulated and compared in this part. To see the difference here, the inlet velocity changes on the setup used in the experiment. According to the air velocity measurements mentioned in Chapter 3, the average velocity for supply air is 0.34 m/s, and the average for exhaust air is 0.28 m/s.

5.3.4.1. (*3-1*) 0.2 m/s

The first case is the 0.2 m/s for supply air and exhaust air. Figure 5.57 illustrates the temperature distribution of tubes and inlet temperature of 34°C and outlet temperature of 21°C. It is obvious from the figures that there is a difference in the temperature of the tubes. The difference can be seen clearly in Figures 5.57 and 5.58. As can be seen, only the 1st, 2nd, 3rd, 4th tubes reach the outdoor temperature of 34°C, while the 5th tube reaches 32°C and the remaining tubes reach 27-28°C. In the case of exhaust, the 7th 8th 9th and 10th tubes have reached the indoor temperature.

Figure 5.58 shows the liquid fraction distribution of this system, and the charging and discharging process take 20-minute cycles. In general, 100% melting is seen in 1st 2nd 3rd $4^{th,}$ and 5th while the 9th PCM melts at 80%, the PCM inside the 6th $8^{th,}$ and 10th tube melts at 75%, the 7th tube melts at 50%.
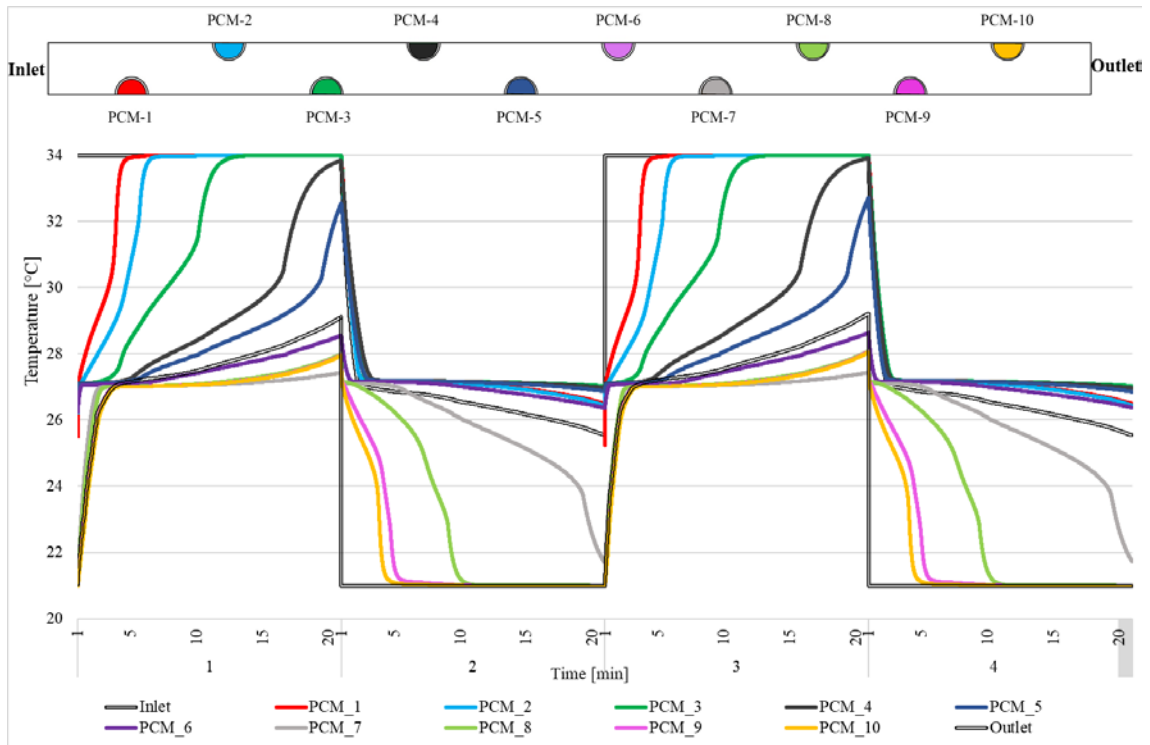
Figure 5.57. Cyclic results for Ø4.76 mm tube with 0.2 m/s.
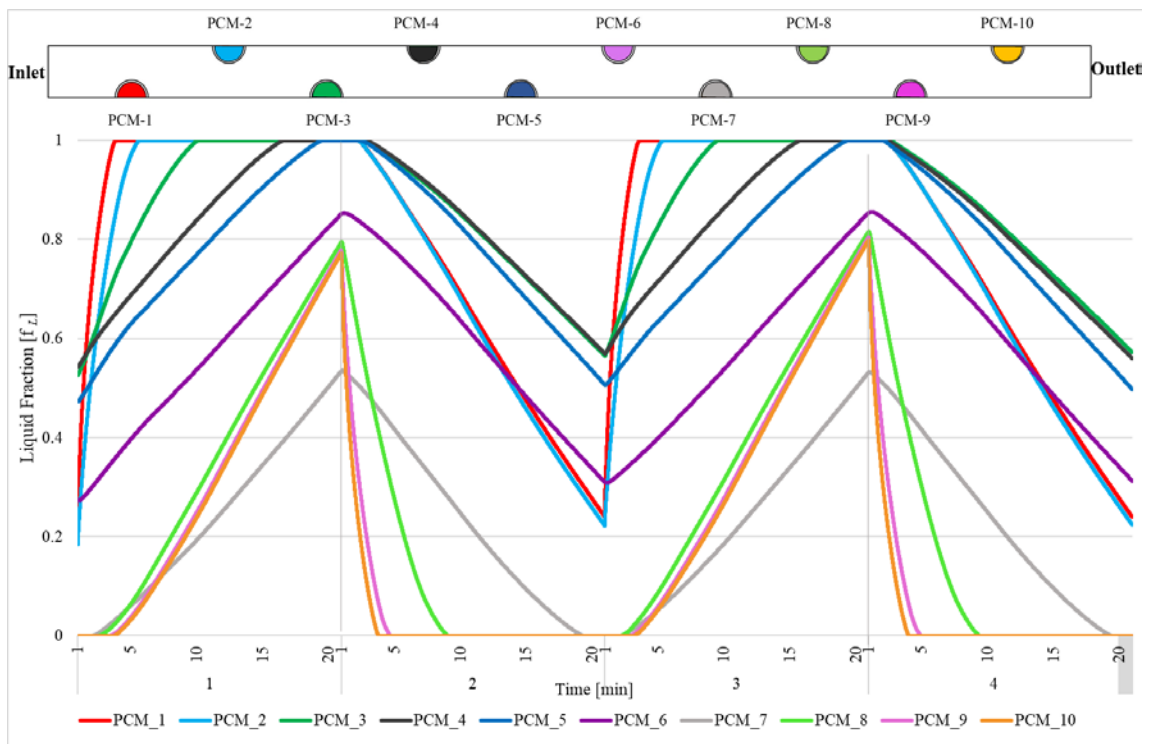
Figure 5.58. Melting/ solidification results for Ø4.76 mm tube with 0.2 m/s.

160

5.3.4.2. (*3-2*) 0.5 m/s

Figures 5.59 and 5.60 show the simulation results of 0.5 m/s inlet and outlet fluid velocities. This figure represents the PCM melting interfaces by 10 tubes with lines. And two of them are inlet and outlet temperature as constant. In Figure 5.59, almost all tubes reached outdoor temperature, only the 7th and 9th tubes remained at 29°C. 0.5 m/s is not enough in 20-minute for the whole system to reach the inlet or outlet temperature in supply/exhaust mode. With an increase in the heat transfer fluid velocity, the amount of energy stored in the LHTES in a system, and hence the amount of PCM melted, increases. As expected, there is more heat transferred to the tubes found closer to the inlet in supply mode.
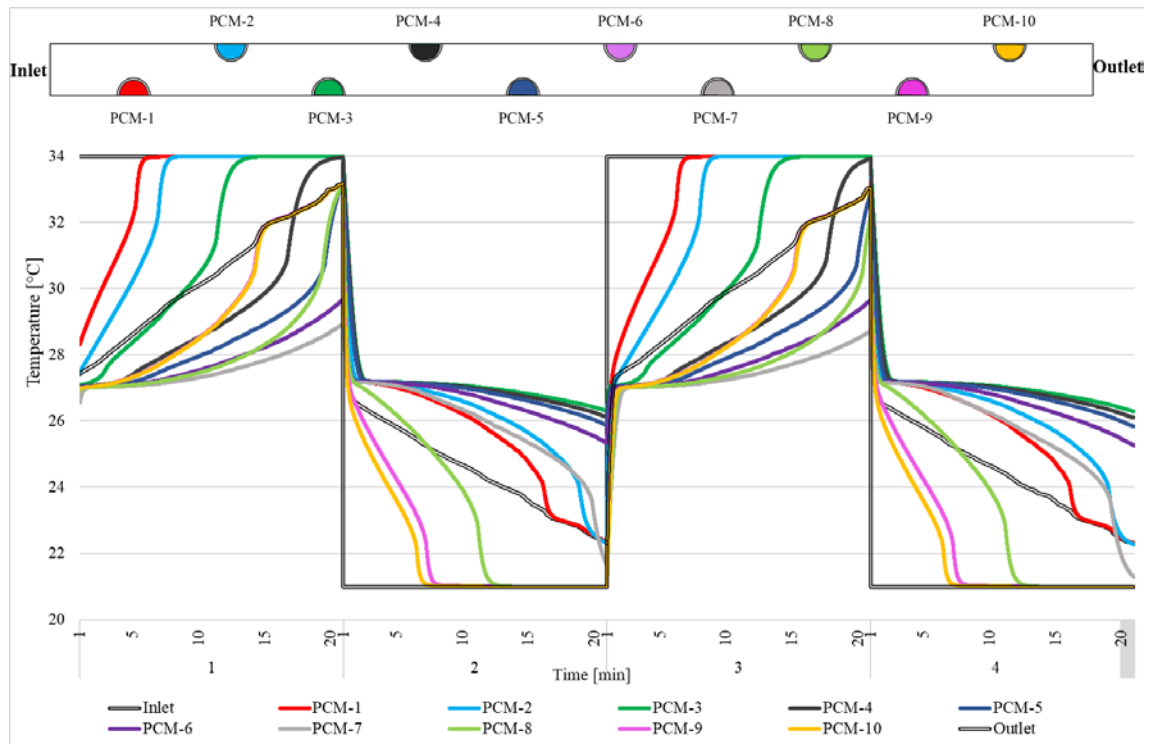
Figure 5.59. Cyclic results for Ø4.76 mm tube with 0.5 m/s.

Figure 5.60 shows the liquid fraction of PCM at a different time step. In this figure, the region of liquid fraction between 0 and 1 indicates the solid-liquid interface region. 0 means solid, 1 is liquid. The solid-liquid interface differs due to air velocity inside the

system. The melting process is seen in every tube except the 7th and 9th tubes. The inlet part of the tube bundle system starts to melt rapidly.
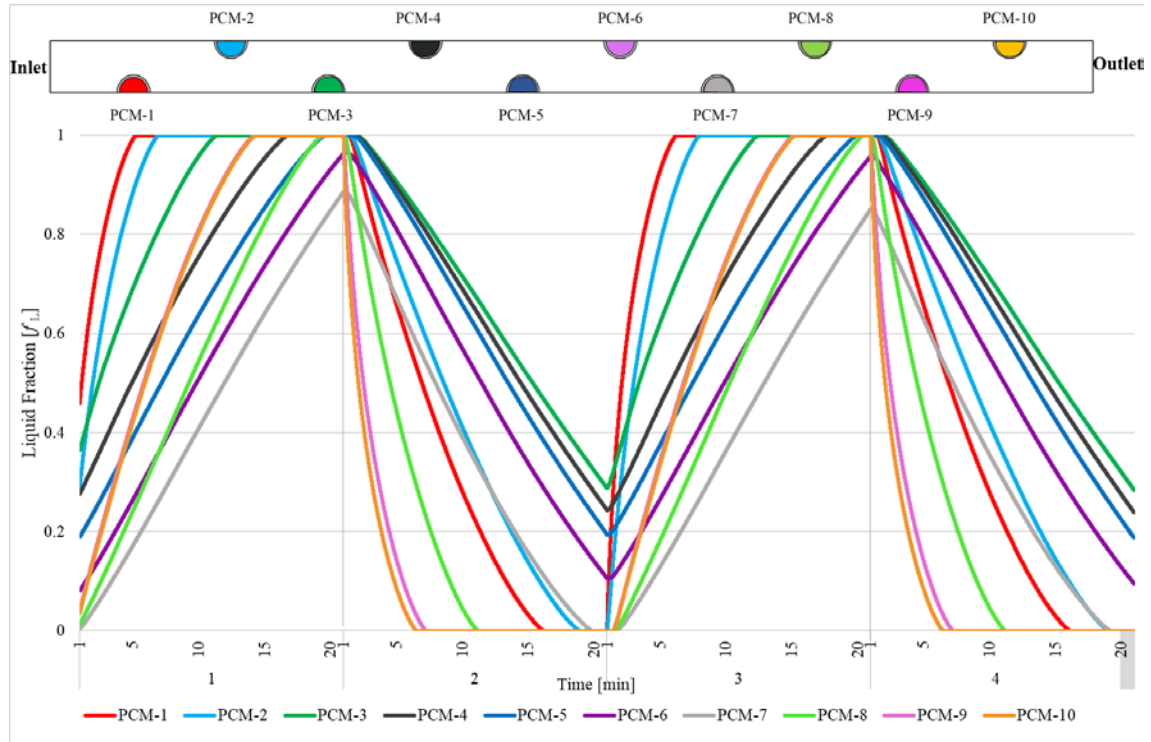
Figure 5.60. Melting/ solidification results for Ø4.76 mm tube with 0.5 m/s.

5.3.4.3. (*3-3*) 1 m/s

In this model, the velocity of air, both inlet and outlet, are changed. The fluid velocity value is 1 m/s. The melting and solidification time and the temperature distribution of these simulations are shown in Figure 5.61 and Figure 5.62. Looking at Figure 5.61, it is seen that the PCM in all the tubes reaches the outdoor temperature within the specified period and reaches 21°C, which is determined as the indoor temperature in exhaust mode. It can be noticed that the temperature rise of the PCM is rapid first 10 minutes due to the high driving force for conduction and discharging curve becomes flat as time progresses after the 10 minutes. HTF receives the heat from the charged PCM.
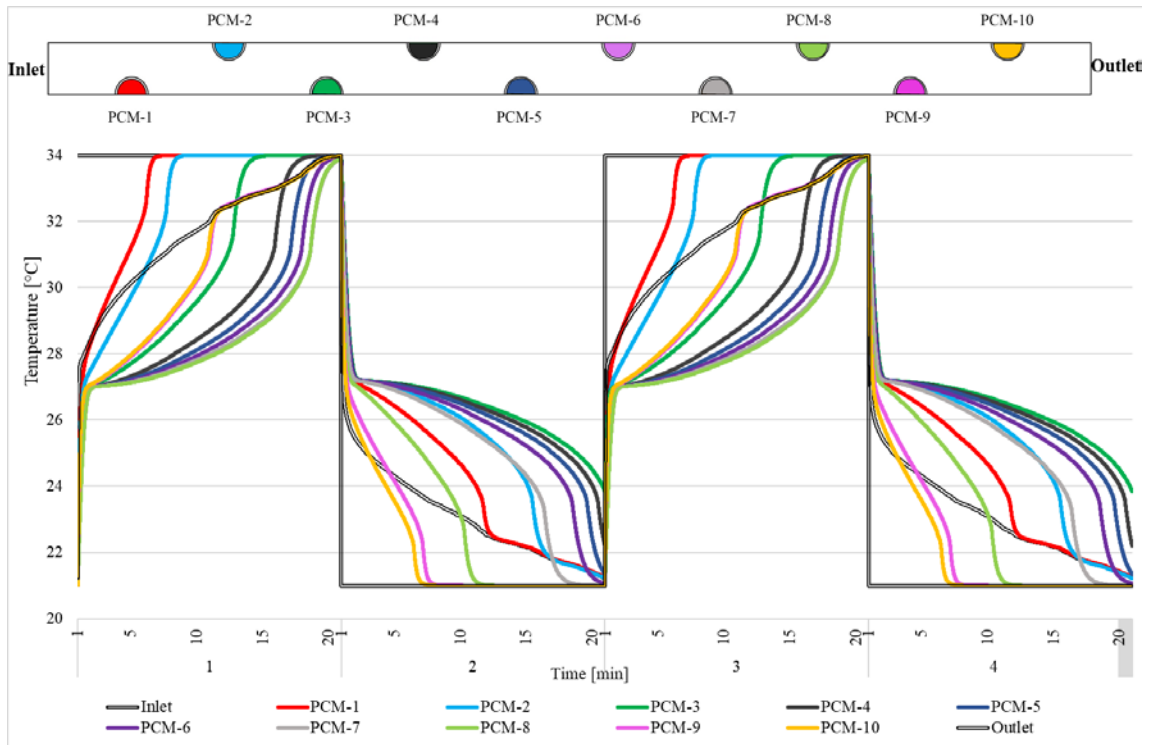
Figure 5.61. Cyclic results for Ø4.76 mm tube with 1 m/s.

Figure 5.62 through the liquid fraction contours at different time intervals of the charging and discharging cycle. The total charging and discharging in this figure are 20-minute. But, looking at Figure 5.62, each tube melt and solidify in a maximum of 15-minute. The time needed to freeze PCM completely is 100% according to the specified cycling time. A significant improvement in the melting and solidification process is observed in 1 m/s compared to 0.2 m/s and 0.5 m/s cases. The effect of the velocity on the melting and solidification rate of PCM and the time required to melt and freeze the PCM completely.
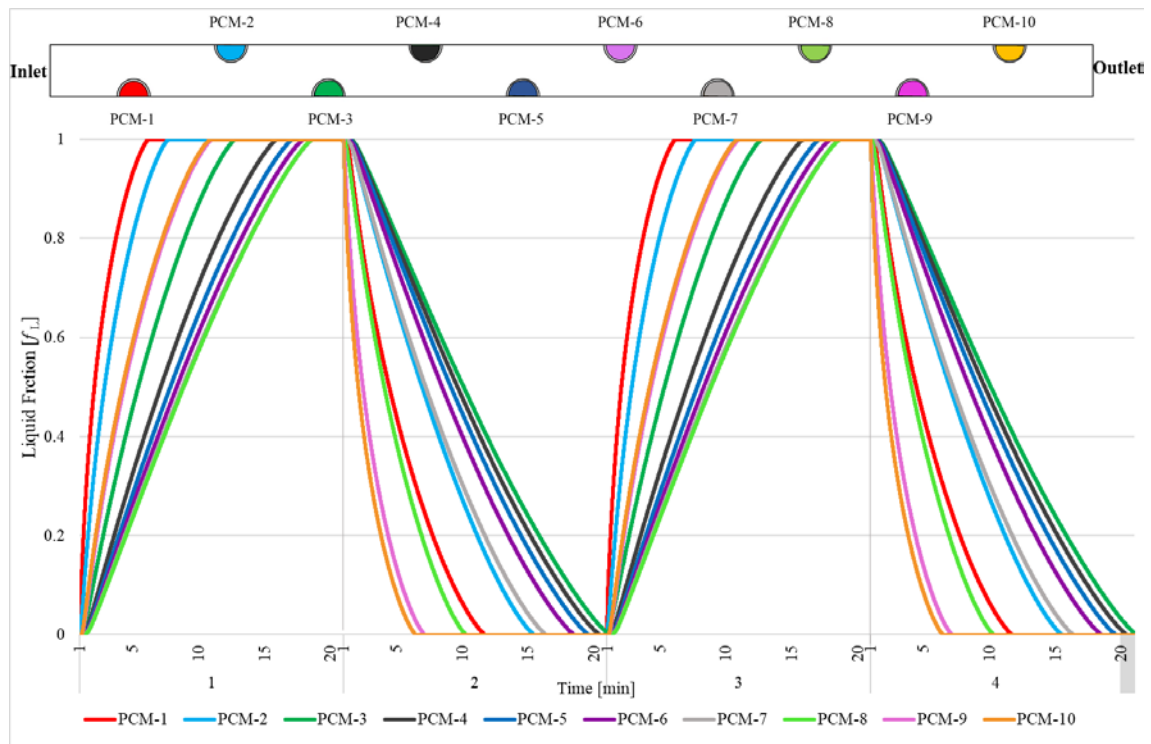
Figure 5.62. Melting/ solidification results for Ø4.76 mm tube with 1 m/s.

5.3.5. (*4*) Combination of PCM at Different Melting Temperatures

According to research, the multi-PCM design improves the dynamic performance of the LHTES by increasing the charging and discharging rate.

Elsanusi and Nsofor (2021) investigated different arrangements of the multiple PCMs' performances of heat exchangers. As a result, natural convection has a positive effect on heat transfer. The parallel arrangement enhances conduction and, in multiple PCMs, reduces complete melting time compared with the single PCM arrangement.

Talukdar et al. (2019) evaluated the solidification /melting behavior of the LHTES solar cold storage unit with the CFD model. With this model, the numerical analysis of charging /discharging of PCM is analyzed for PCM pack thickness and evaporator arrangements. PCM pack sizes are 100 cm x 76 cm x (4.5 cm to 7 cm) and evaporator arrangement of 0, 5, 8, 10 and 12 aluminum fins. The 6.5 cm thick pack with 12 aluminum fins gives the best charging/discharging time.

Aldoss and Rahman (2014) investigated the TES using spherical capsules filled with PCMs of the different melting points at different sections along the bed. Single-PCM design and multi-PCM design of two and three phases are investigated. The results show

that the performance of multi-PCM TES increases as the number of stages increases. Using more than three stages, on the other hand, does not result in any noticeable improvement.

Gong and Mujumdar (1996) analyzed the multiple PCM for shell and tube thermal storage exchangers. Each exchanger uses a different PCM. In this paper, numerical studies were carried out to investigate the cyclic energy charge/discharge processes. The result is that the overall exergy efficiency of the three-stage PCMs system was found to be 74% higher than that of the single-PCM system.

According to these studies, this case focused on the combination of various PCM in the tube bundle system. In this case, it is expected to increase the system's thermal performance, as emphasized in the literature.

5.3.5.1. (*4-1*) Combination 1: RT27 and RT24

Based on the previous analysis results, the melting temperature variation is selected to match the HTF temperature profile throughout the system. Looking at the previous analyzes, it is seen that PCMs close to the inlet reach the outdoor temperature and melt faster, while PCMs in the tubes close to the outlet melt later or do not melt completely. Therefore, the first five tubes were filled with RT27 and the remaining five tubes with RT24 (Figure 5.63). The purpose of this is to maximize the heat transfer rate between PCMs and HTF.
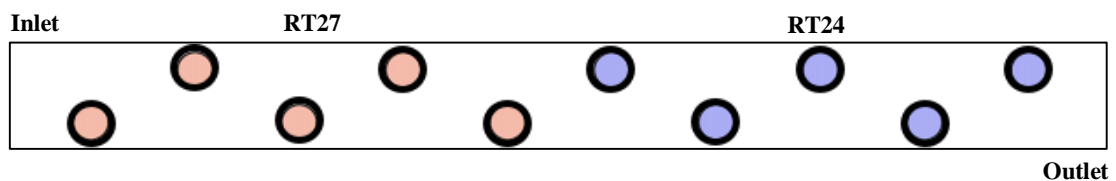
Figure 5.63. The prototype tube bundle system geometry with two different PCM.

The simulation results are shared by filling the system with an indoor temperature of 21°C and an outdoor temperature of 34°C with PCM with 2 different melting points. RT27 is a phase change material that melts/solidifies at 27°C, while RT24 is a phase change material that melts/solidifies at 24°C. 1st 2nd 3rd 4th 5th tube filled with RT27, 6th

7th 8th 9th and 10th tubes filled with RT24. All tubes melt in the charging process and reach the outdoor temperature. However, Figure 5.64 shows that the tubes filled with RT24 do not reach the indoor temperature during the discharging process.
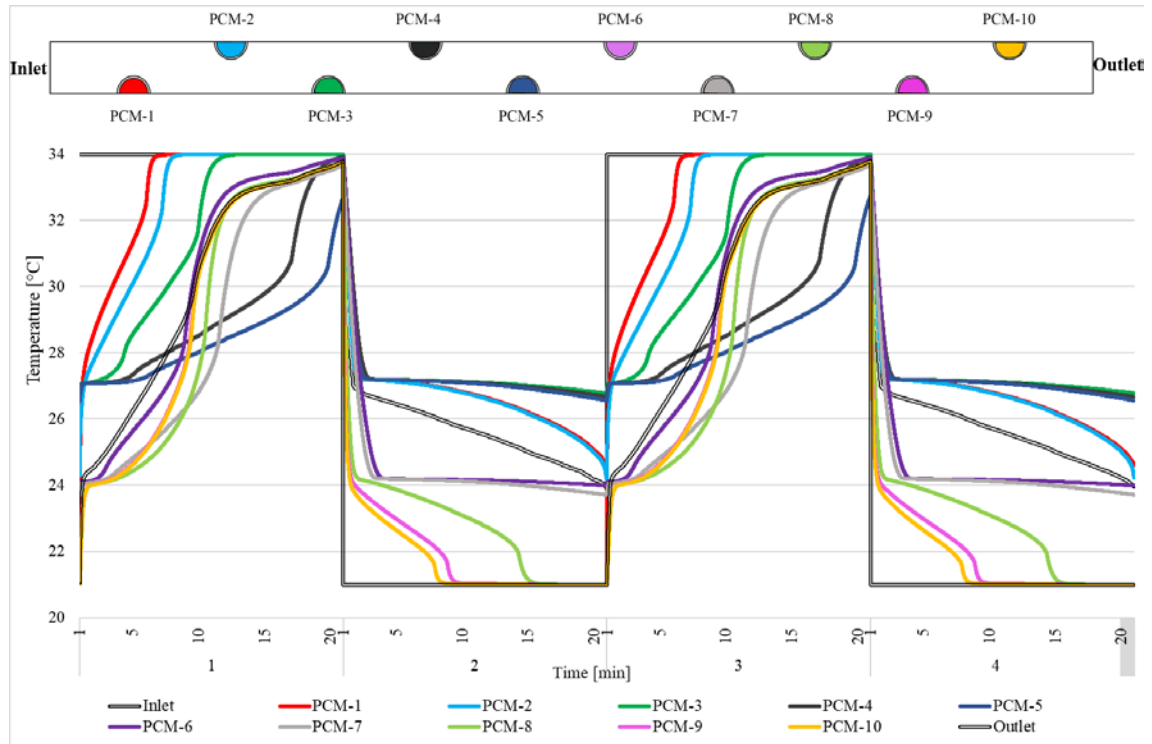
Figure 5.64. Cyclic results for Ø4.76 mm tube with the combination of RT27 and RT24.

Figure 5.65 shows the melting fraction versus time of the PCM during the charging period (melting) and discharging period (solidification). As seen here, PCMs filled with RT27 melt and solidified at full capacity, while tubes filled with RT24 operate at 60% capacity. During the charging period, all tubes melt in the first 10-minute except PCM-4 and PCM-5 tubes.
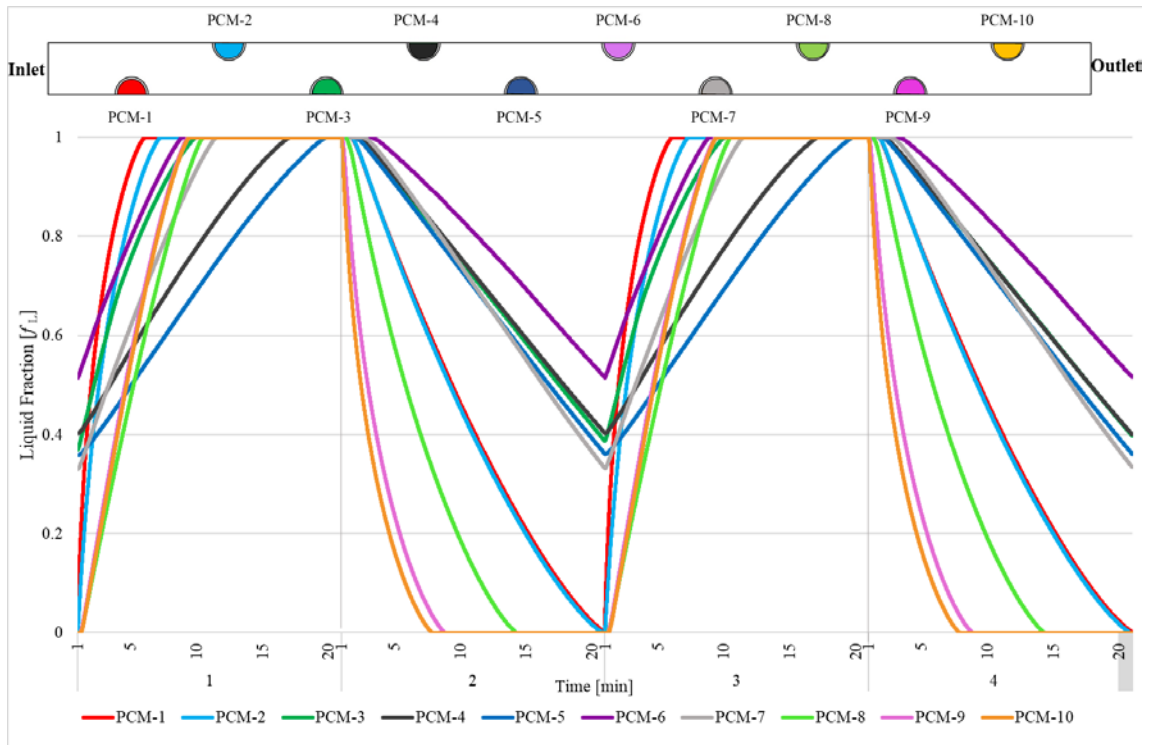
Figure 5.65. Melting/ solidification results for Ø4.76 mm tube with the combination of RT27 and RT24

5.3.5.2. (*4-2*) Combination 2: RT27, RT26, and RT24

In this case, looking at the simulation results with RT27 and RT24, it is seen that especially PCM-4 and PCM-5 melt and solidify later. For this reason, faster melting and solidification are expected in the system by filling the 4th tube and 5th tube with RT26. The 1st 2nd 3rd tubes will be filled with RT27, while the 4th and 5th RT26 will be simulated by filling the remaining tubes with RT24 (Figure 5.66). Tubes are the same as the measurements used in the experiment. The diameter of the tubes is 4.76 mm. And the longitudinal and transverse pitches size is 14 mm.
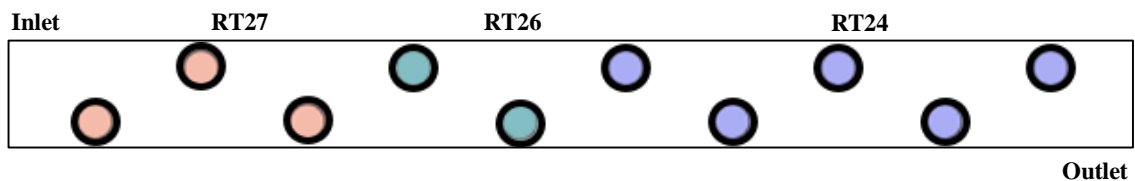
Figure 5.66. The prototype tube bundle system geometry with three different PCM.

Figure 5.67 shows the temperature distribution for 10 tubes. It is seen that all tubes melt in the charging process. In addition, the curve continues until it changes phase according to the melting temperatures of the PCMs in the tubes and reaches the outdoor temperature. In the discharging process, there are 3 different solidification points.
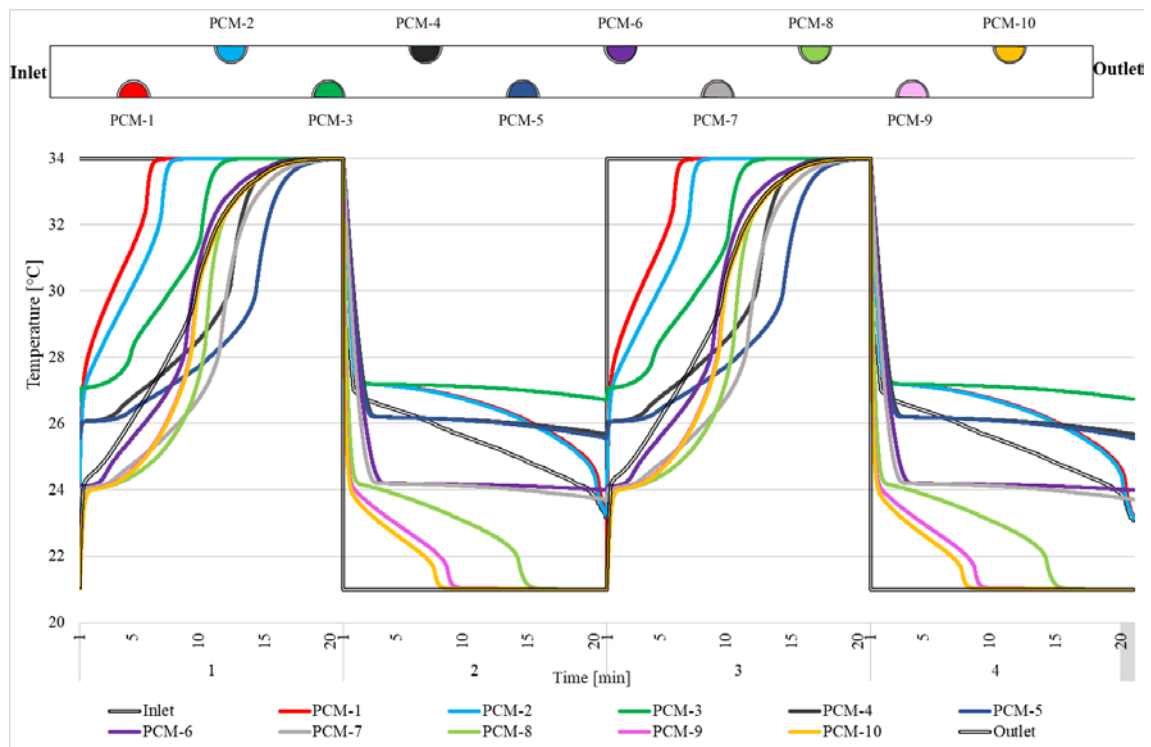
Figure 5.67. Cyclic results for Ø4.76 mm tube with the combination of RT27, RT26, and RT24.

Figure 5.68 shows the melting solidification process for 10 tubes. It is seen that all the tubes melt in the charging process. Especially the shortening of the charging period is an important difference according to the other PCM combination case. It is seen that the tubes in the whole system melt in just 10-minute. PCM-6 solidifies 40% of the discharging process, 3rd 4th 5th 7th tubes 60%, the remaining PCM-1, PCM-2, PCM-8, PCM-9, and PCM-10 100% solidify.
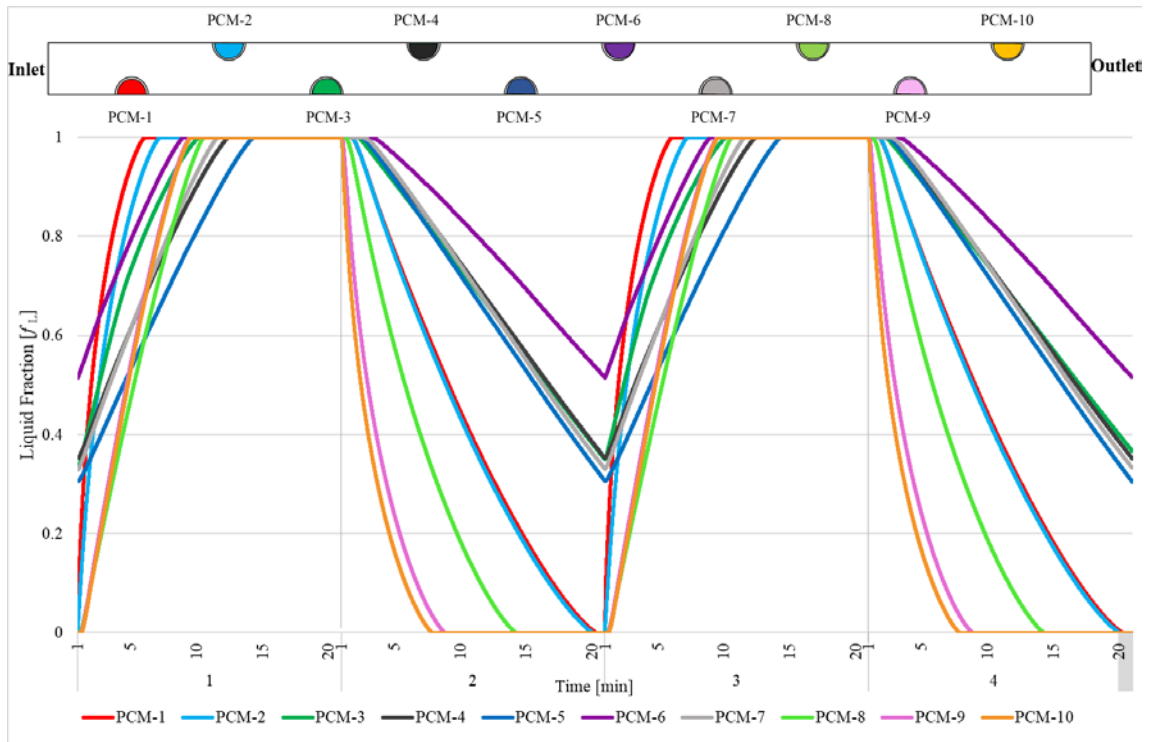
Figure 5.68. Melting/ solidification results for Ø4.76 mm tube with the combination of RT27, RT26, and RT24.

5.3.6. (5) The Case Combination with different PCM and Pitch Size

This simulation study, it is aimed to see the results by combining two different cases. The combination of the case with 3 different PCMs where faster melting and solidification is seen and the combination of 12 mm longitudinal and 12 mm transverse pitch size cases in a 4.76 mm tube is simulated. The first 6 tubes are filled with RT27, the next two with RT26, and the last 4 tubes near the outlet with RT24. In this case, the first six tubes were filled with RT27, the next two with RT26, and the last four tubes near the outlet with RT24 (Figure 5.69).
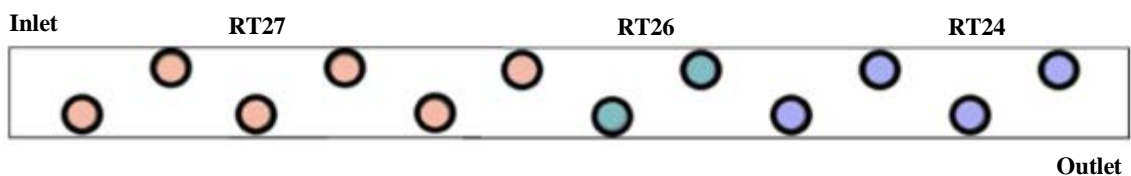
Figure 5.69. The prototype tube bundle system geometry with three different PCM with 12 mm longitudinal, 12 mm transverse pitches.

169

It is seen in Figure 5.70 that when 3 different PCMs with 3 different melting points are used in the system, all tubes reach the outdoor temperature in the charging process, which is 34°C. However, in the discharging process, the tubes cannot reach 21°C, which is the indoor temperature, except for tubes 10, 11, and 12. The 1st and 9th tubes drop to 23°C, the 7th and 8th tubes drop to 26°C, and the remaining tubes to 27°C.
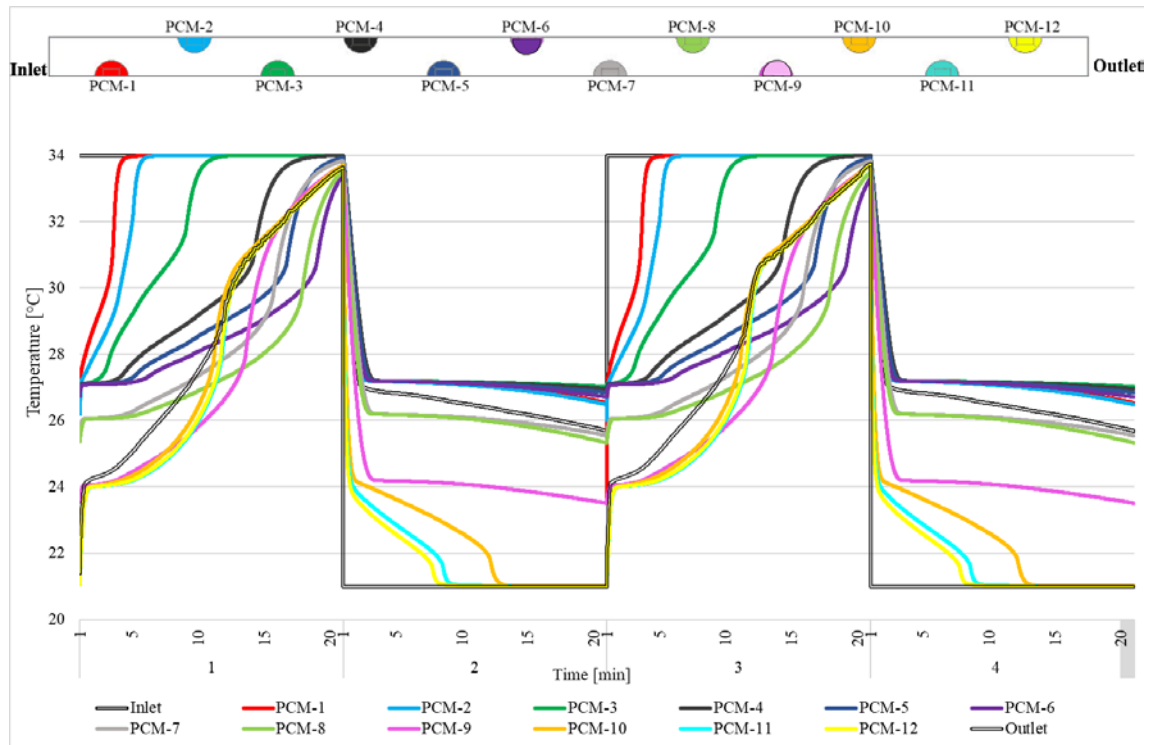
Figure 5.70. Cyclic results for Ø4.76 mm tube with the combination of RT27, RT26, and RT24 with 12 mm longitudinal, 12 mm transverse pitches.

Figure 5.71 shows the simulation results when the system, consisting of tubes with a diameter of 4.76 mm and has a 12 mm longitudinal 12 mm transverse pitch size, is filled with 3 different PCMs. Tube-1 and tube-2 melt within the first minutes. Then the PCM in the 3rd tube changes phase. The 3rd tube is followed by PCM-10, 11, and 12. After the 10th minute, the 4th tube, 9th tube, 7th 5th 8th, and 6th tube melt, respectively. In exhaust mode, while 100% of the 10th 11th, and 12th tubes solidify, the 2nd tube, 1st tube 8th tube, 9th tube 7th tube 6th tube 5th tube 4th tube, and finally 3rd tube solidify respectively.
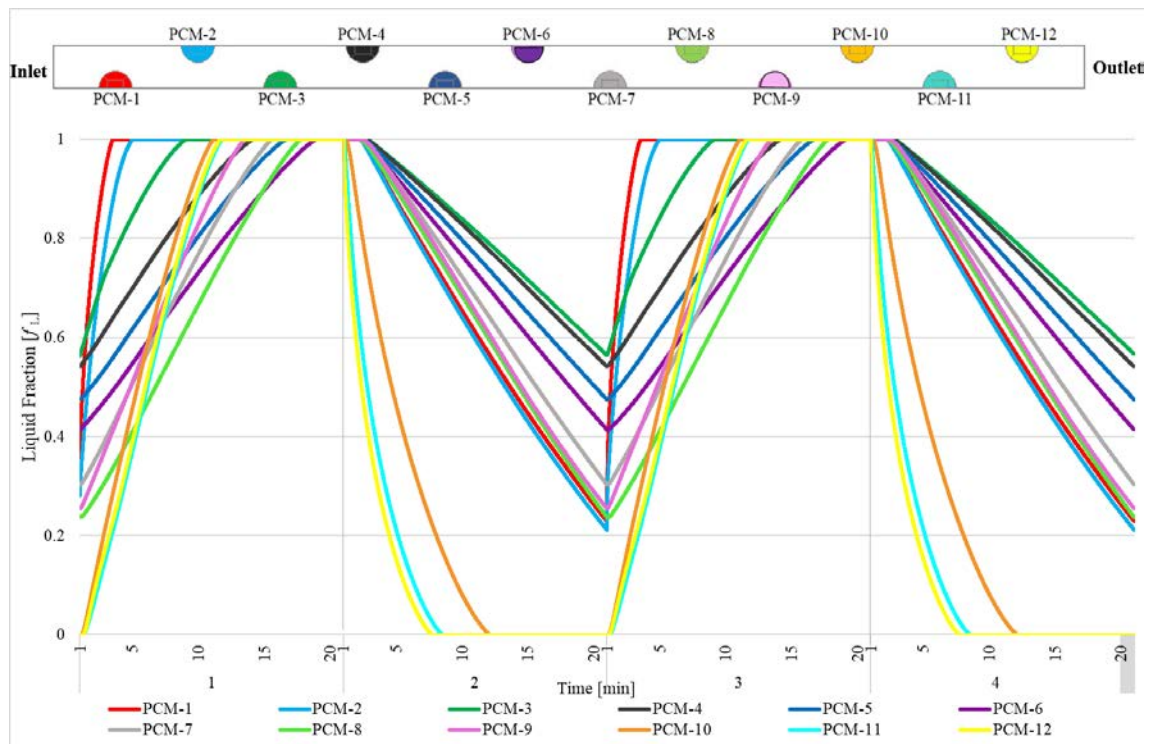
Figure 5.71. Melting/ solidification results for Ø4.76 mm tube with the combination of RT27, RT26, and RT24 with 12 mm longitudinal, 12 mm transverse pitches

5.3.7. Cross Analysis of the Tube Bundle Unit

During the liquid to solid or solid to liquid phase changes in the PCM, latent heat *hsf* (kJ/kg) is stored/released per unit mass are different from each other. While RT27 heat of fusion is 184 kJ/kg, RT26's heat storage capacity is 180 kJ/kg, and RT24 is 160 kJ/kg. So, all calculations are the result of the entire system. Calculated according to the PCM mass in all the tubes in the system.

Table 5.7 shows the results of the cases calculation results of energy stored/released, and also the other important parameter for the HRV unit is pressure drop. In all cases, the operating time is 20-minute. And all cases are operated simultaneously in summer conditions. It was determined as the indoor environment (21°C) and outdoor environment (34°C) in exhaust and supply mode. In the first study, 4 different pitch sizes (Case 1) are investigated on a 3 mm diameter tube. It is calculated that the heat transfer increase is greater in the 4th simulation with a lower pitch size. When the tube shape is changed (Case 2), it appears to be a promising technique for heat transfer enhancement compared to conventional cylindrical tubes. In the experiments, the measured velocity

171

value is 0.34m/s from the inlet, 0.28 m/s from the outlet. So, in Case 3, the air velocity value has changed both inlet and outlet. As velocity increases, heat transfer increases. In Case 4 and 5, that can be seen the series arrangement compared to the single PCM enhances the solidification and melting performance. As seen in the 5th simulation, the heat transfer increases or decreases in direct proportion to the PCM mass in the system.

According to these results, the values of exhaust and supply, unlike the experiments, are the same (or very close); It is related to the fact that the fan has the same performance in both directions in the simulations. The HTC increases as the inlet velocity increases due to the increased convective effect and turbulence. (Swain and Das 2016) In addition to this result, as seen in the parametric velocity values in Table 5.7, the parameter that has the most effect on energy storage is the change in velocity. In this table, the comparison of the airside pressure drops of 14 simulations made on five different cases is also available in Table 5.7.

Table 5.7. Total heat capacity of the units for all cases.

Cases			Exhaust (kJ)	Supply (kJ)	Pressure Drop (Pa)
(1) Tube Diameter	*(1-1)* (3mm)	*(1-1-1)* L: 14 mm, T:14 mm	19.71	19.68	10.75
		(1-1-2) L: 12 mm, T:14 mm	25.06	25.06	29.40
		(1-1-3) L: 10 mm, T:14 mm	27.70	27.71	27.43
		(1-1-4) L: 10 mm, T:10 mm	34.53	34.51	25.97
	(1-2) (4.76 mm)	*(1-2-1)* L: 16 mm, T:16 mm	32.80	32.81	22.41
		(P) L: 14mm, T:14mm	34.80	34.82	34.35
		(1-2-2) L: 12 mm, T:12 mm	45.77	45.77	38.40
(2) Tube Shape	Oval		30.26	30.26	16.61
(3) Air Velocity	*(3-1)* 0.2 m/s		30.50	30.50	17.27
	(3-2) 0.5 m/s		40.48	40.40	40.65
	(3-3) 1 m/s		48.81	48.81	80.72
(4) PCM Combination	*(4-1)* (L: 14 mm, T:14 mm) + RT27+RT24		25.21	25.21	34.41
	(4-2) (L: 14 mm, T:14 mm) + RT27+RT26+RT24		28.60	28.60	34.39
(5) Case Combination	(L: 12 mm, T:12 mm) + (RT27+RT26+RT24)		37.9	37.9	38.41

*P: Prototype results

5.4. Simulations of Prototype Using Different Climatic Data

The tube bundle prototype produced within the scope of this thesis is analyzed the energy performance in three different climatic conditions aimed to guide the designer in selecting the wall integrated ventilation system in different climates. The heat recovery system operated based on the monthly average daily temperature in 20-minute cycles with the same inlet and outlet velocity. Erzurum is selected as the pilot city for the continental climate, İzmir is selected as the pilot city for the mild climate, and Singapore is selected as the pilot city for the tropical climate. In this section, the tube bundle is briefly summarized, then the climate choices and analyses on the 3 selected cities are detailed.

5.4.1. Tube bundle prototype

The height of the one tube is 15 cm, and the tube's outer diameter is 4.76 mm. Also, these tube bundle transverse and longitudinal pitch is 1.4 cm. The diagonal pitch size is 1.565 cm in these simulations. As seen in Figure 5.72, there are physical boundaries between inlet and outlet. The inlet side is the outdoor environment, and the outlet side represents the indoor environment. The inlet velocity is defined as 0.34 m/s, and the outlet velocity from the outlet is 0.28 m/s. All simulations are solved in a 2D plane. To ensure that the predicted temperature changes are not affected by the initial conditions, the analysis has been analyzed for at least 27 hours. All results are for 24 hours a day.
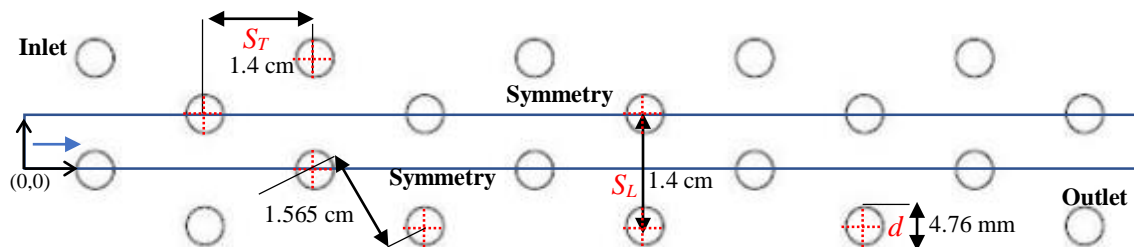
Figure 5.72. Plan of the tube bundle prototype for climate simulations.

5.4.2. Climatic data

This thesis selected cities based on their climates according to Köppen type climate zones (Table 5.8). The mean value of meteorological events such as humidity, air movement, and solar radiation is referred to as climatic temperature. Physical variables that influence climate include geographical location, altitude above sea level, atmospheric layer quality, and surface cover. These are the data that may be used to save energy and improve the comfort of a building (Pekdogan 2015). For the climatic Wladimir, Köppen's classification is the most popular one of all the others. According to this system, there are 5 main climate groups (tropical, dry, mild, continental, and polar).

Table 5.8. Basic features of Köppen-Geiger climate classification.
(Source: Ma et al. 2021)

Climate Groups	Basic features
Tropical	$T_{min} \geq 18°C$
Dry	$P_{threshold} x10 > P_{mean\ annual\ precipitation}$
Mild	$T_{max} \geq 10°C$ $18°C > T_{min} > 0°C$
Continental	$T_{max} > 10°C$ $T_{min} \leq 0°C$
Polar	$T_{max} < 10°C$

According to the classification, 3 main climate types have been determined in Turkey. The widest distribution is the mid-climate type. The second most common climate type is characterized as a continental climate. another is the dry climate, which corresponds to the areas with the lowest precipitation in Turkey. (Yılmaz and Çiçek 2018) In terms of this standard, Erzurum is selected as the pilot city for the continental climate zone (Eastern Anatolia Region), İzmir is selected as the pilot city for the mild climate zone (Aegean Region), and Singapore is selected as the pilot city for tropical climate zone. In addition, these climates were determined by considering the temperature distributions during the day and yearly. Although a PCM that will operate throughout the year is not possible for Erzurum and İzmir, it shows the system's operating performance in climates that dominate summer conditions for İzmir and winter conditions for Erzurum.

Since Singapore has similar climatic conditions throughout the year, the system's performance has been examined.

5.4.2.1. Continental Climate: Erzurum

In a continental climate zone, the temperature point to below 0°C, generally in winters. In this zone, the lowest average temperature is approximate -20°C. During the summer, precipitation comes in the form of rain, while it comes in snow during the winter. Snow usually begins to fall in October and continues until the middle of May, but the summer season is short and cool. And the wind's effect makes already difficult weather conditions much tougher. This study which is selected Erzurum city from the continental climate zone. With 39° 9' latitude, 41° 3' longitude, and 1757 m above sea level, Erzurum province is one of Turkey's highest and coldest provinces. Figure 5.73 shows the temperature distribution whole year for Erzurum. And the highest on average in August, and January is the coldest month of the year.
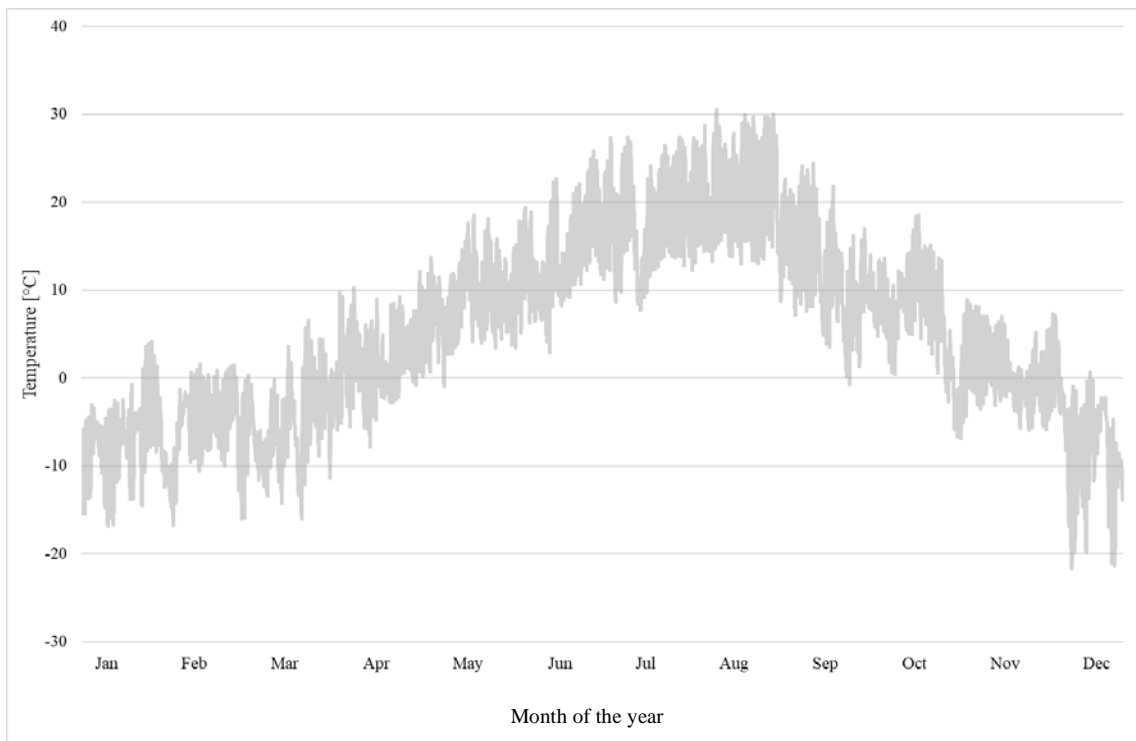
Figure 5.73. Erzurum's highest and lowest temperatures throughout the year (2005-2016)

For the outdoor temperature, simulations are made over two different months. These are January and February. Figure 5.74 shows the monthly average of the daily temperature distribution of Erzurum from 2005 to 2016. Although three months are shared in this graph, simulations are made for January and February because December and February temperature distributions are similar. These data are developed using Photovoltaic Geographical Information System (PVGIS). These interactive maps represent all countries and continents (Pekdogan and Başaran 2017).
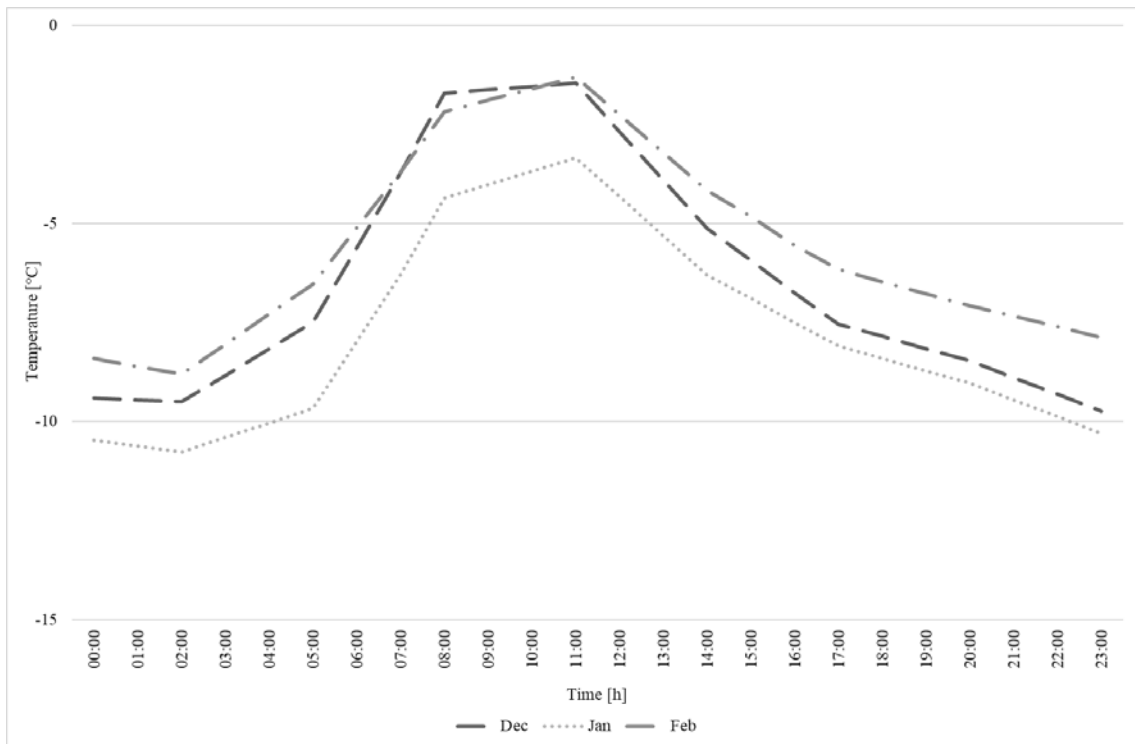
Figure 5.74. Monthly average of the daily temperature distribution of Erzurum.

The possible melting and solidifying process depend on the outdoor climate. These simulations are made according to the prototype used in the experiment and are simulated in winter conditions for Erzurum. The phase change material's melting and a solidification point of 15°C is chosen for Erzurum, and the indoor temperature is assumed to be 20°C. Different indoor temperatures are considered for each season since the comfort room temperature changes throughout the year. In January, February, March, November, and December, the comfort temperature is expected to be 20°C, 22°C in April, May, September, and October, and 24°C in June, July, and August (Arıcı et al. 2020).

For Erzurum, January, and February are simulated. Figure 5.75 shows the heat recovery system operates based on the monthly average of daily temperature in 20-minute cycles for January. The melting and solidifying temperature is 15°C, and the indoor temperature 20°C. The PCM appears to have completely solidified and completely melted in January. PCM's melt solidification cycle occurs every 20-minute. All tubes reach the inlet and outlet temperature in discharging and charging process.
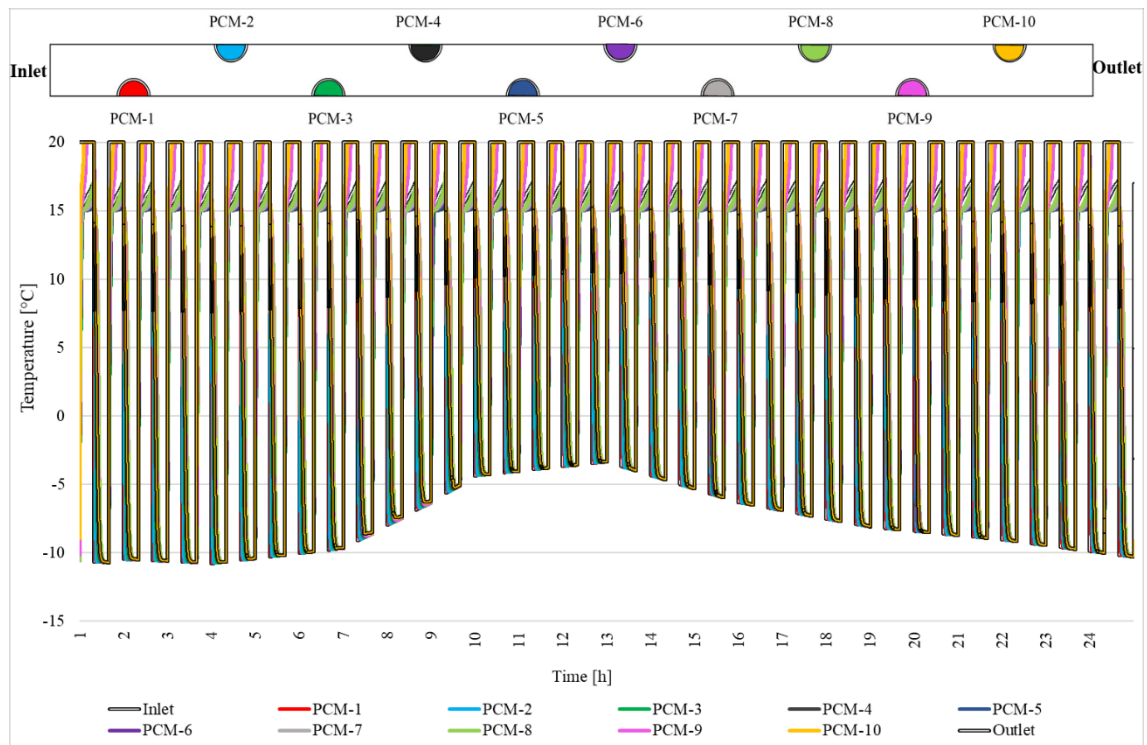
Figure 5.75. Daily simulation results for January in Erzurum.

Figure 5.76 shows the charging and discharging cycle of the heat recovery system for Erzurum in January. The inlet temperatures are the monthly average of the daily temperature, and the outlet temperature, which is indoor temperature, is 20°C. Discharging process and charging process follow each other. PCMs in all tubes change phase. It can be noticed that the temperature rise of the PCM melts and solidifies before 20-minute. When looking at Figure 5.76, after approximately 10-minute the charging and the discharging curve becomes flat.
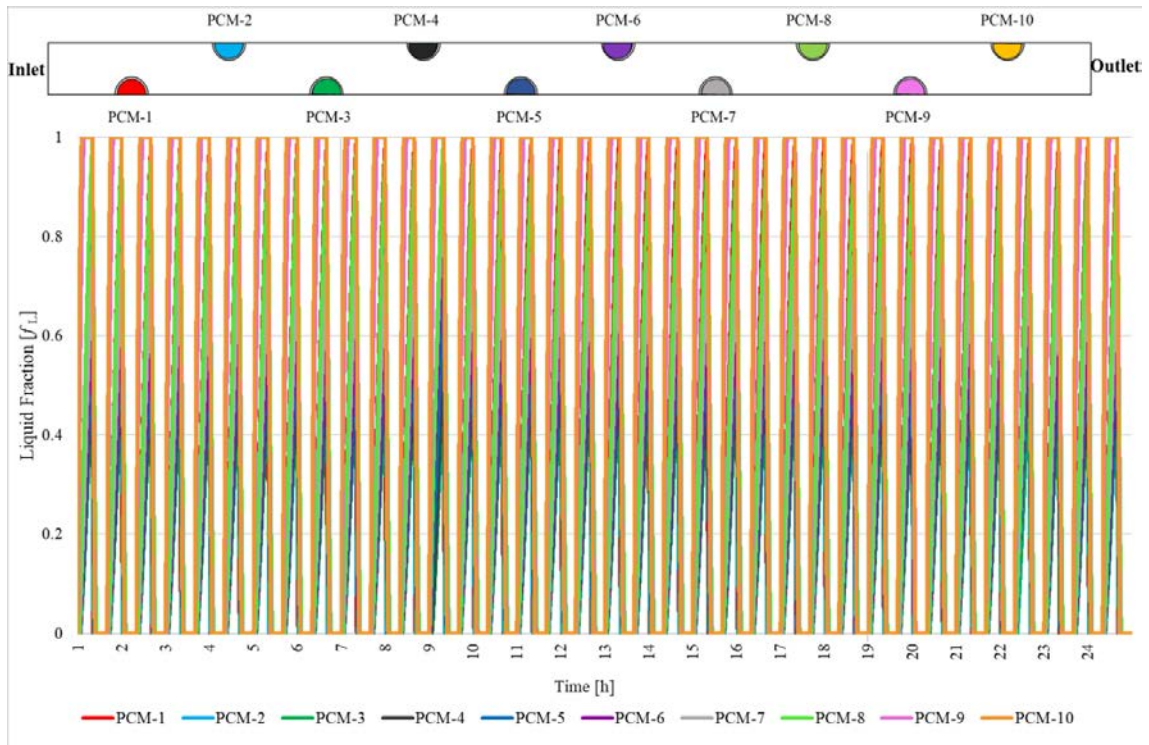
Figure 5.76. Erzurum, melting/solidification results for January in Erzurum.

Figure 5.77 is related to 24 hours operation time in February. The February average temperature is almost the same as in January in Erzurum. And still subzero cold and which is approximate -3°C. Also, the average low temperature is -9°C. Same as the January result, after the 10 minutes, there are no differences in PCM temperature. Because the system reaches the thermal balance, after 10 minutes in the system, PCMs are not melting or solidifying. In the simulation, the outdoor temperature is assigned a different value for each second. According to the change in outdoor temperature, all PCMs in the system reaches that temperature and reach 20°C, which is given as the indoor temperature, while the system is in supply mode.

Figure 5.78 represents the time-related melting and solidifying graphs for 20-minute operating according to Erzurum outdoor temperature daily data. It is seen that the PCMs inside the tubes close to the inlet is melted first. In exhaust mode and supply mode, the melting and solidification process has completely occurred approximately 10 minutes.
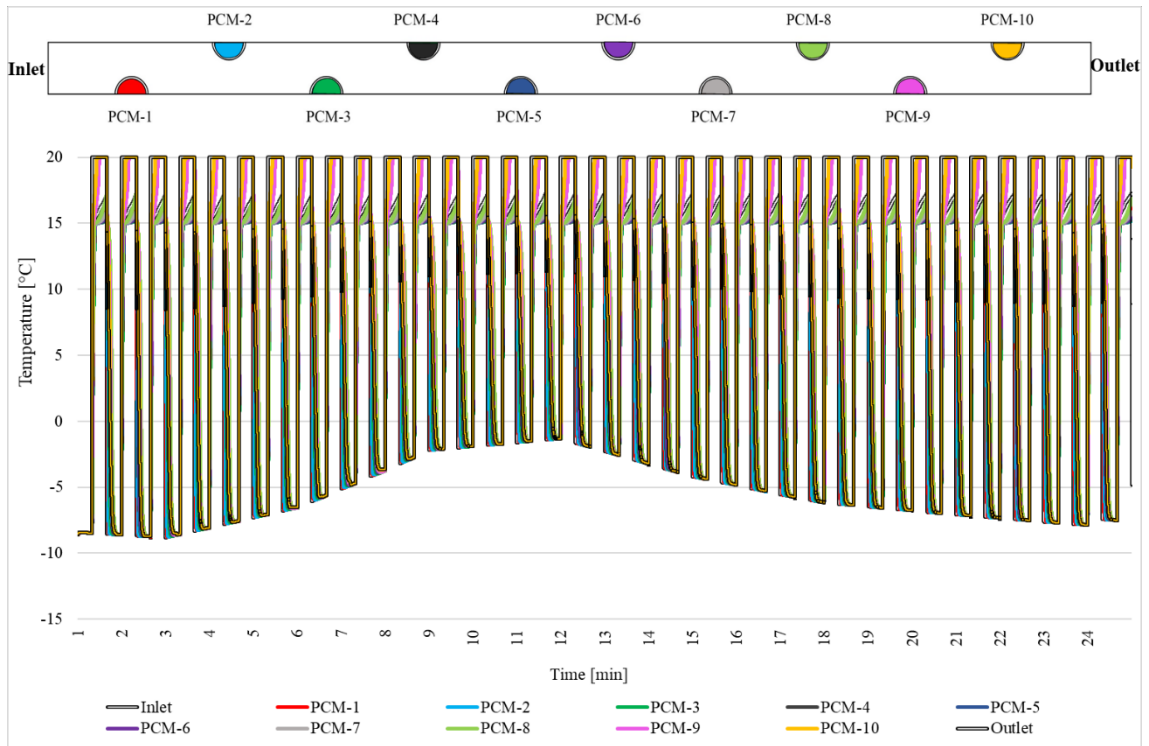
Figure 5.77. Daily simulation results for February in Erzurum.
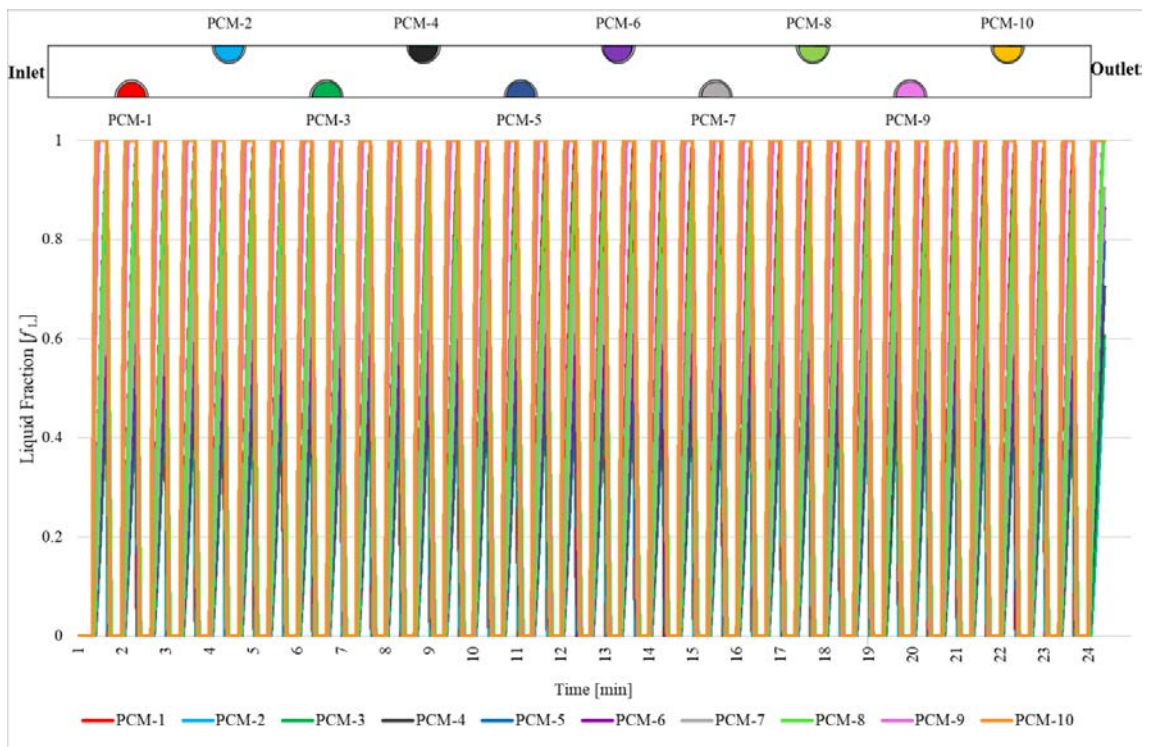
Figure 5.78. Erzurum, melting/solidification results for February in Erzurum.

179

5.4.2.2. Mild Climate: Izmir

The climate of Izmir is temperate/mild. The most significant characteristics of mild climate are intense rainfall, high humidity ratio, and hot weather. The temperature difference between winter and summer is negligible. There is more heavy rainfall during the winter months than in the summer months. Izmir, with temperature in the range of an average high of 30°C. In June, the average low temperature is 20°C. The average sunshine in Izmir is a minimum of 11 hours a day. İzmir province is located at 38º 4' latitude, 27º 2' longitude, and 25 meters above sea level. Figure 5.79 shows the temperature distribution whole year for Izmir. And the highest on average in July and January is the coldest month of the year.
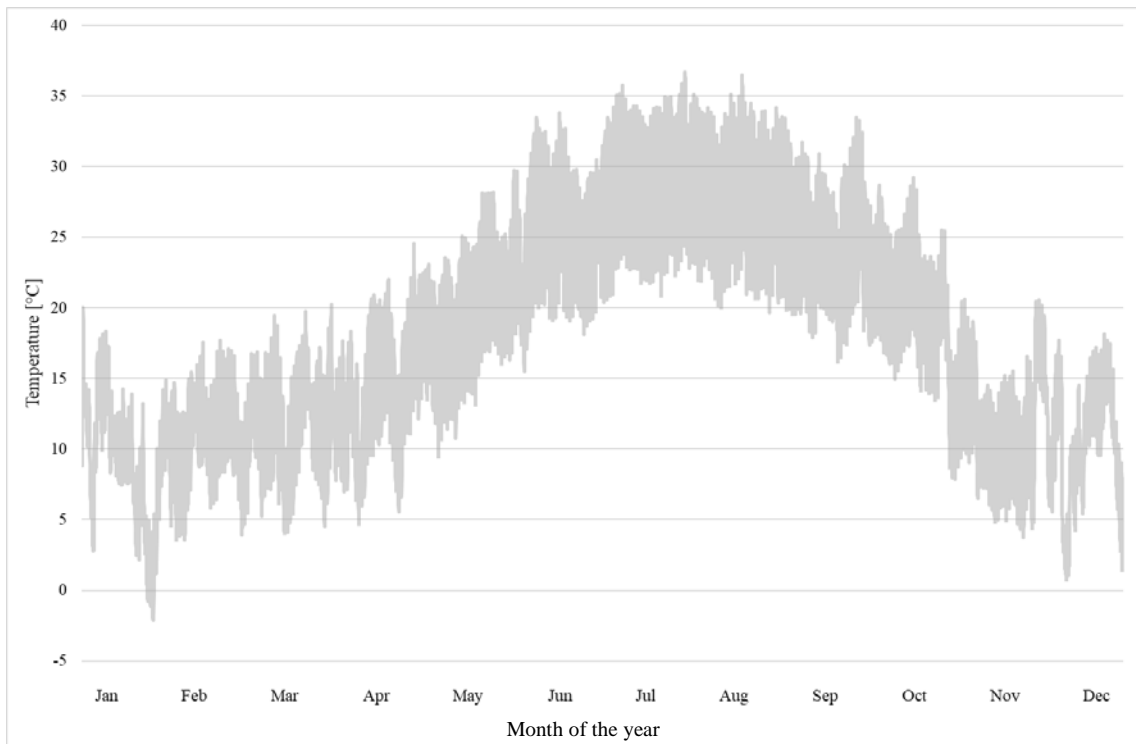
Figure 5.79. İzmir highest and lowest temperatures throughout the year (2005-2016).

Using this climate data as input, simulations were carried out for June and July. Figure 5.80 shows the monthly average of the daily temperature distribution of İzmir. As seen in Figure 5.80, the hottest month on average in July. In June, with temperature in the

range of an average high of 30°C and an average low of 20°C. With an average high temperature of 33°C and an average low temperature of 22°C in July. Last month of the summer in İzmir, August average high temperature is 32°C, and the average low temperature is 22°C. Although 3 months are shared in this graph, simulations were made for June and July, since the temperature distribution in July and August is similar. And in these three months the temperature, which increases especially after 07.00, falls below 27°C after 18.00. Also, the average length of the day is approximately 12 hours in June, July, and August.
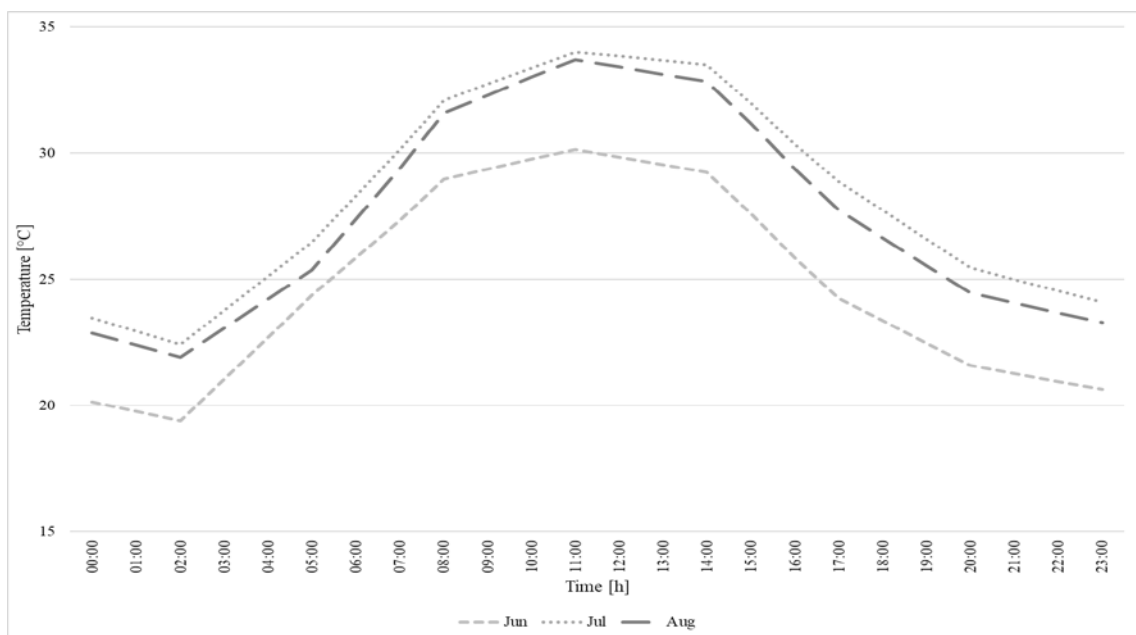
Figure 5.80. Monthly average of the daily temperature distribution of Izmir in the summer season.

All PCMs in the system completely melting degree is 27°C. So, during the day when its temperature reaches 27°C it starts to melt and after the completion of the melting process, its temperature will reach outdoor temperature. In accordance with the assumption, its temperature starts to decrease at midnight. This decrease continues till it reaches indoor temperature which is 24°C and after the completion of the freezing point, its temperature decreases to 20°C. For the Izmir, all PCMs in the systems completely melt at 27°C. So, during the day when its temperature reaches 27°C it starts to melt and after the completion of the melting process, its temperature will reach outdoor temperature.

Following the assumption, its temperature starts to decrease at midnight. This decrease continues till it reaches completely solidifying.

With the increase in outdoor temperature, the system starts operating again and works all day long. Figure 5.81 is related to June the tube bundle system temperature results and Figure 5.83 represents the July results for İzmir. Also, Figures 5.82 and 5.84 show the liquid fraction results of the tube bundle system for the İzmir summer season. Based on the indoor temperature of 24°C, looking at the June results, the time interval when the PCM in the system exceeds 27°C and changes phase is between 08.00 and 17.00. Especially between 12:00 and 13:00, the PCM inside the tubes in the system reaches 30°C. However, there is no phase change in the remaining hours and the temperature drops down to 20°C, which is the outdoor temperature.
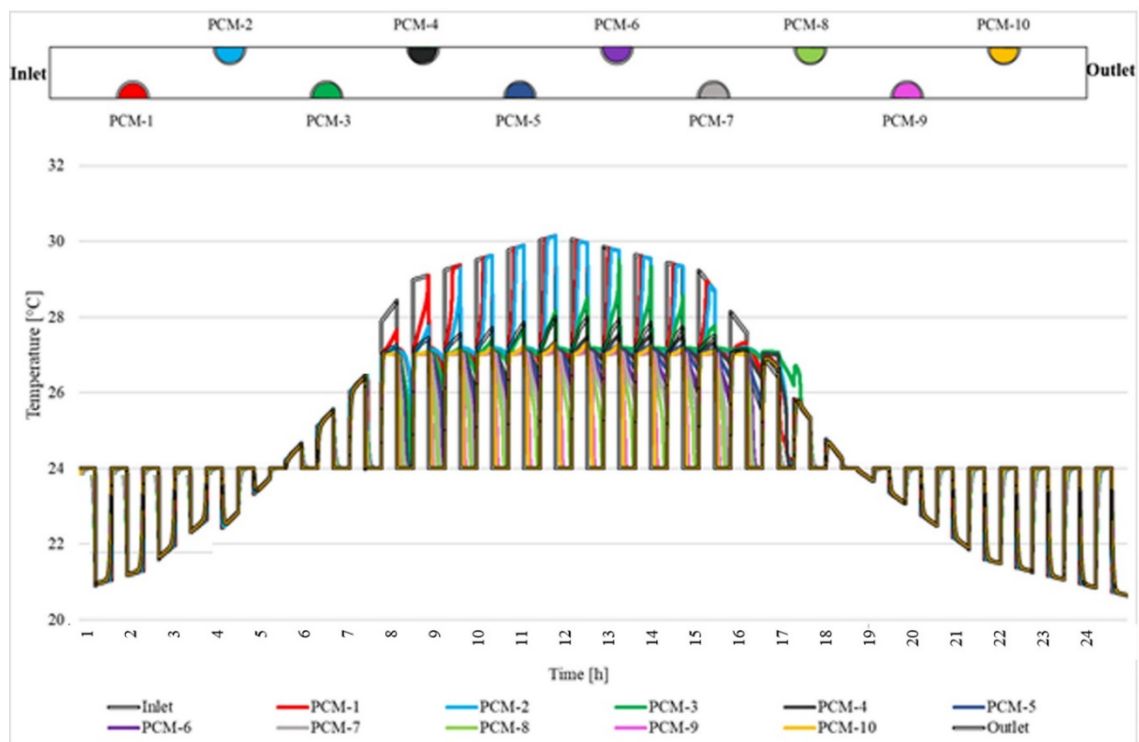
Figure 5.81. Daily simulation results for June in İzmir.

Figure 5.82 shows the melting/solidification results for the monthly average of daily temperature for June in İzmir. When the melting solidification process is examined, while full melting and solidification take place in the 1st, 2nd, and 3rd tube, a phase change of 60% is observed in the 4th and 10th tubes, and 20% in the 5th, 6th, 7th, 8th, and 9th tubes.

In general, the most efficient time of the system is between 10:00 and 16:00. While melting and solidification are observed in all tubes between the specified hours, no phase change is observed in some at other hour intervals.
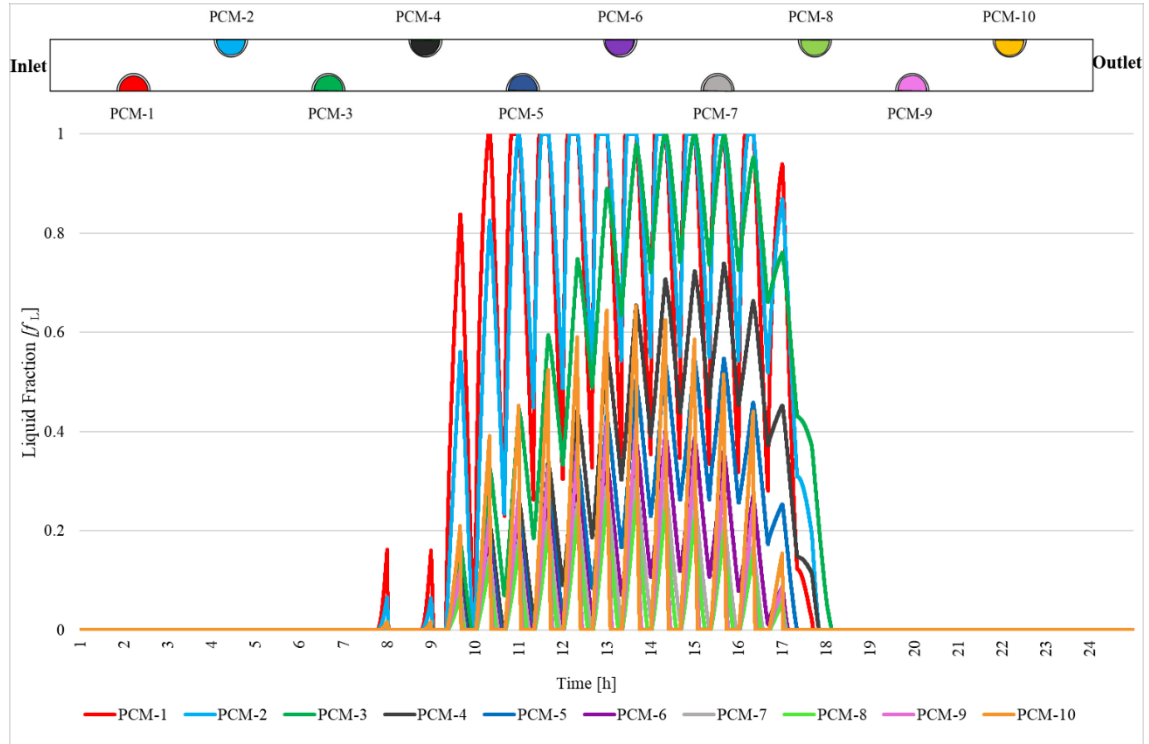
Figure 5.82. İzmir, melting/solidification results for June in İzmir.

Figures 5.83 and 5.84 refer to 24 hours operating time for the tube bundle HRV system July results for İzmir. Figure 5.83 shows the PCM chosen for İzmir melts and solidifies at 27°C. As seen in this graph, while melting and solidification are observed in certain time intervals, the temperature of the PCMs inside the tubes changes along with the outside temperature in the remaining times. Phase change starts after 07:00 in the morning and continues until 21:00. The melting and solidification of PCM in all tubes are only observed between 12:00 and 13:00.

Figure 5.84 shows the July melting and solidification results for İzmir. As seen in this graph, the phase changes of the tubes start at 08:00 in the morning and continue until 22:00. While a phase change of a maximum of 40% is observed in the morning hours, the phase change is observed in almost all tubes from 12:00 until 19:00. Especially 1st, 2nd, 3rd tubes change phase more efficiently than others.

183
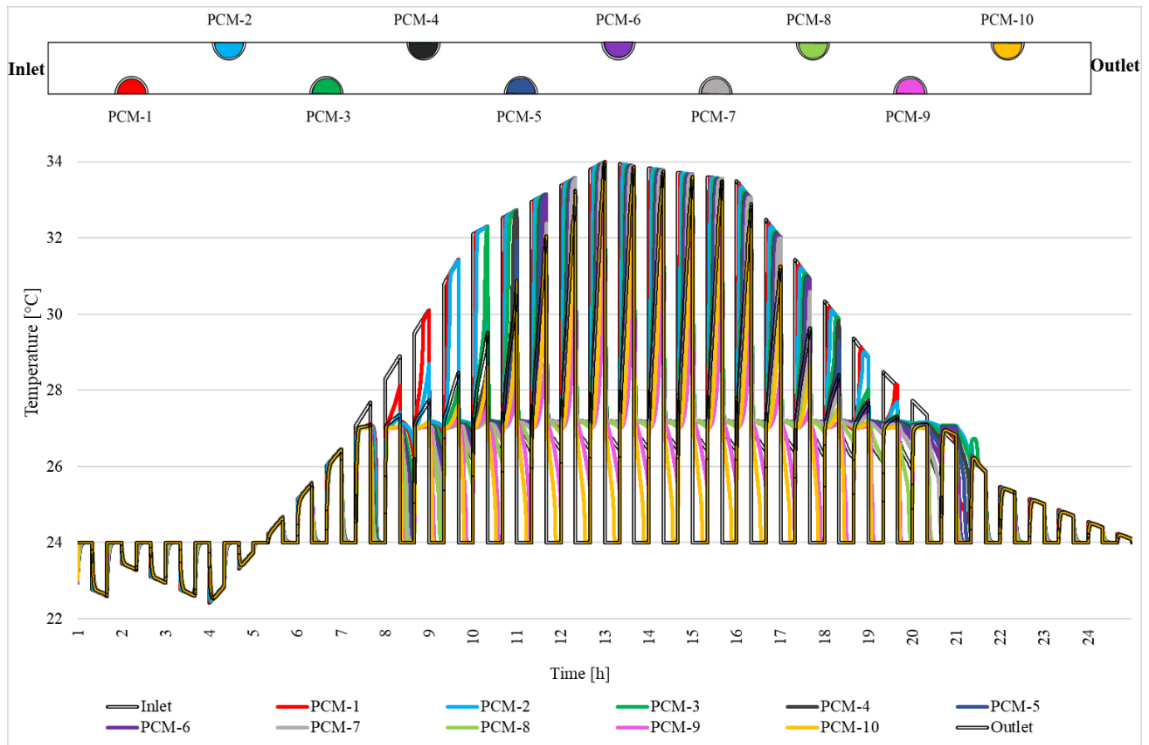
Figure 5.83. Daily simulation results for July in İzmir.
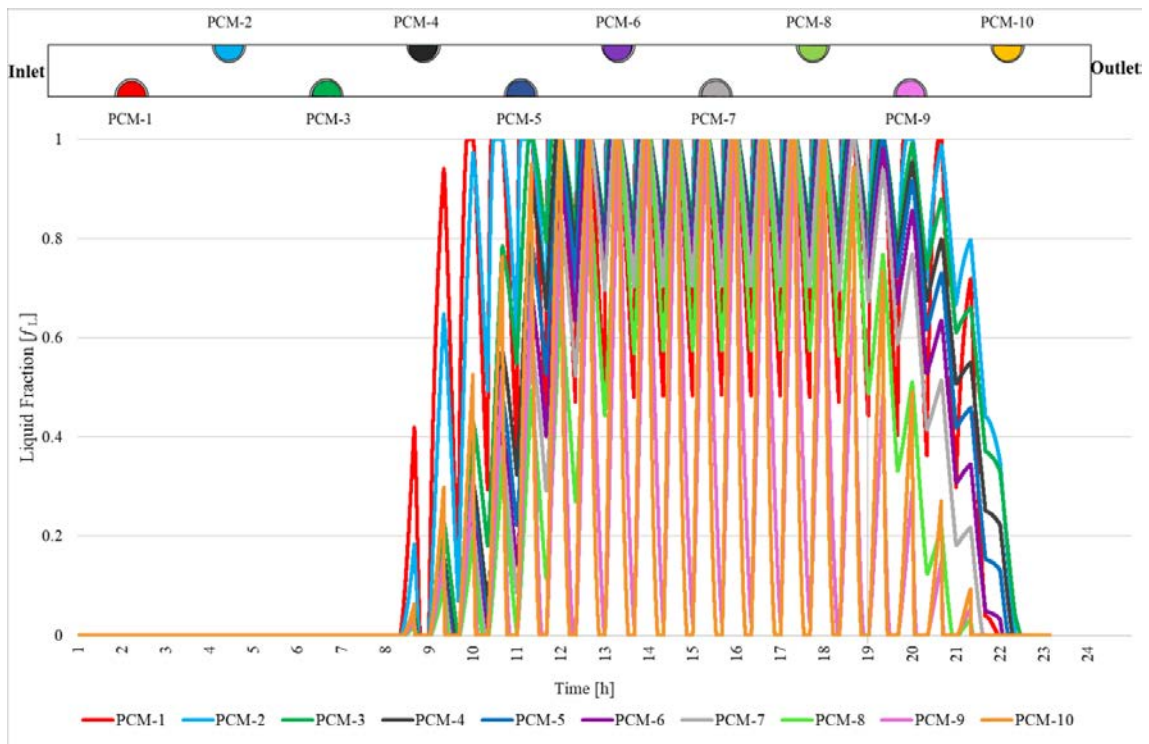
Figure 5.84. İzmir, melting/solidification results for July in İzmir.

5.4.2.3. Tropic Climate: Singapore

Due to Singapore's proximity to the Equator, there is only one season. The climate type seen in Singapore is the tropical climate type. All seasons of the year are quite hot and humid. The average temperature is between 25°C and 31°C. April is the warmest month and January is the coolest month in Singapore. The daytime length in Singapore remains 12 hours in all seasons. The latitude of Singapore is 1°.3', and the longitude is 103°.8'. So, this city-state is located just 1-degree north of the equator. Because of this, the Singapore climate is tropical. Figure 5.85 shows the yearly variation of the Singapore climate. And the temperatures in Singapore are very little from month to month and generally, the minimum degree is 25°C, the maximum degree is 31°C. December and January are the coolest months of the year. May, June, and July have the highest average of the monthly temperature data.
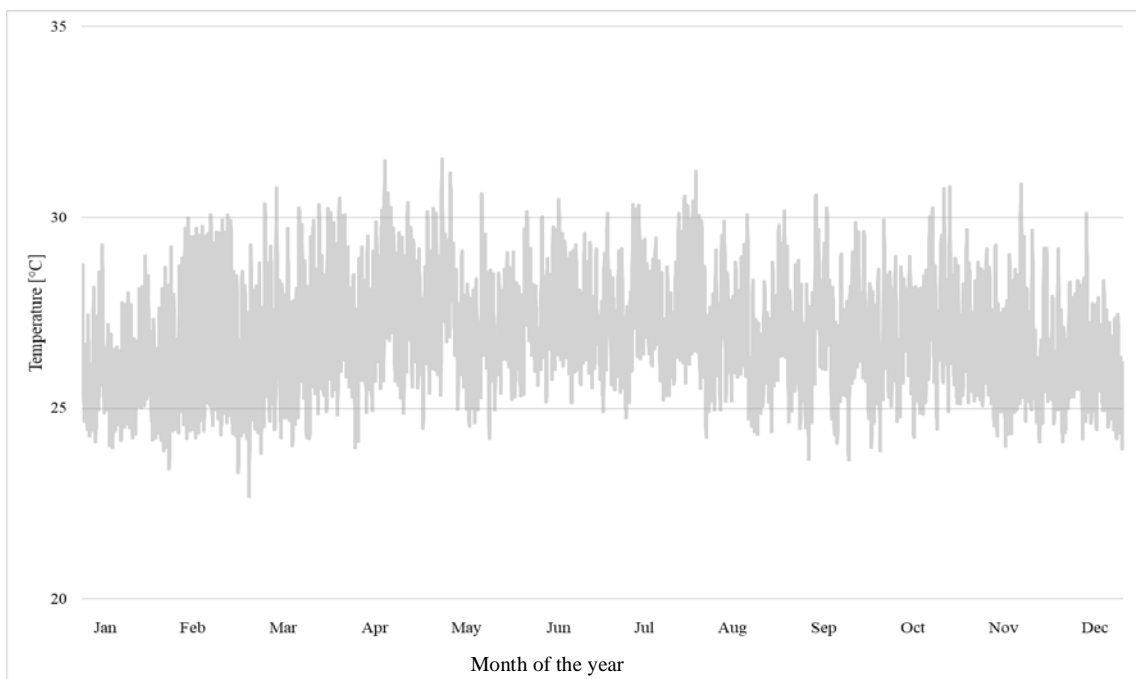
Figure 5.85. Singapore highest and lowest temperatures throughout the year (2005-2016)

Three months have been selected according to the monthly highest and coldest average temperature values given in Figure 5.85, as shown in Figure 5.86. These simulations are tried in 3 different months and are simulated in January, April, and July.

185

Figure 5.86 shows the monthly average of the daily data for selected months. It drops below 25 °C only between 17.00 and 23.00 in January and usually starts to rise at 00.00 and reaches its highest level at 05.00. The lowest level is seen at 20.00 hours. However, looking at the graph, the temperature values for April and July are almost the same. It is observed that there is a 2°C difference with January.
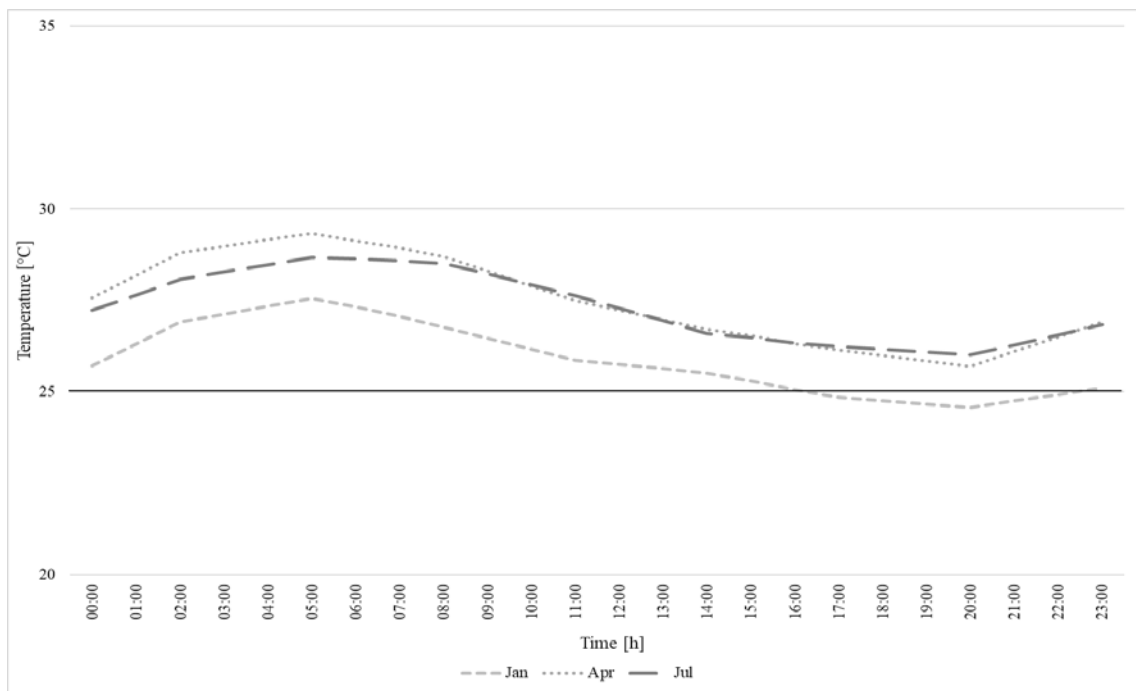
Figure 5.86. Monthly average of the daily temperature distribution of Singapore for January, April, and July.

PCM melting at 24°C is chosen considering the average temperature of Singapore. According to Vimalanathan and Babu (2014), The ideal indoor temperature at 21°C enhanced Singapore's office workers' productivity and health. So, simulations are carried out by assuming a constant indoor temperature of 21°C. Complete melting and solidification are not seen in every tube throughout the day, but the system operates all day and night. Figure 5.87 represents the heat recovery system operating based on the monthly average daily temperature for January. According to 21°C indoor temperature and transient outdoor temperature, the system works daily. When looking at the tubes, it reaches more indoor and outdoor temperatures in the morning hours, while the PCM in any tube does not reach the outdoor temperature in the evening, especially between 18.00 and 23.00.

186
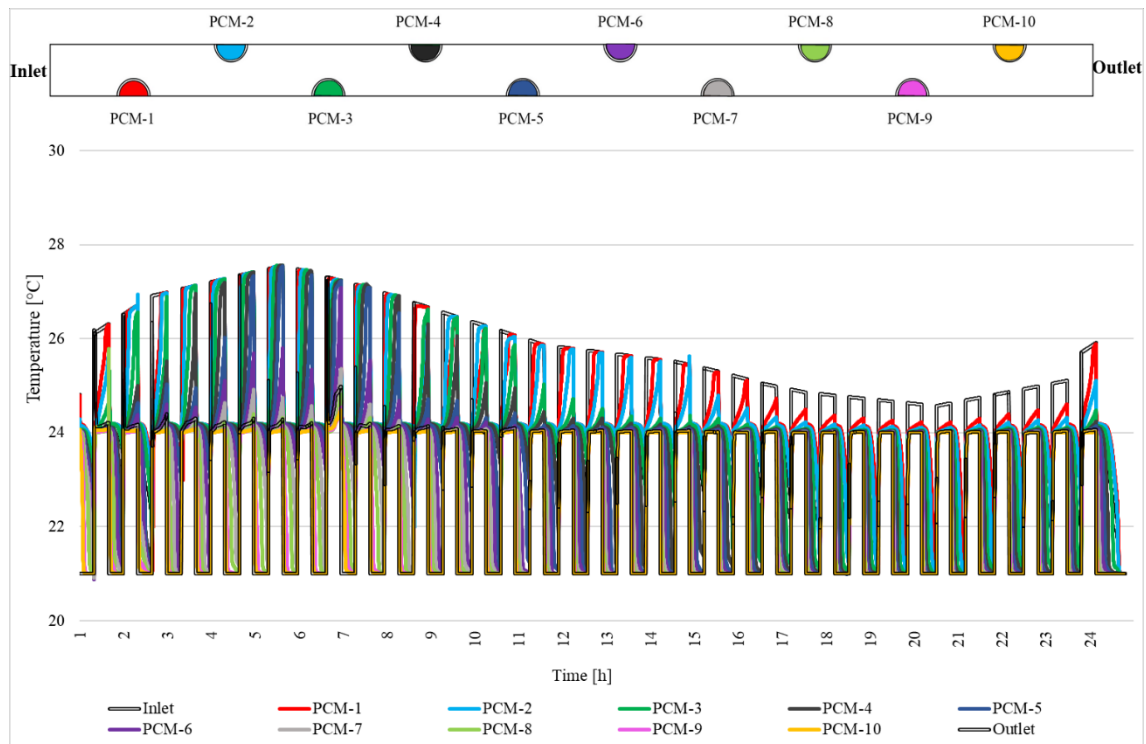
Figure 5.87. Daily simulation results for January in Singapore.

In Figure 5.88, the melting and solidification results are examined. The PCM in all the tubes has the highest percentage between 05.00-10.00 hours. The lowest melting/solidification ratio is observed in the evening hours. Especially 1st tube 2nd tube 3rd tube has the highest melting rate. While 8th, 9th, and 10th tubes change phase %40, 4th, 5th, 6th, and 7th tubes change phase %60. After 17.00, the liquid fraction decreases below 0.2 in all tubes except the 1st tube. The most fluctuation is seen in the 1st and 2nd tubes throughout the day.

The average temperature in April is 27°C. The highest temperature is 31°C while the lowest is 24°C. Here, eight hours of sunshine each day for April. In Figure 5.89, more melting and solidification are observed during the hours when the air temperature is the highest, while less energy is stored or released in the system in the evening hours. The phase change material melts at 24°C which melts and solidifies around all day. The PCM in each tube does not reach the indoor and outdoor temperatures all day. As shown in the graph, the 1st 2nd 3rd tube melts and solidifies the most, while the 4th 5th 6th 7th tube reaches the outdoor temperature between 05.00-12.00. After 12.00, there is no fully melting and solidification in these tubes. In addition, tube 8, 9, and 10 reach a level 1°C lower than the outdoor temperature between 05.00-12.00.
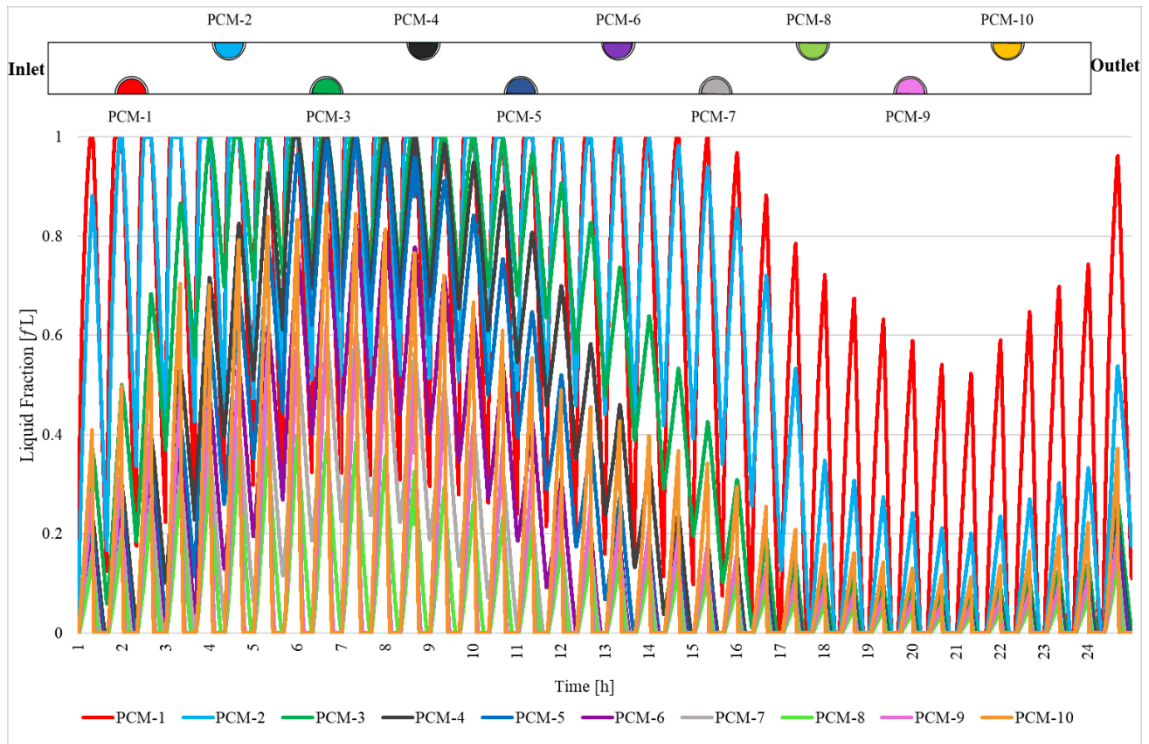
Figure 5.88. Singapore, melting/solidification results for January in Singapore.
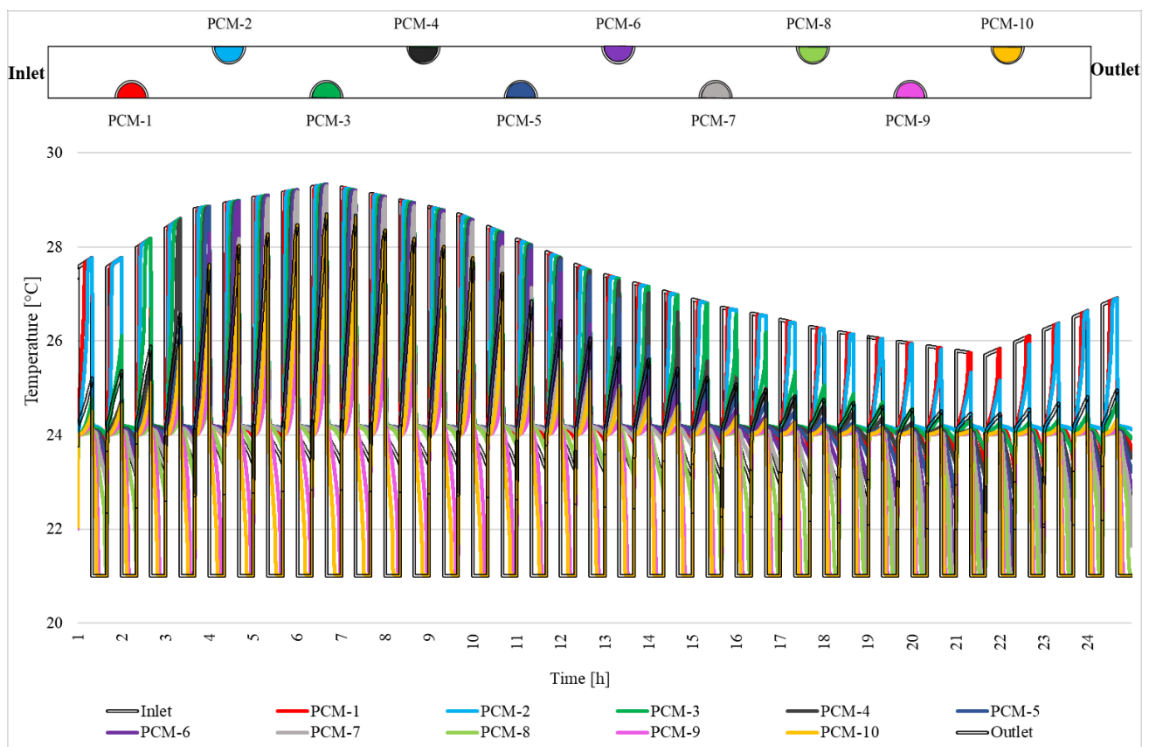
Figure 5.89. Daily simulation results for April in Singapore.

Looking at the melting solidification rates of April in Figure 5.90, almost the entire system is operating at all hours. However, while full melting and solidification are observed between 05.00-12.00, the system's performance decreases depending on the outdoor temperature. PCM-1 and PCM-2 work at %100 all day long. Other tubes melt and solidify by %60.
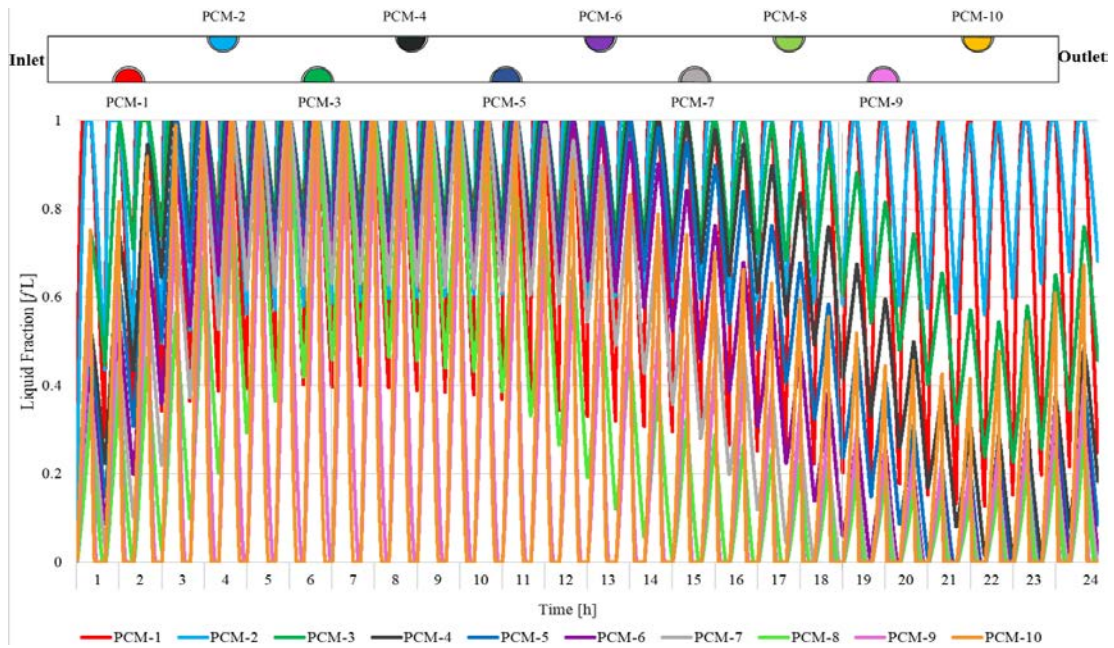
Figure 5.90. Singapore, melting/solidification results for April in Singapore.

Figures 5.91 and 5.92 refer to 24 hours operating time for the tube bundle HRV system July results for Singapore. The average daily temperature of around 27°C in July. In the heat of the day, the temperatures jump up to 31°C. In Singapore, it gets around 8 hours of sunshine in July. July has one of the highest average monthly temperatures. Figure 5.91 shows the PCM chosen for Singapore melts and solidifies 24°C. As seen in this graph, melting and solidification are observed all day. Although not all tubes reach the outdoor temperature, the most phase change is observed between 05.00-14.00.

When looking at the melt-solidification rates of July from Figure 5.92, almost the entire system is operating all day. However, while full melting and solidification are observed between 05.00-14.00, the system operates 80% depending on the outdoor temperature. In July, when the difference between the outdoor and indoor temperatures is greater, the system works more efficiently than in April.
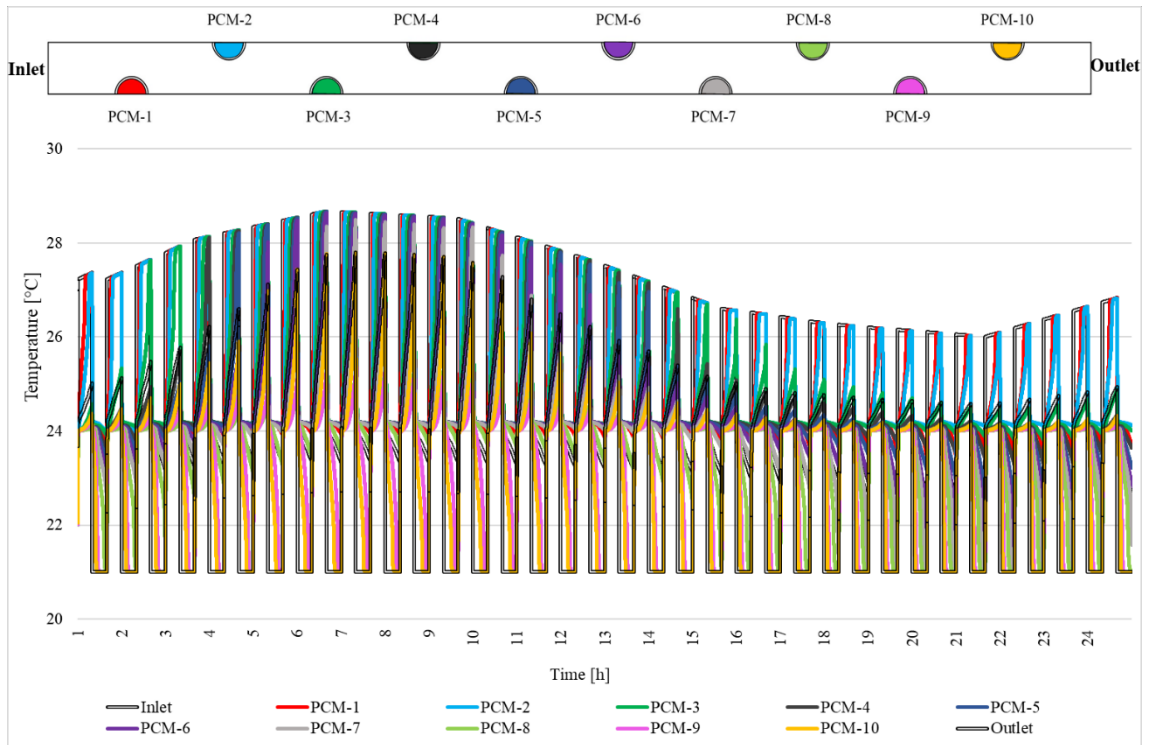
Figure 5.91. Daily simulation results for July in Singapore.
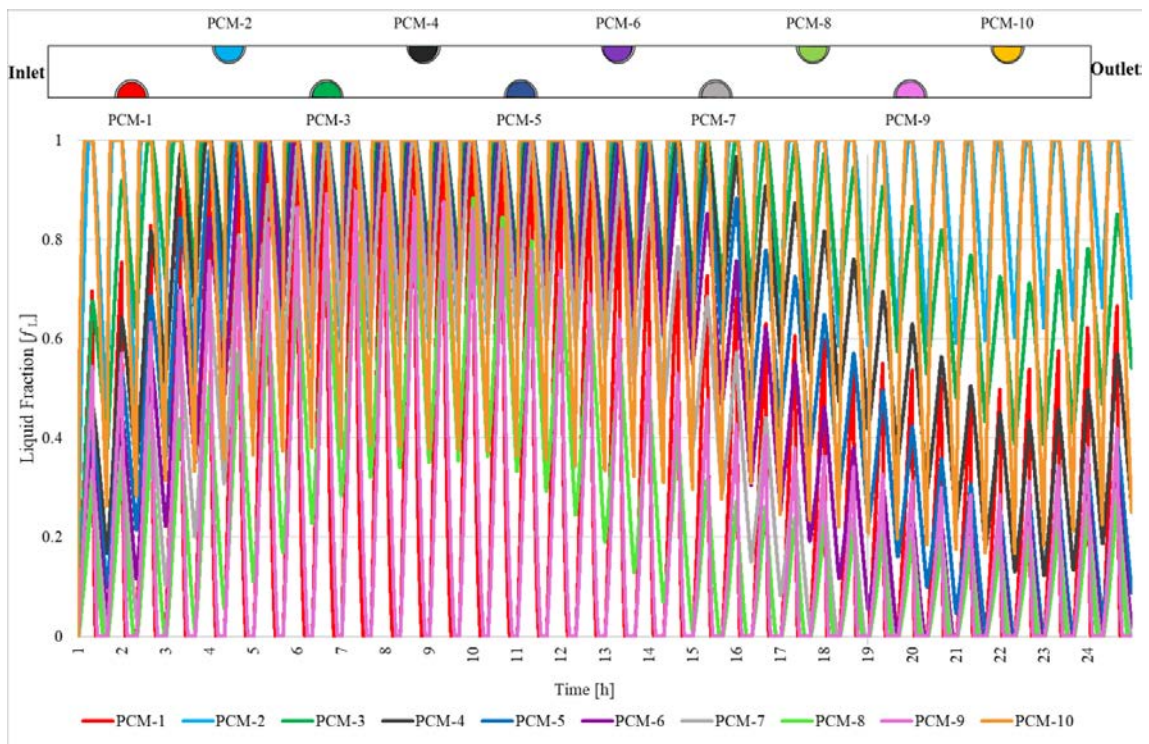
Figure 5.92. Singapore, melting/solidification results for July in Singapore.

5.4.3. Data Reduction

Figure 5.93 shows the results of the tube bundle HRV system with PCM obtained from simulations according to different climatic data. The red lines show the supply values in this figure, and the blue ones show the exhaust values. Here, two months are chosen from the winter conditions for Erzurum: January and February. Simulation has been made according to summer conditions for Izmir and the results of June and July are seen. For Singapore, simulations are made for 3 different months above, and April and July are shared here. Since the temperature distribution in Singapore is similar throughout the year, the results are expected to be the same all year.

This figure shows the calculation results of energy stored/released. The simulations are made according to the inlet and outlet velocity values obtained in the experiments. These are 0.34 m/s for inlet and 0.28 m/s for outlet. Outdoor temperatures are simulated using climate data. Indoor temperatures are selected differently for each city. While PCM melting at 15°C is chosen for Erzurum, the indoor temperature is accepted as 20°C. PCM melting at 27°C is chosen for Izmir, and the indoor temperature is determined as 24°C. For Singapore, the indoor temperature is 21°C with PCM melting at 24°C. While the average heat storage capacity is 38 kJ for Erzurum, it is 15 kJ for Izmir during the operating hours. And for Singapore, the average value is 21 kJ. It is seen that the system works all day long in winter conditions for Erzurum. For Singapore, the highest release rate of stored heat occurred between 00.00 and 09.00 hours. For İzmir, only the system stored/ released heat between 08:00 and 18:00. The highest storage values for Erzurum are observed between 00.00 and 03.00 when the outdoor temperature is the lowest. For İzmir, the system stores or releases heat at the highest outdoor temperature.
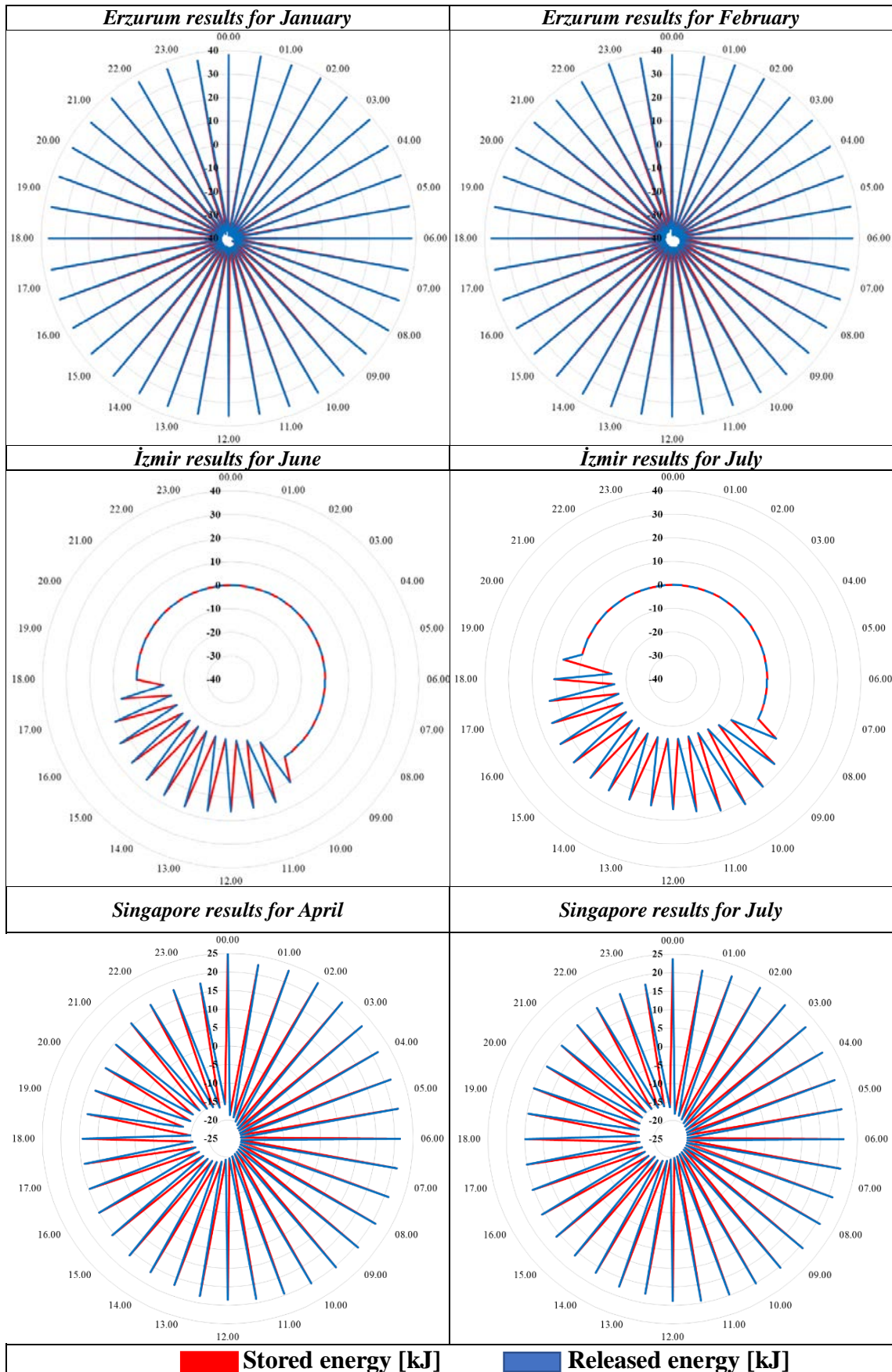
Figure 5.93. Total heat capacity of the tube bundle unit according to a monthly average of the daily data

5.5. Summary

This chapter contains 4 subtitles. The first section is the experimental results, the second section is the numerical results, the third section is the refinement of the tube bundle HRV system, and the fourth section is the simulations made in different climates. In this chapter, both ceramic systems stored sensible energy and tube bundle system stored latent energy were tested experimentally and analytically. After experimental and numerical results, six alternative cases were simulated to improve the total heat capacity. In addition, the thermal behavior of the system in 3 different climates was investigated.

In the first section, experimental results were explained. These units tested charging-discharging cycles to identify the temperature characteristics and evaluate the heat exchangers' energy capacity and losses. In order to evaluate the method of charging-discharging cycle test, the SHS module and LHS module have been experimented with in the laboratory. Then the detailed results in transient state different operation times for two systems were analyzed and discussed from the quantitative way. The efficiency results were shared for both systems by comparing.

In this case of the studied heat recovery ventilation units, the airflow generated large differences in the supply and exhaust efficiency. Also, the pressure differences are affected by the airflow rates in this ventilation system. And the higher-pressure rise is affected by the airflow balance difference of the unit with an axial fan. So, this resulted in the change in heat recovery system efficiency because of the stack effect pressure. Also, experimental studies all have some limitations. To more accurate temperature distribution in the heat exchanger materials could be observed by taking more measurements while the system is working.

In the second section, numerical results were represented. For the ceramic system, the simulation results and experimental results show that in winter conditions, the heat transfer rate was the best result when the system was operated for the 2-minute cycle. In addition, the best performance according to efficiency results is the 2-minute operation time.

For the tube bundle system, according to the experiments, the melting/solidifying results show that 20-minute of operation time gives the best thermal performance for maintaining a comfortable indoor temperature with the least energy consumption

according to the storage rate. When looking at the numerical results 15-minute and 20-minute mean heat transfer rates are very close to each other.

The third section discusses the CFD simulations' modifications for tube bundle decentralized heat recovery systems with six alternative HRV unit alteration approaches. Several alternative HRV unit changes can improve tube bundle heat transfer, according to the literature. To get the best performance out of the PCM tubes, the diameter, pitch size, various PCM solidification/melting temperatures, tube geometry, and air velocity are all examined using CFD modeling. Most previous experimental and computational research on flows in tube bundles concentrated on changing the size of the tubes, the form of the tubes, the system inlet air velocity, and the PCM combinations utilized in the system. The effect of system modifications was simulated and modeled in this study, and the results were reported in this section. The heat transfer has been calculated from the measured temperatures, inlet and outlet fluid temperatures, and pressure drops. The following conclusions were obtained from the simulations:

Unlike the experiments, the values of exhaust and supply are the same (or very close) in these results; this is due to the fact that the fan has the same performance in both directions in the simulations.

According to pressure drop results, the oval tube bundle has an advantage in airside convection heat transfer than the round tube bundle with the same arrangement in crossflow.

The heat transfer for staggered tube bundles is not independent of the pitch, at least an extended longitudinal pitch.

The heat transfer increases with the transverse row number for the tube bundle. And the heat transfer decreases with an increasing transverse pitch size.

The heat transfer in the system increases or decreases in direct proportion to the PCM mass. As the number of tubes increases, the amount of PCM that changes phase increases, so the heat transfer increases.

Pressure drop and heat transfer are directly proportional to increasing velocity. As seen in Table 1, 0.2 m/s, 0.5 m/s, and 1m/s results increase or decrease depending on the velocity.

As a result, the tube bundle performance evaluation criterion variations with the transverse and longitudinal tube pitches indicate that better performances can be achieved by reducing the tube pitch. This section shows that different geometries give different results at different flow conditions. The selection of the appropriate geometry for the tube

bundle does not always depend on the size, but the thermodynamic properties of the PCMs are just as important.

In the fourth section, the simulations were made under three different climatic conditions. In this section, according to the Köppen climate standard, Erzurum, Izmir, and Singapore are selected as the pilot city for continental climate, mild climate, and tropical climate, respectively. The analysis of the present study shows:

Decentralized HRV systems that store the latent heat energy in the tube bundle containing the PCM and the PCM with a fixed melting point are unsuitable for ventilation energy savings in some climatic zones.

Erzurum's heating load is more than the cooling load. On the other hand, in İzmir, the cooling load is higher than the heating load. So, this system is effective when used in Erzurum during the winter months and when used in İzmir during the summer months. Therefore, the designers need to consider the prevailing loads for efficient utilization of the latent HRV system.

Although the system cannot be used every month for Erzurum and İzmir, this wall integrated LHTES tube bundle HRV unit can be used every month in Singapore. because the temperature difference throughout the year in Singapore is low. This system is more efficient in Singapore than the other cities Thus, it is suitable for tropical climate.

CHAPTER 6

CONCLUSIONS AND RECOMMENDATIONS

This study investigated two different types of decentralized HRV units experimentally and numerically. These two systems are ceramic HRV unit and tube bundle HRV unit. A decentralized wall integrated HRV system with PCM, which has more energy storage capacity as an alternative to the system with ceramic units on the market, was designed and prototyped, and energy and flow numerical and experimental analyses were performed. For this purpose, the real-scale experiments were carried out in the Building Physics Laboratory of the Faculty of Architecture, Izmir Institute of Technology. The experimental tests of the ceramic HRV unit and tube bundle HRV unit took place in a controlled environment in different cases, where two HRV units were inside two wall integrated ducts for controlled parametric studies. The wall divides conditioned spaces that represent the indoors and the outdoors. During these experiments, the systems placed inside two ducts run synchronously. In an experimental set, the performance of the HRV units with SHTES and in another experimental set LHTES and their axial fan was experimentally investigated under different operating conditions. Afterward, ventilation performances for supply and exhaust were also analyzed to provide new experimental data under controlled ambient conditions.

The main findings for the ceramic HRV unit can be listed as follows:

For experimental results:

- The average supply air velocity results are 0.215 m/s, and the exhaust velocity is 0.165 m/s. These average values were measured at two different positions in the ducts due to the airflow direction because of providing a fully developed flow.

- The fan produces an average pressure difference of 4.82 Pa when the system is operating for 1-minute, 4.90 Pa when it is operating for 2-minute, 5.10 Pa when it is operating for 5-minute, and 4.82 Pa when it is operating for 7.5-minute.

- It is observed that the temperature of the ceramic materials increased between 1°C and 3°C depending on the position of the thermocouples in the ceramics during the 1-minute operating time. The air energy change of the unit for a 1-minute cycle is 5.098 kJ.

- When the operating time was the 2-minute cycle, the temperatures of the ceramic materials increased by up to 7°C depending on the measuring locations. The air energy change of the unit for a 2-minute cycle is 10.607 kJ.

- When the system was operated for 5-minute, the temperature of the interior of the ceramic approached the indoor temperature. In addition, a temperature difference of 10°C occurs in ceramics depending on the thermocouple positions. The air energy change of the unit for a 5-minute cycle is 20.732 kJ.

- The ceramic is approximately equal to both indoor and outdoor temperatures when the system is operated for 7.5-minute. The temperature value of the thermocouples in the ceramic showed an increase of a maximum of 11°C. The air energy change of the unit for a 7.5-minute cycle is 29.281 kJ.

- During the 10-minute cycle, there is a decrease or increase in the temperature of the ceramic materials of approximately 12°C. The high-temperature variation in the ceramic indicates that the most energy storage is achieved during a 10-minute cycle. The air energy change of the unit for a 10-minute cycle is 36.532 kJ.

On the other hand, by evaluating the experimental results, considering the average heat transfer rate instead of the total heat capacity of the unit in certain periods at different time steps; It has been seen that the HRV unit performs best in 2-minute cycles out of 1, 5, 7.5 and 10-minute cycles.

- For 1 min, 2 min, 5 min, 7.5 min, and 10 min operating time for winter conditions for ceramic HRV unit, the supply efficiency results are 75%, 82%, 76%, 73%, and 77%, and the exhaust efficiency results are 73%, 67%, 73%, 58%, and 62% respectively. And the average result is 77% for supply efficiency, and exhaust efficiency is 65%.

- For summer conditions, the unit is operated 7.5-minute, the supply efficiency result is 89%, exhaust efficiency is 61%, for 10-minute operating time results are 81% and 45% supply and exhaust efficiency, respectively.

The main findings for the tube bundle HRV unit can be listed as follows:

For experimental results:

- The average velocity for supply air is 0.344 m/s, and the average for exhaust air is 0.282 m/s for the tube bundle HRV prototype. The points that provided the nearest values to the calculated average velocity values were selected to represent the average velocity.

- The pressure difference between two fans for 15-minute, 20-minute, and 30-minute airflow from the outdoor to the indoor environment is 9.74 Pa, 9.78 Pa, and 9.57 Pa, respectively.

- When the system is operated for 15 min, all PCMs in the temperature trend inside the tubes do not reach 27°C, which is the melting/solidifying temperature, thus they are not fully melted. There is not enough time to stabilize the temperature distribution of the PCMs inside all the tubes. The air energy change of the latent HRV prototype for a 15-minute cycle in supply mode is 16.12 kJ.

- When the system operates for 20 min, the temperature increases inside the tube bundle, and the melting and solidification process of the PCM performs better than the 15 min cycle. The air energy change of the latent HRV prototype for a 20-minute cycle in supply mode is 27.24 kJ.

- PCM completely melts and completely solidifies 30 min. after fully melting/solidifying, the temperatures of the thermocouples increase. This indicates that SHTES follows LHTES. Thus, the temperatures of these thermocouples get very close to the indoor or outdoor environment when the system operates for 30 min. Air energy change of the latent HRV prototype for a 30-minute cycle in supply mode is 34.12 kJ.

According to experimental results, the mean heat transfer rate for tube bundle HRV system for 20-minute cycle gives the best result in supply mode is 22.7 W and exhaust mode is 18.4 W.

- For 15 min, 20 min, and 30 min operating time for summer conditions for tube bundle HRV unit, the supply efficiency results are 51%, 54%, and 46%, and the exhaust efficiency results are 23%, 29%, and 24% respectively. And the average result is 50% for supply efficiency, and exhaust efficiency is 25%.

ANSYS was used to simulate the control system, provide the necessary boundary conditions required by the FLUENT model, and calculate the energy requirements of the systems. With these results, simulations of operating conditions were examined, and the ability of a building simulation tool to provide modeling and performance prediction of these systems was tested. The ceramic and tube bundle systems were simulated in these simulations for this study. The fluids for the two systems are Newtonian and incompressible, and the Boussinesq approximation is utilized to account for the buoyancy term in the momentum equation. The flow is time-dependent, and the cartesian coordinate

system is 2D, no-slip conditions are valid for all boundaries, also viscous dissipation and radiation effects are neglected.

The mesh resolution can affect the result of a CFD simulation. So, many mesh structures were analyzed, and these can be classified as very coarse, coarse, medium, fine, very fine, ultra-fine. To provide the cyclic steady-state and eliminate the boundary condition that affects the simulations were analyzed with at least 50 consecutive cycles. While the system was operated from outdoor to indoor and from indoor to outdoor, stability was achieved in cycles, and the difference between the last two cycles is only 2%.

The main findings for the ceramic HRV unit can be listed as follows:

For numerical results:

• A mesh structure was created by using quadrilateral elements with edge sizing and face meshing features for a ceramic cell.

• The average temperature values standard deviation for the charging process is 0.65%, for the discharging process, it is 1.59% compared with CFD and experimental study results.

• For a 1-minute cycle, initially, the rise in the average volume temperature of ceramic and air was rapid and decreases with time. And the inlet temperature and ceramic reach a maximum of 15°C. The outlet temperature drops to 11°C. 1-minute operation time is not enough to charge and discharge processes. The energy change of the unit for a 1-minute cycle is 5.11 kJ.

• For a 2-minute operating time, the inlet temperature rises to a maximum of 17°C, the fluid inside the ceramic and ceramic rises to 19°C. The outlet temperature drops to 7°C while the system operates from outdoor to indoor. The energy change of the unit for a 2-minute cycle is 10.32 kJ.

• For 5 min, 7.5 min, and 10 min cycles, the temperature rise of ceramic is rapid first 150 s due to the high driving force for conduction, and discharging curve becomes flat as time progresses after the 150 s. The average system temperature reaches the inlet and outlet temperature in discharging and charging process. The energy change of the unit for 5 min, 7.5 min, and 10 min cycle results are 21.20 kJ, 30.91 kJ, and 30.91 kJ, respectively.

The main findings for the tube bundle HRV unit can be listed as follows:

For numerical results:

- A mesh structure was created by using quadrilateral and triangular elements with edge sizing and face meshing features for the tube bundle computational domain.

- As a result, while the average temperature values standard deviation for the charging process is 1.32%, for the discharging process, it is 1.38% compared with numerical solutions and experimental study results.

- PCM has no fully melting and solidifying process in the time-related melting and solidifying graphs for 15-minute operating. The energy change of the latent HRV unit for a 15-minute cycle is 26.94 kJ.

- For the 20-minute cyclic result, unlike the results of 15-minute, PCMs in all tubes melt and solidify except only 2 tubes. According to supply mode, the solidification process is not completely occurred. The energy change of the latent HRV unit for a 20-minute cycle is 31.99 kJ.

- During the 30-minute operating time, all PCM melted in the system and solidified except only 2 tubes. All the tubes reached the outside temperature. The energy change of the latent HRV unit for a 30-minute cycle is 41.94 kJ.

This thesis dissertation made different simulations by changing the LHTES HRV unit tube bundle dimensions, the tubes' shapes, air velocity, and the PCM material used for enhanced heat transfer.

For numerical results of refinement of the prototype:

- 1st case: 4 different pitch sizes were investigated on a tube diameter of 3 mm. In the simulation with 10 mm longitudinal and 10 mm transverse pitch sizes, it was calculated that the heat transfer increase is greater with a lower pitch size. According to the simulation results on the same tube diameter, the heat capacity increases as the longitudinal and transverse pitch size decreases. Also, the pressure drop increases.

- 2nd case: When the tube shape is changed, it appears to be a promising technique for heat transfer enhancement, especially the pressure drop results are compared to conventional cylindrical tubes.

- 3rd case: In the experiments, the measured velocity value is 0.34 m/s from the inlet, 0.28 m/s from the outlet. So, in case 3, the air velocity value has changed both inlet and outlet. 0.2 m/s, 0.5 m/s, and 1 m/s were simulated. As a result, heat transfer and the pressure drop increase if velocity increases.

- 4th case: In cases 4 and 5, it can be seen that the series arrangement improves solidification and melting performance compared to a single PCM. However, the heat storage capacities of the PCMs used in this case are different from each other. Therefore, there is a lower total heat storage capacity when compared.

- 5th case: The heat transfer increases or decreases in direct proportion to the PCM mass in the system. So, PCM's thermal energy storage capacity depends on the amount of PCM.

The tube bundle prototype produced within the scope of this thesis was analyzed the energy performance in three different climatic conditions was aimed to guide the designer in the selection of the wall integrated ventilation system in different climates. The heat recovery system operated based on the monthly average daily temperature in 20-minute cycles with the same inlet and outlet velocity. Erzurum is selected as the pilot city for the continental climate zone, İzmir is selected as the pilot city for the mild climate zone, and Singapore is selected as the pilot city for the tropical climate zone.

For numerical results of different climatic conditions:

- For Erzurum: the outdoor temperature simulations are made over two different months. These are January and February. The phase change material's melting/solidification point of 15°C is chosen, and the indoor temperature is assumed to be 20°C. The average outdoor temperature is -5°C. The PCM was completely solidified and completely melted in January and February. All tubes reached the inlet and outlet temperature in discharging and charging process. The average heat storage capacity is 38 kJ for Erzurum, according to simulation results.

- For Izmir: the simulations were carried out for June and July. The PCM melting and a solidification temperature is 27°C, and the indoor temperature is assumed to be 24°C. The average outdoor temperature for June and July is 30°C. For June, the system operated between 08:00 and 18:00. For July, the phase changes of the tubes start at 08:00 in the morning and continue until 22:00. While melting/solidification was observed in all tubes between the specified hours, no phase change was observed at other hour intervals. The average heat storage capacity is 15 kJ for Izmir during operating hours.

- For Singapore: these simulations were carried out in 3 different months and are simulated in January, April, and July. PCM melting at 24°C is chosen considering the average temperature of Singapore. And the indoor temperature is 21°C as a constant. The

melting and solidification were observed all day and all year. The average heat storage capacity value is 21 kJ.

This thesis contributes to the studies on the integration of PCMs and thus latent heat storage materials into HRV equipment used in the facades of buildings. The prototype proposed in the study was analyzed both experimentally and numerically. It is an alternative to the wall integrated sensible heat recovery ventilation systems available in the market. Such a wall integrated latent heat recovery ventilation system has no example in the literature. The proposed unit has a flexible model adaptable to different climatic conditions. It is also a system that can be developed and changed.

Some of the possible future work on this prototype is to consider different fans for more efficient ventilation performance, experimentally test it in different indoor and outdoor conditions, as well as experimentally and numerically investigate changes in the levels of IAQ variables, including relative humidity and CO_2 levels.

REFERENCES

Abdeen, Ahmed, Ahmed A Serageldin, Mona GE Ibrahim, Abbas El-Zafarany, Shinichi Ookawara, and Ryo Murata. 2019. "Solar chimney optimization for enhancing thermal comfort in Egypt: An experimental and numerical study." *Solar Energy* 180: 524-536.

Abduljalil, A, and Sohif Bin Mat Al-abidi. 2013. "K. Sopian, MY Sulaiman and Abdulrahman Th. Mohammed, CFD applications for latent heat thermal energy storage: a review." *Renewable and sustainable energy reviews* 20: 353-363.

Abdul-Wahab, Sabah Ahmed, Stephen Chin Fah En, Ali Elkamel, Lena Ahmadi, and Kaan Yetilmezsoy. 2015. "A review of standards and guidelines set by international bodies for the parameters of indoor air quality." *Atmospheric Pollution Research* 6 (5): 751-767.

Abhat, A. 1983. "Low temperature latent heat thermal energy storage: heat storage materials." *Solar energy* 30 (4): 313-332.

Afshari, Reza. 2020. Indoor air quality and severity of COVID-19: where communicable and non-communicable preventive measures meet. Mashhad University of Medical Sciences.

Agyenim, Francis, Neil Hewitt, Philip Eames, and Mervyn Smyth. 2010. "A review of materials, heat transfer and phase change problem formulation for latent heat thermal energy storage systems (LHTES)." *Renewable and sustainable energy reviews* 14 (2): 615-628.

Ahmad, Mardiana Idayu, and Saffa Riffat. 2020. *Energy Recovery Technology for Building Applications*. Springer.

Akeiber, Hussein, Payam Nejat, Muhd Zaimi Abd Majid, Mazlan A Wahid, Fatemeh Jomehzadeh, Iman Zeynali Famileh, John Kaiser Calautit, Ben Richard Hughes, and Sheikh Ahmad Zaki. 2016. "A review on phase change material (PCM) for sustainable passive cooling in building envelopes." *Renewable and Sustainable Energy Reviews* 60: 1470-1497.

Albatayneh, Aiman, Dariusz Alterman, and Adrian Page. 2018. "Adaptation the use of CFD modelling for building thermal simulation." Proceedings of the 2018 International Conference on Software Engineering and Information Management.

Albatayneh, Aiman, Dariusz Alterman, Adrian Page, and Behdad Moghtaderi. 2019. "The significance of the adaptive thermal comfort limits on the air-conditioning loads in a temperate climate." *Sustainability* 11 (2): 328.

Aldoss, Taha K, and Muhammad M Rahman. 2014. "Comparison between the single-PCM and multi-PCM thermal energy storage design." *Energy conversion and management* 83: 79-87.

Ali, Muzaffar, and Mukhtar Hussain Sahir. 2013. "Optimization of Heating, Ventilation, and Air-Conditioning (HVAC) System Configurations." Thesis, University of Engineering & Technology, Taxila.

Alizadeh, M, and SM Sadrameli. 2016. "Development of free cooling based ventilation technology for buildings: Thermal energy storage (TES) unit, performance enhancement techniques and design considerations–A review." *Renewable and Sustainable Energy Reviews* 58: 619-645.

Al-Jeebori, Abbas AS. 2008. "Thermal Design of Tube Banks in Cross Flow Based on Minimum Thermodynamic Losses." *Al-Qadisiyah Journal for Engineering Sciences* 1 (2): 133-143.

Anderson, Brian. 2006. "Energy performance of buildings directive." *BRE, April*.

Apte, Michael G. 2000. "Associations between indoor CO2 concentrations and sick building syndrome symptoms in US office buildings: an analysis of the 1994-1996 BASE study data." *Indoor air* 10 (4).

Arıcı, Müslüm, Feyza Bilgin, Sandro Nižetić, and Hasan Karabay. 2020. "PCM integrated to external building walls: An optimization study on maximum activation of latent heat." *Applied Thermal Engineering* 165: 114560.

Arkar, C, and S Medved. 2007. "Free cooling of a building using PCM heat storage integrated into the ventilation system." *Solar energy* 81 (9): 1078-1087.

ASHRAE. *ANSI/ASHRAE STANDARD 111-2008 Measurement, Testing, Adjusting, and Balancing of Building HVAC Systems*; 2008.

Asker, Mustafa, Ersin Alptekin, Ayça Tokuç, Mehmet Akif Ezan, and Hadi Ganjehsarabi. 2018. "Numerical Simulation of Building Wall Integrated with Phase Change Material: A Case Study of a Mediterranean City Izmir, Turkey." In *The Role of Exergy in Energy and the Environment*, 757-768. Springer.

Association for Environment Conscious Building (AECB), http://www.aecb.net/goldstandardpdf.php.

Astolfi, Arianna, and Franco Pellerey. 2008. "Subjective and objective assessment of acoustical and overall environmental quality in secondary school classrooms." *The Journal of the Acoustical Society of America* 123 (1): 163-173.

Averfalk, Helge, Paul Ingvarsson, Urban Persson, Mei Gong, and Sven Werner. 2017. "Large heat pumps in Swedish district heating systems." *Renewable and Sustainable Energy Reviews* 79: 1275-1284.

Balci, Ozan M, Mehmet A Ezan, and Kutbettin Z Turhan. 2019. "A heat recovery unit with phase change material for combi-boilers." *Energy Storage* 1 (5): e81.

Baldini, Luca, Moon Keun Kim, and Hansjürg Leibundgut. 2014. "Decentralized cooling and dehumidification with a 3 stage LowEx heat exchanger for free reheating." *Energy and buildings* 76: 270-277.

Baranova, Daria, Daniil Sovetnikov, Daria Semashkina, and Anatolijs Borodinecs. 2017. "Correlation of energy efficiency and thermal comfort depending on the ventilation strategy." *Procedia Engineering* 205: 503-510.

Bas, Halit, and Veysel Ozceyhan. 2012. "Heat transfer enhancement in a tube with twisted tape inserts placed separately from the tube wall." *Experimental Thermal and Fluid Science* 41: 51-58.

Başaran, Tahsin, and Tuğba İnan. 2016. "Experimental investigation of the pressure loss through a double skin facade by using perforated plates." *Energy and Buildings* 133: 628-639.

Benyahia, Nabil, Mohamed Aksouh, Amina Mataoui, and Hakan F Oztop. 2020. "Coupling turbulent natural convection-radiation-conduction in differentially heated cavity with high aspect ratio." *International Journal of Thermal Sciences* 158: 106518.

Bern, Marshall W, and Paul E Plassmann. 2000. *Mesh Generation*. Vol. 6.

Bernard, H Russell, and Harvey Russell Bernard. 2013. *Social research methods: Qualitative and quantitative approaches*. Sage.

Bernold, Leonhard E, and Tai Sik Lee. 2010. "Experimental research in construction." *Journal of Construction Engineering and Management* 136 (1): 26-35.

Bland, Ashley, Martin Khzouz, Thomas Statheros, and Evangelos I Gkanas. 2017. "PCMs for residential building applications: A short review focused on disadvantages and proposals for future development." *Buildings* 7 (3): 78.

Bonato, Paolo, Matteo D'Antoni, and Roberto Fedrizzi. 2020. "Modelling and simulation-based analysis of a façade-integrated decentralized ventilation unit." *Journal of Building Engineering* 29: 101183.

Buddhi, D, and RL Sawhney. 1994. "Proc: Thermal energy storage and energy conversion." *School of Energy and Environmental Studies, Devi Ahilya University, Indore, India*.

Bulut, Hüsamettin. 2011. "Havalandırma ve iç hava kalitesi açısından CO2 miktarının analizi." *Ulusal Tesisat Mühendisliği Kongresi*: 13-16.

Building Energy Performance (BEP) (in Turkish). https://www.mevzuat.gov.tr/mevzuat?MevzuatNo=13594&MevzuatTur=7&MevzuatTertip=5. (Accessed 10.09.2018).

Building Research Establishment Environmental Assessment Method (BREEAM), BRE Global Ltd. What Is BREEAM? *www.breeam.org/about.jsp?id=66* 2015.

BS EN 15251. BS EN 15251. 2007. *Indoor Environ. input parameters Des. Assess. energy Perform. Build.*

Calautit, John Kaiser, and Ben Richard Hughes. 2014. "Integration and application of passive cooling within a wind tower for hot climates." *HVAC&R Research* 20 (7): 722-730.

Campos-Celador, Álvaro, Gonzalo Diarce, Pello Larrinaga, and Ane Miren García-Romero. 2020. "A simple method for the design of thermal energy storage systems." *Energy Storage* 2 (6): e140.

Capeluto, Isaac Guedi, and Boris Plotnikov. 2017. "A method for the generation of climate-based, context-dependent parametric solar envelopes." *Architectural Science Review* 60 (5): 395-407.

Carbonare, N, T Pflug, C Bongs, and A Wagner. 2019. "Comfort-oriented control strategies for decentralized ventilation using co-simulation." IOP Conference Series: Materials Science and Engineering.

Carlucci, Salvatore, Lujian Bai, Richard de Dear, and Liu Yang. 2018. "Review of adaptive thermal comfort models in built environmental regulatory documents." *Building and Environment* 137: 73-89.

Celik, Ismail, and Gusheng Hu. 2004. "Single grid error estimation using error transport equation." *J. Fluids Eng.* 126 (5): 778-790.

Cengel, Yunus A. 2010. *Fluid mechanics*. Tata McGraw-Hill Education.

Cengel, Yunus A, and Afshin J Ghajar. 2007. "Heat and mass transfer." *A practical approach.*

Chandel, SS, and Tanya Agarwal. 2017. "Review of cooling techniques using phase change materials for enhancing efficiency of photovoltaic power systems." *Renewable and Sustainable Energy Reviews* 73: 1342-1351.

Chorin, Alexandre Joel. 1968. "Numerical solution of the Navier-Stokes equations." *Mathematics of computation* 22 (104): 745-762.

CIBSE, TM36. 2005. "Climate change and the indoor environment: impacts and adaptation." *Chartered Institution of Building Services Engineers, London.*

CIBSE, TM52. 2013. "Environmental Design." *Chartered Institution of Building Services Engineers, London.*

CIBSE, TM59. 2013. "Assess Overheating Risk in Homes." *Chartered Institution of Building Services Engineers, London.*

Clausen, Geo, and David P Wyon. 2008. "The combined effects of many different indoor environmental factors on acceptability and office work performance." *HVAC&R Research* 14 (1): 103-113.

Coley, David, Tristan Kershaw, and Matt Eames. 2012. "A comparison of structural and behavioural adaptations to future proofing buildings against higher temperatures." *Building and Environment* 55: 159-166.

Collyer, Anna. 2019. "Independent review of the Greenhouse and Energy Minimum Standards (GEMS) Act 2012."

Comite'Europe'en de Normalisation, CEN. 2007. "Indoor environmental input parameters for design and assessment of energy performance of buildings addressing indoor air quality, thermal environment, lighting and acoustics." *EN 15251*.

Council, National Research, and Green Schools. 2007. "Attributes for health and learning." *National Academy of Sciences USA, Washington*.

Creswell, John W. 2002. *Educational research: Planning, conducting, and evaluating quantitative*. Prentice Hall Upper Saddle River, NJ.

Creswell, John W, and J David Creswell. 2017. *Research design: Qualitative, quantitative, and mixed methods approaches*. Sage publications.

Cuce, Pinar Mert, and Saffa Riffat. 2015. "A comprehensive review of heat recovery systems for building applications." *Renewable and Sustainable Energy Reviews* 47: 665-682.

Culha, Oguzhan, Huseyin Gunerhan, Emrah Biyik, Orhan Ekren, and Arif Hepbasli. 2015. "Heat exchanger applications in wastewater source heat pumps for buildings: A key review." *Energy and Buildings* 104: 215-232.

Daisey, Joan M, William J Angell, and Michael G Apte. 2003. "Indoor air quality, ventilation and health symptoms in schools: an analysis of existing information." *Indoor air* 13 (LBNL-48287).

Dardir, Mohamed, Karthik Panchabikesan, Fariborz Haghighat, Mohamed El Mankibi, and Yanping Yuan. 2019. "Opportunities and challenges of PCM-to-air heat exchangers (PAHXs) for building free cooling applications—A comprehensive review." *Journal of Energy Storage* 22: 157-175.

Diallo, Thierno MO, Xudong Zhao, Antoine Dugue, Paul Bonnamy, Francisco Javier Miguel, Asier Martinez, Theodoros Theodosiou, Jing-Sheng Liu, and Nathan Brown. 2017. "Numerical investigation of the energy performance of an Opaque Ventilated Façade system employing a smart modular heat recovery unit and a latent heat thermal energy system." *Applied energy* 205: 130-152.

Dincer, Ibrahim, and Mehmet Akif Ezan. 2018. *Heat storage: A unique solution for energy systems*. Springer.

DIN EN 12599-Ventilation for buildings-Test procedures and measurement methods to hand over air conditioning and ventilation systems.

DIN EN 16211-Ventilation for buildings. Measurement of air flows on site. Methods.

Driels, Morris R, and Young S Shin. 2004. *Determining the number of iterations for Monte Carlo simulations of weapon effectiveness.*

Duffield, John S, and Brian Woodall. 2011. "Japan's new basic energy plan." *Energy Policy* 39 (6): 3741-3749.

Durakovic, Benjamin, and Muris Torlak. 2017. "Experimental and numerical study of a PCM window model as a thermal energy storage unit." *International Journal of Low-Carbon Technologies* 12 (3): 272-280.

Eiamsa-ard, Smith, Chinaruk Thianpong, and Pongjet Promvonge. 2006. "Experimental investigation of heat transfer and flow friction in a circular tube fitted with regularly spaced twisted tape elements." *International Communications in Heat and Mass Transfer* 33 (10): 1225-1233.

El Fouih, Younness, Pascal Stabat, Philippe Rivière, Phuong Hoang, and Valérie Archambault. 2012. "Adequacy of air-to-air heat recovery ventilation system applied in low energy buildings." *Energy and Buildings* 54: 29-39.

El Mankibi, Mohamed, Nikolaos Stathopoulos, Niousha Rezai, and Amine Zoubir. 2015. "Optimization of an Air-PCM heat exchanger and elaboration of peak power reduction strategies." *Energy and Buildings* 106: 74-86.

Ellis, MW, and EH Mathews. 2002. "Needs and trends in building and HVAC system design tools." *Building and environment* 37 (5): 461-470.

Elsaid, Ashraf Mimi, and M Salem Ahmed. 2021. "Indoor Air Quality Strategies for Air-Conditioning and Ventilation Systems with the Spread of the Global Coronavirus (COVID-19) Epidemic: Improvements and Recommendations." *Environmental Research*: 111314.

Elsanusi, Omer S, and Emmanuel C Nsofor. 2021. "Melting of multiple PCMs with different arrangements inside a heat exchanger for energy storage." *Applied thermal engineering* 185: 116046.

ElSorady, Dalia A, and Sahar M Rizk. 2020. "LEED v4. 1 operations & maintenance for existing buildings and compliance assessment: Bayt Al-Suhaymi, Historic Cairo." *Alexandria Engineering Journal* 59 (1): 519-531.

Energy Performance of Buildings Directive. *Struct. Surv.* 2005. https://doi.org/10.1108/ss.2005.11023aab.001.

Energy Performance of Buildings Directive. *Struct. Surv.* 2010.

EN 13141-8:2014. Ventilation for buildings. Performance testing of components/products for residential ventilation. Performance testing of un-ducted mechanical supply and exhaust ventilation units (including heat recovery) for mechanical ventilation systems intended for a2014.

Erdem, IŞIK, and Serkan Çibuk. 2015. "Yemekhaneler ve kantinlerde iç hava kalitesi ile ilgili ölçüm sonuçları ve analizi-Tunceli Üniversitesi örneği." *Dicle Üniversitesi Mühendislik Fakültesi Mühendislik Dergisi* 6 (1): 39-50.

Erguvan, Mustafa, and David W MacPhee. 2019. "Second law optimization of heat exchangers in waste heat recovery." *International Journal of Energy Research* 43 (11): 5714-5734.

Ezan, Mehmet Akif. 2011. "Experimental and numerical investigation of cold thermal energy storage systems." DEÜ Fen Bilimleri Enstitüsü.

Ezan, Mehmet Akif, Muhammet Ozdogan, and Aytunç Erek. 2011. "Experimental study on charging and discharging periods of water in a latent heat storage unit." *International Journal of Thermal Sciences* 50 (11): 2205-2219.

Ezan, Mehmet Akif, Ceren Yüksel, Ersin Alptekin, and Ahmet Yılancı. 2018. "Importance of natural convection on numerical modelling of the building integrated PVP/PCM systems." *Solar Energy* 159: 616-627.

Fanger, Poul O. 1970. "Thermal comfort. Analysis and applications in environmental engineering." *Thermal comfort. Analysis and applications in environmental engineering.*

Filis, Vasileios, Jakub Kolarik, and Kevin Michael Smith. 2021. "The impact of wind pressure and stack effect on the performance of room ventilation units with heat recovery." *Energy and Buildings* 234: 110689.

Fiorentini, Massimo, Paul Cooper, and Zhenjun Ma. 2015. "Development and optimization of an innovative HVAC system with integrated PVT and PCM thermal storage for a net-zero energy retrofitted house." *Energy and Buildings* 94: 21-32.

Fisk, William J. 2017. "The ventilation problem in schools: literature review." *Indoor Air* 27 (6): 1039-1051.

Fluent, ANSYS. 2011. "Ansys fluent theory guide." *ANSYS Inc., USA* 15317: 724-746.

Fonseca, Ana, Isabel Abreu, Maria João Guerreiro, Cristina Abreu, Ricardo Silva, and Nelson Barros. 2019. "Indoor Air Quality and Sustainability Management—Case Study in Three Portuguese Healthcare Units." *Sustainability* 11 (1): 101.

Fountain, M, and Edward A Arens. 1993. "Air movement and thermal comfort." *ASHRAE journal* 35 (8): 26-30.

Frontczak, Monika, Stefano Schiavon, John Goins, Edward Arens, Hui Zhang, and Pawel Wargocki. 2012. "Quantitative relationships between occupant satisfaction and satisfaction aspects of indoor environmental quality and building design." *Indoor air* 22 (2): 119-131.

Gasia, Jaume, Jan Diriken, Malcolm Bourke, Johan Van Bael, and Luisa F Cabeza. 2017. "Comparative study of the thermal performance of four different shell-and-tube heat exchangers used as latent heat thermal energy storage systems." *Renewable Energy* 114: 934-944.

George, PL, and H Borouchaki. 2000. "Quality mesh generation." *Comptes Rendus de l'Académie des Sciences Paris* 328: 505-518.

Gheorghe, Iuliana Florentina, and Barbu Ion. 2011. "The effects of air pollutants on vegetation and the role of vegetation in reducing atmospheric pollution." *The impact of air pollution on health, economy, environment and agricultural sources*: 241-280.

Godish, Thad. 2016. *Indoor environmental quality*. CRC press.

Godish, Thad, Wayne T Davis, and Joshua S Fu. 2014. *Air quality*. CRC Press.

Goetzler, William, Matt Guernsey, Jim Young, Jay Fujrman, and Amar Abdelaziz. 2016. *The future of air conditioning for buildings.* Navigant Consulting, Burlington, MA (United States).

Gong, Zhen-Xiang, and Aran S Mujumdar. 1996. "Finite element analysis of a multistage latent heat thermal storage system." *Numerical Heat Transfer, Part A Applications* 30 (7): 669-684.

Goodfellow, Howard D, and Esko Tahti. 2001. *Industrial ventilation design guidebook.* Academic press.

Greenhouse and Energy Minimum Standards Act 2012. https://www.legislation.gov.au/Details/C2018C00454. (Accessed 10.09.2018).

Grignon-Massé, Laurent, Jérôme Adnot, and Philippe Rivière. 2008. "Towards Adaptive PMV/PPD Indices for European Climates…." *Scaling up: building tomorrow's solutions-Proceedings from the ACEEE 2008 Summer Study on Energy Efficiency in Buildings*.

Guide, A. 2006. "Environmental design." *Chartered Institute of Building Services Engineers (CIBSE)*.

Gümüş, Veysel, Seven, Alaattin, and Şimşek, Oğuz. "Eğimli kritik altı açık kanal akımının sayısal modellemesi." *Gümüşhane Üniversitesi Fen Bilimleri Enstitüsü Dergisi* 11 (1): 73-90.

Guo, Haibo, Lu Huang, Wenjie Song, Xinyue Wang, Hongnan Wang, and Xinning Zhao. 2020. "Evaluation of the summer overheating phenomenon in reinforced concrete and cross laminated timber residential buildings in the cold and severe cold regions of China." *Energies* 13 (23): 6305.

Gupta, Naveen Kumar, Arun Kumar Tiwari, and Subrata Kumar Ghosh. 2018. "Heat transfer mechanisms in heat pipes using nanofluids–A review." *Experimental Thermal and Fluid Science* 90: 84-100.

Gürel, Barış. 2020. "A numerical investigation of the melting heat transfer characteristics of phase change materials in different plate heat exchanger (latent heat thermal energy storage) systems." *International Journal of Heat and Mass Transfer* 148: 119117.

Hekmat, Dariusch, Helmut E Feustel, and Mark P Modera. 1986. "Impacts of ventilation strategies on energy consumption and indoor air quality in single-family residences." *Energy and Buildings* 9 (3): 239-251.

Holman, Jack Philip. 2012. "Experimental methods for engineers."

Hu, Yue, Per Kvols Heiselberg, Hicham Johra, and Rui Guo. 2020. "Experimental and numerical study of a PCM solar air heat exchanger and its ventilation preheating effectiveness." *Renewable Energy* 145: 106-115.

İnan, Tuğba, Tahsin Başaran, and Aytunç Erek. 2017. "Experimental and numerical investigation of forced convection in a double skin façade." *Energies* 10 (9): 1364.

İnan, Tuğba, Tahsin Başaran, and Mehmet Akif Ezan. 2016. "Experimental and numerical investigation of natural convection in a double skin facade." *Applied Thermal Engineering* 106: 1225-1235.

Incropera, Frank P, David P DeWitt, Theodore L Bergman, and Adrienne S Lavine. 2007. "heat and mass transfer-Incropera 6e." *Fundamentals of Heat and Mass Transfer* 997.

Jang, Jiin-Yuh, and Jyh-Yau Yang. 1998. "Experimental and 3-D numerical analysis of the thermal-hydraulic characteristics of elliptic finned-tube heat exchangers." *Heat Transfer Engineering* 19 (4): 55-67.

Jokisalo, Juha, Jarek Kurnitski, Mika Vuolle, and Antti Torkki. 2003. "Performance of balanced ventilation with heat recovery in residential buildings in a cold climate." *International Journal of Ventilation* 2 (3): 223-236.

Kakac, Sadik, Hongtan Liu, and Anchasa Pramuanjaroenkij. 2002. *Heat exchangers: selection, rating, and thermal design*. CRC press.

Kalnæs, Simen Edsjø, and Bjørn Petter Jelle. 2015. "Phase change materials and products for building applications: A state-of-the-art review and future research opportunities." *Energy and Buildings* 94: 150-176.

Karaçavuş, Berrin, And Kadir Aydın. 2017. "Boru Demetleri Üzerinde Çapraz Akışta Nusselt Sayısının Nümerik İncelenmesi." TESKON.

Karimi, Mohsen, G Akdogan, KH Dellimore, and SM Bradshaw. 2012. "Quantification of numerical uncertainty in computational fluid dynamics modelling of hydrocyclones." *Computers & Chemical Engineering* 43: 45-54.

Khan, Muhammad Hammad, and William Pao. 2015. "Thermal comfort analysis of PMV model prediction in air conditioned and naturally ventilated buildings." *Energy Procedia* 75: 1373-1379.

Kim, Moon Keun, and Luca Baldini. 2016. "Energy analysis of a decentralized ventilation system compared with centralized ventilation systems in European climates: Based on review of analyses." *Energy and Buildings* 111: 424-433.

Kim, Nae-Hyun, Kang-Jong Lee, and Yeong-Bin Jeong. 2014. "Airside performance of oval tube heat exchangers having sine wave fins under wet condition." *Applied thermal engineering* 66 (1-2): 580-589.

Köktürk, G, and A Tokuç. 2017. "Vision for wind energy with a smart grid in Izmir." *Renewable and Sustainable energy reviews* 73: 332-345.

Konstantinidis, Christine Vasiliki. 2010. "Integration of thermal energy storage in buildings."

Koper, Piotr, Agnieszka Palmowska, and Agnieszka Myszkowska. 2019. "Research of single room decentralized heat recovery unit." *Architecture Civil Engineering Environment* 12 (4).

Kozielska, Barbara, Anna Mainka, Magdalena Żak, Dorota Kaleta, and Walter Mucha. 2020. "Indoor air quality in residential buildings in Upper Silesia, Poland." *Building and Environment* 177: 106914.

Krainer, A. Passivhaus Contra Bioclimatic Design. *Bauphysik* 2008. https://doi.org/10.1002/bapi.200810051.

Küçüka, Serhan. 2005. "Isı geri kazanım cihazlarının bazı şehirlerdeki yıllık toplam ısıtma ve soğutma kazançları." *Ulusal Tesisat Mühendisliği Kongresi* 1 (7): 46.

Kumar, D Arun, and R Prabu ME. "Investigation of Comparison of Three Different Tube Bundles of Heat Exchanger."

Lai, Dayi, Yue Qi, Junjie Liu, Xilei Dai, Lei Zhao, and Shen Wei. 2018. "Ventilation behavior in residential buildings with mechanical ventilation systems across different climate zones in China." *Building and Environment* 143: 679-690.

Lane, George A. 2018. *Solar Heat Storage: Volume II: Latent Heat Material*. CRC press.

Li, Gang. 2016. "Sensible heat thermal storage energy and exergy performance evaluations." *Renewable and Sustainable Energy Reviews* 53: 897-923.

Li, Hui, Xu Liu, and Guiyin Fang. 2010. "Preparation and characteristics of n-nonadecane/cement composites as thermal energy storage materials in buildings." *Energy and Buildings* 42 (10): 1661-1665.

Li, Xiuzhen, Dongsheng Zhu, Yingde Yin, Shijie Liu, and Xun Mo. 2018. "Experimental study on heat transfer and pressure drop of twisted oval tube bundle in cross flow." *Experimental Thermal and Fluid Science* 99: 251-258.

Liu, Shuli, Muriel Iten, and Ashish Shukla. 2017. "Numerical study on the performance of an air—multiple PCMs unit for free cooling and ventilation." *Energy and Buildings* 151: 520-533.

Ma, Nan, Dorit Aviv, Hongshan Guo, and William W Braham. 2021. "Measuring the right factors: A review of variables and models for thermal comfort and indoor air quality." *Renewable and Sustainable Energy Reviews* 135: 110436.

Maheshwari, A, RP Chhabra, and G Biswas. 2006. "Effect of blockage on drag and heat transfer from a single sphere and an in-line array of three spheres." *Powder technology* 168 (2): 74-83.

Mahler, B, and R Himmler. 2008. "Results of the evaluation study DeAL Decentralized facade integrated ventilation systems."

Malekzadeh, Fatemeh Malek. 2015. "Integration of phase change materials in commercial buildings for thermal regulation and energy efficiency." The University of Arizona.

Manz, H, H Huber, A Schälin, A Weber, M Ferrazzini, and M Studer. 2000. "Performance of single room ventilation units with recuperative or regenerative heat recovery." *Energy and Buildings* 31 (1): 37-47.

Mardiana-Idayu, A, and Saffa B Riffat. 2011. "An experimental study on the performance of enthalpy recovery system for building applications." *Energy and Buildings* 43 (9): 2533-2538.

Markov, Detelin. 2002. "Standards in thermal comfort." *Annual International Course: Ventilation and Indoor Climate, Sofia*: 147-157.

Maroni, Marco, Bernd Seifert, and Thomas Lindvall. 1995. *Indoor air quality: a comprehensive reference book*. Elsevier.

McDowall, Robert. 2007. *Fundamentals of HVAC systems: SI edition*. Academic Press.

Megahed, Naglaa A, and Ehab M Ghoneim. 2020. "Indoor Air Quality: Rethinking rules of building design strategies in post-pandemic architecture." *Environmental Research*: 110471.

Mehling, Harald, and Luisa F Cabeza. 2008. *Heat and cold storage with PCM*. Vol. 308. Springer.

Mentese, Sibel, Nihal Arzu Mirici, Tolga Elbir, Elif Palaz, Deniz Tasdibi Mumcuoğlu, Osman Cotuker, Coskun Bakar, Sibel Oymak, and Muserref Tatman Otkun. 2020. "A long-term multi-parametric monitoring study: Indoor air quality (IAQ) and the sources of the pollutants, prevalence of sick building syndrome (SBS) symptoms, and respiratory health indicators." *Atmospheric Pollution Research* 11 (12): 2270-2281.

Merzkirch, Alexander, Stefan Maas, Frank Scholzen, and Daniele Waldmann. 2016. "Field tests of centralized and decentralized ventilation units in residential buildings–Specific fan power, heat recovery efficiency, shortcuts and volume flow unbalances." *Energy and buildings* 116: 376-383.

Metin, Cagri, Servet Giray Hacipasaoglu, Ersin Alptekin, and Mehmet Akif Ezan. 2019. "Implementation of enhanced thermal conductivity approach to an LHTES system with in-line spherical capsules." *Energy Storage* 1 (1): e39.

Mikola, Alo, Raimo Simson, and Jarek Kurnitski. 2019. "The impact of air pressure conditions on the performance of single room ventilation units in multi-story buildings." *Energies* 12 (13): 2633.

Mishra, Akanksha, A Shukla, and Atul Sharma. 2015. "Latent heat storage through phase change materials." *Resonance* 20 (6): 532-541.

Mitova, Maya I, Camille Cluse, Catherine G Goujon-Ginglinger, Samuel Kleinhans, Michel Rotach, and Manuel Tharin. 2020. "Human chemical signature: Investigation on the influence of human presence and selected activities on concentrations of airborne constituents." *Environmental Pollution* 257: 113518.

Moore, Nick. 2006. *How to do research: a practical guide to designing and managing research projects*. Facet publishing.

Murgul, Vera, Dusan Vuksanovic, Nikolay Vatin, and Viktor Pukhkal. 2014. "Decentralized ventilation systems with exhaust air heat recovery in the case of residential buildings." Applied Mechanics and materials.

Murray, Portia, Adam M Rysanek, Jovan Pantelic, Matthias Mast, and Arno Schlueter. 2015. "On decentralized air-conditioning for hot and humid climates: Performance characterization of a small capacity dedicated outdoor air system with built-in sensible and latent energy recovery wheels." *Energy Procedia* 78: 3471-3476.

Myong, Ji-Hyun, Byung-Nam Choi, Min-Geon Go, and Nae-Hyun Kim. 2021. "Experimental investigation on the airside heat transfer and pressure drop of the fin-and-tube heat exchangers having oval tubes." *Experimental Heat Transfer*: 1-16.

Nichols, BD, CW Hirt, and RS Hotchkiss. 1981. "Volume of fluid (VOF) method for the dynamics of free boundaries." *Journal of Computational Physics* 39 (1): 201-225.

Nicol, Fergus. 2013. *The Limits of Thermal Comfort: Avoiding Overheating in European Buildings: CIBSE TM52, 2013*. Cibse.

No, Compilation. 2008. "National Greenhouse and Energy Reporting (Measurement) Determination 2008."

O'Connor, Dominic, John Kaiser S Calautit, and Ben Richard Hughes. 2016. "A review of heat recovery technology for passive ventilation applications." *Renewable and Sustainable Energy Reviews* 54: 1481-1493.

Olesen, Bjarne W, and KC Parsons. 2002. "Introduction to thermal comfort standards and to the proposed new version of EN ISO 7730." *Energy and buildings* 34 (6): 537-548.

Olivier, David. 2008. "The carbonlite energy performance standards." AECB 15th Conference.

Özbalta, T, and İ Çakmanus. 2008. "Binalarda Sürdürülebilirlik: Ömür boyu maliyete ilişkin yaklaşımlar." *Doğa Sektörel Yayınları, İstanbul*.

Özdamar, Melek, and Umaroğullari, Filiz. 2017. "Bir Ofis Yapısı Örneğinde Isıl Konfor ve İç Hava Kalitesinin İncelenmesi." *Megaron* 12 (1).

Pagkalos, Christos, George Dogkas, Maria K Koukou, John Konstantaras, Kostas Lymperis, and Michail Gr Vrachopoulos. 2020. "Evaluation of water and paraffin PCM as storage media for use in thermal energy storage applications: A numerical approach." *International Journal of Thermofluids* 1: 100006.

Park, JS, N-Y Jee, and J-W Jeong. 2014. "Effects of types of ventilation system on indoor particle concentrations in residential buildings." *Indoor Air* 24 (6): 629-638.

Park, Seong Hyun, Yong Gap Park, and Man Yeong Ha. 2020. "A numerical study on the effect of the number and arrangement of tubes on the melting performance of phase change material in a multi-tube latent thermal energy storage system." *Journal of Energy Storage* 32: 101780.

Pause, B. 2010. "Phase change materials and their application in coatings and laminates for textiles." In *Smart Textile Coatings and Laminates*, 236-250. Elsevier.

Pekdoğan, Tugce. 2015. "An investigation of transient thermal behaviors of building external walls." İzmir Institute of Technology.

Pekdogan, Tugce, and Tahsin Basaran. 2017. "Thermal performance of different exterior wall structures based on wall orientation." *Applied Thermal Engineering* 112: 15-24.

Pekdogan, Tugce, Ayça Tokuç, Mehmet Akif Ezan, and Tahsin Başaran. 2021a. "Experimental investigation of a decentralized heat recovery ventilation system." *Journal of Building Engineering* 35: 102009.

Pekdogan, Tugce, Ayça Tokuç, Mehmet Akif Ezan, and Tahsin Başaran. 2021b. "Experimental investigation on heat transfer and air flow behavior of latent heat storage unit in a facade integrated ventilation system." *Journal of Energy Storage* 44: 103367.

Pérez-Lombard, Luis, José Ortiz, and Christine Pout. 2008. "A review on buildings energy consumption information." *Energy and buildings* 40 (3): 394-398.

Permana, Ikhwan, Tri Ayodha Ajiwiguna, and Mukhammad Ramdlan Kirom. 2019. "Comparison of heat transfer coefficient on single tube and multi tube heat exchanger." Journal of Physics: Conference Series.

Persily, Andrew, and Lilian de Jonge. 2017. "Carbon dioxide generation rates for building occupants." *Indoor air* 27 (5): 868-879.

Prior, J. 1993. "Building research establishment environmental assessment method." *BREEAM) Version* 1: 93.

Promoppatum, Patcharapit, Shi-Chune Yao, Thomas Hultz, and Dave Agee. 2017. "Experimental and numerical investigation of the cross-flow PCM heat exchanger for the energy saving of building HVAC." *Energy and Buildings* 138: 468-478.

Qi, MW, XF Li, LB Weschler, and J Sundell. 2014. "CO_2 generation rate in Chinese people." *Indoor Air* 24 (6): 559-566.

Rehm, Bill, Jerome Schubert, Arash Haghshenas, Amir Saman Paknejad, and Jim Hughes. 2013. *Managed pressure drilling*. Elsevier.

Republic of Turkey General Directorate of State Meteorological Service. https://www.mgm.gov.tr/veridegerlendirme/il-ve-ilceler-istatistik.aspx?k=H (Accessed 18. 09. 2021).

Roache, Patrick J. 1993. "A method for uniform reporting of grid refinement studies." *ASME-PUBLICATIONS-FED* 158: 109-109.

Roy, Uttam, and Pranab Kanti Roy. 2020. "Advances in heat intensification techniques in shell and tube heat exchanger." In *Advanced Analytic and Control Techniques for Thermal Systems with Heat Exchangers*, 197-207. Elsevier.

Rubitherm Technologies GmbH. Rubitherm GmbH. *Rubitherm GmbH*. 2016.

Russell, Marion, Max Sherman, and Armin Rudd. 2007. "Review of residential ventilation technologies." *Hvac&R Research* 13 (2): 325-348.

Sakhaei, Mehryar, I Ashtiani Abdi, Farhad Sabri, and Kamel Hooman. 2020. "Experimental and numerical analysis of transient heat transfer from inclined tube bundles." *Journal of Thermal Analysis and Calorimetry* 140 (3): 1413-1426.

Sandberg, M, and B Moshfegh. 1996. "Investigation of fluid flow and heat transfer in a vertical channel heated from one side by PV elements, part II-Experimental study." *Renewable Energy* 8 (1-4): 254-258.

Sassi, Paola. 2017. "Thermal comfort and indoor air quality in super-insulated housing with natural and decentralized ventilation systems in the south of the UK." *Architectural Science Review* 60 (3): 167-179.

Schröder, Elisabeth, Klaus Neumaier, Fabian Nagel, and Christian Vetter. 2014. "Study on heat transfer in heat exchangers for a new supercritical organic Rankine cycle." *Heat transfer engineering* 35 (18): 1505-1519.

Seppanen, Olli, and William J Fisk. 2001. "Association of ventilation system type with SBS symptoms in office workers."

Settimo, Gaetano, Maurizio Manigrasso, and Pasquale Avino. 2020. "Indoor air quality: A focus on the European legislation and state-of-the-art research in Italy." *Atmosphere* 11 (4): 370.

Seyam, Shaimaa. 2018. "Types of HVAC systems." *HVAC System*: 49-66.

Shah, Karnav N, Priyank D Patel, Kush V Mahant, and Chetan O Yadav. 2013. "CFD analysis of heat exchanger over a staggered tube bank for different angle arrangement of tube bundles." *Int J Eng* 2: 1-5.

Shao, L, SB Riffat, and G Gan. 1998. "Heat recovery with low pressure loss for natural veltilation." *Energy and Buildings* 28 (2): 179-184.

Sharma, Atul. 2009. "Tyagi, VV Chen, CR Buddhi, D." *Renewable and Sustainable Energy Reviews* 13: 318-45.

Soares, Nelson, José J Costa, Adélio Rodrigues Gaspar, and Paulo Santos. 2013. "Review of passive PCM latent heat thermal energy storage systems towards buildings' energy efficiency." *Energy and buildings* 59: 82-103.

Ekren, Orhan, Ziya Haktan Karadeniz, Ibrahim Atmaca, Tugba Ugranli-Cicek, Sait C. Sofuoglu, and Macit Toksoy. "Assessment and improvement of indoor environmental quality in a primary school." *Science and Technology for the Built Environment* 23, no. 2 (2017): 391-402. Stathopoulos, N, M El Mankibi, and Mattheos Santamouris. 2017. "Numerical calibration and experimental validation of a PCM-Air heat exchanger model." *Applied Thermal Engineering* 114: 1064-1072.

Stritih, U, VV Tyagi, R Stropnik, H Paksoy, F Haghighat, and M Mastani Joybari. 2018. "Integration of passive PCM technologies for net-zero energy buildings." *Sustainable cities and society* 41: 286-295.

Sublett, James L. 2011. "Effectiveness of air filters and air cleaners in allergic respiratory diseases: a review of the recent literature." *Current allergy and asthma reports* 11 (5): 395-402.

Sutherland, Ken, and George Chase. 2011. *Filters and filtration handbook*. Elsevier.

Swain, Abhilas, and Mihir Kumar Das. 2016. "Convective heat transfer and pressure drop over elliptical and flattened tube." *Heat Transfer—Asian Research* 45 (5): 462-481.

Szokolay, Steven. 2012. *Introduction to architectural science*. Routledge.

Talukdar, Shaon, Hasan Mohammad Mostafa Afroz, Md Anowar Hossain, MA Aziz, and Md Monir Hossain. 2019. "Heat transfer enhancement of charging and discharging of phase change materials and size optimization of a latent thermal energy storage system for solar cold storage application." *Journal of Energy Storage* 24: 100797.

Tan, Zhi-Zhong, Ling Zhou, and Da-feng Luo. 2015. "Resistance and capacitance of 4× n cobweb network and two conjectures." *International Journal of Circuit Theory and Applications* 43 (3): 329-341.

Taufiq, BN, Haji Hassan Masjuki, TMI Mahlia, Rahman Saidur, MS Faizul, and E Niza Mohamad. 2007. "Second law analysis for optimal thermal design of radial fin geometry by convection." *Applied Thermal Engineering* 27 (8-9): 1363-1370.

Teke, Ahmet, and Oğuzhan Timur. 2014. "Assessing the energy efficiency improvement potentials of HVAC systems considering economic and environmental aspects at the hospitals." *Renewable and Sustainable Energy Reviews* 33: 224-235.

The Ministry of Housing and Urban-Rural Development (MOHURD) http://english.www.gov.cn/state_council/2014/09/09/content_281474986284089.htm. (Accessed 10.09.2018).

Tokuç, Ayça, Tahsin Başaran, and S Cengiz Yesügey. 2015. "An experimental and numerical investigation on the use of phase change materials in building elements: The case of a flat roof in Istanbul." *Energy and buildings* 102: 91-104.

Tommerup, Henrik, and Svend Svendsen. 2006. "Energy savings in Danish residential building stock." *Energy and buildings* 38 (6): 618-626.

Vakhshouri, Amir Reza. 2020. "Paraffin as phase change material." *Paraffin Overview*: 1-23.

Van Berkel, S, KD Pressnail, and MF Touchie. 2014. "Residential ventilation: a review of established systems and a preliminary laboratory investigation of an innovative fine wire heat recovery ventilator." *Proc. 14th CCBST, Toronto, Canada*: 381-390.

Verriele, M, Coralie Schoemaecker, Benjamin Hanoune, N Leclerc, Sébastien Germain, V Gaudion, and N Locoge. 2016. "The MERMAID study: indoor and outdoor average pollutant concentrations in 10 low-energy school buildings in France." *Indoor Air* 26 (5): 702-713.

Vimalanathan, Komalanathan, and Thangavelu Ramesh Babu. "The effect of indoor office environment on the work performance, health and well-being of office workers." *Journal of environmental health science and engineering* 12, no. 1 (2014): 1-8.

Wallner, Peter, Peter Tappler, Ute Munoz, Bernhard Damberger, Anna Wanka, Michael Kundi, and Hans-Peter Hutter. 2017. "Health and wellbeing of occupants in highly energy efficient buildings: A field study." *International journal of environmental research and public health* 14 (3): 314.

Wang, Chun-Yan, Akihiro Isoda, Mao-Song Li, and Dao-Long Wang. 2007. "Growth and eco-physiological performance of cotton under water stress conditions." *Agricultural Sciences in China* 6 (8): 949-955.

Weinläder, Helmut, Werner Körner, and Birgit Strieder. 2014. "A ventilated cooling ceiling with integrated latent heat storage—monitoring results." *Energy and buildings* 82: 65-72.

Willink, R, and R Willink. 2013. "Guide to the Expression of Uncertainty in Measurement." *Measurement Uncertainty and Probability; Cambridge University Press: Cambridge, UK*: 237-244.

Wong, Ling Tim, Kwok Wai Mui, and PS Hui. 2008. "A multivariate-logistic model for acceptance of indoor environmental quality (IEQ) in offices." *Building and environment* 43 (1): 1-6.

Wouters, P, P Barles, Å Blomsterberg, P Bulsing, W De Gids, Ch Delmotte, JC Faÿsse, C Filleux, P Hardegger, and V Leal. 2001. "Towards improved performances of mechanical ventilation systems." *Joule TIP-Vent project*.

Wu, Felicia, David Jacobs, Clifford Mitchell, David Miller, and Meryl H Karol. 2007. "Improving indoor environmental quality for public health: impediments and policy recommendations." *Environmental health perspectives* 115 (6): 953-957.

Xing, Tao, and Frederick Stern. 2010. "Factors of safety for Richardson extrapolation." *Journal of Fluids Engineering* 132 (6).

Xu, Qi, Saffa Riffat, and Shihao Zhang. 2019. "Review of heat recovery technologies for building applications." *Energies* 12 (7): 1285.

Yeang, Ken. 2006. "Ecodesign: A manual for ecological design."

Yıldırım, Nazım Haydar, Emre Kahraman, Ahmet Berk Yılmaz, Ersin Alptekin, Ayça Tokuç, Mehmet Akif Ezan, And Aytunç Erek. 2017. "Bir Gizli Isıl Enerji Depolama Tankının Akış Modülünün 2 Boyutlu Sayısal İncelenmesi.". TESKON.

Yılmaz, Erkan, and İhsan Çiçek. 2018. "Detailed Köppen-Geiger climate regions of Turkey Türkiye'nin detaylandırılmış Köppen-Geiger iklim bölgeleri." *Journal of Human Sciences* 15 (1): 225-242.

Yılmaz, Tuncay. "Isı Geri Kazanım Sistemleri."

Zemitis, Jurgis, Anatolijs Borodinecs, Aleksandrs Geikins, Targo Kalamees, and Kalle Kuusk. 2016. "Ventilation system design in three European geo cluster." *Energy Procedia* 96: 285-293.

Zender–Świercz, Ewa. 2020. "Improvement of indoor air quality by way of using decentralized ventilation." *Journal of Building Engineering* 32: 101663.

Zeng, Cheng, Shuli Liu, and Ashish Shukla. 2017. "A review on the air-to-air heat and mass exchanger technologies for building applications." *Renewable and Sustainable Energy Reviews* 75: 753-774.

Zhai, Zhiqiang. 2006. "Application of computational fluid dynamics in building design: aspects and trends." *Indoor and built environment* 15 (4): 305-313.

Zhang, Yi, Jonathan A Wright, and Vic I Hanby. 2006. "Energy aspects of HVAC system configurations—problem definition and test cases." *HVAC&R Research* 12 (S3): 871-888.

Zhukauskas, A. 1972. "Heat transfer from a single tubes and banks of tubes in crossflow." *Advances in Heat Transfer* 8: 843-865.

APPENDICES

APPENDIX A

THE AIR VELOCITY METER CALIBRATION RESULTS

TÜRKAK
TÜRK AKREDİTASYON KURUMU
TURKISH ACCREDITATION AGENCY
tarafından akredite edilmiş

AVL Kalibrasyon Laboratuvarı

İvedik O.S.B Dericiler Sit. 1385. Sok No: 10 Ostim / Ankara
T: +90 (312) 394 15 50 F: +90 (312) 394 15 53 E: bilgi@avl.com.tr

Kalibrasyon Sertifikası
Calibration Certificate

AB-0089-K

194735

10.19

Cihazın Sahibi / adresi:	İYTE MİMARLIK FAKÜLTESİ
Customer / Address:	İyte Mimarlık Fakültesi Dekanlığı Urla / İZMİR
İstek Numarası:	T-0919-073 / 1
Order No:	
Makina / Cihaz:	Hava Hızı Ölçer
Instrument / Device:	Anemometer
İmalatçı	BLİTZSENS
Manufacturer:	
Tip:	VS-C2-1-A
Type:	
Seri Numarası:	19100914522700
Serial Number:	
Kalibrasyon Tarihi:	11.10.2019
Date of Calibration:	
Sertifikanın Sayfa Sayısı:	4
Number of Pages:	

Bu kalibrasyon sertifikası, Uluslararası Birimler Sisteminde (SI) tanımlanmış birimleri realize eden ulusal ölçüm standartlarına izlenebilirliği belgeler.
This calibration certificate documents the traceability to national standards, which realize the unit of measurement according to the International System of Units (SI).

Kalibrasyon laboratuvarı olarak faaliyet gösteren AVL Kalibrasyon Laboratuvarı, TÜRKAK'tan AB-0089-K dosya numarası ile TS EN ISO/IEC 17025-2017 standardına göre akredite edilmiştir.
AVL Kalibrasyon Laboratuvarı is accredited by TÜRKAK under registration number AB-0089-K for TS EN ISO/IEC 17025-2017 as test laboratory.

Türk Akreditasyon Kurumu(TÜRKAK) deney raporlarının tanınması konusunda Avrupa Akreditasyon Birliği (EA) ve Uluslararası Laboratuvar Akreditasyon Birliği (ILAC) ile karşılıklı tanınma antlaşmasını imzalamıştır.
The Turkish Accreditation Agency (TURKAK) is signatory to the multilateral agreements of the European co-operation for the Accreditation(EA) and of the International Laboratory Accreditation (ILAC) for the Mutual recognation of test reports.

Ölçüm sonuçları, genişletilmiş ölçüm belirsizlikleri ve kalibrasyon metotları bu sertifikanın tamamlayıcı kısmı olan takip eden sayfalarda verilmiştir.
The measurements, the uncertainties with confidence probability and calibration methods are given on the following pages which are part of this certificate.

Mühür / Kaşe	Tarih	Kalibrasyon Personeli	Onaylayan
Seal	*Date*	*Calibrated by*	*Approval*
	11.10.2019	**Veli BAYDIR**	**Younes NEVAYESHİRAZİ**
		Dijital İmzalı	Dijital İmzalı

Bu sertifika 5070 sayılı kanununa göre güvenli elektronik imza ile imzalanmıştır. Belge teyidi için sayfalarda yer alan karekodu okutabilirsiniz.
This certificate is signed using secure digital signature according to article of law, number 5070. For confirmation, read the QR Code using QR Code reader.

SRT.LBBR.211

1. Cihaza Ait Bilgiler
Device to be Calibrated

Cihazın Adı : Hava Hızı Ölçer
Name of the Instrument   *Anemometer*

İmalatçısı : BLİTZSENS
Manufacturer

Model / Tipi : VS-C2-1-A
Model / Type

Seri Numarası : 19100914522700
Serial Number

Çözünürlüğü :
Resolution

2. Kalibrasyon Yeri ve ve Cihaz Kabulu
Calibration Place and Receipt of Device

Kalibrasyon Yeri : Laboratuvar   **Laboratuvar Kabul Tarihi** : 09.10.2019
Calibration Place   *Laboratory*   *Receipt Date of Device*

3. Kalibrasyon Metodu
Calibration Method

Kalibrasyon, hava hızının karşılaştırma metodu ile rüzgar tüneli içerisinde gerçekleştirilmiştir. Referans sensör ve test altındaki cihaz rüzgar tünelinin ölçüm alanına yerleştirilmiştir. Test altındaki cihazın ölçüm değeri ve genişletilmiş belirsizliği 5 ölçümün ortalaması alınarak hesaplanmıştır. Her ölçüm 30 saniyede bir kalibrasyon sistemi ile otomatik olarak alınmıştır. Kalibrasyon PR.LBBR.211 prosedürüne uygun olarak gerçekleştirilmiştir.

Calibration is performed according to comparison method of air velocity inside a wind tunnel. The reference sensor and test instrument is positioned inside the test section of tunnel. The expanded uncertainty of measurement and the average value of the test instrument is calculated by 5 measured data in series, in the interval of 30 seconds. Calibration is performed according to PR.LBBR.211 procedure.

4. Kalibrasyonda Kullanılan Referans Cihazlar
Reference Equipments Used During Calibration

Cihaz *Device*	İmalatçı *Manufacturer*	Seri No *Serial No*	Sertifika No *Certificate No*	İzlenebilirlik *Tracebility*
Sıcaklık ve Nem Ölçer	Extech	12081741	193712	AVL
Anemometre	TSI Instruments	67030043	4331	Westenberg
Dijital Multimetre	**Fluke**	**3352008**	**E1807373**	**Netes**

Kalibrasyon işlemi Westenberg Engineering marka eiffel tipi rüzgar tüneli kullanılarak gerçekleştirilmektedir.

Calibration is performed using an eiffel type wind tunnel manufactured by Westenberg Engineering.

222

AVL AKUSTİK VİBRASYON

KALİBRASYON LABORATUVARI

5. Çevresel Şartlar
Enviromental Conditions

Ölçüm Measurement	Sıcaklık Temperature	Bağıl Nem Relative Humidity	Basınç Pressure	Yoğunluk Density
	°C	%	mbar	kg / m^3
1	23,900	38,700	916,000	1,070
2	24,100	38,600	916,000	1,069
3	24,100	38,200	917,000	1,069
4	24,200	38,100	917,000	1,069
5	24,300	39,300	917,000	1,069

6. Kalibrasyon Sonuçları
Calibration Results

Ölçülen Akış Measured Flow		Ölçüm Belirsizliği Measurement Uncertainty	
Referans Cihaz Reference Instrument	Test Cihazı Test Instrument	Belirsizlik Uncertainty	Bağıl Relative
m/s	mA	± m/s	± %
0,196	6,625	0,018	8,946
0,397	10,263	0,012	2,938
0,591	13,047	0,011	1,857
0,789	15,613	0,011	1,351
0,988	19,009	0,010	1,029

SRT.LBBR.211

7. Uygunluk Beyanı

Statement of Complience

Ölçüm sonuçları ve ölçüm belirsizliği yukarıda verilmiştir. Kullanıcı bunları dikkate alarak uygunluğuna karar vermelidir. Beyan edilen genişletilmiş belirsizlik değeri standart belirsizliğin normal dağılımı için; yaklaşık % 95 güvenirlik seviyesini sağlayan k=2 kapsam faktörü ile çarpımının sonucudur. Standart ölçüm belirsizliği GUM ve EA-4/02 dokümanlarına uygun olarak belirlenmiştir. Ölçüm sonuçları, genişletilmiş ölçüm belirsizlikleri ve kalibrasyon metotları bu sertifikanın tamamlayıcı bir bölümüdür.

The measurement results and measurement uncertinity were given above. The user have to consider the results and decide compliance of the device. The reported expended uncertainity of measurement is stated as the standart uncertainity of multitude by coverage factor k=2, which for a normal distribution corresponds to covarage of approximately 95%. The standard measurement uncertainty is defined according to the GUM and EA-4/02 documents. Measurement results, the expanded measurement uncertainty of measurement and calibration methods, is an integral part of the this certificate.

8. Açıklamalar

Remarks

Bu sertifikada bulunan sonuçlar cihazın kalibrasyon tarihindeki durumu kapsar ve uzun dönem kararlığı hakkında bir öngörü içermez.

The result reported in this certificate refer to the condition of the instrument on the date of calibration and carry no implication regarding the long-term stability of the instrument.

APPENDIX B

THE FAN MANUFACTURER DOCUMENT/ FAN CHARACTERISTICS

Characteristics	
Schematics	
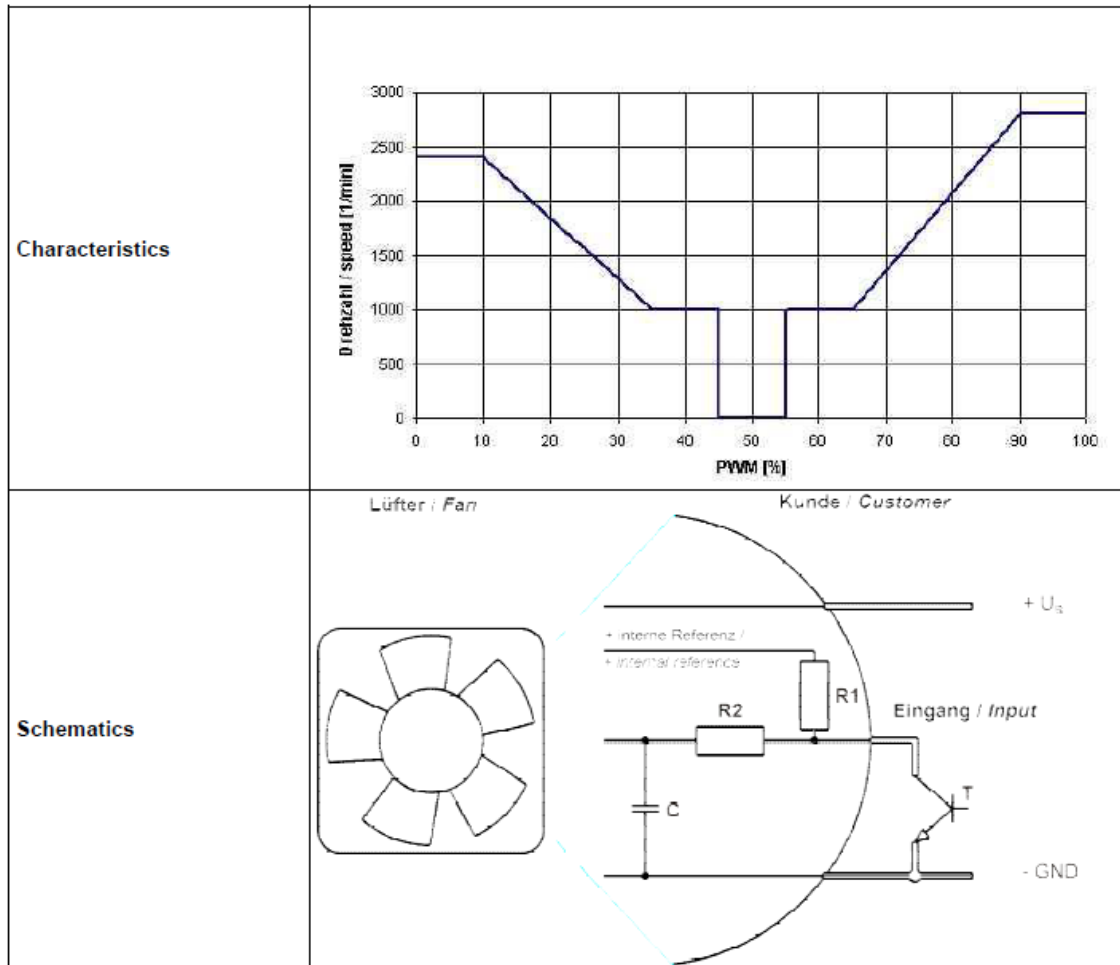
APPENDIX C

THE MULTICHANNEL DATALOGGER TEMPERATURE CALIBRATION RESULTS

APPENDIX C.1. 0-7°C Range

MMO KALMEM

Kalibrasyon Laboratuvarı ve Metroloji Eğitim Merkezi

Kalibrasyon Sertifikası

Calibration Certificate

TÜRKAK

Kalibrasyon
TS EN ISO/IEC 17025
AB-0070-K

AB-0070-K

19.SCK.0538

02.2019

Cihaz / Ekipman *Device / Equipment*	:	ÇOK KANALLI SICAKLIK KAYDEDİCİ *Multi Channel Temperature Logger*
Üretici Firma *Manufacturer*	:	HIOKI
Seri No *Serial No*	:	120611260
Tip / Model *Tip / Model*	:	LR8402-20 (K/T)
Talep Eden / Adresi *Issued For /Address*	:	**İzmir Yüksek Teknoloji Enstitüsü Proje Koordinasyon Uygulama ve Araştırma Merkezi** Gülbahçe Kampusu 35430 URLA İZMİR
Talep Numarası *Order no*	:	EK19000149/1
Kalibrasyon Tarihi *Date of Calibration*	:	15.02.2019
Sertifika Sayfa Sayısı *Page Number*	:	3

Bu kalibrasyon sertifikası, Uluslararası Birimler Sisteminde (SI) tanımlanmış birimleri realize eden ulusal ölçüm standartlarına izlenebilirliği belgeler. Kalibrasyon laboratuvarı olarak faaliyet gösteren MMO KALMEM, TÜRKAK'tan AB-0070-K ile TS EN ISO/IEC 17025:2012 standardına göre akredite edilmiştir. Türk Akreditasyon Kurumu(TÜRKAK) kalibrasyon sertifikalarının tanınırlığı konusunda Avrupa Akreditasyon Birliği(EA) ile Çok Taraflı Anlaşma ve Uluslararası Laboratuvar Akreditasyon Birliği(ILAC) ile karşılıklı tanıma anlaşması imzalamıştır. Ölçüm sonuçları, genişletilmiş ölçüm belirsizlikleri ve kalibrasyon metotları bu sertifikanın tamamlayıcı kısmı olan takip eden sayfalarda verilmiştir.

This calibration certificate documents the traceabilty to national standards, which realize the unit of measurement according to the International System of Units (SI). MMO KALMEM accredited by TÜRKAK under registration number AB-0070-K for TS EN ISO/IEC 17025:2012 as Calibration Laboratory. Turkish Accreditation Agency (TURKAK) is a signatory to the European co-operation for Accreditation (EA) Multilateral Agreement (MLA) and to the International Laboratory Accreditation Cooperation (ILAC) Mutual Recognition Arrangement (MRA) for the recognition of calibration certificates. The measurements, the uncertainties with confidence probability and calibration methods are given on the following pages which are partof this certificate.

Mühür *Seal*	**Tarih** *Date of Issue*	**Kalibrasyonu Yapan** *Calibrated by*	**Laboratuvar Müdürü** *Head of the Calibration Laboratory*
MMO KALMEM	18.02.2019 11:32:52	GÜVEN KAÇAR	ALPER TORTOÇ
		Dijital olarak imzalayan: GÜVEN KAÇAR	Dijital olarak imzalayan: ALPER TORTOÇ

EKC.05.12 18.07.2016 Rev:00

226

MMO KALMEM
Sanayinin Hizmetinde

Sayfa No: 2/3

Page Number

1. Kalibrasyonda Kullanılan Referans:

Cihaz / Ekipman	Üretici	Seri No	İzlenebilirlik
Sıcaklık Sensörü Pt100	ISOTECH	EK 05.02	MMO KALMEM
Sıcaklık Kalibratörü	Beamex	EK.03.01	MMO KALMEM
Sıvı Banyo	UMS	EK 05.11	MMO KALMEM
Termometre	-	EK 05.24	MMO KALMEM

2. Kalibre Edilen Cihazın Özellikleri:

Cihazın Adı	Ölçüm Aralığı	Çözünürlük	Okunabilirlik
Dijital Göstergeli Sıcaklık Ölçer	0 ... 7 °C	0,01 °C	0,01 °C

3. Ortam Şartları :

Sıcaklık: (23 ± 3) °C   Bağıl Nem   : % (45 ± 15)

4. Kalibrasyon Yöntemi ve Prosedü

Cihazın kalibrasyonu *EURAMET* kalibrasyon dokümanlarına uygun olarak KALMEM tarafından hazırlanmış olan EKT 05.03 No'lu talimata göre gerçekleştirilmiştir. Kalibrasyon kararlı sıcaklık ortamında, referans cihazdan ölçülen sıcaklık değerleri ile cihazın gösterge değerlerinin karşılaştırılması yöntemi ile gerçekleştirilmiştir.

5. Kalibrasyon Belirsizliği

Ölçüm belirsizlikleri sonuç tablosunda verilmiştir. Beyan edilen genişletilmiş belirsizlik değeri, standart belirsizliğin normal dağılım için yaklaşık %95 güvenilirlik seviyesini sağlayan k=2 kapsam faktörü ile çarpımının sonucudur. Standart ölçüm belirsizliği GUM ve EA-4/02 dokümanlarına uygun olarak hesaplanmıştır. Ölçüm belirsizliği uzun zaman kararlılığını kapsamamaktadır.

6. Fonksiyon ve Göz Kontrolü

Fonksiyon ve göz kontrolünde hasar veya eksiklik görülmemiştir.

8. Açıklamalar

Kalibrasyon sonuçları sadece yukarıda belirtilen cihaza ait olup, kalibrasyon tarihinden itibaren ve sertifikada verilmiş olan şartlarda geçerlidir. Cihazın uygun aralıklarla kalibrasyonunun gerçekleşmesinden kullanıcı sorumludur.

9. Kalibrasyon Etiketinin Yeri

Kalibrasyon etiketi cihazın ön tarafına yapıştırılmıştır.

EKC.05.12   18.07.2016   Rev:00

A_ 251 sok. no: 33 d: 1-2 Manavkuyu Bayraklı İZMİR T_ (0232) 348 40 50 F_ (0232) 348 63 98 W_ www.kalmem.org | kalmem@mmo.org.tr

227

7. Kalibrasyon Sonuçları

Yapılan ölçümlerin sonucunda aşağıdaki değerler elde edilmiştir.

Ölçüm Bölgesi	Referans °C	Ölçülen °C	Sapma °C	Belirsizlik °C	Ölçüm Bölgesi	Referans °C	Ölçülen °C	Sapma °C	Belirsizlik °C
UNIT-1 -1	0,00	0,03	0,03	0,035	UNIT-1 -1	7,00	6,94	-0,06	0,070
UNIT-1 -2	0,00	0,16	0,16	0,035	UNIT-1 -2	7,00	7,00	0,00	0,070
UNIT-1 -3	0,00	0,18	0,18	0,035	UNIT-1 -3	7,00	7,07	0,07	0,070
UNIT-1 -4	0,00	0,11	0,11	0,035	UNIT-1 -4	7,00	6,99	-0,01	0,070
UNIT-1 -5	0,00	0,02	0,02	0,035	UNIT-1 -5	7,00	6,90	-0,10	0,070
UNIT-1 -6	0,00	0,02	0,02	0,035	UNIT-1 -6	7,00	6,90	-0,10	0,070
UNIT-1 -7	0,00	0,12	0,12	0,035	UNIT-1 -7	7,00	6,75	-0,25	0,070
UNIT-1 -8	0,00	-0,13	-0,13	0,035	UNIT-1 -8	7,00	6,78	-0,22	0,070
UNIT-1 -9	0,00	-0,16	-0,16	0,035	UNIT-1 -9	7,00	6,72	-0,28	0,070
UNIT-1 -10	0,00	-0,10	-0,10	0,035	UNIT-1 -10	7,00	6,76	-0,24	0,070
UNIT-2 -1	0,00	0,10	0,10	0,035	UNIT-2 -1	7,00	7,10	0,10	0,070
UNIT-2 -2	0,00	0,09	0,09	0,035	UNIT-2 -2	7,00	7,15	0,15	0,070
UNIT-2 -3	0,00	0,08	0,08	0,035	UNIT-2 -3	7,00	7,05	0,05	0,070
UNIT-2 -4	0,00	0,07	0,07	0,035	UNIT-2 -4	7,00	7,05	0,05	0,070
UNIT-2 -5	0,00	0,08	0,08	0,035	UNIT-2 -5	7,00	7,09	0,09	0,070
UNIT-2 -6	0,00	-0,05	-0,05	0,035	UNIT-2 -6	7,00	6,90	-0,10	0,070
UNIT-2 -7	0,00	-0,13	-0,13	0,035	UNIT-2 -7	7,00	6,95	-0,05	0,070
UNIT-2 -8	0,00	-0,08	-0,08	0,035	UNIT-2 -8	7,00	6,93	-0,07	0,070
UNIT-2 -9	0,00	-0,09	-0,09	0,035	UNIT-2 -9	7,00	6,91	-0,09	0,070
UNIT-2 -10	0,00	-0,02	-0,02	0,035	UNIT-2 -10	7,00	7,03	0,03	0,070
UNIT-2 -11	0,00	0,00	0,00	0,035	UNIT-2 -11	7,00	7,00	0,00	0,070
UNIT-2 -12	0,00	0,00	0,00	0,035	UNIT-2 -12	7,00	7,04	0,04	0,070
UNIT-2 -13	0,00	0,06	0,06	0,035	UNIT-2 -13	7,00	7,10	0,10	0,070
UNIT-2 -14	0,00	-0,04	-0,04	0,035	UNIT-2 -14	7,00	6,95	-0,05	0,070
UNIT-2 -15	0,00	-0,02	-0,02	0,035	UNIT-2 -15	7,00	7,00	0,00	0,070
UNIT-4 -1	0,00	0,20	0,20	0,035	UNIT-4 -1	7,00	7,09	0,09	0,070
UNIT-4 -2	0,00	0,15	0,15	0,035	UNIT-4 -2	7,00	7,15	0,15	0,070
UNIT-4 -3	0,00	0,22	0,22	0,035	UNIT-4 -3	7,00	7,13	0,13	0,070
UNIT-4 -4	0,00	0,21	0,21	0,035	UNIT-4 -4	7,00	7,22	0,22	0,070
UNIT-4 -5	0,00	0,21	0,21	0,035	UNIT-4 -5	7,00	7,16	0,16	0,070
UNIT-4 -6	0,00	0,18	0,18	0,035	UNIT-4 -6	7,00	7,14	0,14	0,070
UNIT-4 -7	0,00	0,18	0,18	0,035	UNIT-4 -7	7,00	7,15	0,15	0,070
UNIT-4 -8	0,00	0,18	0,18	0,035	UNIT-4 -8	7,00	7,08	0,08	0,070
UNIT-4 -9	0,00	0,19	0,19	0,035	UNIT-4 -9	7,00	7,18	0,18	0,070
UNIT-4 -10	0,00	0,28	0,28	0,035	UNIT-4 -10	7,00	7,12	0,12	0,070
UNIT-4 -11	0,00	0,27	0,27	0,035	UNIT-4 -11	7,00	7,15	0,15	0,070
UNIT-4 -12	0,00	0,25	0,25	0,035	UNIT-4 -12	7,00	7,18	0,18	0,070
UNIT-4 -13	0,00	0,30	0,30	0,035	UNIT-4 -13	7,00	7,13	0,13	0,070
UNIT-4 -14	0,00	0,30	0,30	0,035	UNIT-4 -14	7,00	7,19	0,19	0,070
UNIT-4 -15	0,00	0,36	0,36	0,035	UNIT-4 -15	7,00	7,16	0,16	0,070

Rev:00

18.07.2016

EKC.05.12

Kalibrasyon başında ve sonunda alınan   0,00 °C

değerleri arasındaki fark histeresiz hatası olarak belirsizliğe eklenmiştir.

A_ 251 sok. no: 33 d: 1-2 Manavkuyu Bayraklı İZMİR **T_** (0232) 348 40 50 **F_** (0232) 348 63 98 **W_** www.kalmem.org | kalmem@mmo.org.tr

228

APPENDIX C.2. 14-21°C Range

MMO KALMEM

Kalibrasyon Laboratuvarı ve Metroloji Eğitim Merkezi

Kalibrasyon Sertifikası

Calibration Certificate

AB-0070-K

19.SCK.0539

02.2019

Cihaz / Ekipman *Device / Equipment*	:	ÇOK KANALLI SICAKLIK KAYDEDİCİ *Multi Channel Temperature Logger*
Üretici Firma *Manufacturer*	:	HIOKI
Seri No *Serial No*	:	120611260
Tip / Model *Tip / Model*	:	LR8402-20 (K/T)
Talep Eden / Adresi *Issued For /Address*	:	**İzmir Yüksek Teknoloji Enstitüsü Proje Koordinasyon Uygulama ve Araştırma Merkezi** Gülbahçe Kampusu 35430 URLA İZMİR
Talep Numarası *Order no*	:	EK19000149/2
Kalibrasyon Tarihi *Date of Calibration*	:	15.02.2019
Sertifika Sayfa Sayısı *Page Number*	:	3

Bu kalibrasyon sertifikası, Uluslararası Birimler Sisteminde (SI) tanımlanmış birimleri realize eden ulusal ölçüm standartlarına izlenebilirliği belgeler. Kalibrasyon laboratuvarı olarak faaliyet gösteren MMO KALMEM, TÜRKAK'tan AB-0070-K ile TS EN ISO/IEC 17025:2012 standardına göre akredite edilmiştir. Türk Akreditasyon Kurumu(TÜRKAK) kalibrasyon sertifikalarının tanınırlığı konusunda Avrupa Akreditasyon Birliği(EA) ile Çok Taraflı Anlaşma ve Uluslararası Laboratuvar Akreditasyon Birliği(ILAC) ile karşılıklı tanıma anlaşması imzalamıştır. Ölçüm sonuçları, genişletilmiş ölçüm belirsizlikleri ve kalibrasyon metotları bu sertifikanın tamamlayıcı kısmı olan takip eden sayfalarda verilmiştir.

This calibration certificate documents the traceabilty to national standards, which realize the unit of measurement according to the International System of Units (SI). MMO KALMEM accredited by TÜRKAK under registration number AB-0070-K for TS EN ISO/IEC 17025:2012 as Calibration Laboratory. Turkish Accreditation Agency (TURKAK) is a signatory to the European co-operation for Accreditation (EA) Multilateral Agreement (MLA) and to the International Laboratory Accreditation Cooperation (ILAC) Mutual Recognition Arrangement (MRA) for the recognition of calibration certificates. The measurements, the uncertainties with confidence probability and calibration methods are given on the following pages which are partof this certificate.

Mühür *Seal*	**Tarih** *Date of Issue*	**Kalibrasyonu Yapan** *Calibrated by*	**Laboratuvar Müdürü** *Head of the Calibration Laboratory*
	18.02.2019 11:32:52	GÜVEN KAÇAR Dijital olarak imzalayan: GÜVEN KAÇAR	ALPER TORTOÇ Dijital olarak imzalayan: ALPER TORTOÇ

EKC.05.12 18.07.2016 Rev:00

243 Sok. No:17 D:6 Manavkuyu-Bayraklı / İZMİR - Turkey   (0232) 348 40 50   (0232) 348 63 98   www.kalmem.org   kalmem@mmo.org.tr

Sayfa No: 2/3
Page Number

1. Kalibrasyonda Kullanılan Referans:

Cihaz / Ekipman	Üretici	Seri No	İzlenebilirlik
Sıcaklık Sensörü Pt100-2	KMP	EK 05.39	AB 0059-K
Sıcaklık Kalibratörü	Beamex	EK.03.01	MMO KALMEM
Sıvı Banyo	UMS	EK 05.11	MMO KALMEM
Termometre	-	EK 05.24	MMO KALMEM

2. Kalibre Edilen Cihazın Özellikleri:

Cihazın Adı	Ölçüm Aralığı	Çözünürlük	Okunabilirlik
Dijital Göstergeli Sıcaklık Ölçer	14 ... 21 °C	0,01 °C	0,01 °C

3. Ortam Şartları :

Sıcaklık: (23 ± 3) °C   Bağıl Nem   : % (45 ± 15)

4. Kalibrasyon Yöntemi ve Prosedü

Cihazın kalibrasyonu *EURAMET* kalibrasyon dokümanlarına uygun olarak KALMEM tarafından hazırlanmış olan EKT 05.03 No'lu talimata göre gerçekleştirilmiştir. Kalibrasyon kararlı sıcaklık ortamında, referans cihazdan ölçülen sıcaklık değerleri ile cihazın gösterge değerlerinin karşılaştırılması yöntemi ile gerçekleştirilmiştir.

5. Kalibrasyon Belirsizliği

Ölçüm belirsizlikleri sonuç tablosunda verilmiştir. Beyan edilen genişletilmiş belirsizlik değeri, standart belirsizliğin normal dağılım için yaklaşık %95 güvenilirlik seviyesini sağlayan k=2 kapsam faktörü ile çarpımının sonucudur. Standart ölçüm belirsizliği GUM ve EA-4/02 dokümanlarına uygun olarak hesaplanmıştır. Ölçüm belirsizliği uzun zaman kararlılığını kapsamamaktadır.

6. Fonksiyon ve Göz Kontrolü

Fonksiyon ve göz kontrolünde hasar veya eksiklik görülmemiştir.

8. Açıklamalar

Kalibrasyon sonuçları sadece yukarıda belirtilen cihaza ait olup, kalibrasyon tarihinden itibaren ve sertifikada verilmiş olan şartlarda geçerlidir. Cihazın uygun aralıklarla kalibrasyonunun gerçekleşmesinden kullanıcı sorumludur.

9. Kalibrasyon Etiketinin Yeri

Kalibrasyon etiketi cihazın ön tarafına yapıştırılmıştır.

EKC.05.12   18.07.2016   Rev:00

A_ 251 sok. no: 33 d: 1-2 Manavkuyu Bayraklı İZMİR T_ (0232) 348 40 50 F_ (0232) 348 63 98 W_ www.kalmem.org | kalmem@mmo.org.tr

230

Sayfa No: 3/3

Page Number

7. Kalibrasyon Sonuçları

Yapılan ölçümlerin sonucunda aşağıdaki değerler elde edilmiştir.

Ölçüm Bölgesi	Referans °C	Ölçülen °C	Sapma °C	Belirsizlik °C	Ölçüm Bölgesi	Referans °C	Ölçülen °C	Sapma °C	Belirsizlik °C
UNIT-1 -1	14,00	14,10	0,10	0,070	UNIT-1 -1	21,00	21,15	0,15	0,115
UNIT-1 -2	14,00	14,10	0,10	0,070	UNIT-1 -2	21,00	21,13	0,13	0,115
UNIT-1 -3	14,00	14,21	0,21	0,070	UNIT-1 -3	21,00	21,20	0,20	0,115
UNIT-1 -4	14,00	14,19	0,19	0,070	UNIT-1 -4	21,00	21,07	0,07	0,115
UNIT-1 -5	14,00	14,07	0,07	0,070	UNIT-1 -5	21,00	21,01	0,01	0,115
UNIT-1 -6	14,00	14,07	0,07	0,070	UNIT-1 -6	21,00	21,90	0,90	0,115
UNIT-1 -7	14,00	13,96	-0,04	0,070	UNIT-1 -7	21,00	20,82	-0,18	0,115
UNIT-1 -8	14,00	13,97	-0,03	0,070	UNIT-1 -8	21,00	20,80	-0,20	0,115
UNIT-1 -9	14,00	13,96	-0,04	0,070	UNIT-1 -9	21,00	20,74	-0,26	0,115
UNIT-1 -10	14,00	13,95	-0,05	0,070	UNIT-1 -10	21,00	20,76	-0,24	0,115
UNIT-2 -1	14,00	14,13	0,13	0,070	UNIT-2 -1	21,00	21,08	0,08	0,115
UNIT-2 -2	14,00	14,15	0,15	0,070	UNIT-2 -2	21,00	21,01	0,01	0,115
UNIT-2 -3	14,00	14,14	0,14	0,070	UNIT-2 -3	21,00	20,93	-0,07	0,115
UNIT-2 -4	14,00	14,13	0,13	0,070	UNIT-2 -4	21,00	21,01	0,01	0,115
UNIT-2 -5	14,00	14,21	0,21	0,070	UNIT-2 -5	21,00	21,00	0,00	0,115
UNIT-2 -6	14,00	14,01	0,01	0,070	UNIT-2 -6	21,00	20,93	-0,07	0,115
UNIT-2 -7	14,00	14,04	0,04	0,070	UNIT-2 -7	21,00	20,90	-0,10	0,115
UNIT-2 -8	14,00	13,99	-0,01	0,070	UNIT-2 -8	21,00	20,85	-0,15	0,115
UNIT-2 -9	14,00	14,07	0,07	0,070	UNIT-2 -9	21,00	20,92	-0,08	0,115
UNIT-2 -10	14,00	14,09	0,09	0,070	UNIT-2 -10	21,00	20,93	-0,07	0,115
UNIT-2 -11	14,00	14,12	0,12	0,070	UNIT-2 -11	21,00	21,01	0,01	0,115
UNIT-2 -12	14,00	14,16	0,16	0,070	UNIT-2 -12	21,00	21,00	0,00	0,115
UNIT-2 -13	14,00	14,14	0,14	0,070	UNIT-2 -13	21,00	21,06	0,06	0,115
UNIT-2 -14	14,00	14,18	0,18	0,070	UNIT-2 -14	21,00	21,00	0,00	0,115
UNIT-2 -15	14,00	14,12	0,12	0,070	UNIT-2 -15	21,00	21,08	0,08	0,115
UNIT-4 -1	14,00	14,26	0,26	0,070	UNIT-4 -1	21,00	21,17	0,17	0,115
UNIT-4 -2	14,00	14,17	0,17	0,070	UNIT-4 -2	21,00	21,11	0,11	0,115
UNIT-4 -3	14,00	14,24	0,24	0,070	UNIT-4 -3	21,00	21,10	0,10	0,115
UNIT-4 -4	14,00	14,21	0,21	0,070	UNIT-4 -4	21,00	21,14	0,14	0,115
UNIT-4 -5	14,00	14,19	0,19	0,070	UNIT-4 -5	21,00	21,09	0,09	0,115
UNIT-4 -6	14,00	14,25	0,25	0,070	UNIT-4 -6	21,00	21,12	0,12	0,115
UNIT-4 -7	14,00	14,15	0,15	0,070	UNIT-4 -7	21,00	21,03	0,03	0,115
UNIT-4 -8	14,00	14,29	0,29	0,070	UNIT-4 -8	21,00	21,08	0,08	02,115
UNIT-4 -9	14,00	14,31	0,31	0,070	UNIT-4 -9	21,00	21,08	0,08	0,115
UNIT-4 -10	14,00	14,30	0,30	0,070	UNIT-4 -10	21,00	21,12	0,12	0,115
UNIT-4 -11	14,00	14,34	0,34	0,070	UNIT-4 -11	21,00	21,15	0,15	0,115
UNIT-4 -12	14,00	14,26	0,26	0,070	UNIT-4 -12	21,00	21,08	0,08	0,115
UNIT-4 -13	14,00	14,32	0,32	0,070	UNIT-4 -13	21,00	21,17	0,17	0,115
UNIT-4 -14	14,00	14,36	0,36	0,070	UNIT-4 -14	21,00	21,15	0,15	0,115
UNIT-4 -15	14,00	14,30	0,30	0,070	UNIT-4 -15	21,00	21,27	0,27	0,115

Rev:00

18.07.2016

EKC.05.12

Kalibrasyon başında ve sonunda alınan   14,00 °C

değerleri arasındaki fark histeresiz hatası olarak belirsizliğe eklenmiştir.

APPENDIX C.3. 28-35°C Range

MMO KALMEM

Kalibrasyon Laboratuvarı ve Metroloji Eğitim Merkezi

Kalibrasyon Sertifikası

Calibration Certificate

AB-0070-K

19.SCK.0540

02.2019

Cihaz / Ekipman *Device / Equipment*	:	ÇOK KANALLI SICAKLIK KAYDEDİCİ *Multi Channel Temperature Logger*
Üretici Firma *Manufacturer*	:	HIOKI
Seri No *Serial No*	:	120611260
Tip / Model *Tip / Model*	:	LR8402-20 (K/T)
Talep Eden / Adresi *Issued For /Address*	:	**İzmir Yüksek Teknoloji Enstitüsü Proje Koordinasyon Uygulama ve Araştırma Merkezi** Gülbahçe Kampusu 35430 URLA İZMİR
Talep Numarası *Order no*	:	EK19000149/3
Kalibrasyon Tarihi *Date of Calibration*	:	15.02.2019
Sertifika Sayfa Sayısı *Page Number*	:	3

Bu kalibrasyon sertifikası, Uluslararası Birimler Sisteminde (SI) tanımlanmış birimleri realize eden ulusal ölçüm standartlarına izlenebilirliği belgeler. Kalibrasyon laboratuvarı olarak faaliyet gösteren MMO KALMEM, TÜRKAK'tan AB-0070-K ile TS EN ISO/IEC 17025:2012 standardına göre akredite edilmiştir. Türk Akreditasyon Kurumu(TÜRKAK) kalibrasyon sertifikalarının tanınırlığı konusunda Avrupa Akreditasyon Birliği(EA) ile Çok Taraflı Anlaşma ve Uluslararası Laboratuvar Akreditasyon Birliği(ILAC) ile karşılıklı tanıma anlaşması imzalamıştır. Ölçüm sonuçları, genişletilmiş ölçüm belirsizlikleri ve kalibrasyon metotları bu sertifikanın tamamlayıcı kısmı olan takip eden sayfalarda verilmiştir.

This calibration certificate documents the traceabilty to national standards, which realize the unit of measurement according to the International System of Units (SI). MMO KALMEM accredited by TÜRKAK under registration number AB-0070-K for TS EN ISO/IEC 17025:2012 as Calibration Laboratory. Turkish Accreditation Agency (TURKAK) is a signatory to the European co-operation for Accreditation (EA) Multilateral Agreement (MLA) and to the International Laboratory Accreditation Cooperation (ILAC) Mutual Recognition Arrangement (MRA) for the recognition of calibration certificates. The measurements, the uncertainties with confidence probability and calibration methods are given on the following pages which are partof this certificate.

Mühür *Seal*	**Tarih** *Date of Issue*	**Kalibrasyonu Yapan** *Calibrated by*	**Laboratuvar Müdürü** *Head of the Calibration Laboratory*
	18.02.2019 11:32:52	GÜVEN KAÇAR Dijital olarak imzalayan: GÜVEN KAÇAR	ALPER TORTOÇ Dijital olarak imzalayan: ALPER TORTOÇ

EKC.05.12 18.07.2016 Rev:00

Bu sertifika MMO KALMEM'in yazılı izni olmadan kısmen çoğaltılıp kopyalanamaz. İmzasız ve mühürsüz sertifikalar geçersizdir.

This certificate shall not be reproduced other than in full except with the full permission of MMO KALMEM Calibration certificate without signature and seal are not valid.

243 Sok. No:17 D:6 Manavkuyu-Bayraklı / İZMİR - Turkey   (0232) 348 40 50   (0232) 348 63 98   www.kalmem.org   kalmem@mmo.org.tr

MMO KALMEM
Sanayinin Hizmetinde

1. Kalibrasyonda Kullanılan Referans:

Cihaz / Ekipman	Üretici	Seri No	İzlenebilirlik
Sıcaklık Sensörü Pt100-2	KMP	EK 05.39	AB 0059-K
Sıcaklık Kalibratörü	Beamex	EK.03.01	MMO KALMEM
Sıvı Banyo	UMS	EK 05.11	MMO KALMEM
Termometre	-	EK 05.24	MMO KALMEM

2. Kalibre Edilen Cihazın Özellikleri:

Cihazın Adı	Ölçüm Aralığı	Çözünürlük	Okunabilirlik
Dijital Göstergeli Sıcaklık Ölçer	28 ... 35 °C	0,01 °C	0,01 °C

3. Ortam Şartları :

Sıcaklık: (23 ± 3) °C   Bağıl Nem   : % (45 ± 15)

4. Kalibrasyon Yöntemi ve Prosedü

Cihazın kalibrasyonu *EURAMET* kalibrasyon dokümanlarına uygun olarak KALMEM tarafından hazırlanmış olan EKT 05.03 No'lu talimata göre gerçekleştirilmiştir. Kalibrasyon kararlı sıcaklık ortamında, referans cihazdan ölçülen sıcaklık değerleri ile cihazın gösterge değerlerinin karşılaştırılması yöntemi ile gerçekleştirilmiştir.

5. Kalibrasyon Belirsizliği

Ölçüm belirsizlikleri sonuç tablosunda verilmiştir. Beyan edilen genişletilmiş belirsizlik değeri, standart belirsizliğin normal dağılım için yaklaşık %95 güvenilirlik seviyesini sağlayan k=2 kapsam faktörü ile çarpımının sonucudur. Standart ölçüm belirsizliği GUM ve EA-4/02 dokümanlarına uygun olarak hesaplanmıştır. Ölçüm belirsizliği uzun zaman kararlılığını kapsamamaktadır.

6. Fonksiyon ve Göz Kontrolü

Fonksiyon ve göz kontrolünde hasar veya eksiklik görülmemiştir.

8. Açıklamalar

Kalibrasyon sonuçları sadece yukarıda belirtilen cihaza ait olup, kalibrasyon tarihinden itibaren ve sertifikada verilmiş olan şartlarda geçerlidir. Cihazın uygun aralıklarla kalibrasyonunun gerçekleşmesinden kullanıcı sorumludur.

9. Kalibrasyon Etiketinin Yeri

Kalibrasyon etiketi cihazın ön tarafına yapıştırılmıştır.

EKC.05.12   18.07.2016   Rev:00

MMO KALMEM
Sanayinin Hizmetinde

Sayfa No: 3/3

Page Number

7. Kalibrasyon Sonuçları

Yapılan ölçümlerin sonucunda aşağıdaki değerler elde edilmiştir.

Ölçüm Bölgesi	Referans °C	Ölçülen °C	Sapma °C	Belirsizlik °C	Ölçüm Bölgesi	Referans °C	Ölçülen °C	Sapma °C	Belirsizlik °C
UNIT-1 -1	28,00	27,97	-0,03	0,115	UNIT-1 -1	35,00	35,14	0,14	0,138
UNIT-1 -2	28,00	28,00	0,00	0,115	UNIT-1 -2	35,00	35,14	0,14	0,138
UNIT-1 -3	28,00	28,05	0,05	0,115	UNIT-1 -3	35,00	35,24	0,24	0,138
UNIT-1 -4	28,00	28,03	0,03	0,115	UNIT-1 -4	35,00	35,18	0,18	0,138
UNIT-1 -5	28,00	27,94	-0,06	0,115	UNIT-1 -5	35,00	35,06	0,06	0,138
UNIT-1 -6	28,00	27,87	-0,13	0,115	UNIT-1 -6	35,00	35,04	0,04	0,138
UNIT-1 -7	28,00	27,89	-0,11	0,115	UNIT-1 -7	35,00	34,94	-0,06	0,138
UNIT-1 -8	28,00	27,91	-0,09	0,115	UNIT-1 -8	35,00	35,00	0,00	0,138
UNIT-1 -9	28,00	27,93	-0,07	0,115	UNIT-1 -9	35,00	34,97	-0,03	0,138
UNIT-1 -10	28,00	28,00	0,00	0,115	UNIT-1 -10	35,00	35,03	0,03	0,138
UNIT-2 -1	28,00	28,04	0,04	0,115	UNIT-2 -1	35,00	35,20	0,20	0,138
UNIT-2 -2	28,00	28,00	0,00	0,115	UNIT-2 -2	35,00	35,20	0,20	0,138
UNIT-2 -3	28,00	28,05	0,05	0,115	UNIT-2 -3	35,00	35,16	0,16	0,138
UNIT-2 -4	28,00	28,02	0,02	0,115	UNIT-2 -4	35,00	35,18	0,18	0,138
UNIT-2 -5	28,00	28,03	0,03	0,115	UNIT-2 -5	35,00	35,18	0,18	0,138
UNIT-2 -6	28,00	28,11	0,11	0,115	UNIT-2 -6	35,00	35,20	0,20	0,138
UNIT-2 -7	28,00	27,96	-0,04	0,115	UNIT-2 -7	35,00	35,13	0,13	0,138
UNIT-2 -8	28,00	28,00	0,00	0,115	UNIT-2 -8	35,00	35,19	0,19	0,138
UNIT-2 -9	28,00	28,03	0,03	0,115	UNIT-2 -9	35,00	35,19	0,19	0,138
UNIT-2 -10	28,00	28,10	0,10	0,115	UNIT-2 -10	35,00	35,27	0,27	0,138
UNIT-2 -11	28,00	28,13	0,13	0,115	UNIT-2 -11	35,00	35,25	0,25	0,138
UNIT-2 -12	28,00	28,04	0,04	0,115	UNIT-2 -12	35,00	35,29	0,29	0,138
UNIT-2 -13	28,00	28,15	0,15	0,115	UNIT-2 -13	35,00	35,29	0,29	0,138
UNIT-2 -14	28,00	28,05	0,05	0,115	UNIT-2 -14	35,00	35,28	0,28	0,138
UNIT-2 -15	28,00	28,06	0,06	0,115	UNIT-2 -15	35,00	35,33	0,33	0,138
UNIT-4 -1	28,00	28,25	0,25	0,115	UNIT-4 -1	35,00	35,15	0,15	0,138
UNIT-4 -2	28,00	28,22	0,22	0,115	UNIT-4 -2	35,00	35,13	0,13	0,138
UNIT-4 -3	28,00	28,24	0,24	0,115	UNIT-4 -3	35,00	35,12	0,12	0,138
UNIT-4 -4	28,00	28,18	0,18	0,115	UNIT-4 -4	35,00	35,01	0,01	0,138
UNIT-4 -5	28,00	28,24	0,24	0,115	UNIT-4 -5	35,00	35,07	0,07	0,138
UNIT-4 -6	28,00	28,18	0,18	0,115	UNIT-4 -6	35,00	35,06	0,06	0,138
UNIT-4 -7	28,00	28,24	0,24	0,115	UNIT-4 -7	35,00	35,01	0,01	0,138
UNIT-4 -8	28,00	28,15	0,15	0,115	UNIT-4 -8	35,00	35,10	0,10	02.138
UNIT-4 -9	28,00	28,25	0,25	0,115	UNIT-4 -9	35,00	35,15	0,15	0,138
UNIT-4 -10	28,00	28,22	0,22	0,115	UNIT-4 -10	35,00	35,10	0,10	0,138
UNIT-4 -11	28,00	28,25	0,25	0,115	UNIT-4 -11	35,00	35,15	0,15	0,138
UNIT-4 -12	28,00	28,25	0,25	0,115	UNIT-4 -12	35,00	35,12	0,12	0,138
UNIT-4 -13	28,00	28,23	0,23	0,115	UNIT-4 -13	35,00	35,14	0,14	0,138
UNIT-4 -14	28,00	28,32	0,32	0,115	UNIT-4 -14	35,00	35,10	0,10	0,138
UNIT-4 -15	28,00	28,25	0,25	0,115	UNIT-4 -15	35,00	35,20	0,20	0,138

Kalibrasyon başında ve sonunda alınan   28,00 °C

değerleri arasındaki fark histeresiz hatası olarak belirsizliğe eklenmiştir.

Rev:00
18.07.2016
EKC.05.12

A_ 251 sok. no: 33 d: 1-2 Manavkuyu Bayraklı İZMİR T_ (0232) 348 40 50 F_ (0232) 348 63 98 W_ www.kalmem.org | kalmem@mmo.org.tr

234

APPENDIX C.4. 42°C

MMO KALMEM
Kalibrasyon Laboratuvarı ve Metroloji Eğitim Merkezi
Kalibrasyon Sertifikası
Calibration Certificate

AB-0070-K

19.SCK.0541

02.2019

Cihaz / Ekipman *Device / Equipment*	:	ÇOK KANALLI SICAKLIK KAYDEDİCİ *Multi Channel Temperature Logger*
Üretici Firma *Manufacturer*	:	HIOKI
Seri No *Serial No*	:	120611260
Tip / Model *Tip / Model*	:	LR8402-20 (J/T)
Talep Eden / Adresi *Issued For /Address*	:	**İzmir Yüksek Teknoloji Enstitüsü Proje Koordinasyon Uygulama ve Araştırma Merkezi** Gülbahçe Kampusu 35430 URLA İZMİR
Talep Numarası *Order no*	:	EK19000149/4
Kalibrasyon Tarihi *Date of Calibration*	:	15.02.2019
Sertifika Sayfa Sayısı *Page Number*	:	3

Bu kalibrasyon sertifikası, Uluslararası Birimler Sisteminde (SI) tanımlanmış birimleri realize eden ulusal ölçüm standartlarına izlenebilirliği belgeler. Kalibrasyon laboratuvarı olarak faaliyet gösteren MMO KALMEM, TÜRKAK'tan AB-0070-K ile TS EN ISO/IEC 17025:2012 standardına göre akredite edilmiştir. Türk Akreditasyon Kurumu(TÜRKAK) kalibrasyon sertifikalarının tanınırlığı konusunda Avrupa Akreditasyon Birliği(EA) ile Çok Taraflı Anlaşma ve Uluslararası Laboratuvar Akreditasyon Birliği(ILAC) ile karşılıklı tanıma anlaşması imzalamıştır. Ölçüm sonuçları, genişletilmiş ölçüm belirsizlikleri ve kalibrasyon metotları bu sertifikanın tamamlayıcı kısmı olan takip eden sayfalarda verilmiştir.

This calibration certificate documents the traceabilty to national standards, which realize the unit of measurement according to the International System of Units (SI). MMO KALMEM accredited by TÜRKAK under registration number AB-0070-K for TS EN ISO/IEC 17025:2012 as Calibration Laboratory. Turkish Accreditation Agency (TURKAK) is a signatory to the European co-operation for Accreditation (EA) Multilateral Agreement (MLA) and to the International Laboratory Accreditation Cooperation (ILAC) Mutual Recognition Arrangement (MRA) for the recognition of calibration certificates. The measurements, the uncertainties with confidence probability and calibration methods are given on the following pages which are partof this certificate.

Mühür *Seal*	**Tarih** *Date of Issue*	**Kalibrasyonu Yapan** *Calibrated by*	**Laboratuvar Müdürü** *Head of the Calibration Laboratory*
	18.02.2019 11:32:52	GÜVEN KAÇAR Dijital olarak imzalayan: GÜVEN KAÇAR	ALPER TORTOÇ Dijital olarak imzalayan: ALPER TORTOÇ

EKC.05.12 18.07.2016 Rev:00

243 Sok. No:17 D:6 Manavkuyu-Bayraklı / İZMİR - Turkey   (0232) 348 40 50   (0232) 348 63 98   www.kalmem.org   kalmem@mmo.org.tr

Sayfa No: 2/3

Page Number

1. Kalibrasyonda Kullanılan Referans:

Cihaz / Ekipman	Üretici	Seri No	İzlenebilirlik
Sıcaklık Sensörü Pt100	ISOTECH	EK 05.02	MMO KALMEM
Sıcaklık Kalibratörü	Beamex	EK.03.01	MMO KALMEM
Sıvı Banyo	UMS	EK 05.11	MMO KALMEM
Termometre	-	EK 05.24	MMO KALMEM

2. Kalibre Edilen Cihazın Özellikleri:

Cihazın Adı	Ölçüm Aralığı	Çözünürlük	Okunabilirlik
Dijital Göstergeli Sıcaklık Ölçer	42 ... 42 °C	0,01 °C	0,01 °C

3. Ortam Şartları :

Sıcaklık: (23 ± 3) °C   Bağıl Nem   : % (45 ± 15)

4. Kalibrasyon Yöntemi ve Prosedü

Cihazın kalibrasyonu *EURAMET* kalibrasyon dokümanlarına uygun olarak KALMEM tarafından hazırlanmış olan EKT 05.03 No'lu talimata göre gerçekleştirilmiştir. Kalibrasyon kararlı sıcaklık ortamında, referans cihazdan ölçülen sıcaklık değerleri ile cihazın gösterge değerlerinin karşılaştırılması yöntemi ile gerçekleştirilmiştir.

5. Kalibrasyon Belirsizliği

Ölçüm belirsizlikleri sonuç tablosunda verilmiştir. Beyan edilen genişletilmiş belirsizlik değeri, standart belirsizliğin normal dağılım için yaklaşık %95 güvenilirlik seviyesini sağlayan k=2 kapsam faktörü ile çarpımının sonucudur. Standart ölçüm belirsizliği GUM ve EA-4/02 dokümanlarına uygun olarak hesaplanmıştır. Ölçüm belirsizliği uzun zaman kararlılığını kapsamamaktadır.

6. Fonksiyon ve Göz Kontrolü

Fonksiyon ve göz kontrolünde hasar veya eksiklik görülmemiştir.

8. Açıklamalar

Kalibrasyon sonuçları sadece yukarıda belirtilen cihaza ait olup, kalibrasyon tarihinden itibaren ve sertifikada verilmiş olan şartlarda geçerlidir. Cihazın uygun aralıklarla kalibrasyonunun gerçekleşmesinden kullanıcı sorumludur.

9. Kalibrasyon Etiketinin Yeri

Kalibrasyon etiketi cihazın ön tarafına yapıştırılmıştır.

EKC.05.12   18.07.2016   Rev:00

MMO KALMEM
Sanayinin Hizmetinde

tmmob makina mühendisleri odası

Sayfa No: 3/3
Page Number

7. Kalibrasyon Sonuçları

Yapılan ölçümlerin sonucunda aşağıdaki değerler elde edilmiştir.

Ölçüm Bölgesi	Referans °C	Ölçülen °C	Sapma °C	Belirsizlik °C
UNIT-1 -1	42,00	42,10	0,10	0,170
UNIT-1 -2	42,00	42,20	0,20	0,170
UNIT-1 -3	42,00	42,24	0,24	0,170
UNIT-1 -4	42,00	42,18	0,18	0,170
UNIT-1 -5	42,00	42,10	0,10	0,170
UNIT-1 -6	42,00	42,05	0,05	0,170
UNIT-1 -7	42,00	41,96	-0,04	0,170
UNIT-1 -8	42,00	41,99	-0,01	0,170
UNIT-1 -9	42,00	41,97	-0,03	0,170
UNIT-1 -10	42,00	42,02	0,02	0,170
UNIT-2 -1	42,00	42,24	0,24	0,170
UNIT-2 -2	42,00	42,15	0,15	0,170
UNIT-2 -3	42,00	42,14	0,14	0,170
UNIT-2 -4	42,00	42,18	0,18	0,170
UNIT-2 -5	42,00	42,19	0,19	0,170
UNIT-2 -6	42,00	42,25	0,25	0,170
UNIT-2 -7	42,00	42,17	0,17	0,170
UNIT-2 -8	42,00	42,16	0,16	0,170
UNIT-2 -9	42,00	42,21	0,21	0,170
UNIT-2 -10	42,00	42,23	0,23	0,170
UNIT-2 -11	42,00	42,30	0,30	0,170
UNIT-2 -12	42,00	42,24	0,24	0,170
UNIT-2 -13	42,00	42,29	0,29	0,170
UNIT-2 -14	42,00	42,22	0,22	0,170
UNIT-2 -15	42,00	42,23	0,23	0,170
UNIT-4 -1	42,00	42,07	0,07	0,170
UNIT-4 -2	42,00	42,19	0,19	0,170
UNIT-4 -3	42,00	42,10	0,10	0,170
UNIT-4 -4	42,00	42,02	0,02	0,170
UNIT-4 -5	42,00	42,20	0,20	0,170
UNIT-4 -6	42,00	42,07	0,07	0,170
UNIT-4 -7	42,00	42,05	0,05	0,170
UNIT-4 -8	42,00	42,13	0,13	0,170
UNIT-4 -9	42,00	42,06	0,06	0,170
UNIT-4 -10	42,00	42,13	0,13	0,170
UNIT-4 -11	42,00	42,22	0,22	0,170
UNIT-4 -12	42,00	42,04	0,04	0,170
UNIT-4 -13	42,00	42,20	0,20	0,170
UNIT-4 -14	42,00	42,13	0,13	0,170
UNIT-4 -15	42,00	42,12	0,12	0,170

Kalibrasyon başında ve sonunda alınan 42,00 °C değerleri arasındaki fark histeresiz hatası olarak belirsizliğe eklenmiştir.

EKC.05.12   18.07.2016   Rev:00

VITA

PERSONAL

Surname Name: Pekdoğan Tuğçe

EDUCATION

Ph.D.	İzmir Institute of Technology. The Graduate School. Department of Architecture (2016-2022)
Thesis	"Experimental and Numerical Investigation of a Heat Recovery Ventilation Unit with Phase Change Material for Building Facades"
M.Sc.	İzmir Institute of Technology. The Graduate School. Department of Architecture (2013-2016)
Thesis	"An Investigation of Transient Thermal Behaviours of Building External Walls"
B.Arch.	Eastern Mediterranean University. Faculty of Architecture (2008-2013)

ACADEMIC EXPERIENCES

İzmir Institute of Technology. Department of Architecture (2014-2022)

Adana Alparslan Türkeş Science and Technology University. Department of Architecture (2014-ongoing)

PUBLICATIONS

Pekdogan, Tugce, Ayça Tokuç, Mehmet Akif Ezan, and Tahsin Başaran. "Experimental investigation on heat transfer and air flow behavior of latent heat storage unit in a facade integrated ventilation system." *Journal of Energy Storage* 44 (2021): 103367.

Pekdogan, Tugce, Ayça Tokuç, Mehmet Akif Ezan, and Tahsin Başaran. "Experimental investigation of a decentralized heat recovery ventilation system." *Journal of Building Engineering* 35 (2021): 102009.

Pekdogan, Tugce, Sedat Akkurt, and Tahsin Basaran. "A full 34 factorial experimental design for the low energy building's external wall." *Thermal Science* 24, no. 2 Part B (2020): 1261-1273.

Pekdogan, Tugce, and Tahsin Basaran. "Thermal performance of different exterior wall structures based on wall orientation." *Applied Thermal Engineering* 112 (2017): 15-24.